UNIVERSITÀ DEGLI STUDI DI PAVIA

SCIENTIFICA ACTA

QUADERNI DEL DOTTORATO

VOLUME XVIII ANNO XVIII NUMERO 1

15 MARZO 2003

ISTITUTO NAZIONALE DI FISICA NUCLEARE

CENTRO STAMPA - DIPARTIMENTI FISICI
Via Bassi, 6 27100 Pavia

INDEX

UNIVERSITÀ DEGLI STUDI DI PAVIA

FACOLTÀ DI SCIENZE MATEMATICHE FISICHE E NATURALI
Dipartimento di Fisica "Alessandro Volta"
Dottorato di Ricerca in Fisica – XV Ciclo

Fluctuating diamagnetism and ^{89}Y NMR quantities from the underdoped to the overdoped regime in YBCO superconductors

by

PATRIZIA TEDESCO

A Doctoral Dissertation
In Partial Fulfillment of the Requirements for the Degree of
Dottorato di Ricerca in Fisica

February 2003

Contents

Introduction and overview of the thesis

In spite of intense research efforts along the last fifteen years, relevant microscopic aspects of high temperature superconductors ($\mathrm{HT_CSC}$) are still under debate. One of the major challenges for understanding the microscopic mechanism underlying superconductivity in cuprates involves to the evolution of their properties with the carrier concentration, from the underdoped regime to the Fermi liquid metal (overdoped phase) passing through an anomalous metal.[1] This thesis work deals with the above mentioned issue. In particular, in the thesis the fluctuating diamagnetism above the critical temperature and the microscopic quantities conveyed by ^{89}Y NMR in the $Y_1Ba_2Cu_3O_{7-\delta}$ (YBCO) family are studied upon variation of the number of carriers in the CuO_2 planes.
It is known that in the compounds of that family the superconducting properties depend in a complicate way from the oxygen in the chains (which controls the number of holes in the superconducting CuO_2 planes) and possibly from the oxygen ordering along the chains. Therefore the heterovalent substitution by Ca^{2+} for Y^{3+} is the best way to obtain the underdoped regime starting from ideally chain-empty $YBCO_6$ and the overdoped regime from chain-full $YBCO_7$, without affecting the chains.

In $\mathrm{HT_CSC}$, because of the small coherence length, high transition temperature T_C and marked anisotropy, a strong enhancement

---

[1] Optimally doped indicates the sample having highest transition temperature T_C. The samples with hole concentration n_h smaller or greater than the optimally one are called respectively underdoped and overdoped. T_C as function of n_h has a bell-bottomed trend and for particular values of the carrier concentration T_C goes to zero (see Fig. 1.2).

of the superconducting fluctuations (SF) with respect to conventional superconductors is induced. In cuprates the transition region is considerably smeared by SF's, which can be detected in a wide temperature range, up to 10-15 K above T_C. The formation of fluctuating Cooper pairs results in the appearance of a diamagnetic contribution to the magnetization, $-M_{fl}(T,H)$, on approaching the transition from above. In general the magnetization of layered superconductors can be theoretically described in the framework of the Ginzburg Landau (GL) scheme, with the Lawrence-Doniach Hamiltonian, in the vicinity of the transition temperature and for magnetic field $H \ll H_{C2}(0)$ ($H_{C2}(0)$ critical field at which the superconductivity is destroyed), when the contribution of short-wavelength fluctuations is negligible (see References [1, 2, 3, 4] and references therein). The size of fluctuating pairs $\xi(T)$ grows when T approaches T_C and consequently $-M_{fl}(T,H)$ should diverge near the transition for any small fixed magnetic field, being equal zero for $H = 0$. On the other hand very strong magnetic fields, comparable to $H_{C2}(0)$, must suppress SF. Therefore, the isothermal magnetization curve $-M_{fl}(T = const, H)$ vs H has to exhibit an upturn. This upturn can be quantitatively described in the framework of the exactly solvable, for any magnetic field, zero-dimensional model[2], namely superconducting granula at size much smaller than the coherence length. The experimental curves of M_{fl} vs T obtained for conventional BCS superconductors show that the magnetization is quenched for fields as small as $\sim 10^{-2} H_{c2}(0)$ (see Ref. [2]). The value of the upturn field H_{up} in the magnetization curves can be considered inversely proportional to the coherence length[2, 4]. In HT$_C$SC the coherence length is so short that the decrease of the diamagnetic magnetization on increasing the magnetic field, for $T \approx T_C$, has not yet been observed.

In the YBCO:Ca samples studied in this thesis and having hole content n_h different from the optimal one, marked deviations from the behavior expected in the framework of the GL scenario have been evidenced. The isochamp magnetization $-M_{fl}(H = const, T)$ vs T is strongly enhanced with respect to the one in the optimally doped compound and the isothermal magnetization curves $-M_{fl}(T = const, H)$ vs H show the upturn with the field, for $H \ll H_{C2}$.

The presence of local, non-percolating, superconducting droplets has been considered as a source of the "anomalous"diamagnetism above T_C. A test of this hypothesis has been offered from the search of magnetic-history dependent effects. It is known that in YBCO the irreversibility temperature is not far from T_C and therefore if the anomalous FD has to be attributed to locally SC droplets with $T_C^{\mathrm{local}} > T_C^{\mathrm{resistive}}$ (bulk transition temperature), then differences should be detected between zero-field-cooled and field-cooled magnetization measurements. The experimental findings regarding the fluctuating diamagnetism are examined in the light of a theory of phase fluctuations which takes into account the presence of mesoscopic "islands" with non-zero average order parameter. This theoretical approach successfully accounts for all the magnetization curves, by considering the possibility that the superconducting islands are above or below the local irreversibility temperature. A full account of most of the experimental findings is thus achieved.

NMR spettroscopy allows one to study several microscopic properties of $\mathrm{HT_CSC}$, including in particular the correlated spin dynamics. Information on the internal fields, antiferromagnetic (AF) Cu^{2+} correlation, density of states around the Fermi level, the spin gap and/or the charge gap opening up at a temperature T^* above the superconducting transition temperature T_C in underdoped samples can be derived by NMR spectra and relaxation measurements[5]. The coexistence of superconductivity and magnetism can also be studied.

In the SC compounds of YBCO family, ^{89}Y nucleus, lacking of the quadrupole moment and filtering out the AF correlation between Cu^{2+} pseudo-localized magnetic moments, is particularly suitable to study the evolution with doping of the properties related to the fermionic excitations spectrum of the carriers. From Knight shift $\mathrm{K_S}$ and, to a less extent, from spin-lattice relaxation time $\mathrm{T_1}$ measurements the evolution with doping of the phase diagram and in particular of the density of states $\rho(\mathrm{E_F})$ around the Fermi level, have already been studied.

In this work the results obtained by a comprehensive ^{89}Y NMR study are presented. Measurements of line width, $\delta\nu$, Knight shift, $\mathrm{K_S}$, echo dephasing time, $\mathrm{T_2}$, and the spin-lattice relaxation time, $\mathrm{T_1}$, in the temperature range $1.6 \div 300$ K have been performed, in YBCO-type SC's spanning from underdoped to the overdoped regime. The evolution of the NMR quantities with doping is discussed both in terms of modification of the density of states $\rho(E_F)$

and under the hypothesis of a generalized spin susceptibility that includes the contributions due to excitations of charge and spin degrees freedom. In the overdoped regime a non-conventional relationship between K_S and T_1 is evidenced. In the underdoped phases the effects of the spin gap opening in T_1 and K_S measurements are pointed out. In the superconducting state of overdoped compounds, the relaxation rates show the temperature behavior somewhat expected (i.e. $\propto 1/T^3$), with a slight shoulder around the irreversibility temperature that can be attributed to the thermal motions of the flux lattice lines. In underdoped compounds $\delta\nu$ increases for decreasing temperature, while T_2^{-1} shows a sharp peak at $T \approx 7$ K and increases again with decreasing temperature below about ≈ 4 K. The spin-lattice relaxation rate T_1^{-1} shows a maximum at the temperature generally called spin-glass freezing temperature, $T_g \approx 8K$. Correspondently the recovery law is not a single exponential, but takes a stretched exponential character. The behavior of the relaxation rate in underdoped regimes is discussed in terms of low energy excitations due to sliding motion of orbital currents coexisting with d-wave superconducting state. The overall of experimental results suggest that different dynamics drive the longitudinal and the transverse fluctuations of the local field to Y site and that a certain revision of the commonly accepted view for the microscopic magnetic properties in YBCO compounds would be required in order to account for all the experimental findings.

In the following an outline of the thesis is reported.

The central body of the report is constituted by two Chapters in which the experimental results regarding the fluctuating diamagnetism and the ^{89}Y NMR quantities behavior, from underdoped to overdoped regimes, are described, respectively.
The first Chapter, instead, is devoted to the synthesis and the characterization of our YBCO:Ca compounds. The structural, electronic and magnetic properties of YBCO:Ca's resulting from XRPD (X-Ray Powder Diffraction), SEM (Scanning Electronic Microsopy), EDS (Energy Dispersive Spectrometry), as well as from SQUID (Superconductor Quantum Interference Device) measurements, are described.
Chapter 2, the one about fluctuating diamagnetism, is organized as follows. First a short introduction to the theory of SF, in particular

the Ginsburg-Landau scenario, is presented. The results obtained in optimally doped YBCO samples are reported and briefly discussed, as an example where the GL theory is substancially applicable. Then the magnetization curves obtained in overdoped and underdoped samples are presented. A new elaboration of the theory for phase fluctuations of the order parameter in a layered liquid of vortices is shown to account for the experimental observations.
In the first part of Chapter 3 the NMR quantities T_1, T_2, K_S, $\delta\nu$ are defined, with a recall of the basic theoretical background useful for the subsequent discussion. Then the experimental results of ^{89}Y NMR are reported. Finally a comprehensive analysis of the data and summarizing remarks are given.
Appendix A of the thesis describes the diamagnetic fluctuations expected in BCS superconductor and the illustrative example of MgB_2 is discussed. The breakdown of the finite-field theoretical description, with the onset of the upturn in the magnetization curves, is emphasized.
Appendix B is devoted to the theory for the precursor diamagnetism in underdoped and overdoped compounds in the framework of the approach based on the phase fluctuations in a liquid of vortices.
In Appendix C an overview of the experimental results regarding the effect of the magnetic field on the SF's, as detected by NMR measurements, is reported and briefly discussed.

Chapter 1

General properties, synthesis and characterization of $Y_{1-x}Ca_xBa_2Cu_3O_y$ superconducting compounds

First a brief recall on structural and electronic properties of the YBCO compounds is given, with emphasis on the effects of Ca^{2+} for Y^{3+} substitution. Then the procedure used to synthesize the underdoped and overdoped YBCO:Ca compounds is described. Finally the structural and magnetic characterization of the samples used in the NMR and SQUID measurements is reported.

1.1 Structural, electronic and magnetic properties of YBCO-type crystals.

From the discovery of superconductivity in YBCO compounds[6] several heterovalent and isovalent substitutions for Y^{3+} or Ba^{2+} have been devised in order to investigate the general properties and their relationships in these materials[7, 8]. In particular the heterovalent substitutions are of considerable interest, since they can substantially change the effective copper valence and the carrier concentration in CuO_2 planes. In $R_1Ba_2Cu_3O_y$ (with R trivalent lanthanide ion or Y) the carrier density can be enhanced either by increasing the oxygen stoichiometry or by on-site cationic substitutions with dopants of lower valence state. By increasing the oxygen stoichiometry, the copper valence in general can not be increased beyond its optimal value (in correspondence to the maximum in the transition temperature T_C), due to structural instability. Furthermore also the oxygen order in the chain seems to plays a relevant role in superconducting properties[9, 10, 11, 12]. The $Y_{1-x}Ca_xBa_2Cu_3O_6$ compound for $x > 0.1$[13] is an underdoped chain empty superconductor, while the parent compound $Y_1Ba_2Cu_3O_6$ is an antiferromagnetic insulator. The compound $Y_{1-x}Ca_xBa_2Cu_3O_7$, instead, is an overdoped chain full superconductor, $Y_1Ba_2Cu_3O_7$ being only slightly overdoped[14]. As a consequence the heterovalent substitution of Y^{3+} by Ca^{2+} allows to explore the whole phase diagram from the underdoped to the overdoped superconducting regime.

$YBa_2Cu_3O_7$ has a triple-perovskite structure[15, 16, 17] and can be regarded as built up by intercalation, along c-axis, of metallic CuO_2 planes with two different insulating block layers: Y and $BaO - CuO_z - BaO$, where z is the occupancy of the oxygen site O(1) (see Fig. 1.1). The presence of the CuO chains causes the b lattice parameter (along the chain direction) to be longer than a, so that the structure is orthorhombic. When all of the oxygen is removed from the chains, as in $YBa_2Cu_3O_6$, the structure is tetragonal, and the material is an antiferromagnetic insulator. In the cuprates the superconductivity is due to electron vacancies (or hole) in $Cu0_2$ planes. These holes have prevalently O2p character. The average occupancy z of the oxygen sites in CuO chains controls the density of the holes in the CuO_2 planes. The distribution of holes between the chains and planes is stabilized electrostatically by displacements within the BaO layers. The hole density in the CuO_2 planes determines T_C. In particular T_C vs the doped hole concentration in the cuprates follows an universal approximately parabolic curve (see Fig. 1.2)[13]

$$\frac{T_C}{T_{C,max}} = 1 - 82.6(n_h - 0.16)^2 \tag{1.1}$$

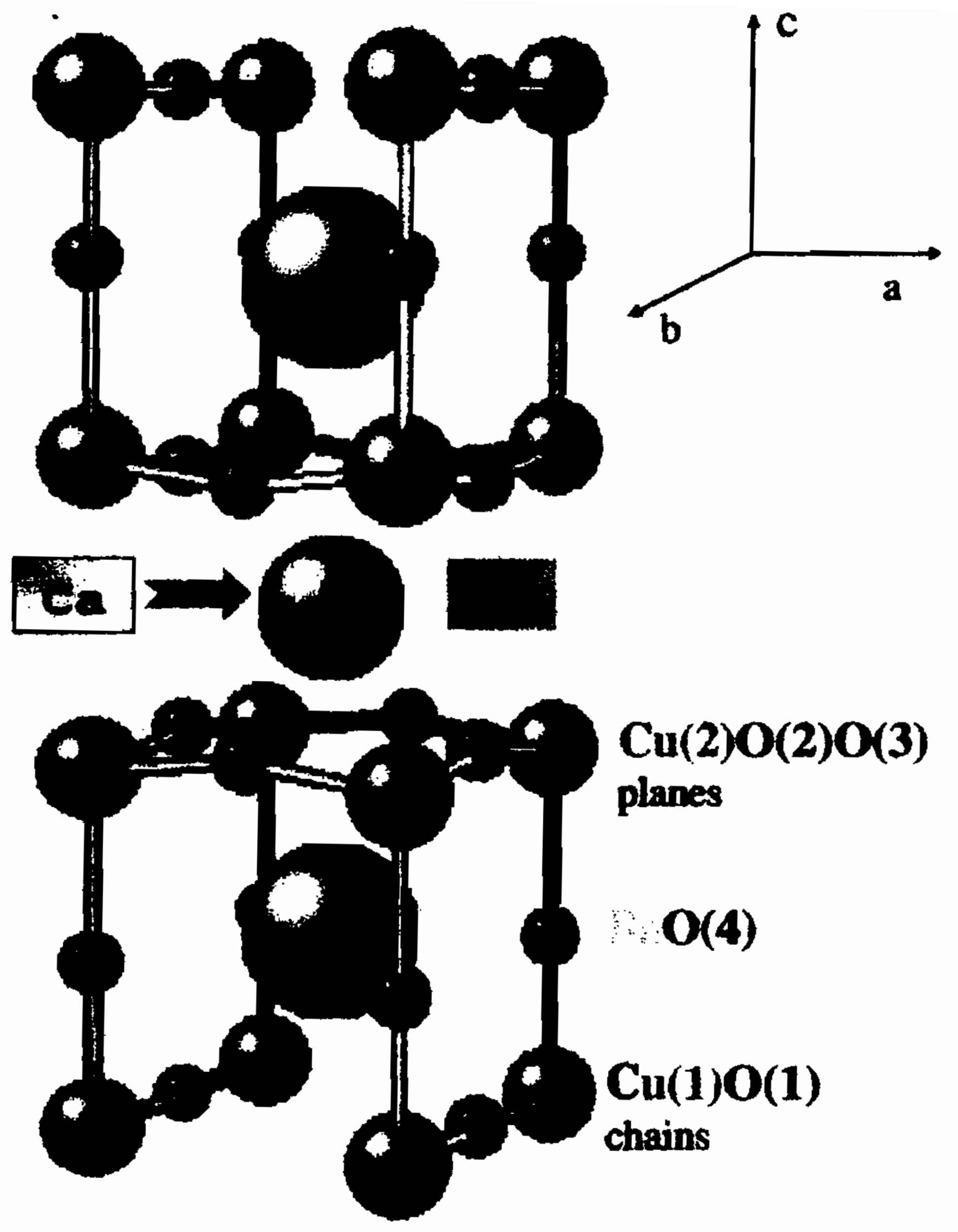

Figure 1.1: The crystalline structure of $Y_1Ba_2Cu_3O_7$. In YBCO:Ca compounds some Y^{3+} ions are substituted by Ca^{2+} ions.

where n_h is the fraction of holes per Cu atom in CuO_2 sheet, and $T_{C,max}$ is the maximum of value of T_C for the particular compound (i.e. $T_{C,max} = 92$ K for $YBa_2Cu_3O_{6+z}$).

The oxygen content in CuO chains drives a phase transition from a high-temperature tetragonal to a low-temperature orthorhombic structure[18] (see Fig. 1.3). The superconducting transition temperature T_C appears correlated to this behavior.

The Y ion is surrounded by eight oxygens atoms, the Ba atoms form a ionic bond with the 10 oxygen neighbors. A key role is played by the Cu coordination. In fact the filling and ordering of $Cu(1) - O_z$ chains control the filling of valence bands, and hence the electronic and magnetic properties of $YBa_2Cu_3O_{6+z}$. The Cu(2) atoms in the planes are coordinated with five oxygen neighbors (square pyramidal coordination). In the tetragonal structure with empty chains the Cu(1) in the chains is twofold coordinated with the O(4) atoms along c direction (linear coordination). In the orthorhombic structure with full chains the Cu(1) is fourfold coordinated with oxygen O(1) along b direction and O(4) along c direction (square planar coordination). For arbitrary z the oxygen in the Cu(1) layer cluster into chains so to maximize the number of two or four-fold coordinated Cu(1) sites. Another limiting case is that in which every oxygen is isolated and sits between two threefold coordinated Cu(1) atoms. It must be noted that when oxygen atoms are added to an empty chain, they can obtain only half of the charge they require from their Cu(1) neighbors. Thus, either holes must be created in the chains, or electrons must be transferred from the planes to the chains, thus creating holes in the planes. It is worthy to note that the displacement from Ba and O(1) along *c*-axis strongly contracts with increasing z in the orthorhombic phase, consistent with plane-to-chain charge transfer (see Ref. [16] and references therein). In the full reduced compound $YBa_2Cu_30_6$ the Cu(2) ions have magnetic moments, while the two-fold coordinated Cu(1) sites are non-magnetic. The Cu moments within the CuO_2 planes order antiferromagnetically because of nearest-neighbor superexchange interaction, and the planes couple together antiferromagnetically along the *c*-axis. In $YBa_2Cu_3O_{6+z}$ the magnetic order is not destroyed by mobile holes until the tetragonal-orthorhombic phase boundary is reached. The simplified phase diagram for $YBa_2Cu_3O_{7-\delta}$ is shown in Fig. 1.4.

In the oxygen annealed $YBa_2CuO_3O_{7-\delta}$ compounds ($\delta \approx 0$), the heterovalent substitution of Ca^{2+} for Y^{3+} decreases the su-

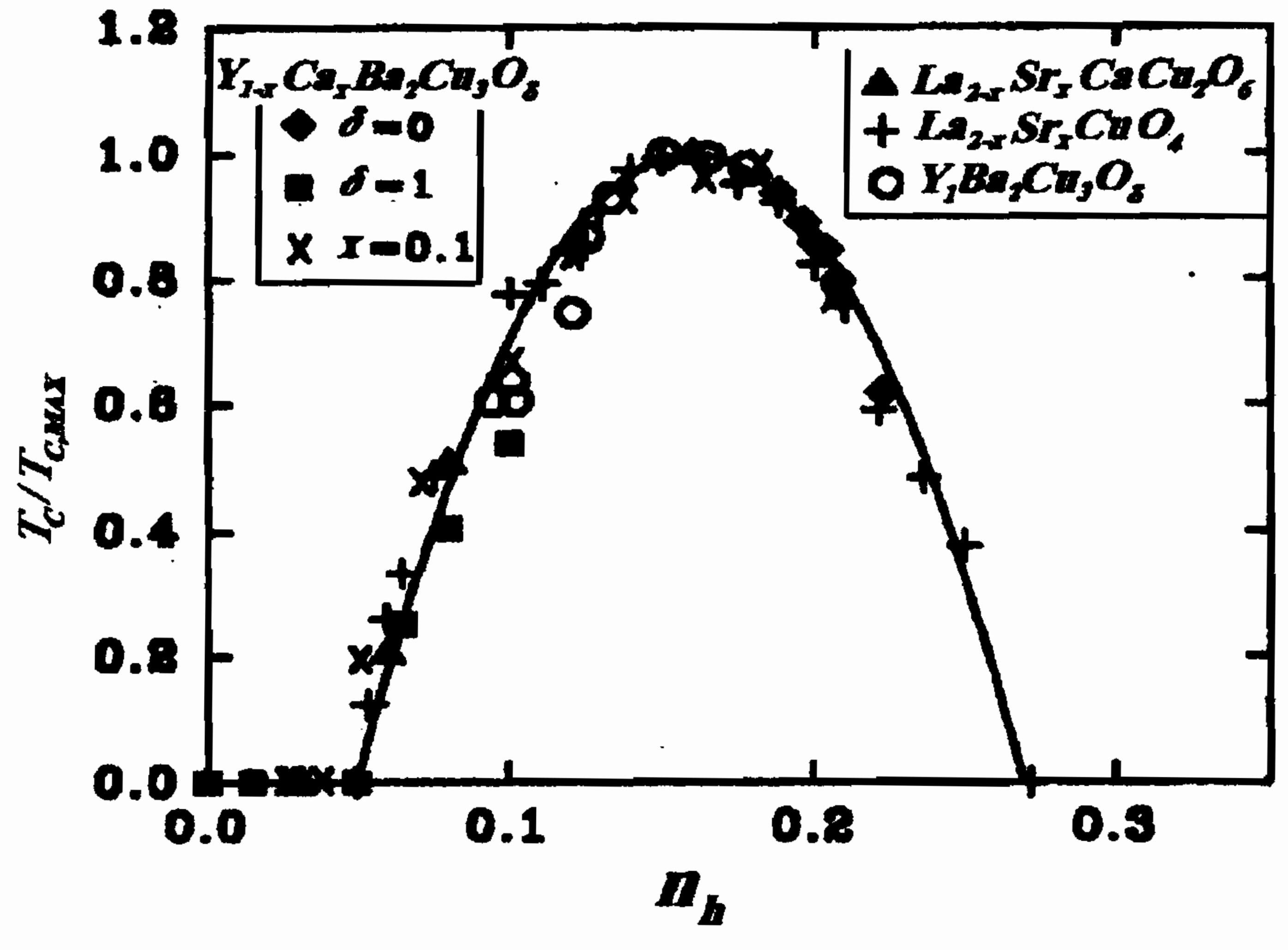

Figure 1.2: T_C values vs hole concentration n_h. T_C values are normalized to $T_{C,max}$. (Fig. from Ref. [13]).

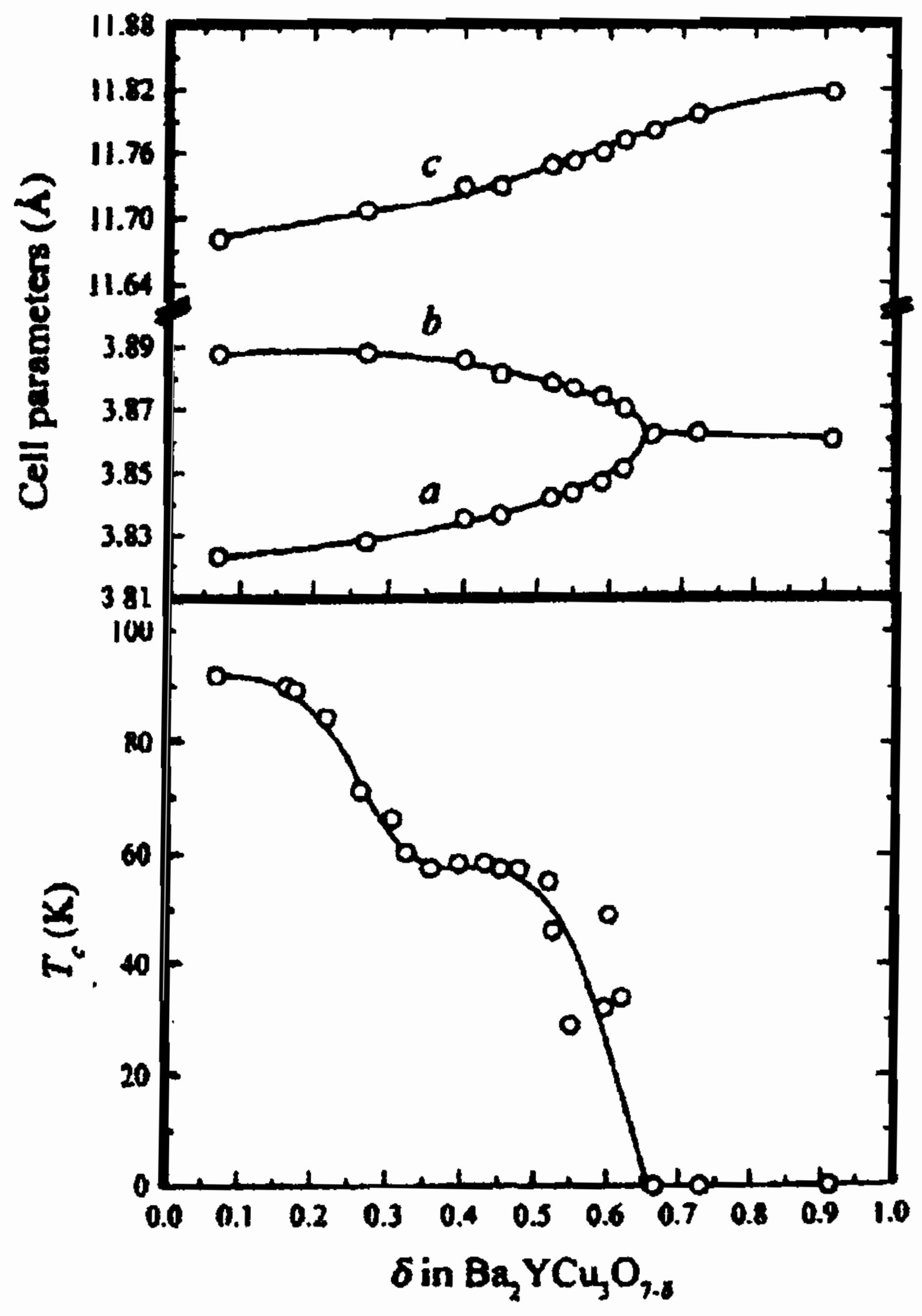

t!

Figure 1.3: Cell parameter (top) and superconducting transition temperature (bottom) vs δ for $YBa_2Cu_3O_{7-\delta}$. (Fig. from Ref. [18]).

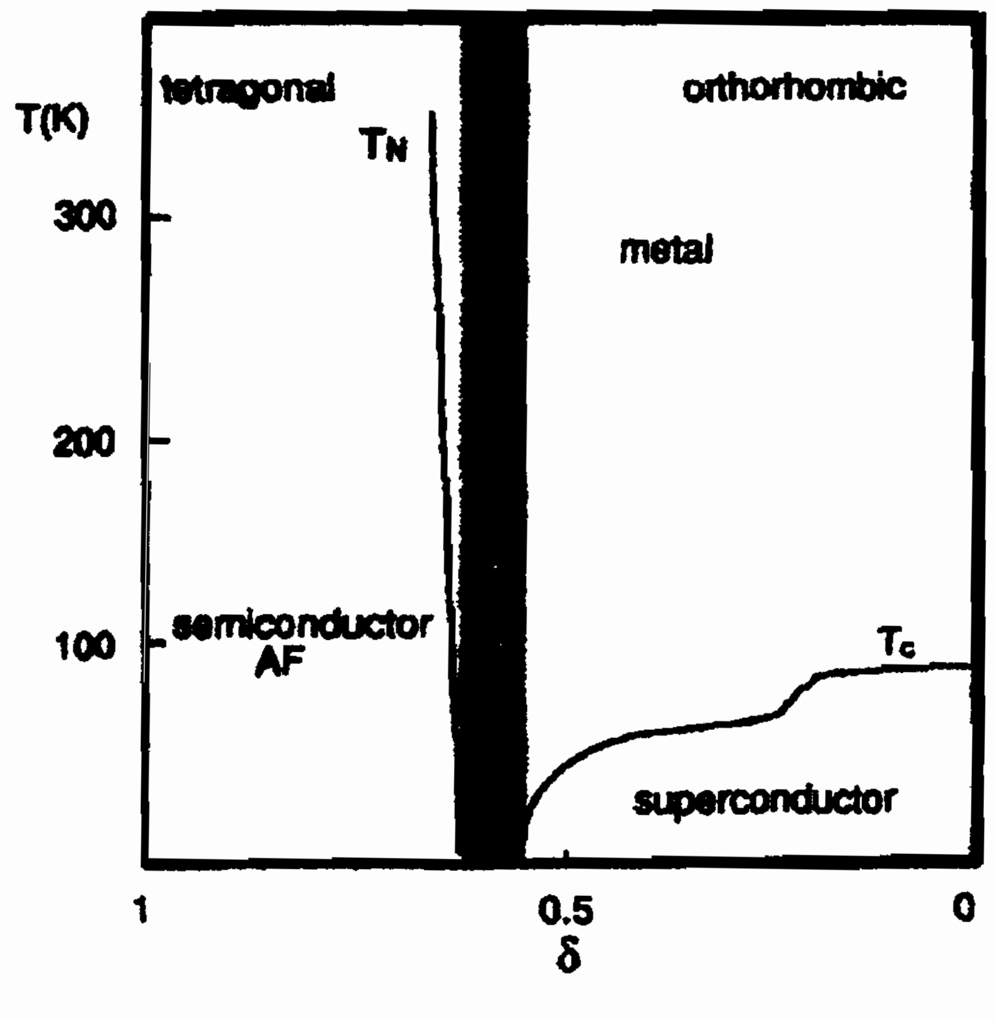

Figure 1.4: Schematic phase diagram for $YBa_2Cu_3O_{7-\delta}$. (Fig. from Ref. [17]).

perconducting transition temperature (T_C), while in the of oxygen deficient systems ($0.4 \leq \delta \leq 0.8$) T_C is enhanced[20, 21, 19]. In particular the occurrence of superconductivity is also been reported in tetragonal $YBa_2Cu_3O_6$ system on partial replacement of Y by Ca[19, 20, 24, 22, 23] (see Fig. 1.5). The substitution of Ca^{2+} onto Y^{3+} sites causes the increase of hole concentration in the CuO_2 plane without provision of holes from the CuO chain site. In fact the Cu-O bond distance in the chain is constant while the Cu(2)-O(2) bond distance in the planes decreases with increase of Ca^{2+} as shown by neutron diffraction measurements for underdoped samples[21]. Furthermore in tetragonal fully reduced sam-

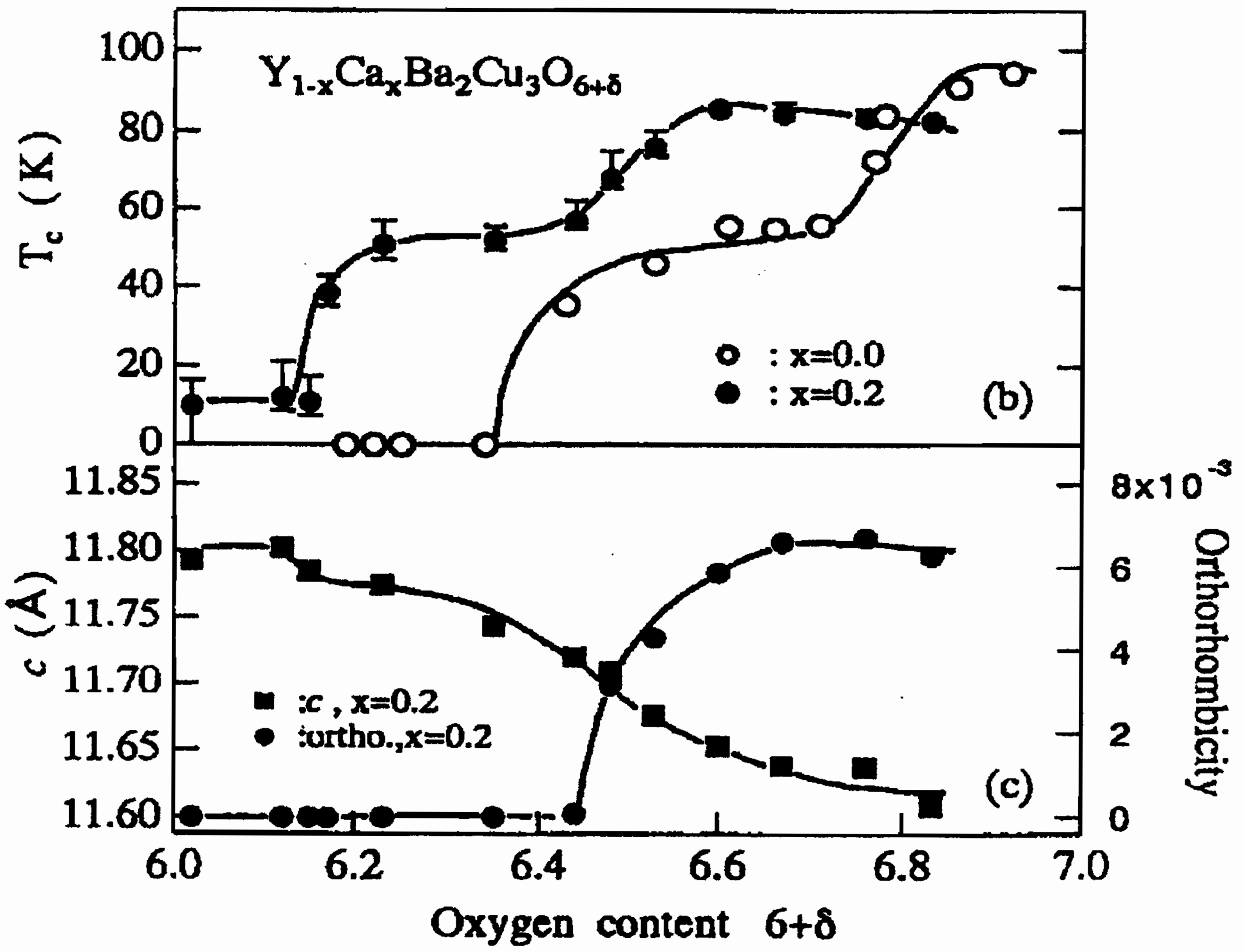

Figure 1.5: (b) Dependence of T_C on oxygen content z in $Y_{1-x}Ca_xBa_2Cu_3O_{6+z}$ per x=0.0 (open circles) and x=0.2 (solid circles). The transition temperature have been estimated by resistivity measurements. (c) Dependence of lattice constant c (left scale and squares) and orthorhombicity, defined as $\frac{b-a}{b+a}$ (right scale and circles), on z in $Y_{1-x}Ca_xBa_2Cu_3O_{6+z}$. Solid lines are only to guide the eye. (Fig. from Ref. [19]).

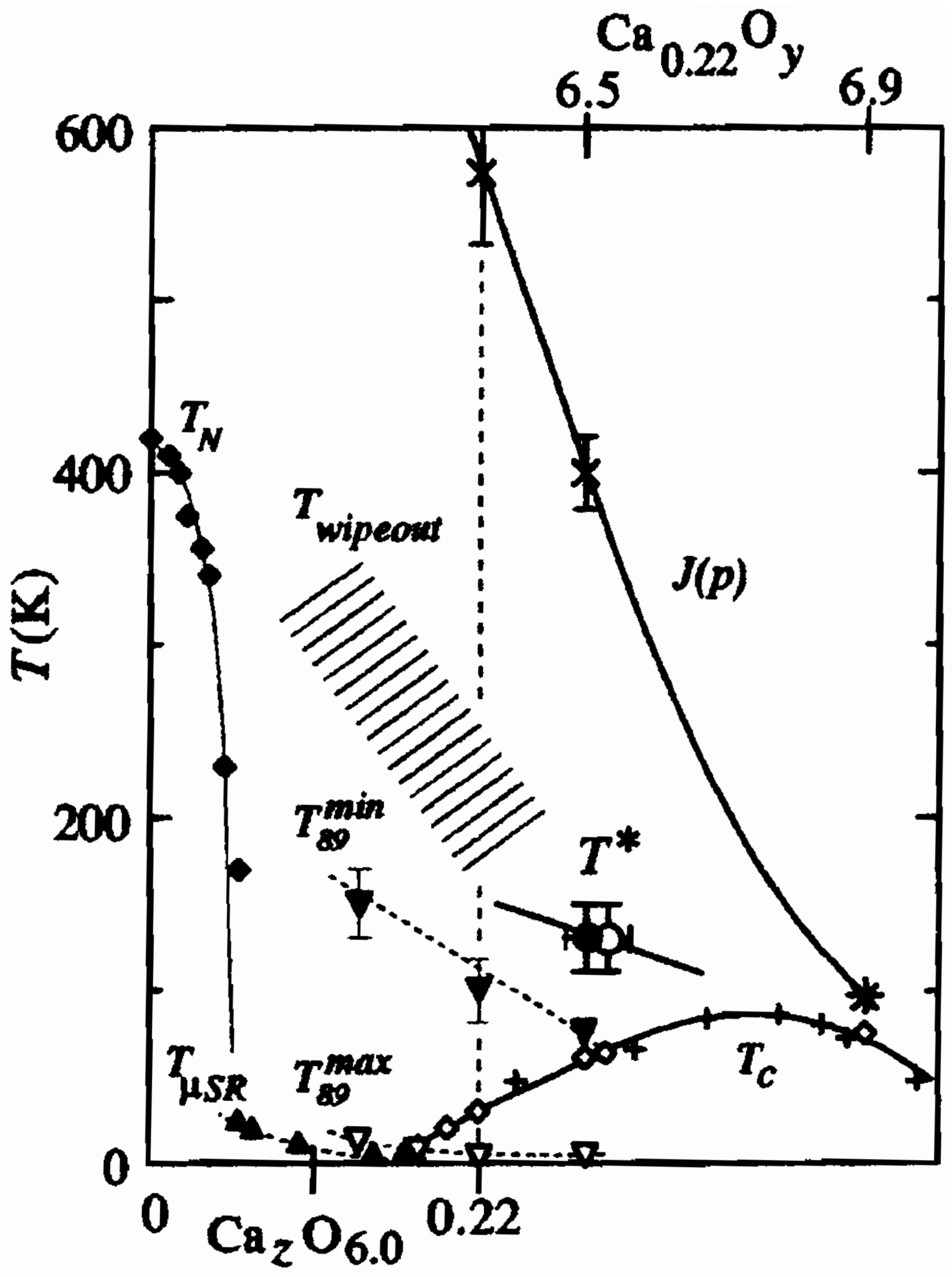

Figure 1.6: Phase diagram of $Y_{1-x}Ca_xBa_2Cu_3O_y$ as a function of Ca_x substitution for fixed y=6.0 to the left of vertical dashed line, and as a function of O_y concentration for fixed x=0.22 to the right. (Fig. from Ref. [29])

ples and in orthorhombic fully oxygenated samples the valence of Cu(1) and Cu(2) remains constant after the heterovalent substitution $Ca^{2+} \rightarrow Y^{3+}$[26, 25, 27]. Therefore this substitution allows one to drive the compounds from the underdoped to the overdoped regime and to explore the full phase diagram of the HT_CSC superconductor. In Fig.s 1.6 and 1.7 the phase diagrams proposed respectively by Niedermayer et al.[28] and Singer et al.[29] are reported. For lower values of hole concentration the compounds are still antiferromagnets. For intermediate values there is a spin glass phase with a "spin-freezing" temperature T_g, finally for hole concentration in the plane larger than $n_h \simeq 0.06$ the compounds are superconductor. In the superconducting phase for underdoped regime there is a kind of coexistence between the superconducting and magnetic phase. As we will discuss in detail in Chapter 3 the transition at T_g could rather be ascribed to the slowing down of orbital currents rather than to the freezing of magnetic moment. In underdoped and optimally doped compounds in Fig. 1.6 the pseudo gap opening at temperatures T^* above T_C is evidenced.

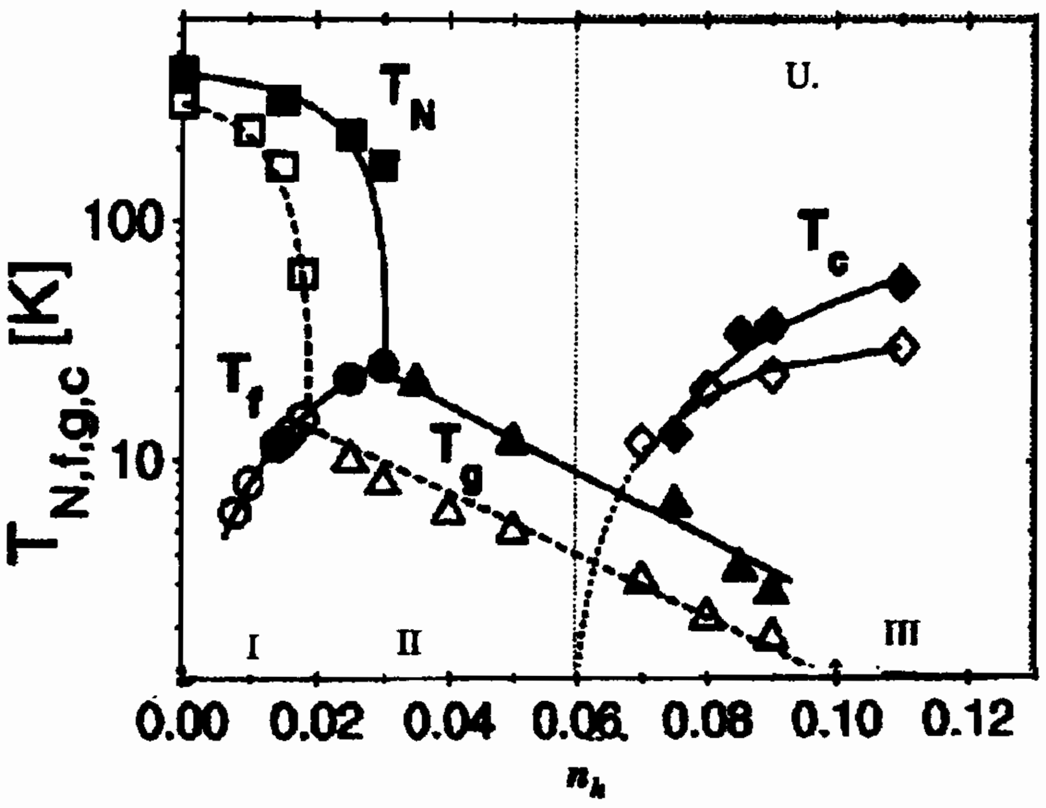

Figure 1.7: Phase diagrams as a function of the hole concentration per CuO_2 sheet for $La_{2-x}Sr_xCuO_4$ (open symbols) and $Y_{1-x}Ca_xBa_2Cu_3O_{6.02}$ (solid symbols). In regime I, two transitions are observed. The transition at which the Cu^{2+} spins order into a 3D AF state at the Neel temperatures T_N (squares) and a freezing transition of the spins of the doped holes at T_f. T_g indicates a transition into a spin-glass-like state (up triangles, regime II) with strong magnetic correlations which coexist with superconductivity in regime III. (Fig. from Ref. [28])

1.2 Synthesis of the compounds

The samples of chemical composition $Y_{1-x}Ca_xBa_2Cu_3O_y$ were prepared by conventional solid state reactions mixing by ball-milling stoichiometric amounts of Y_20_3, $CaCO_3$, $BaCO_3$ and CuO, according to the following reaction

$$\frac{1-x}{2}Y_20_3 + xCaCO_3 + 2BaCO_3 + 3CuO \rightarrow$$
$$Y_{1-x}Ca_xBa_2Cu_3O_{\frac{13-x}{2}} + (2+x)CO_2$$

The $Y_{1-x}Ca_xBa_2Cu_3O_y$ phase was obtained by calcination of the precursor by heating at 915° C for 20 h in air followed by quenching at room temperature. This process was repeated three times with two intermediate grindings to give single phase powders. Then the samples were annealed at 400° C in flowing oxygen for 5 days to obtain the overdoped full oxygen samples $y \simeq 7$, while the samples were heated at 500° C in vacuum for six days in order to obtain underdoped YBCO:Ca $y \simeq 6$. The final oxygen content turned out $y = 6.97 \pm 0.02$ for overdoped YBCO (estimated by thermogravimetry analysis) and $y = 6.10 \pm 0.05$ for the underdoped

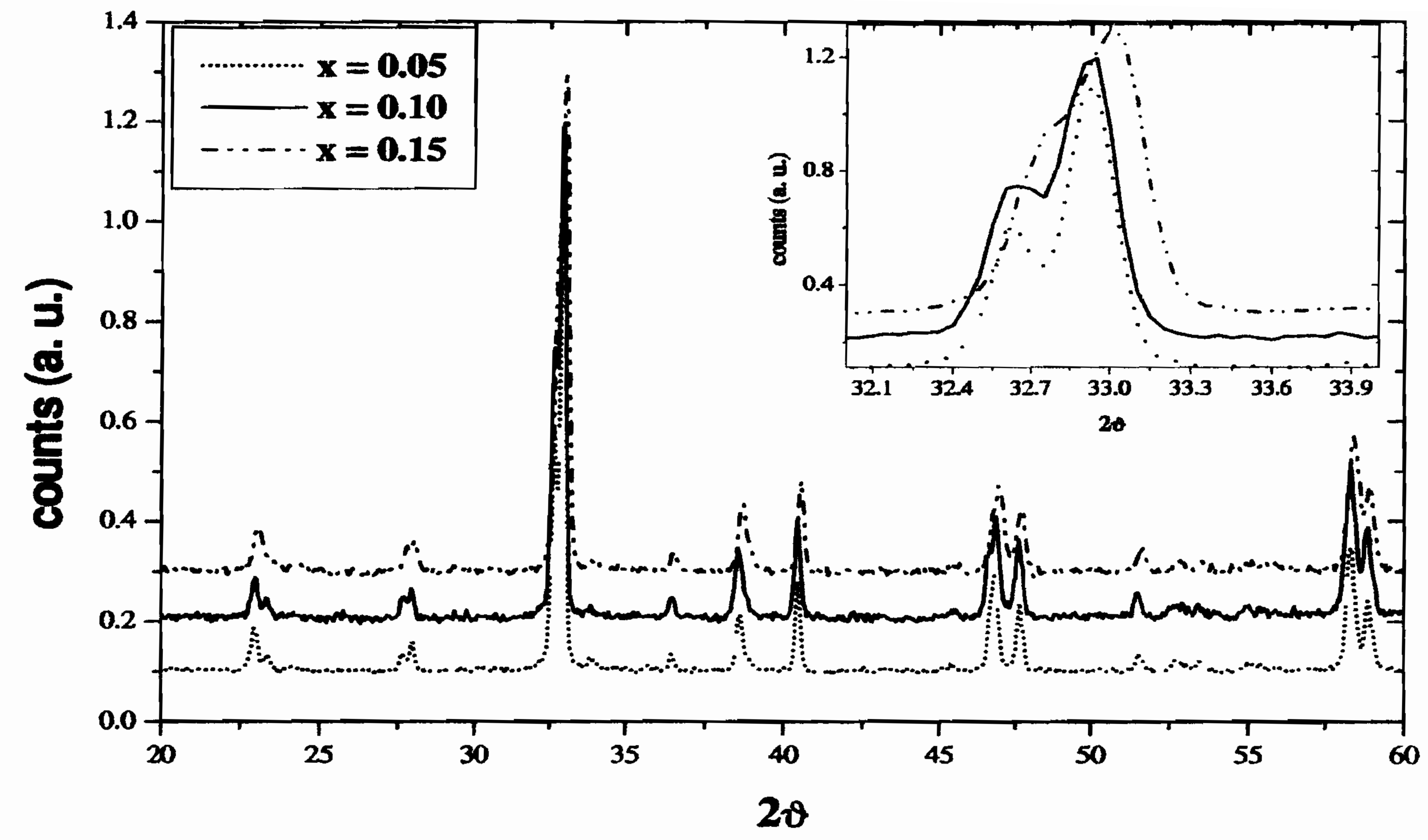

Figure 1.8: XRPD pattern for some YBCO:Ca samples before the annealing in controlled atmosphere.

samples (estimated with loss of mass measurements). Some samples were oriented by hardening in a strong magnetic field (9 Tesla) after mixing with epoxy resin.

1.3 Structural and magnetic characterizations.

X-Ray Powder Diffraction (performed by means of a Philips PW 1700 diffractometer) was used to test if the samples were single phase. Fig. 1.8 shows the XRPD pattern before oxygenation or deoxygenation for some samples at different values of Ca content (x=0.05, x=0.10, x=0.15) (orthorhombic crystal structure). Fig. 1.9 shows the XRPD pattern for underdoped compounds at x=0.15 ($T_C(0) = 20$ K) and x=0.25 ($T_C(0) = 35$ K). One can see from the inset that these samples have tetragonal structure.

Also the ^{63}Cu NQR spectra and ^{89}Y NMR spectra have been used to test the quality of some of the samples. The ^{63}Cu NQR linewidth turned out to have practically the values reported in the literature, thus indicating the lack of unusual lattice defects and/or stresses.

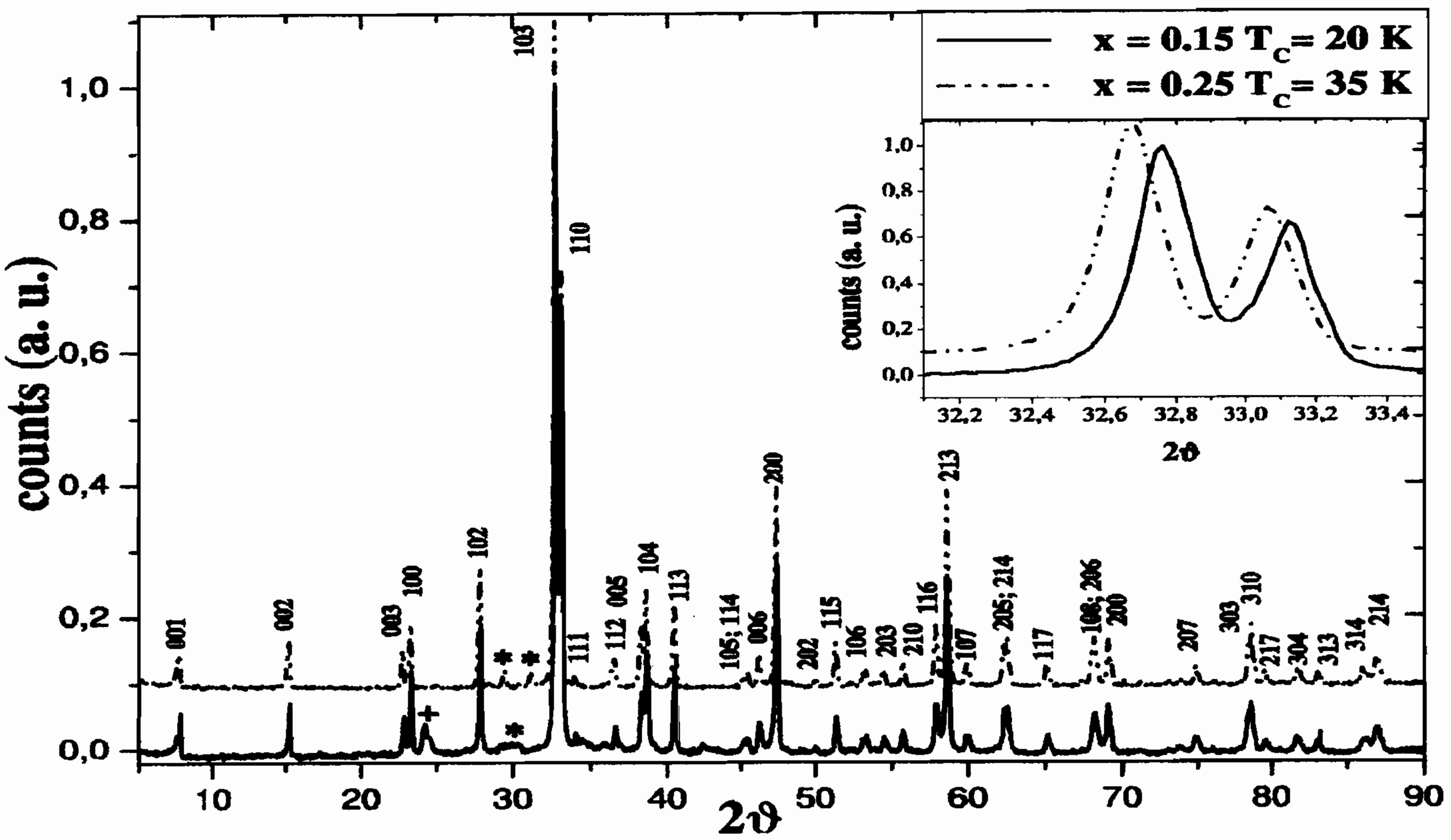

Figure 1.9: XRDP pattern for YBCO:Ca underdoped samples (y ≈ 6.1). ⋆ indicates the $BaCO_2$ impurity.

The ^{89}Y NMR spectra do not evidence any of static phase separation, the linewidth being only slightly larger than in the single crystal[30]. A larger linewidth is likely to be due to the distribution of demagnetization factors. The linewidth is only slightly doping dependent, the spectra of underdoped and overdoped samples being well distinguished in frequency. Therefore it can be concluded that the samples do not appear the superposition of macroscopic regions at different doping amounts, similarly to what observed in Ref. [30]. This observation has a certain relevance in the interpretation of the anomalous diamagnetism observed in underdoped and overdoped compounds, as we shall see at §2.2. Furthermore details on the ^{89}Y NMR linewidth will be given at §3.3.
The powder is formed by grains of 10-30 μm, as evidenced by scanning electron microscopy (Fig. 1.10 part a)). The local stoichiometry was tested by Energy Dispersive Spectrometry on various zones of the samples of dimensions $30 \div 500$ μm. The EDS spectra (see Fig. 1.10 part b)) shows the presence only of Y, Ca, Ba, Cu, O atoms and gives the expected atom percent. The relative concentration of Y and Ca is approximately the nominal one, with some regions (30 μm size) reacher in Ba and Cu. In the remaining part

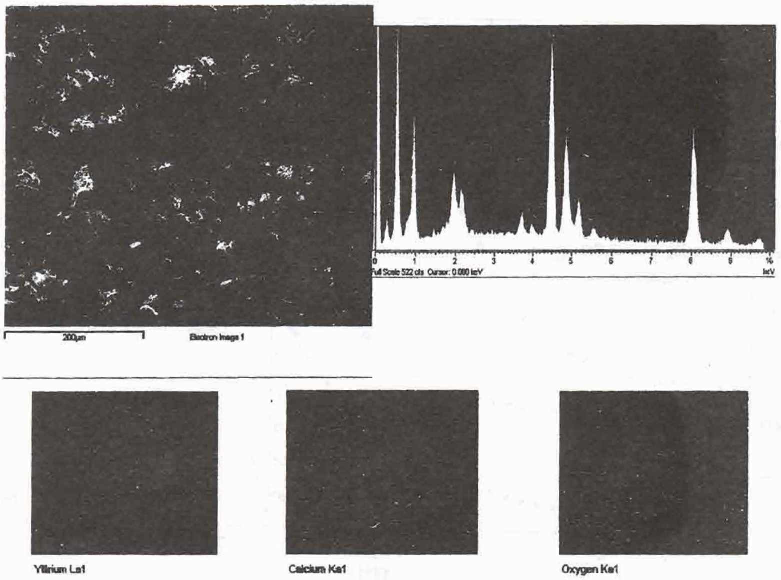

Figure 1.10: a) SEM image of YBCO:Ca underdoped sample at x=0.25. b) EDS spectra. c) The maps of the Y, Ca, O atoms in the sample region shown in part a) of the Figure.

of the samples the element maps (Fig. 1.10 part c)) show an uniform distribution of Ca, Y and O. Magnetization measurements have been carried out in oriented powders by means of a Quantum Design MPMS-XL7 SQUID magnetometer. The transition temperatures $T_C(H=0)=T_C(0)$ were estimated from the magnetization curves vs. T at small fields (20 Oersted), by extrapolating at M=0 the linear behavior of χ occurring below T_C, as shown in the insets in Fig. 1.11. The values of $T_C(0)$ are collected in Table 1.3, where the numbers of holes n_h, as evaluated from the expression 1.1, are also reported. It is worth noting that because of the enhanced fluctuating diamagnetism some uncertainties in the estimate of $T_C(0)$ are present, particularly in strongly underdoped samples. These uncertainties do not affect the discussion (Chapter 2) about the anomalous diamagnetism, which is detected in a temperature range well above $T_C(0)$.

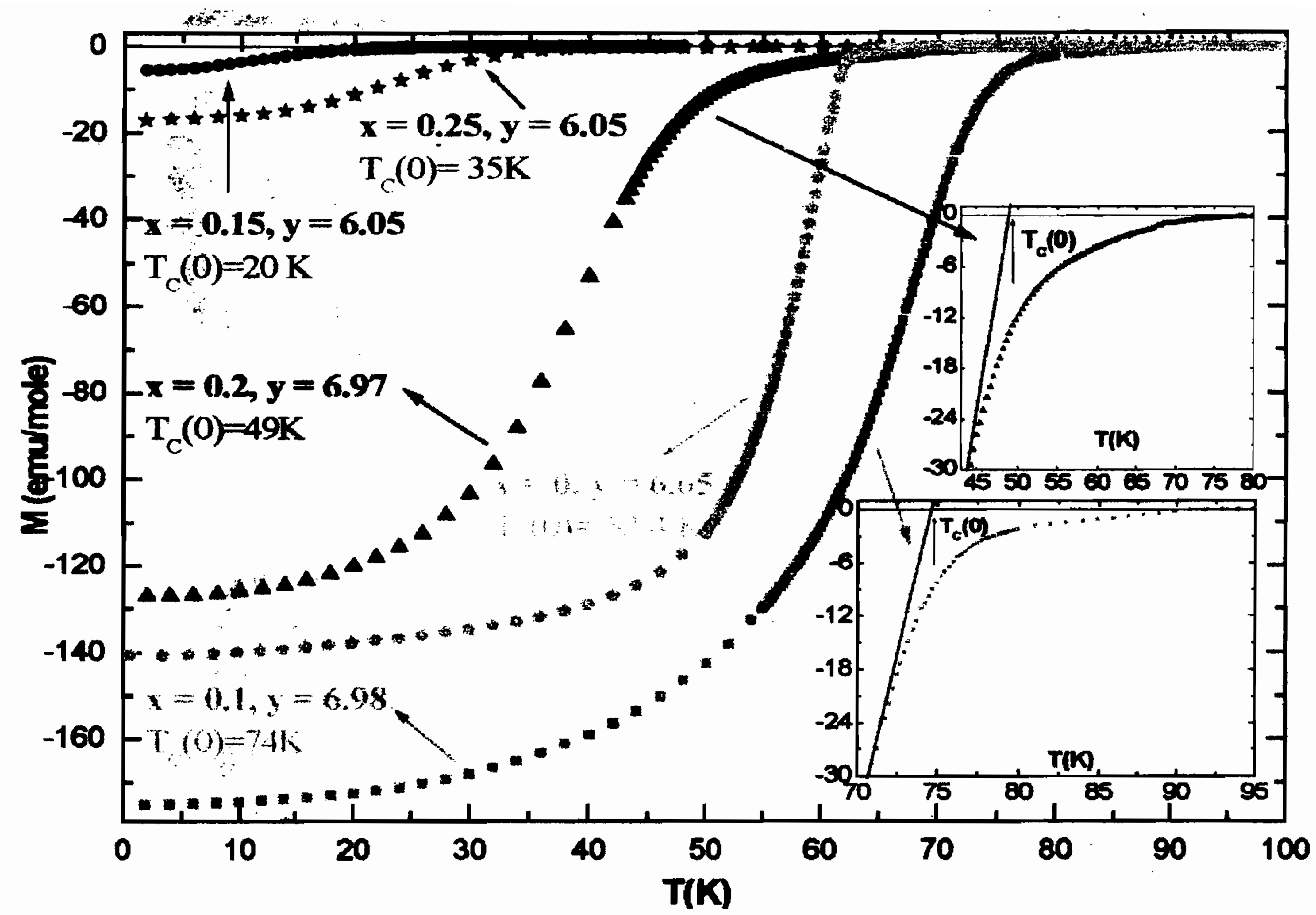

Figure 1.11: Some magnetization data in low field, parallel to the c-axis, as a function of temperature in oriented powders of $Y_{1-x}Ca_xBa_2Cu_3O_y$. The values of the magnetization measured from 250 K down to 90 K, with a positive Pauli-like temperature independent term, are not reported in the figure. In the insets the blow-up for the estimate of $T_C(0)$ is shown.

Table 1.1: Superconducting transition temperature in overdoped and underdoped $Y_{1-x}Ca_xBa_2Cu_3O_y$ and estimated number of holes n_h per CuO_2 unit.

x	y	T_C(K)	n_h
0	6.65	62.5	0.12
0.05	6.97	82.0	0.18
0.1	6.96	73.0	0.20
0.1	6.96	70.0	0.21
0.2	6.98	49.5	0.23
0.25	6.10	35.00± 1	0.07
0.15	6.10	34.00± 1	0.07
≈ 0.15	6.05	20.00± 2	0.06
0.1	6.10	14.00± 2	0.06

Chapter 2

Anomalous doping dependence of the fluctuation-induced diamagnetism above T_C

In the first part of this Chapter a brief recall of the conventional theoretical approach to superconducting fluctuations (Ginzburg-Landau and Lawrence-Doniach scenario) is presented. In the second part of the Chapter the SQUID magnetization measurements, performed in order to analyze the doping dependence of the fluctuating diamagnetism above the superconducting transition temperature T_C, are discussed. The samples that have been investigated are oriented powders of optimally doped $\mathrm{Y_1Ba_2Cu_3O_7}$, underdoped chain-disordered $\mathrm{Y_1Ba_2Cu_3O_{6.65}}$ and finally samples of $\mathrm{Y_{1-x}Ca_xBa_2Cu_3O_y}$, with x ranging from 0 to 0.2, for $\mathrm{y} \approx 6.1$ (underdoped almost chain empty) and $\mathrm{y} \approx 6.97$ (overdoped practically chain full). It will be shown that in optimally doped compounds the diamagnetic susceptibility and the magnetization curves $-M_{fl}(T = const)$ vs. H are rather well justified on the basis of an anisotropic Ginzburg-Landau (GL) functional. At variance, in underdoped and overdoped regimes an anomalous diamagnetism is observed, with a large enhancement respect to the GL value and shapes of the magnetization curves strongly different from the one expected in that framework. The anomalies are discussed in terms of phase fluctuations of the order parameter in a layered system of vortices related to charge inhomogeneities inducing local, non percolating, superconducting regions with $T_C^{(loc)}$ higher than the resistive transition temperature T_C.

2.1 Conventional superconducting fluctuations theories.

2.1.1 The Ginzburg-Landau scenario

To the superconducting transition one associates a complex order parameter: $\psi(\vec{r}) = |\psi(\vec{r})| \exp(i\vartheta(\vec{r}))$, where $\vartheta(\vec{r})$ is the phase and $|\psi(\vec{r})|^2$=$\mathrm{n_s}$ represents the local density of the superconducting electrons (Cooper pairs).[1] Thus $|\psi(\vec{r})|^2$ is zero for $T > T_C$, and raises as T decrease for $T < T_C$. The order parameter is a quantity subject to fluctuations: $\langle|\psi(\vec{r})|^2\rangle \neq 0$ also for $T > T_C$.

A general description of superconducting fluctuations is based on the theory of Ginzburg Landau (GL), which is a phenomenological theory to describe the macroscopic behavior of superconductors.[2]

The GL theory postulates the free energy density (f) as a power series expansion of $|\psi|$ [3] and $\nabla\psi$:

$$f = f_{n0} + \alpha\,|\psi|^2 + \frac{\beta}{2}\,|\psi|^4 + \frac{1}{2m^*}\left|\left(\frac{\hbar}{i}\nabla - \frac{e^*}{c}\vec{A}\right)\psi\right|^2 + \frac{h^2}{8\pi} \qquad (2.1)$$

where f_{n0} is the free energy density in the normal state and in absence of magnetic field, $\vec{A}$ is the vector potential, $\alpha = \alpha_0\frac{T-T_C}{T_C} \equiv \alpha_0\varepsilon$, β is a constant, the gradient term is written in a way to satisfy the gauge invariance, and the quantity $h^2/8\pi$ is the energy density of the magnetic field; m^* and e^* are respectively the effective mass and the charge of supercarriers.

The thermal fluctuations from ψ to $\psi + \delta\psi$ increase the free energy

---

[1] According to the Landau theory for second order phase transitions the order parameter goes to zero at the transition point. Therefore, the natural order parameter is proportional to the condensed state wavefunction.

[2] It can be derived in a rigorous way as a limiting case of BCS microscopic theory[31] (see Ref. [32]).

[3] Only the even terms are present, since in general the free energy must be invariant with respect the symmetry group of transformation that leave the system hamiltonian unaltered, and so in this case the free energy must be invariant with respect to the phase variation of order parameter.

by $\sim k_B T$ (k_B is the Boltzmann constant) and, being $e^{-F/k_B T}$ the associated probability, they occur also above T_C where all the superconducting effects arise from the fluctuations.
The differential equations to derive the distribution of the wavefunction ψ and of the magnetic field are obtained by finding the free energy minimum as functional of three independent functions: ψ, ψ^* and $\vec{A}$:[33]

$$\frac{1}{4m}\left(-i\hbar\nabla - \frac{2e}{c}\vec{A}\right)^2 \psi + \alpha\psi + \beta\left|\psi\right|^2\psi = 0 \qquad (2.2)$$

$$\vec{j} = -\frac{ie\hbar}{2m}\left(\psi^*\nabla\psi - \psi\nabla\psi^*\right) - \frac{2e^2}{mc}\left|\psi\right|^2\vec{A} \qquad (2.3)$$

These equations constitute the Ginzburg-Landau complete equation system, considering $m^* = 2m$, $e^* = 2e$, consequently $n_s = n_e/2$, where n_e is the electron density in the condensed state.
The boundary conditions define the following quantities:

the penetration length λ:

$$\lambda(T) = \left[\frac{mc^2\beta}{4\pi e^2\alpha_0\left(T_C - T\right)}\right]^{\frac{1}{2}} \qquad (2.4)$$

the coherence length ξ:

$$\xi(T) = \frac{\hbar}{2(m\alpha_0)^{1/2}(T_C - T)^{1/2}} \equiv \xi_0\varepsilon^{-1/2} \qquad (2.5)$$

with

$$\varepsilon = \left(\frac{T - T_C}{T_C}\right) \qquad (2.6)$$

These are the lengths in which respectively the magnetic field and the distribution of ψ change substantially (see Fig.2.1). ξ is the correlation length of the order parameter fluctuations (as it can be seen afterwards studying the spatial variation of the fluctuations). λ, ξ must be larger than the Cooper pair size, ξ_0, so the hypothesis that all quantities change spatially in a sufficiently smooth way is verified. Near T_C this condition is generally satisfied because both lengths increase near the transition temperature as $(T_C - T)^{-\frac{1}{2}}$.

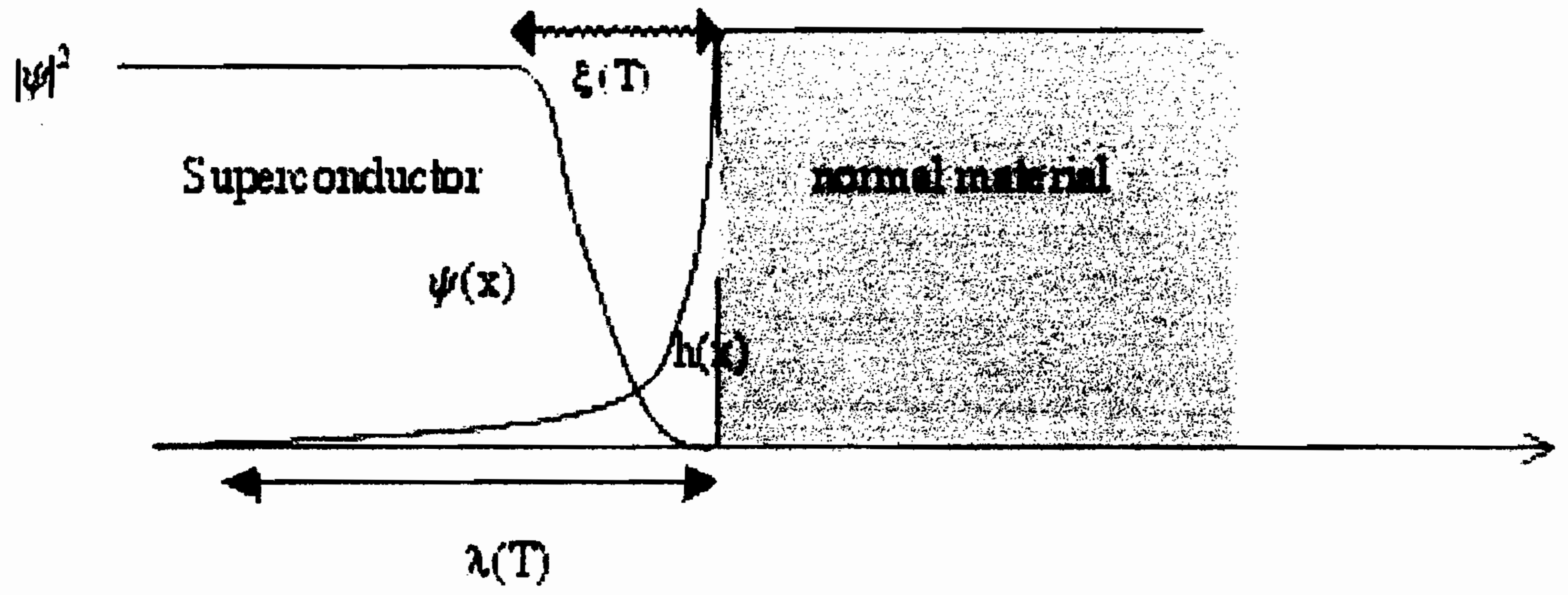

Figure 2.1: Spatial dependence of the order parameter $\psi(x)$ and the magnetic field density $h(x)$ at superconductor-normal interface.

Spatial variation of the fluctuations

The GL free-energy density, Eq. 2.1, neglecting the quartic term in ψ, can be written

$$f = f_{n0} + \alpha \left|\psi\right|^2 + \frac{\hbar^2}{2m^*}\left|\left(\frac{\nabla}{i} - \frac{2\pi\vec{A}}{\Phi_0}\right)\psi\right|^2 \tag{2.7}$$

This assumption is called *Gaussian approximation* and it is valid, for a bulk sample, for T not too close to T_C. In the absence of magnetic field $\vec{A} = 0$, and by writing ψ as an expansion of free-particle eigenfunction

$$\psi(\vec{r}) = \sum_{\vec{k}} \psi_{\vec{k}} e^{i\vec{k}\cdot\vec{r}} \tag{2.8}$$

the free energy density is becomes

$$f = \sum_{\vec{k}} \left(\alpha + \frac{\hbar^2 k^2}{2m^*}\right) |\psi_{\vec{k}}|^2 \tag{2.9}$$

The thermodynamic average of $|\psi_k|^2$ over all possible values of the order parameter reads

$$< |\psi_k|^2 >= \frac{\int |\psi_k|^2 e^{-f/k_BT} D\psi}{\int e^{-f/k_BT} D\psi} = \frac{k_BT}{\alpha(1+k^2\xi^2)} \tag{2.10}$$

The spatial extent of phase coherence above T_C is limited by the fact that ψ is a sum of independent contributions $\psi_{\vec{k}}$ with different wavelengths. The extent of the coherence is described by the correlation function

$$\xi(\vec{R}) = \xi(r, r') \equiv \left\langle \psi^*(\vec{r})\psi(\vec{r'}) \right\rangle = \sum_{\vec{k}} |\psi_{\vec{k}}|^2 e^{i\vec{k}\cdot\vec{R}} \tag{2.11}$$

where $\vec{R} = \vec{r} - \vec{r'}$. Replacing the sum with the integral and considering that $\xi(\vec{R})$ because of the symmetry depends only on the magnitude of R, one has:

$$\xi(R) = \frac{m^* k_B T}{2\pi\hbar^2} \frac{e^{-R/\xi(T)}}{R} \tag{2.12}$$

by substituting $< |\psi|^2 >$ as given by Eq. 2.10.
For external field $H = 0$ the local value of ψ, in fluctuation regime, are correlated over a distance $\xi(T)$. In the presence of field the "radius" of the correlated fluctuations becomes smaller than ξ when H is larger than $\sim \Phi_0/\pi\xi^2 \equiv H_{C2}$ (that is the value of the field in which the sample is no more superconducting), with $\Phi_0 \equiv \frac{\pi\hbar c}{e}$ (see Ref. [2]).

Time dependence of fluctuations

The deviation from equilibrium is given from the general equation of non-equilibrium statistical mechanics:

$$\frac{\partial\psi}{\partial t} = -\frac{1}{\gamma}\frac{\delta f}{\delta\psi^*} \tag{2.13}$$

where γ is the non-critical kinetic coefficient. This time differential equation for ψ (for $T > T_C$), if the electromagnetic potentials and the non linear term in ψ are neglected, can be rewritten in the form

$$-\gamma\hbar\frac{\partial\psi}{\partial t} = \alpha\psi - \frac{\hbar^2}{2m^*}\nabla^2\psi \tag{2.14}$$

For uniform mode, k=0, from Eq.2.10, it is found that the order parameter relaxes exponentially with the Ginzburg-Landau relaxation time:

$$\tau_{GL} = \frac{\hbar\gamma}{\alpha} \propto \varepsilon^{-1} \tag{2.15}$$

This time corresponds to the Cooper pair life time and it is determined by its decay into two free electrons.[4] The superconducting ψ function relaxes exponentially toward its equilibrium value (above T_C this value is zero). At the transition temperature the Cooper pairs start to condensate and $\tau_{GL} = \infty$, as it can be seen from Eq. 2.15. The higher-energy modes, with $k > 0$, decay more rapidly, with relaxation rate

$$\tau_k = \frac{\tau_{GL}}{1 + k^2\xi^2} \tag{2.16}$$

and

$$\left\langle |\psi_{\vec{k}}|^2 \right\rangle = \frac{1}{2\pi} \int_{-\infty}^{\infty} \left\langle |\psi_{\vec{k},\omega}|^2 \right\rangle d\omega \tag{2.17}$$

where $\left\langle |\psi_{\vec{k},\omega}|^2 \right\rangle$ is the power spectrum of $\psi_{\vec{k}}$ in frequency space.
These equations imply that any non-zero value of exponential decays in a time τ_k. The non-zero thermal average of $|\psi_k|^2$ is the one expressed by Eq.2.10. In fact, the exponential decay is compensated by the interaction force between the superconducting electrons and the rest of the thermal bath.
The collective time-dependent correlation function is

$$\left\langle \psi^*_{\vec{k}}(0)\psi_{\vec{k}}(t) \right\rangle = \left\langle |\psi_{\vec{k}}|^2 \right\rangle e^{\frac{-t}{\tau_k}} \tag{2.18}$$

2.1.2 Lawrence-Doniach model and the anisotropic Ginzburg-Landau free energy functional.

The high temperature superconductors (HT$_C$SC) are strongly anisotropic in several properties, owing to their layered structure. Consequently the value of characteristic quantities such as penetration depth, coherence length, critical fields, etc., depend from the magnetic field direction. In anisotropic systems two approaches are

---

[4] The microscopic theory gives: $\tau_{GL} = \frac{\pi\hbar}{8k_B(T-T_C)}$ (see Ref. [1] and references therein).

possible, in principle. For moderate anisotropy the system is usually well described in terms of a continuous anisotropic Ginzburg-Landau theory. In the limiting case of strong anisotropy the two-dimensional (2D) Lawrence-Doniach (LD) model is used and the superconductor is considered as a stack of Josephson junctions, where the Cooper pairs tunnel between the insulating zones and weakly couple the planes.

In the anisotropic GL theory the Eqs. given at §2.1.1 are still valid, provided that the characteristic lengths are defined as follows: $\xi_i = \xi/\sqrt{M_i}$, $\lambda_i = \lambda/\sqrt{M_i}$, with $\lambda = (\lambda_a\lambda_b\lambda_c)^{1/3}$ and $\xi = (\xi_a\xi_b\xi_c)^{1/3}$. The normalized effective mass, M_i, is a tensor and the diagonal elements are so that $M_aM_bM_c = 1$.

ξ_c can be used to define the discreteness of the system, being $\xi_c < \xi_a < \xi_b << \lambda_b < \lambda_a << \lambda_c$. For $\xi_c > s$ (with s inter layer spacing) a continuous system can be considered and the anisotropic GL can be applied, while for $\xi_c < s$ the layered structure is relevant and the Lawrence-Doniach model must be used. On other hand in the GL theory the coherence length depends on temperature and diverges at T_C (see Eq. 2.5) as $\varepsilon^{-\frac{1}{2}}$. Consequently near T_C the continuous GL anisotropic model is anyway appropriate. A crossover 2D-3D can be defined by the condition $\xi_c = s$.

The Lawrence-Doniach (LD) functional[34, 35, 36, 37, 38] is a generalization of the GL theory in which to n-th layer superconductor is associated a 2D order parameter written as

$$\psi_n(\vec{r}) = |\psi_n(\vec{r})|\, e^{i\vartheta_n(\vec{r})} \tag{2.19}$$

where n is the plane label and $\vec{r}$ the in-plane vector position.

In a magnetic field perpendicular to the plane, choosing the gauge $A_z = 0, \vec{A}_{\shortparallel} = \frac{1}{2}\vec{H}\wedge\vec{r}$, the LD functional can be written[2, 1, 33, 39]:

$$\mathcal{F}_{LD}[\psi] = \sum_n \int d^2r \left(\alpha\,|\psi_n|^2 + \frac{\beta}{2}\,|\psi_n|^4 + \right.$$
$$\left. \frac{\hbar^2}{4m}\left|\left(\vec{\nabla}_{\shortparallel} - \frac{2ie}{c\hbar}\vec{A}_{\shortparallel}\right)\psi_n\right|^2 + \mathcal{J}\,|\psi_{n+1} - \psi_n|^2\right), \tag{2.20}$$

where the sum runs over the layers and the integral is over the area of each layer, $\alpha \equiv \alpha_0\varepsilon$ and the phenomenological constant $\mathcal{J}$ is proportional to the Josephson coupling between adjacent planes.

In fact, in the assumption that all $|\psi_n|$ are equal, the last term of Eq. 2.20 becomes $\mathcal{J}|\psi_n|^2[1-\cos(\vartheta_n-\vartheta_{n-1})]$, evidencing the equivalence of this term to a Josephson coupling energy between adjacent planes. In the vicinity of T_c the LD functional is reduced to the GL one, with the effective mass $M=\frac{\hbar^2}{(4\mathcal{J}s^2)}$ along the c-direction. In the GL gaussian region the fourth order term in Eq. 2.20 is omitted and the standard procedure[2, 4, 40] to derive the fluctuation part of the free energy yields

$$F(\varepsilon,H)-F(\varepsilon,0)=-\frac{Vk_BT}{2\pi s\xi_{ab}^2}\mathcal{H}\int_{-\pi}^{\pi}dz\sum_{n=0}\int_{-1/2}^{1/2}dx$$
$$\left[\ln\frac{(2n+1+2x)\mathcal{H}+\frac{\mathcal{L}}{2}(1-\cos z)+\varepsilon}{(2n+1)\mathcal{H}+\frac{\mathcal{L}}{2}(1-\cos z)+\varepsilon}\right]. \qquad (2.21)$$

where the c-axis is along the z direction, $\mathcal{L}=\frac{4\xi_c^2(0)}{s^2}$ is the dimensionless anisotropic parameter and $\mathcal{H}=\frac{H}{H_{c2}(0)}$.

2.1.3 Fluctuating diamagnetism and field dependence

The fluctuating magnetization M_{fl}[5] can be obtained by numerical derivation of Eq. 2.21 with respect to the field[1, 36, 4]. In particular in the limit of weak magnetic field the susceptibility can be obtained in the form

$$\chi_{dia}^{FS}=-\frac{\partial^2F}{\partial H^2}=-\frac{e^2}{3c^2}\frac{1}{s}\frac{k_BT_C}{\pi\hbar^2}\xi_0^2\varepsilon^{-1} \qquad (2.22)$$

Thus a negative divergent behavior of χ_{dia} for $T\longrightarrow T_C^+$ and fluctuating magnetization M_{fl} linear in the field H is expected. Actually Eq. 2.22 has only a limited validity, since even a small field can affect T_C and the SF in a relevant way. An early correction to Eq.2.22, within the GL limits (see Ref.s [1, 4] and references therein), yields

$$M_{fl}\propto\sqrt{H}\mathrm{g}(\varsigma)T \qquad (2.23)$$

---

[5] The relevance of the field dependence of $M_{fl}(H,T)$ for the study of FD has been also recently discussed in the framework of a Gaussian GL approach for non-isotropic systems in Ref. [41].

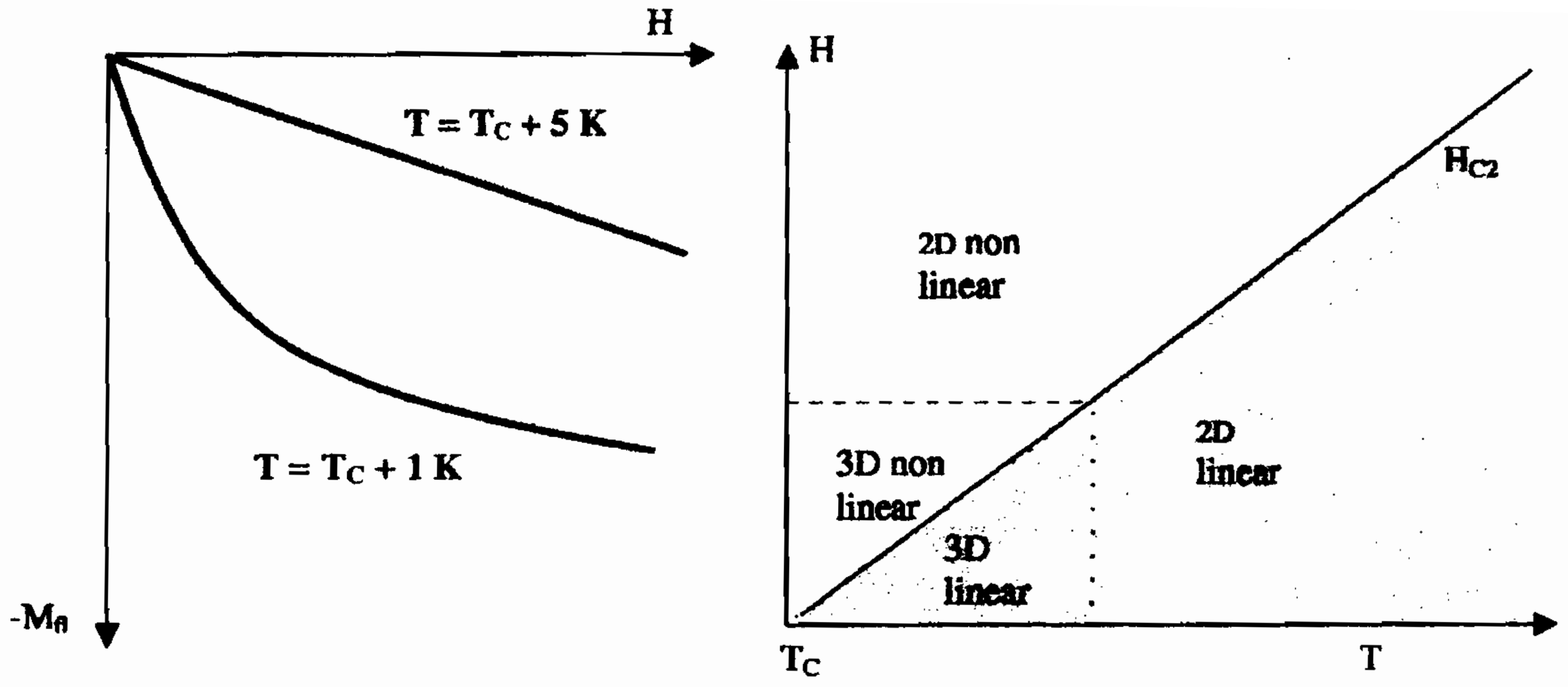

Figure 2.2: Illustrative behavior of typical magnetization curves and the phase diagram showing the dimensional crossover of the SF, as obtained in framework of GL theory and Gaussian approximation (see Refs. quoted in the text).

where g is a function of the variable $\varsigma = \frac{1}{2}\frac{T-T_C(0)}{T_C(0)-T_C(H)}$ such that the Eq. 2.23 implies for $T = T_C(H)$ $M_{fl} \propto \sqrt{H}$, and a divergence of M_{fl} for $T \rightarrow T_C(H)$ of the form $[T - T_{C2}(H)]^{1/2}$ (with $T_{C2}(H) = T_C(H)$ for second-type SC, where the transition is second order).
In Fig. 2.2 the typical magnetization curves and the field crossover[36] from 2D to 3D linear ($M \propto H$) and non linear ($M \propto \sqrt{H}$) regimes , as obtained in the framework of the gaussian approximation of the GL theory, are qualitatively reported.

In the GL theory, as it has been outlined above, several approximations[42] are made:

- the *slow-variation approximation* that requires that ψ varies slowly on the scale of $\xi(0)$. Consequently the theory is valid only for long wavelength fluctuations. This is what allows one to apply to the *Gaussian approximation*;
- the *static approximation* that restricts the validity to GL theory to those fluctuation modes which are long-lived;
- the *non-local electrodynamic corrections are not included.*

These approximations generally lead to theoretical conclusions in rather good agreement with the experimental observation in HT$_C$SC

(as it will be well discussed later on), but do not correctly predict the experimental behavior observed for BCS superconductors, where the limit of evanescent field is abandoned.
The experimental study of magnetization curves as function of temperature for different value of field in conventional BCS superconductors show that on increasing the field the magnetization first goes as $\sqrt{H}$, but around ten Gauss an upturn is observed: M_{fl} is progressively reduced and it is practically quenched for $H \approx H_{C2} \cdot 10^{-2}$ (see Ref.[2], Chapter 8).
The direct observation of magnetization curves in BCS superconductors is not easy because the FD occurs to an extent smaller that in HT_CSC. Recently the direct measurement of magnetization curves has been performed in MgB$_2$ (see Appendix A), essentially a BCS superconductor with $T_C \simeq 39$ K. Furthermore it has been demonstrated that MgB$_2$ is characterized by an anisotropic spectrum of fluctuations, similar to cuprates[43], thus enhancing the FD. The value of the upturn field H$_{\rm up}$ in the magnetization curves can be considered inversely proportional to the coherence length [2, 4]. This explains why in optimally doped high-temperature superconductors, where $\xi(0$ is very small, the Ginzburg-Landau (GL) picture, in general, works pretty well as we shall see in §2.2 for optimally doped YBCO.
It is possible to derive the main aspects of the field dependence of fluctuating diamagnetism for BCS superconductors by means of a simple model. One can think that the fluctuations cause the generation of superconducting "droplets" having size of the order of $\xi(T)$. Then the free energy functional ($F_{LG}[\psi]$), can be calculated in an exact way, for all values of temperature T (including the critical region) and field H, ($H < H_{C2}$), in the assumption that for these droplets one can be rely on the *zero-dimensional approximation*, valid rigorously only for diameter of the grains $d << \xi(T)$ (see Appendix A). Then the expression of magnetization can be written in the form

$$M_{fl}^{0D}(\varepsilon, H) = -\frac{\partial F_0(\varepsilon, H)}{\partial H} = \\ = -\frac{k_B T \frac{2}{5}\frac{\pi^2\xi_0^2}{\Phi_0^2} d^2 H}{(\varepsilon + \frac{\pi^2\xi_0^2}{5\Phi_0^2} H^2 d^2)} \tag{2.24}$$

Since the droplets that yield the most effective diamagnetic screening, have $d = \xi(t)$ from Eq. 2.24 one obtains

$$M_{fl}^{0D} = -k_B T \frac{\frac{2\pi^2\xi_0^4}{5\Phi_0^2\varepsilon}}{(\varepsilon + \frac{\pi^2\xi_0^4 H^2}{5\Phi_0^2\varepsilon})} H. \tag{2.25}$$

From this equation the field at which the magnetization has a minimum can be estimated:

$$H_{up} = \frac{\sqrt{5}\Phi_0\varepsilon}{\pi\xi_0^2} \tag{2.26}$$

and correspondently the value of magnetization at the upturn is

$$M_{up} = -\frac{k_B T\pi}{\sqrt{5}} \frac{\xi_0}{\Phi_0} \varepsilon^{-1}. \tag{2.27}$$

This simple model reproduces qualitatively the magnetization curves in BCS systems (see Fig. A.3 in Appendix A).
In $HT_C SC$ compounds, the coherence length is so short that the field-induced quenching of fluctuating magnetization has not yet been observed as already mentioned. Indicatively for $\xi(0) \simeq 10$ Å and ε in the range $10^{-1} \div 10^{-2}$, H_{up}, from Eq. 2.26, is expected in the range of 10 Tesla. It must be stressed since now that the magnetization curves observed for non-optimally doped YBCO (that will be shown in Fig.s 2.6, 2.7), show an upturn with the field cannot be ascribed to the breakdown of the GL approach of the type commonly observed in BCS superconductors. Furthermore it must be noted that the the upturn on increasing of field, observed in BCS, do not depend on the magnetic history of the sample (see discussion at §2.2).

2.1.4 Main results from scaling arguments

The exponents of the power laws, as the ones characterizing the behavior of the diamagnetic magnetization on approaching T_C, are called *critical exponents*. As it is known a physical system near a transition is characterized by fluctuating quantities, with a correlation function diverging at transition point. A function of a single variable that describe the system can be written as a sum of a singular part and of a regular part:

$$f(X) = f_{sing}(X) + f_{reg}(X). \tag{2.28}$$

By calling X_C the critical value of X and $\Delta X = X - X_C$, the singular part is

$$f_{sing}(X) = (\Delta X)^{\eta} \tilde{f}(X) = (\Delta X)^{\eta}[f_0 + f_1 \Delta X + f_2 \Delta X^2 + ...] \tag{2.29}$$

with $\eta \equiv \lim_{\Delta X \to 0} \frac{log f_{sing}(X)}{log \Delta X}$ *critical exponent.* η is not an integer number and is different from zero.

The scaling hypothesis asserts[44] that a variation of a scaling factor is equivalent to a change of unit length [*hypothesis of Widom generalized homogeneity*], namely

$$f_{sing}(lX) = l^{-D} f_{sing}(X) \tag{2.30}$$

where D is a dimensional index. As consequence the rescaled magnetization curves as a function of reduced temperature must acquire some universal behaviors.

In particular, collapse onto a common function is obtained when $\frac{M_{fl}}{\sqrt{HT}}$ is reported as a function of $\frac{\varepsilon}{H^{\frac{1}{2\nu}}}$, with ν the critical exponent for the coherence length. For example, in YBCO the experimental value of ν is 0.7 [45] (using the gaussian approximation discussed at § 2.1.3 one would have $\nu = 0.5$). For superconductors, the scaling arguments[48, 46, 47, 49], are valid also in the critical region and allow one to include the $|\psi|^4$ term in the functional of Eq. 2.20. We remark that the dimensionality class has to be chosen and obviously no 2D-3D crossover can be studied within scaling observation.

In the scaling approach[48], for superconductors, the singular part of free energy density is expanded in series of ξ^{-D} and in terms of an universal function involving only the number of fluxoid per coherence area, equivalent to the ratio of the magnetic length $(\Phi_0/H)^{1/2}$ and the coherence length: $f = -k_B T \xi^{-D} \Lambda(X)$, $\Lambda(X)$ being the unknown, dimensionless function of the variable $X = (H\xi^2/\Phi_0)$. Then[45, 46, 47]

$$M_{fl} = -\frac{\partial f}{\partial H} = \frac{k_B T}{\Phi_0^{D/2}} H^{\frac{D}{2}-1} m_D(X) \tag{2.31}$$

with $m_D(X) = X^{1-\frac{D}{2}}\frac{d\Lambda}{dx}$.
For 3D isotropic systems $M_{fl} \propto \sqrt{H}$ for $T \approx T_C$ and

$$\frac{M_{fl}(T_C)}{\sqrt{H}} = \frac{k_B T_C}{\Phi_0^{3/2}} m_3(\infty) \tag{2.32}$$

with $m_3(\infty) = -0.32$ as estimated in the Gaussian approximation. The isochamp curves M_{fl} vs T should then cross at T_C when the magnetization is scaled by $\sqrt{H}$.
For 3D anisotropic systems Eq.s 2.31 and 2.32 can still be used in terms of $M_{fl}^{\perp}/\sqrt{H_{\perp}}$, with $m_3(\infty)$ corrected to $m_3^{an}(\infty) = m_3(\infty)\gamma$, $\gamma = (\xi_{\parallel}/\xi_{\perp})$ being the anisotropy parameter.
The above conclusions in general are in good agreement with the experimental results in YBCO optimally doped (see next Section, Fig. 2.4).
In 2D systems the field dependence in Eq. 2.31 erases and the curves M_{fl} vs T for different fields cross at $T_C(0)$ (of coarse a crossover to a 3D regime must occur close to T_C; however the temperature range where the fluctuations take 3D character is usually very narrow and practically unobservable[47]). Generally these 2D scaling conditions are well verified also in YBCO124 even though in a particular range of field, as shown in Ref. [50].

2.2 Fluctuating diamagnetism in optimally-, under- and over-doped YBCO compounds.

The measurements as a function of the field ($0 \div 7$ T) and temperature ($2 \div 300$ K) have been carried out by means of a Quantum Design MPMS-XL7 SQUID magnetometer, allowing one to achieve temperature resolution up to 1 mK and measuring a lowest magnetic moment around 10^{-7} emu. Magnetization measurements, with $\vec{H} \parallel \vec{c}$, at constant field H as a function of temperature, and isothermal magnetization curves M vs H have been performed.
The samples are oriented powders of optimally doped $Y_1Ba_2Cu_3O_7$, underdoped chain disordered $Y_1Ba_2Cu_3O_{6.65}$ and samples of $Y_{1-x}Ca_xBa_2Cu_3O_y$, with x ranging from 0 to 0.2, for $y \approx 6.1$ (underdoped, with almost oxygen empty

chains) and $y \approx 6.97$ (overdoped, with oxygen full chains).
In general two contributions to the magnetization M are present:

$$M = M_P + M_{fl} \simeq \chi_P H + M_{fl} \tag{2.33}$$

The positive term $M_P = \chi_P H$ is a Pauli-like, paramagnetic contribution, with χ_p that does not depend from field. M_P is almost T-independent or only slightly increasing with decreasing temperature in the range ΔT from 200 K down to about 100 K. M_{fl} is a negative diamagnetic contribution that arises on approaching T_C. The M_{fl} term, that it will be reported in the Figures, has been extracted for M vs T curves by subtracting from the raw data the value obtained by extrapolating, for $T \to T_C^+$, the curve M_P vs. T in ΔT, where M_{fl} is practically zero. Thus the possible slight temperature dependence of M_P around T_C was neglected in comparison to the much stronger diamagnetic term.

2.2.1 Magnetization curves in optimally doped YBCO.

In optimally doped YBCO (oriented powders), with $T_C(0) = 92K$, the isothermal (Fig. 2.3) and the isochamp (Fig. 2.4) magnetization curves have been measured for $\vec{H} \parallel \vec{c}$. The magnetization curves M_{fl}, shown in Fig. 2.3, follow the trend expected in the framework of the GL scenario.
In fact M_{fl} turns out proportional to external magnetic field for T rather far from T_C (i.e. $\varepsilon \equiv \frac{T-T_C}{T_C} = 0.090$) and proportional to $\sqrt{H}$ for T near T_C ($\varepsilon = 0.007$). Typical findings in optimally doped YBCO (both single crystals and oriented powders) basically agree with the behavior recalled above (Eq. 2.32), with $m_3^{an}(\infty) = -2,2$ and therefore anisotropy parameter $\gamma \simeq 7$.
In Fig. 2.4 the isochamp magnetization measurements are reported. The scaling predictions for 3D anisotropic systems are well obeyed: the isochamp lines crossing at $T_C(0) \cong 92K$ when M is scaled by $\sqrt{H}$. Thus the experimental results show that the anisotropic GL functional can be used to predict the magnetization curves and the $2D \to 3D$ crossover. Only close to T_C ($\varepsilon \leqslant 3 \cdot 10^{-2}$) and $H \leqslant 1$ Tesla appreciable discrepancies are observed, suggesting a crossover to a region of non-Gaussian SF.

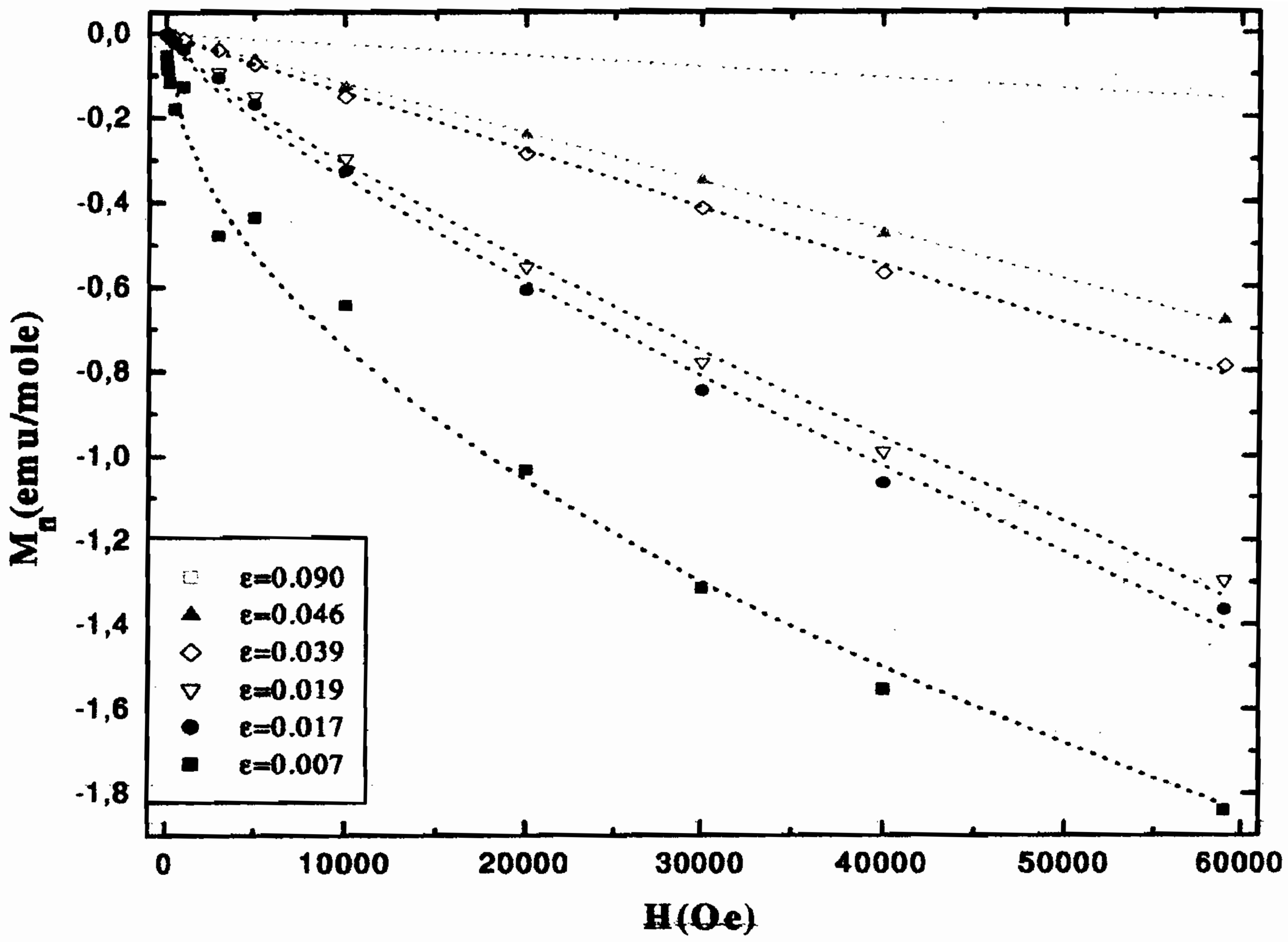

Figure 2.3: Isothermal magnetization curves for different temperatures in optimally doped YBCO. The dashed lines are guides for the eye, according to the linear and non linear regime (see text).

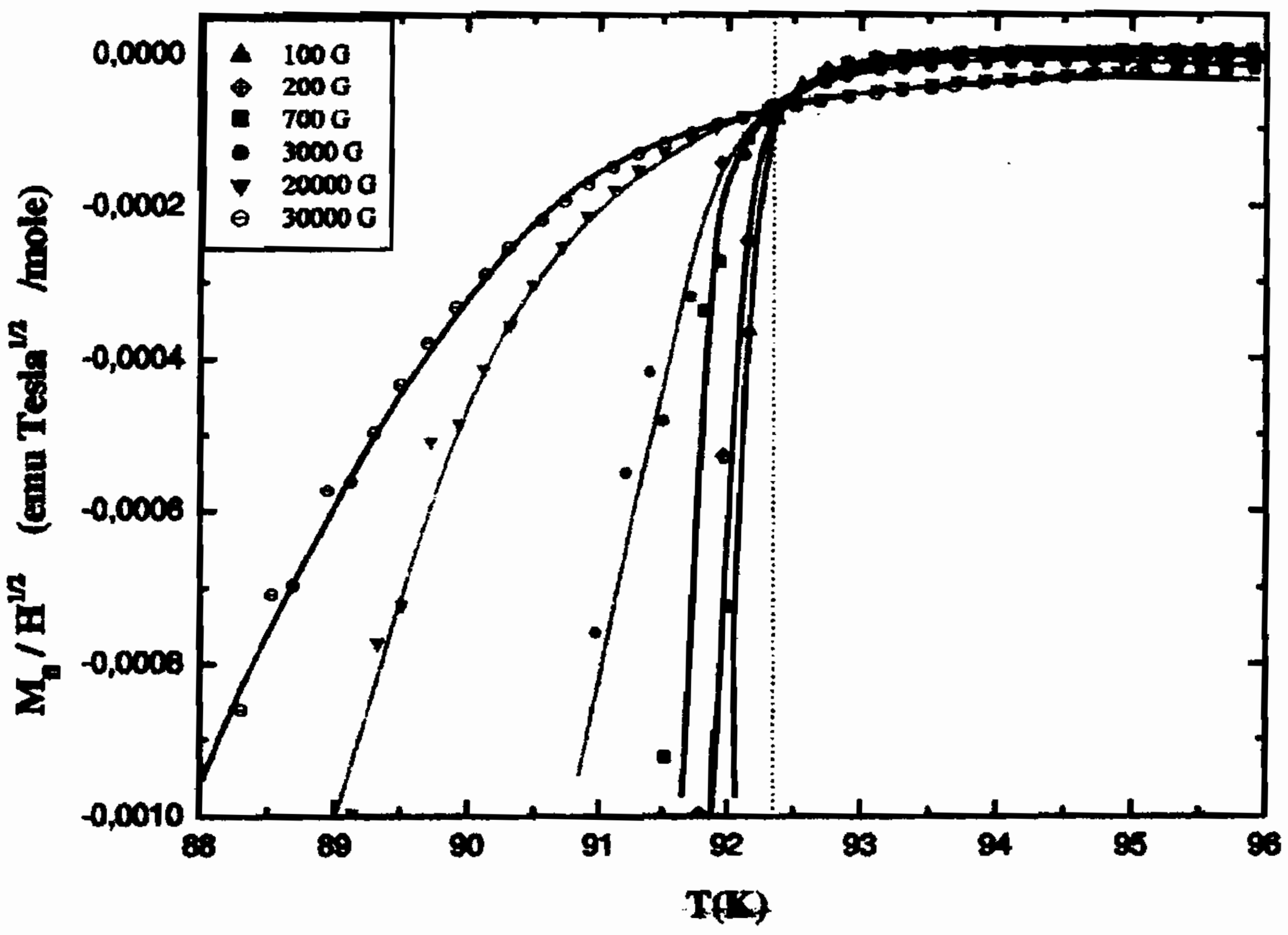

Figure 2.4: Fluctuating magnetization rescaled by $\sqrt{H}$ as a function of temperature for different magnetic field along the c-axis. The lines are guide for the eye.

These few experimental data for optimally doped YBCO123 are recalled here to show the "conventional" behavior of M_{fl} and χ_{dia} for HT$_C$SC, in contrast with the "anomalous" effects found in underdoped and overdoped YBCO[51, 52, 53, 54, 55, 56, 57, 58, 59], to be discussed later on.

2.2.2 Anomalous enhancement of the fluctuations and upturn in the magnetization curves for overdoped and underdoped compounds.

The experimental results of SQUID magnetization measurements in underdoped and overdoped YBCO samples are reported in Fig. 2.5, 2.6, 2.7.
In Fig. 2.5 a marked enhancement of the fluctuating magnetization with respect to optimally doped YBCO is observed. In contrast to optimally doped YBCO, the magnetization curves vs H, for underdoped and overdoped compounds, depart in a drastic way from the ones expected on the basis of GL anisotropic functional (Eq.s 2.22, 2.31). The M_{fl} curves vs T do not cross at any temperature and no collapse onto an universal function is found for $M_{fl}/\sqrt{H}$ or for M_{fl} as a function of $\varepsilon/H^{1/2\nu}$ (see §2.1.4 and §2.2.1).
In Fig. 2.6 the magnetization curves of YBCO$_7$ doped to about 10% in Ca, for two different values of temperatures, are reported in the range $0 \div 7$ T, to allow one to compare them with the analogous curves for optimally doped samples in Fig. 2.3.
In Fig. 2.7 the magnetization curves for differently doped YBCO samples are shown: overdoped samples with x $\simeq$ 0.1, y $\simeq$ 6.96 in part (a) and with x $\simeq$ 0.2, y $\simeq$ 6.98 in part (b); chain empty underdoped samples with x $\simeq$ 0.25, y $\simeq$ 6.1 in part (c) and chain disordered underdoped samples with x $\simeq$ 0, y $\simeq$ 6.65 in part (d).
$|-M_{fl}|$, even relatively far from T_C results linear in H for small fields ($H \lesssim 200$ G for overdoped and $H \lesssim 600$ G for chain empty underdoped), then shows an upturn upon increasing the field and afterwards decreases. In chain-disordered underdoped YBCO (part (d) of Fig. 2.7) the decrease of $|-M_{fl}|$ upon raising of the field is absent, but the magnetization curves however are not described by the GL model.

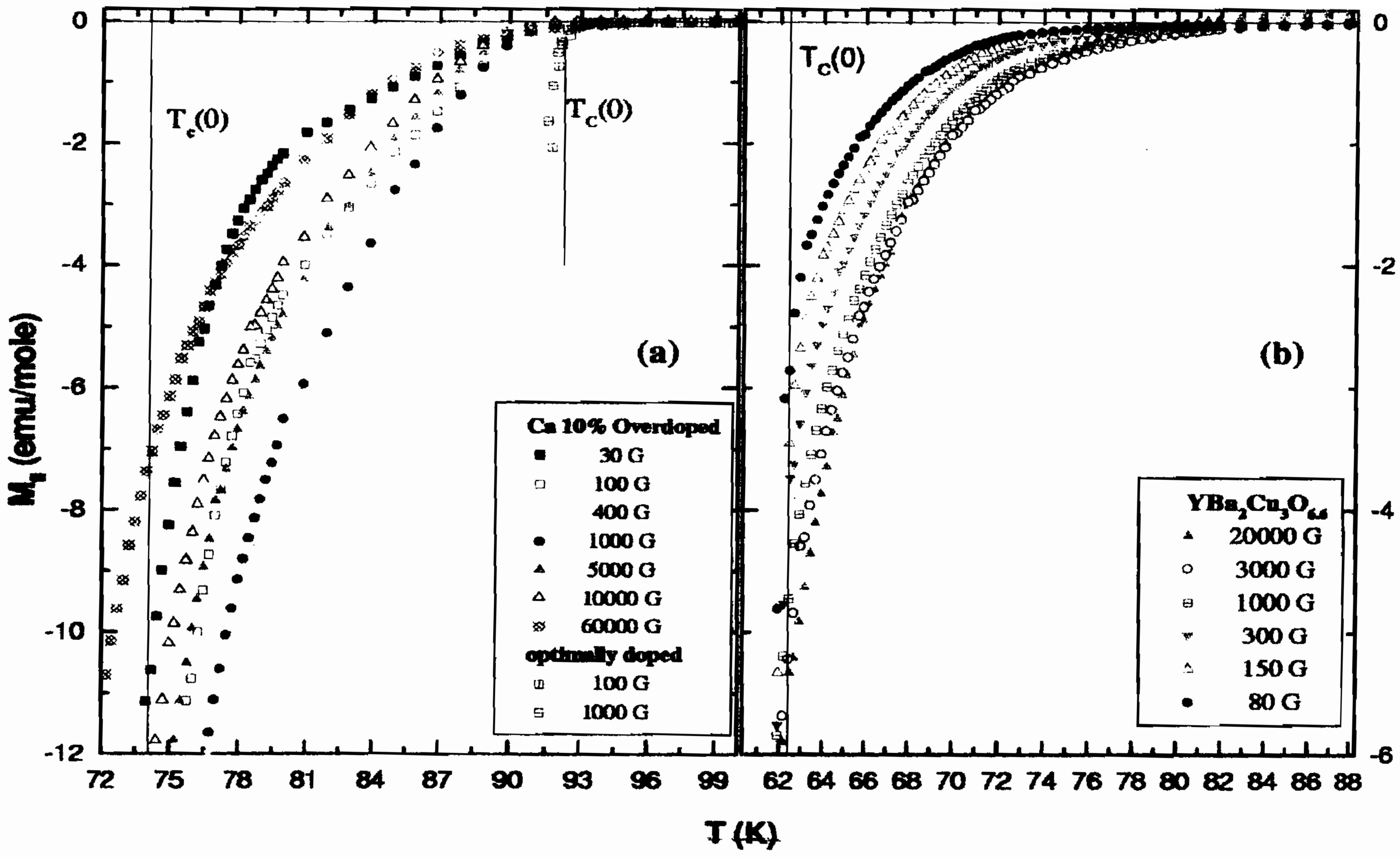

Figure 2.5: Constant field (**H** || **c**) magnetization vs. temperature in overdoped ($x = 0.1$ and $y = 6.96$) (a) and in underdoped ($x = 0$ and $y = 6.65$) (b) YBCO compounds. For comparison in the part a) of the figure the behavior of M_{fl} in optimally doped YBCO is shown.

These magnetization curves, as it has been mentioned in the previous Section, cannot be ascribed to the breakdown of GL framework. commonly observed in BCS superconductors, because in this case H_{up} should be ~ 10 T.

The anomalies presented in underdoped chain-disordered samples have been explained[60] by means a theory for fluctuations of the order parameter phase in a layered liquid of vortices. However it should be stressed that the theoretical description given in Ref. [60] cannot be used in its original form to explain the magnetization curves where the upturn is observed, as well as it cannot justify the history-dependent effects (to be described later on). We are now going to consider in detail the role of charge inhomogeneities in causing regions where the "local" T_C is different from the bulk one, thus inducing a particular type of anomalous diamagnetism.

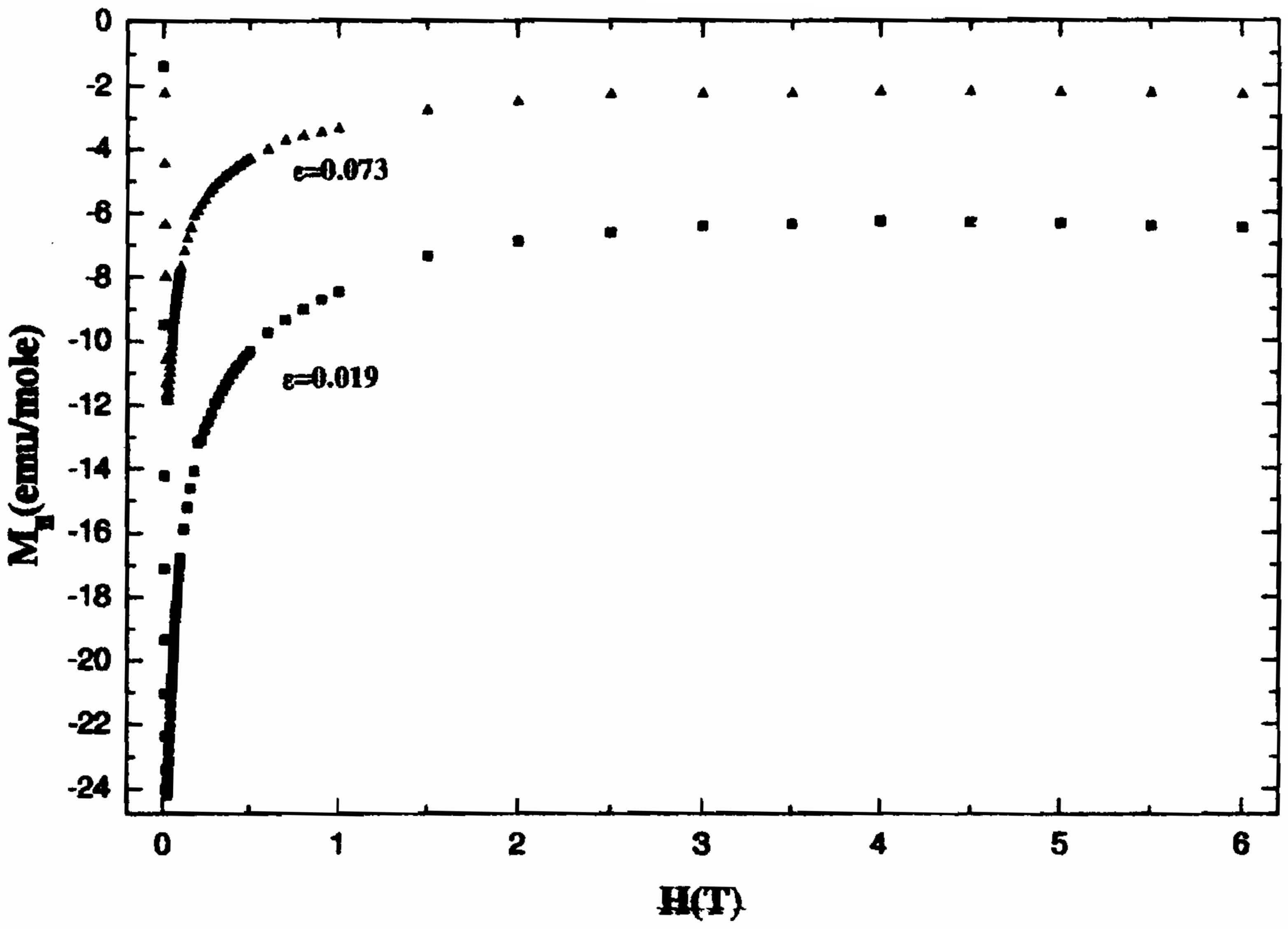

Figure 2.6: Magnetization curves M_{fl} vs. H (after ZFC) in overdoped YBCO:Ca (x=0.1, y=6.96). The anomalies are evident from the comparison between these curves and the ones in optimally doped YBCO (see Fig.2.3) for similar reduced temperature ε.

2.2.3 The picture of superconducting droplets above T_C.

From the volume susceptibility, about 5 K below T_C (see Fig. 2.5), one deduces that a few percents of the total material being superconductor above the resistive transition temperature, could actually justify the screening effects observed as FD. A test of this hypothesis is obtained from the search of magnetic-history dependent effects. It is known, in fact, that in YBCO the irreversibility temperature is not far from T_C and therefore if the anomalous FD has to be attributed to locally SC droplets then one should detect differences between zero field-cooled (ZFC) and field-cooled (FC) magnetization. In Fig.2.8 magnetization curves after zero field cooling and the correspondent values of M_{fl} obtained at the same temperature after cooling in the presence of a given magnetic field, are compared. Furthermore, relaxation effects have been observed. In Fig. 2.9 it is shown how the negative magnetization depends on time, displaying a progressive decrease from the ZFC value towards the

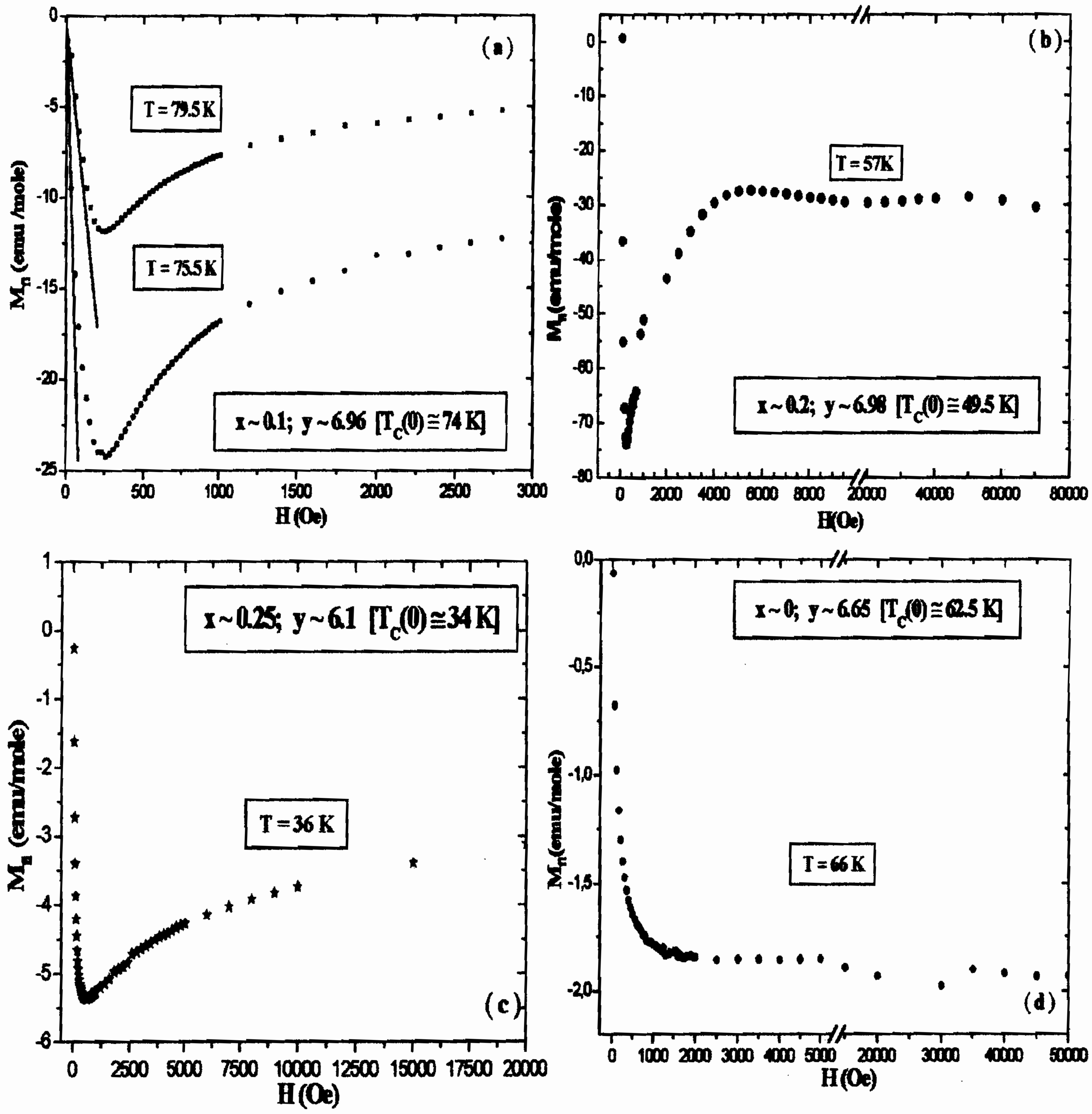

Figure 2.7: Isothermal diamagnetic magnetization vs. H, after zero-field cooling (ZFC) to a certain temperature above $T_C(0)$ for samples with different doping. The sample with y=6.65 and x=0 ($T_C(0) = 62.5K$) is a chain disordered underdoped YBCO. In the part (a) of the figure the solid lines correspond to the diamagnetic susceptibilities estimated in the limit of zero field.

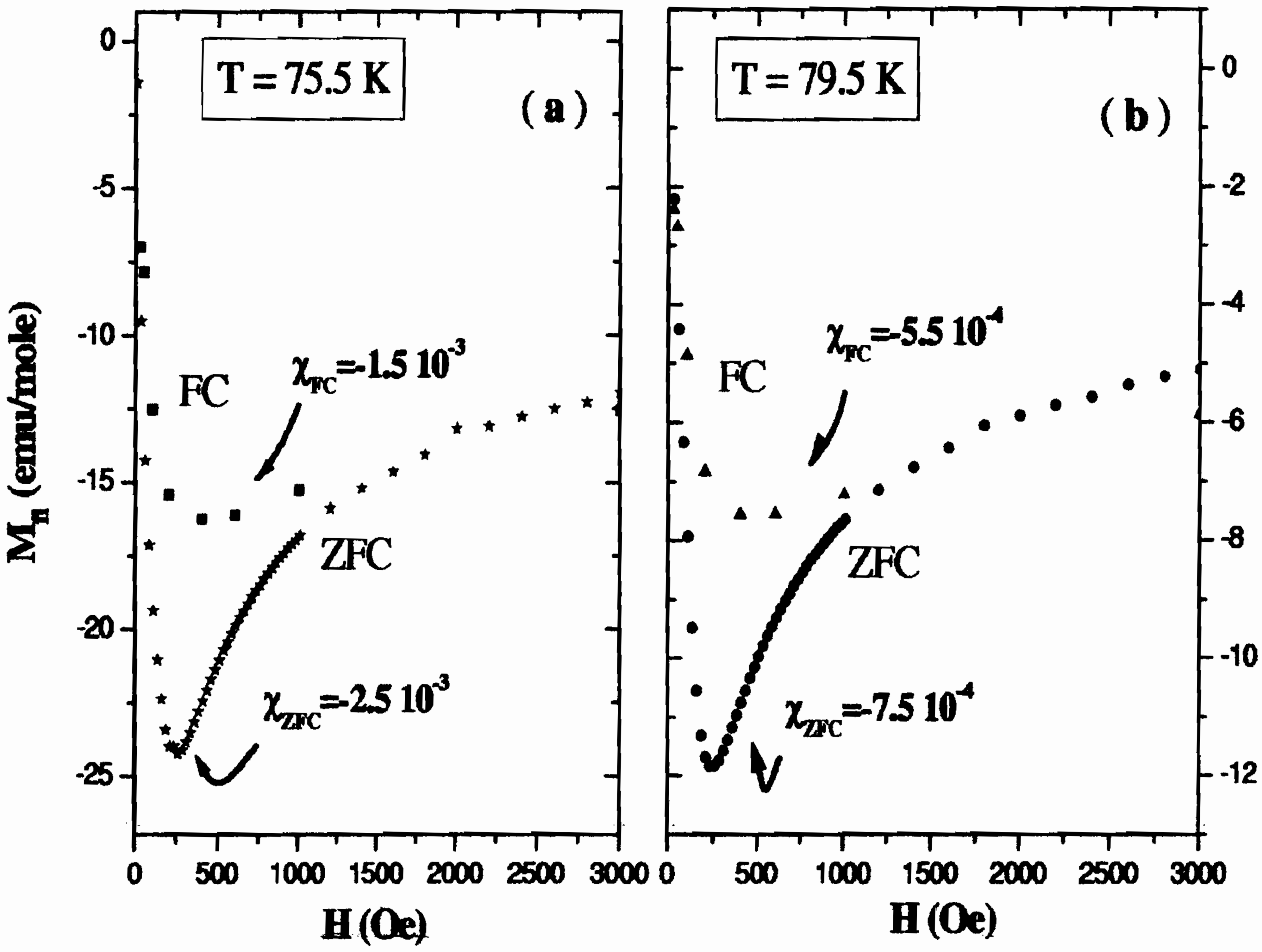

Figure 2.8: Magnetization curves in YBCO:Ca at x=0.1 and y=6.96 by cooling in zero field to a given temperature [a) $T = 75.5K$ and b) $T = 79.5$ K] above the resistive transition temperature and then applying the field (ZFC) and after the application of the field at room temperature, cooling at the same temperature and measuring the correspondent magnetization (FC). The volume susceptibilities in the limit H→ 0 is reported.

one measured in FC condition. The time constant for this relaxation process is close to the one measured in the critical state[61]. As seen in the inset of Fig. 2.9 the local irreversibility temperature of the droplets is above the bulk superconducting transition temperature.

It can be remarked that in underdoped chain-disordered YBCO (see part d) Fig. 2.7) no upturn is observed and the ZFC and FC

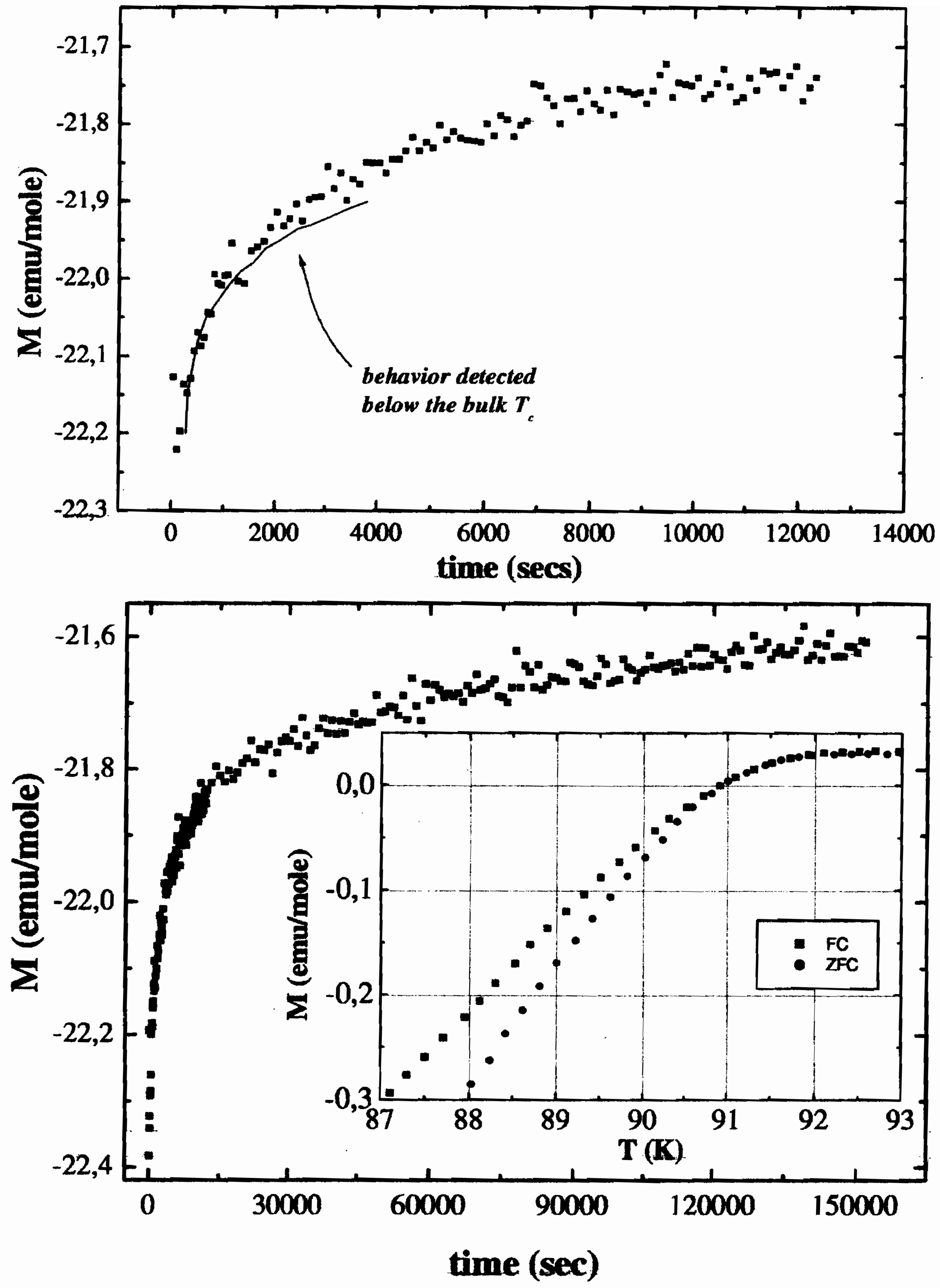

Figure 2.9: Relaxation of the raw magnetization after ZFC and then sudden application of a magnetic field of 260 G, in YBCO:Ca at x=0.1 and y=6.96, at $T = 75.5$ K a) short-term relaxation; b) long-term relaxation. From the comparison of the ZFC and FC magnetization in $H = 20$ G (see inset) an irreversibility temperature of the locally superconducting droplets at highest T_C can be estimated around 90 K. In part a) of the Figure the solid line is the sketchy behavior of the relaxation of the magnetization detected by Yeshurun *et al.* (Ref.[61]) in the critical state, in optimally doped YBCO.

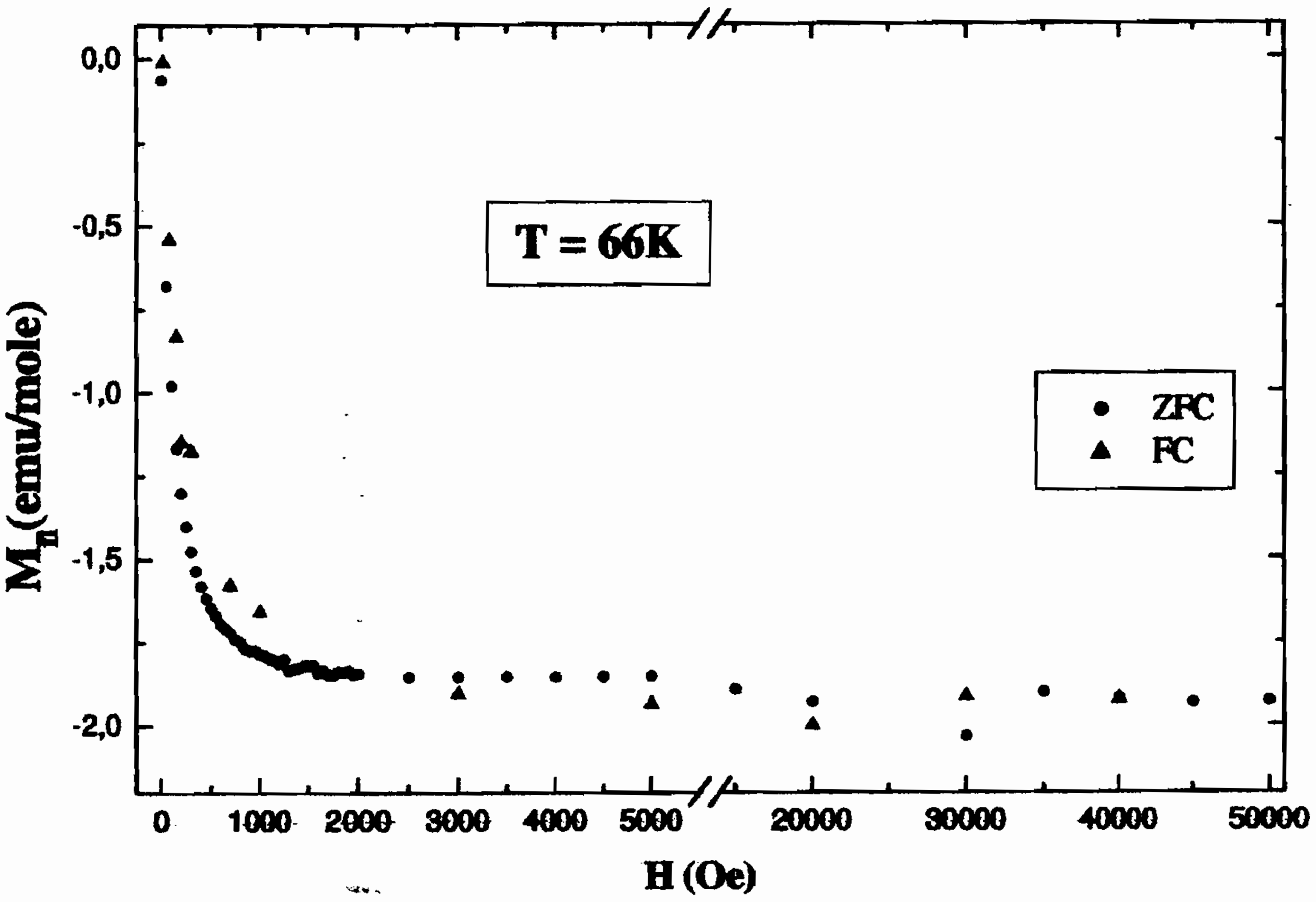

Figure 2.10: ZFC and FC magnetization curves at $T = 66$ K in chain disorder underdoped YBCO (x=0, y=6.65 and $T_C(0) = 62.5$ K)

magnetization curves almost coincide (Fig. 2.10). The explanation that will be supported from our theoretical picture is that the magnetization curves without hysteretic effects refer to superconducting droplets which are above the local irreversibility temperature.

One should observe that the ZFC magnetization curves in chain empty underdoped YBCO:Ca present un upturn for $H \sim 600$ G (see part c Fig.2.7). According to the data in Fig. 2.11 the irreversibility temperature is estimated ~ 54 K. The hysteretic effects can be evidenced by comparing the DC-ZFC magnetization (see part c of Fig. 2.7) with AC-FC susceptibility measurement (see Fig. 2.12). In Fig. 2.12 we report the AC susceptibility measurements vs DC field performed by cooling the sample in the presence of constant field (FC) and for different AC field. It must be noted that the field value at which $\chi = \frac{dM}{dH} = 0$ is $H_{up} \sim$ 1000 G, larger than the value of $\mathrm{H_{up}}$ estimated by ZFC-DC magnetization curve. Also for underdoped samples the shift of $\mathrm{H_{up}}$ for large field in FC curves is evidenced. Furthermore the χ value at small fields from ZFC

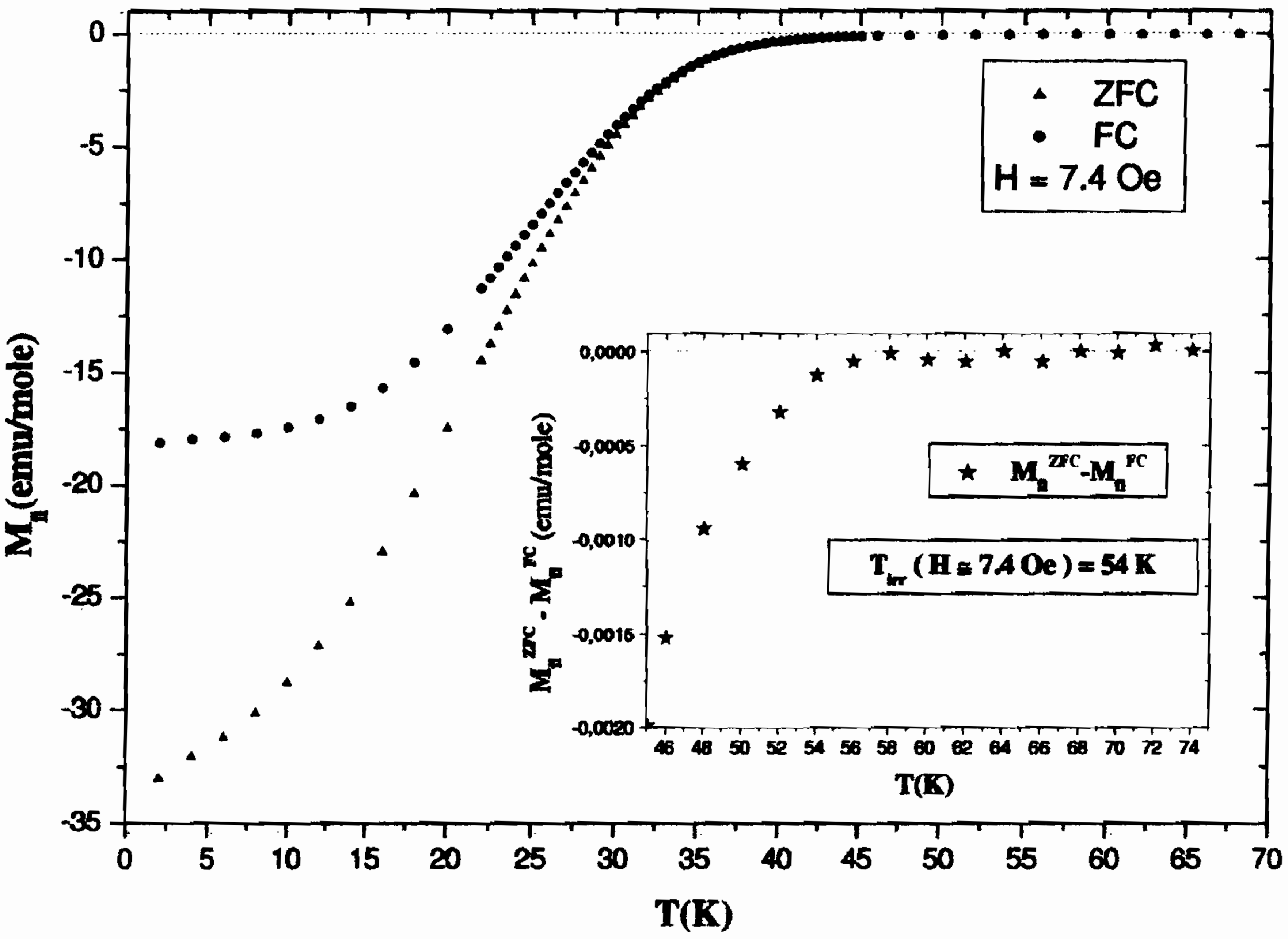

Figure 2.11: The isochamp (H = 7.4 Oe) magnetization curves ZFC and FC vs T in chain empty underdoped YBCO (x = 0.25, y = 6.65 and $T_C(0)$ = 62.5 K). As shown in the inset, the irreversibility temperature can be estimated around 54 K.

magnetization measurements is ($\chi_{vol} = \frac{M_{fl}^{vol}}{H} = 4 * 10^{-4}$) larger than the value of χ_{FC} from AC measurements, demonstrating the presence of irreversibility effects.

One could suspect that the presence of superconducting droplets results from trivial chemical inhomogeneities of the samples. As described in the first Chapter experimental checks like NMR spectra, XRD, EDS allow us to rule out this hypothesis. Furthermore, samples grown with different procedures and already used by other authors, have been also studied, showing the same behavior. It is believed that the charge inhomogeneities do not imply mean the presence of macroscopic parts of the samples at different oxygen and/or calcium content, but it has an intrinsic, character of the type evidenced in the several experiments (see Ref.s [62, 63, 64, 65]). Furthermore it should be remarked that the temperature dependence of the susceptibility above the bulk transition temperature is different from the one occurring in the superconducting state. In

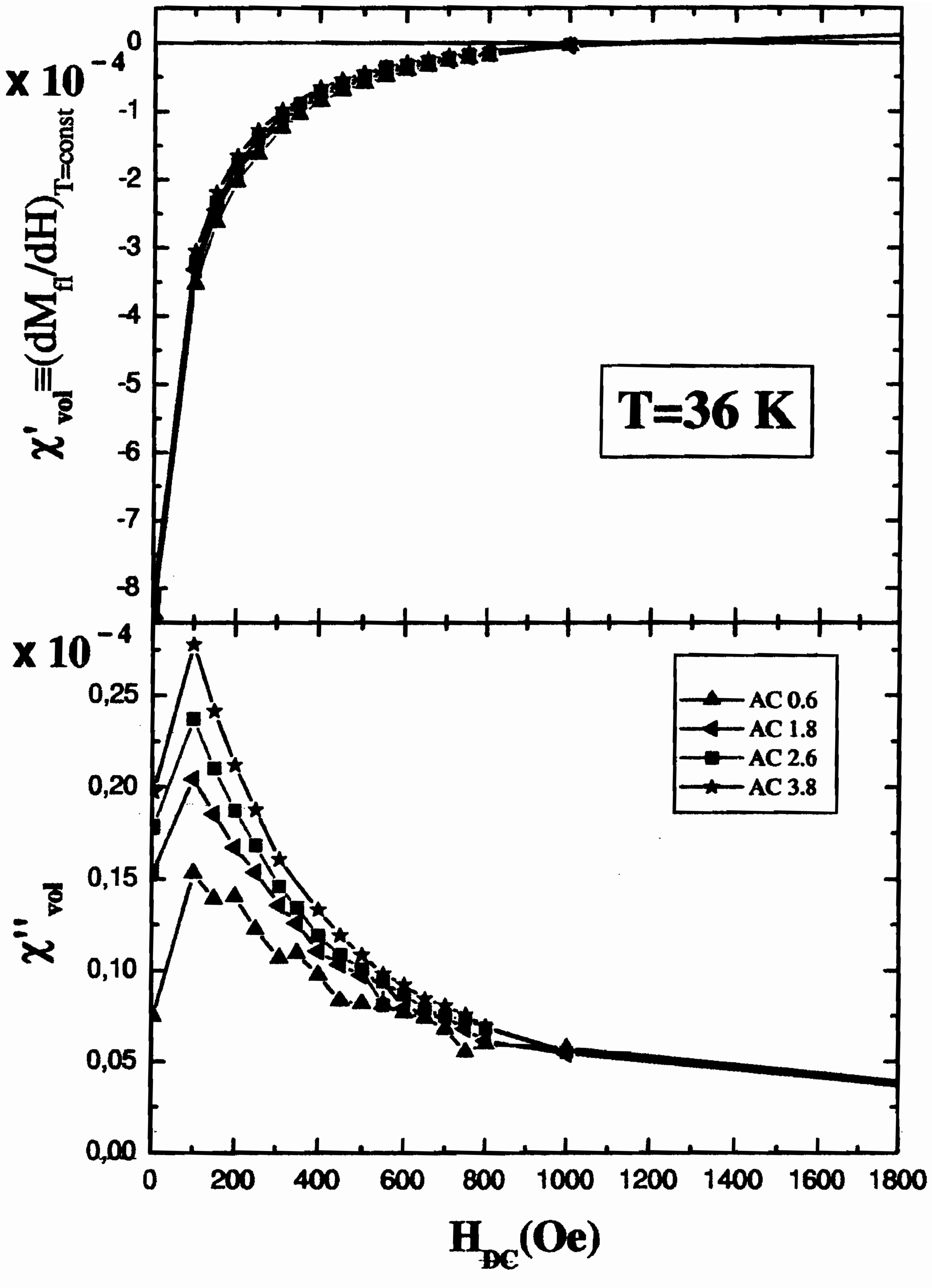

Figure 2.12: The AC susceptibility (from SQUID magnetometer). The figure shows that $\left(\chi' = \frac{dM_{fl}}{dH}\right)$ at $T = 36$ K tends to zero for a certain value of external field ($\sim$ 1000 Oe), corresponding to the upturn in M_{fl} vs. H. In the upper and lower parts of the figure the real and imaginary susceptibilities are reported respectively. The measurements were performed by changing DC field for different values of the amplitude of the AC field, H_{AC}, (reported in the box) and for frequency $\nu = 1$ Hz.

fact, as it can be seen in Fig. 2.13 the temperature dependence of the susceptibility is of the exponential form ($e^{\frac{E_0}{k_B T}}$) only for $T > T_C$.

It must be noted that evidences of the inhomogeneous structure of cuprates have been found by means of neutron and electron diffraction[66, 67, 64], as related to stripes and lattice effects or to local variation in the oxygen concentration, particularly near grain boundaries. Moreover direct evidence of inhomogeneous mag-

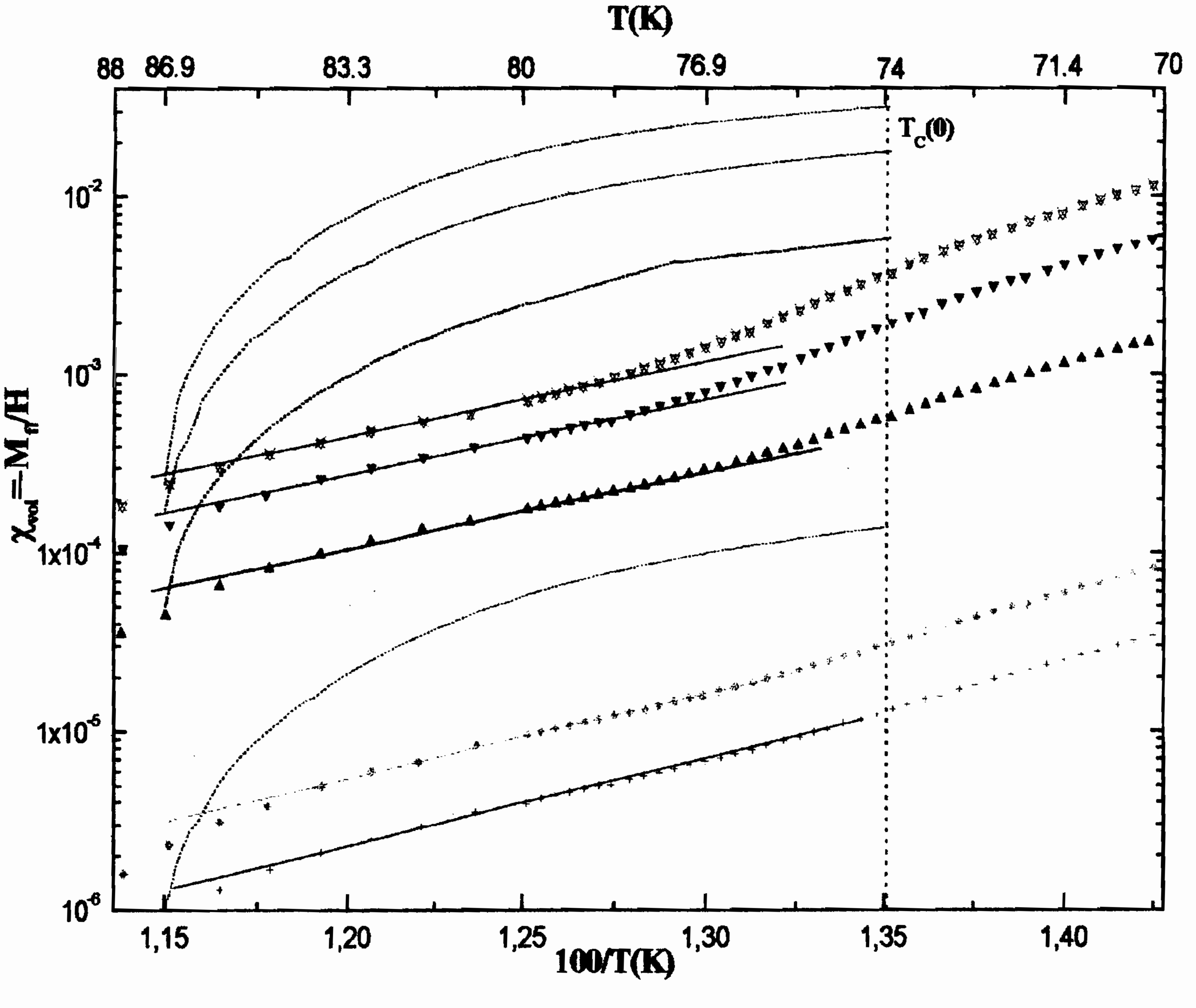

Figure 2.13: Susceptibility as a function of the inverse temperature showing the activated temperature behavior in the sample at y=6.96 and x=0.1. Analogous temperature dependence has been observed in underdoped YBCO compounds. The dashed lines are obtained by transferring above the superconducting temperature $T_C(0)$ the temperature behavior of the bulk susceptibility measured below T_C and by normalizing the data at $T \simeq 88K$

netic domains (few tens of μm in size) showing diamagnetic activity above T_C has been obtained by Iguchi *et al.*[62] by scanning SQUID microscopy, in underdoped LASCO.
Intrinsic inhomogeneities, with spatially dependent critical temperature have been considered as possible cause of pseudogap phenomena[68, 69]. A theory for high temperature superconductivity and pseudogap temperature dependence based on inhomogeneous charge distribution has been recently formulated[70]. In particular a distribution of local clusters, with spatial dependent charge density, $\rho(r)$, different from the average charge density, ρ_m, is considered to lead to the SC transition[70]. When the temperature is decreased, some clusters become superconducting, but they are surrounded by metallic and/or antiferromagnetic insulating domains and, consequently, the whole system is not a superconductor. The number of superconducting clusters increases as the temperature decreases, so that the superconducting regions grow and, eventually, at a temperature T_C, they percolate and can hold a macroscopic dissipationless current.
Ovchinnikov *et al.*[71] have considered the anomalous diamagnetism above T_C induced by non-uniform distribution of magnetic impurities, depressing T_C but leaving "islands" which become superconducting above the resistive transition temperature. As a consequence an anomalous large diamagnetic moment can be detected above T_C and in this way the strong diamagnetic susceptibility observed in overdoped Tl-based cuprates[63] could be explained.
It should be stressed, however, that in this description[71] the magnetization is linear in the field, since the condition of small field is implicitly assumed.

2.2.4 Phase fluctuations of the order parameter.

By taking into account the presence of mesoscopic charge inhomogeneities which cause locally, non percolating, superconducting regions with T_C^{loc} larger than the resistive transition temperature, we are going to outline a theory for the phase fluctuation of the local order parameter which accounts for the anomalous diamagnetism observed in overdoped and underdoped YBCO compounds, as well as for the hysteretic effects. All the details of this theory are given in Appendix B.

One can start by assuming a *frozen amplitude* and taking into account only *phase fluctuations* of the order parameter. In this scenario the unusual magnetization curves detected in underdoped chain disordered YBCO[52] (see part (d) of Fig. 2.7) can be rather well justified. In the original description by Sewer and Beck[60] the anisotropic Lawrence-Doniach functional is rewritten considering the coupling between the parameter order phase and the vector potential describing a homogeneous magnetic field perpendicular to the lattice planes. As a consequence of the thermal excitations there are the phase-field singularities: vortices and antivortices in 2D (*pancakes*) and vortex loops in 3D. The presence of an external magnetic field induces vortex lines extending through the whole sample (see Fig. 2.14). In this model the diamagnetic susceptibility is connected only to the positional correlation function of the vortex line element. For small fields the temperature dependence of the susceptibility is controlled by the vortex loops density n_v: $\chi \propto \frac{1}{n_v}$. The experimental trend of susceptibility as a function of temperature is

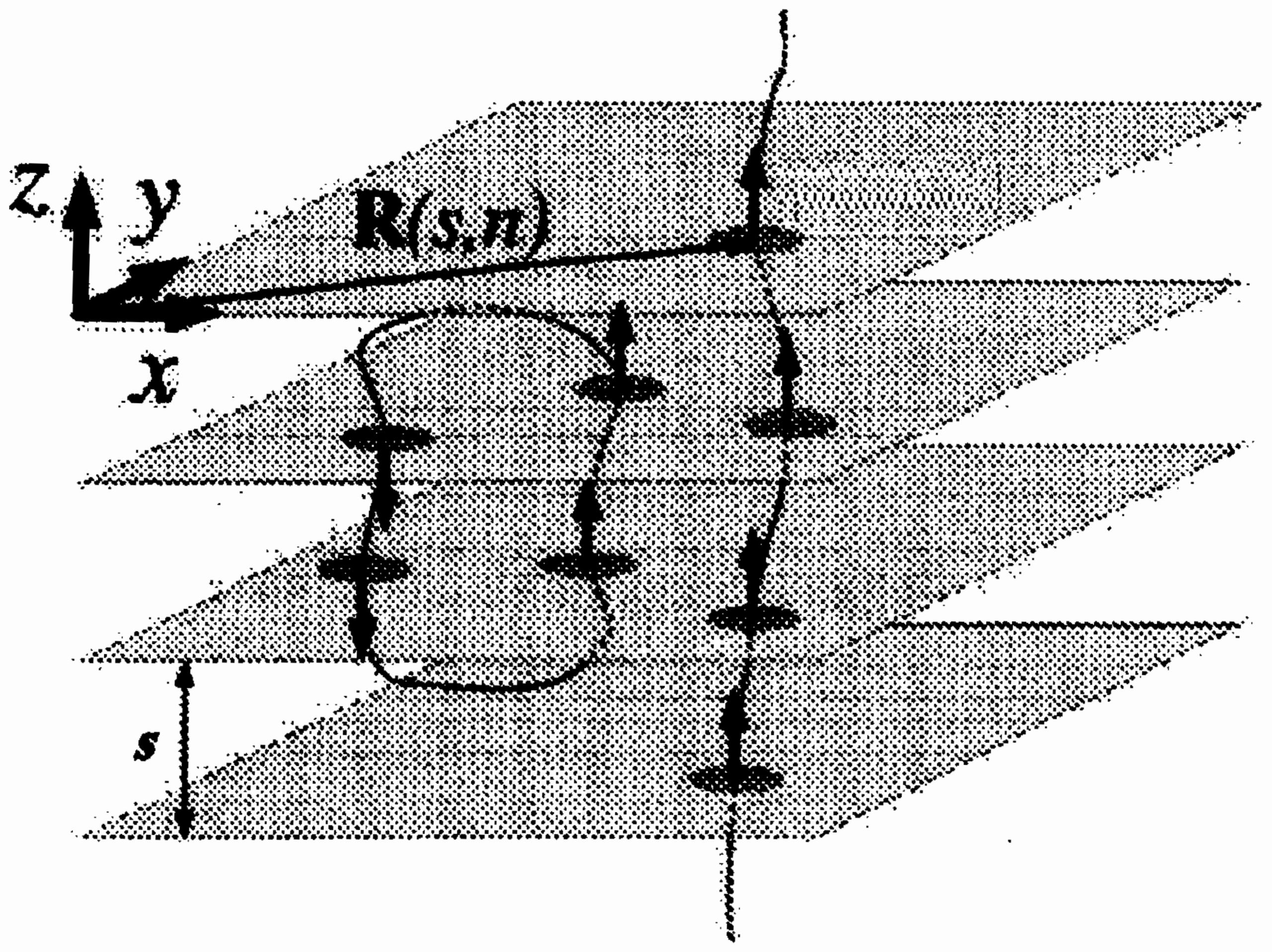

Figure 2.14: Sketch of the 3D thermally excited vortex loop (left) and of a field induced vortex line (right). The gray ellipses represent the vortices antivortices 2D (pancakes). Arrows connecting them are for clarity. (Fig. from Ref. [60])

$$\chi(T, H = 0) \propto e^{\frac{E_0}{k_B T}} \qquad (2.34)$$

corresponding to a thermally activated behavior of n_v:

$$n_v = n_0 e^{-\frac{E_0}{k_B T}} \tag{2.35}$$

according to the general aspects of the XY model[48]. In strong fields, instead, the vortex line elements dominate, the vortex correlations between different layers become relevant and M_{fl} only slightly increases with H and finally it flattens. It should be remarked that *no upturn* in the magnetization curves is predicted, at least for $H << H_{c2}$.
From Fig. 2.13 one sees that the data for χ, defined as $(-M_{fl}/H)$ for $H \rightarrow 0$, obey rather well to Eq. 2.34, in correspondence to $E_0 \simeq 940K$. This value approximately agrees with calculations that yield the activation energy around 10 T_C (see Ref. [60] and references therein). E_0 turns out to depend only slightly from doping and external field. As already mentioned the temperature dependence of the susceptibility above $T_C(0)$ differs from that one measured below T_C, as shown in Fig. 2.13.

Now we are going to modify the theoretical description by Sewer and Beck[60], still keeping their basic idea of *phase fluctuations* but taking into account the *presence of mesoscopic "islands" with non-zero average order parameter amplitude* that can be below or above the local irreversibility temperature.
Eq. 2.20, evidencing the order parameter phase contribution, is rewritten in the form

$$\mathcal{F}_{LD}\left[\theta\right] = \frac{1}{2a^2 s}\sum_l$$

$$\int d^2r \left\{ a^2 J_{\shortparallel} \left(\nabla_{\shortparallel}\theta - \frac{2ie}{c\hbar}\mathbf{A}_{\shortparallel} \right)^2 + J_{\perp}[1-\cos(\theta_{l+1}-\theta_l)] \right\} \tag{2.36}$$

where $J_{\shortparallel} = \dfrac{\pi\hbar^2 n_h}{4m_e}$ and $J_{\perp} = 2\pi\mathcal{J}n_h$ are the order parameter phase coupling constants respectively on the plane and between planes and s is the distance between layers. In Eq. 2.36 the Josephson coupling $[1-\cos(\vartheta_i-\vartheta_j)]$ between neighboring lattice sites in a given layer has been replaced by the phase gradient. In this way the occurrence of superconducting droplets above the critical temperature is assumed, and the order parameter can fluctuate in phase, producing thermal excitations (vortex and antivortex pairs in 2D, vortex loops in an anisotropic system). The potential vector $\mathbf{A}_{\shortparallel}$ in Eq. 2.36 describes both the magnetic field applied parallel to the c - axis and the one induced by thermal fluctuations. By considering, as usual, the partition function $Z = \int D\theta \exp(-\beta \mathcal{F}_{LD}[\theta])$ with $\beta = \frac{1}{k_B T}$, the susceptibility is

$$\chi = \frac{\partial M_{fl}}{\partial H} = \frac{\partial^2 F}{\partial H^2} = \frac{1}{\beta}\left[\frac{1}{Z}\frac{\partial^2 Z}{\partial H^2} - \left(\frac{1}{Z}\frac{\partial Z}{\partial H}\right)^2\right] \tag{2.37}$$

χ is obtained as the sum of three contributions:

$$\chi = \left\langle \frac{\partial^2 \mathcal{F}_{LD}}{\partial^2 H} \right\rangle^2 - \beta \left\langle (\frac{\partial \mathcal{F}_{LD}}{\partial H})^2 \right\rangle + \beta \left(\left\langle \frac{\partial \mathcal{F}_{LD}}{\partial H} \right\rangle \right)^2 \tag{2.38}$$

where $\langle\rangle$ means the thermal average. From the terms in Eq. 2.38 (see Appendix B), the diamagnetic susceptibility is obtained in the form[72, 73]

$$\chi = -\frac{k_B T}{s\Phi_0^2}\frac{1}{(1+2n_3)}\left[1+\left(\frac{H}{H^*}\right)^2 \delta\right]^2$$
$$\left\{\frac{1}{n_v} + \frac{s^2\gamma^2(1+n_3)}{\left[1+\left(\frac{H}{H^*}\right)^2\delta\right]}\right\} + + \frac{47\pi\ R_d^2}{540}\frac{J_{\shortparallel}}{s}\left(\frac{2\pi}{\Phi_0}\right)^2\left(\frac{H}{H^*}\right)^2 \delta \tag{2.39}$$

where $n_3 \cdot s$ is the correlation distance between vortex line in the same position but in different layers, n_v is the areal density of vertical vortex-line, $\gamma = \frac{J_{\shortparallel}}{J_\perp}$, $\delta = \frac{3\pi^2}{4}\frac{J_{\shortparallel}}{k_B T}$ and $H^* = \frac{\Phi_0}{\pi R_d^2}$ an effective critical field, with R_d the average radius of the superconducting islands.

In the limit $H \to 0$ a good agreement of the susceptibility and its temperature dependence with the experimental results is achieved, as in Ref. [60]. The main differences between our susceptibility (Eq. 2.39) and the one given in Ref. [60] consists in the presence of the factor $\left(\frac{H}{H^*}\right)^2$ and of the third, positive term. Is just this term that can cause an inversion in the sign of the susceptibility corresponding to the upturn in the magnetization curves. This phenomenon depends on the dimension of the islands and $\chi = 0$ (i.e. the occurrence of the upturn in M_{fl} vs H) requires $R_d > R_0$ where R_0 depends on some characteristics of the material. By choosing $\gamma = 6$, the interlayer distance $s = 12$Å, $n = 2$, $\frac{J_{\parallel}}{k_B T} = 2.5$, which are typical values for YBCO, for $T = 75.5K$ one estimates $R_0 \simeq 50$Å. In this case for $\chi = 0$ results $\frac{H_{up}}{H^*} \simeq 0.06$ and by considering the experimental value $H_{up} \simeq 250$ G, the effective critical field turns out $H^* \simeq 0.4T$.

The isothermal magnetization curves can be obtained from Eq. 2.39 by means of numerical integration. The shape of these curves depends on the choices of some parameters and by using the values quoted above, with $R_d = 370$ Å one derives the behavior sketched in Fig. 2.15 (a) for an island below the local irreversibility temperature. The same parameters with $T = 66K$, $\frac{J_{\parallel}}{k_B T} = 1.8$ and $R_d = 10$ Å lead to the curve shown in Fig. 2.15 (b) for the magnetization of the island above the irreversibility temperature. From the the differences observed in the magnetization curves between chain-empty and chain-disordered YBCO compounds a role of the chains on favoring the nucleation of local superconducting droplets above T_C can be suspected. In fact, in chain-ordered compounds the droplets have T_C^{loc} smaller than the irreversibility temperature, as evidenced by the presence of irreversibility effects, while in chain disordered samples the T_C^{loc} is higher than T_{irr}. Furthermore the amount of doping is also involved, since a marked variation of T_C with n_h is evidently crucial. In the magnetization curve of chain-ordered underdoped YBCO one sees that after the upturn the magnetization progressively takes the field dependence expected in the in the GL framework (Gaussian approximation) (see Fig. 2.16).

One could remark that in the measurements by Carballeira *et al.*[74] in LASCO at T_C =27.1 K the magnetization curves show only a weak tendency to saturation and no upturn. On the other hand in LASCO at $T_C \simeq 18$ K (therefore more underdoped) scanning

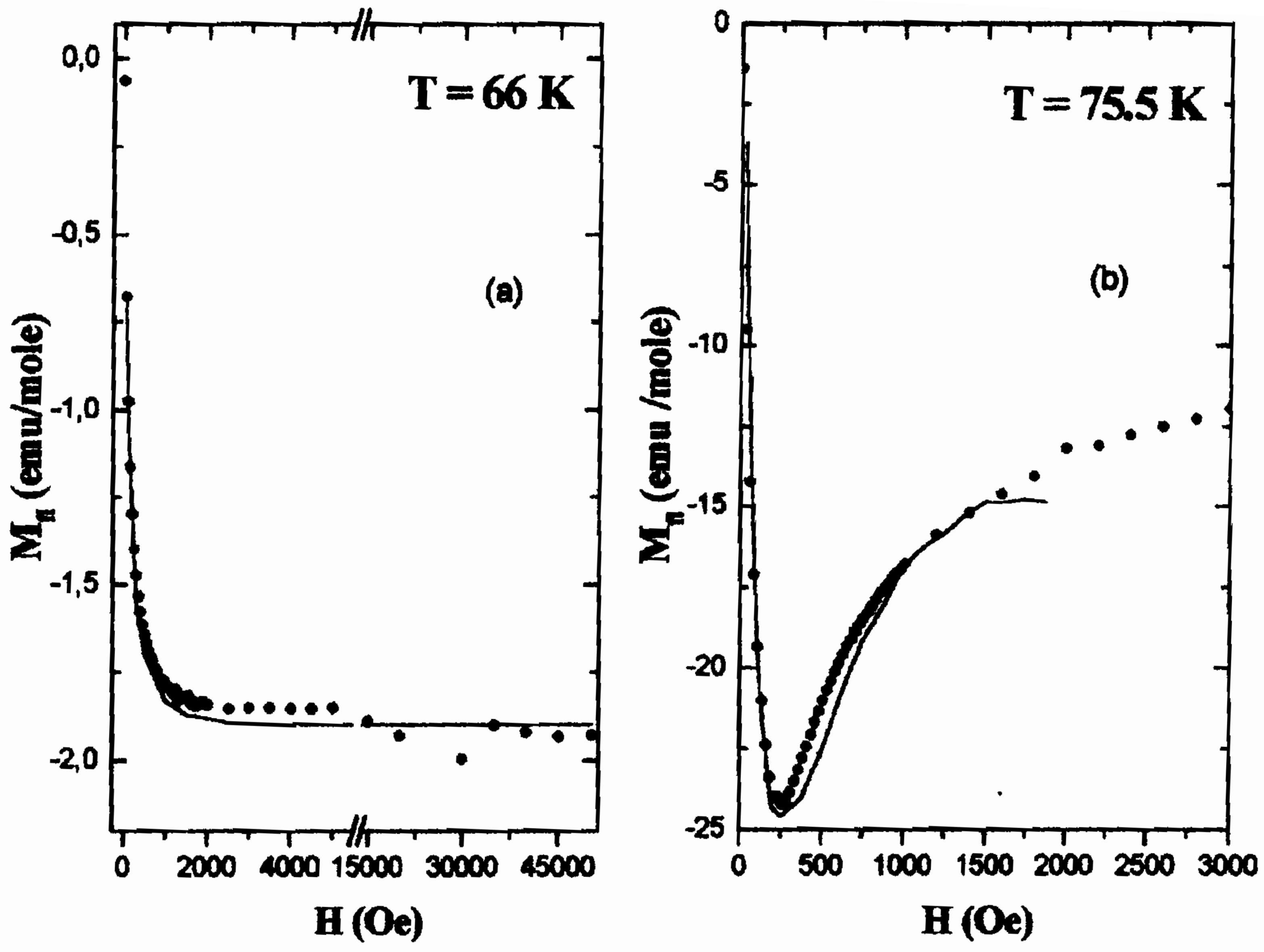

Figure 2.15: Magnetization vs. field at constant temperature for typical YBCO samples and comparison with the theory leading to Eq. 2.39. The solid lines are the theoretical behaviors for M_{fl} obtained from numerical integration of Eq. 2.39 for droplets below and above the local irreversibility temperature.

SQUID microscopy by Iguchi *et al.* [62] does evidence diamagnetic effects to associate to locally superconducting droplets. These droplets should imply a contribution to the magnetization curves similar to the one detected by us in YBCO compounds.
We do not discuss here the case of superconducting LASCO, by only mentioned that in a recent work by Lascialfari *et al.*[75] the upturn of the magnetization at small field is actually detected.
Finally must be noted that the phase fluctuations are not absent in optimally doped, but their effect is less manifest than in underdoped or overdoped compounds, because the T_C as function of n_h changes less rapidly around the optimal value of holes doping. Anyway, at small field an effect of phase fluctuations has been observed also in optimally doped YBCO (data not reported).

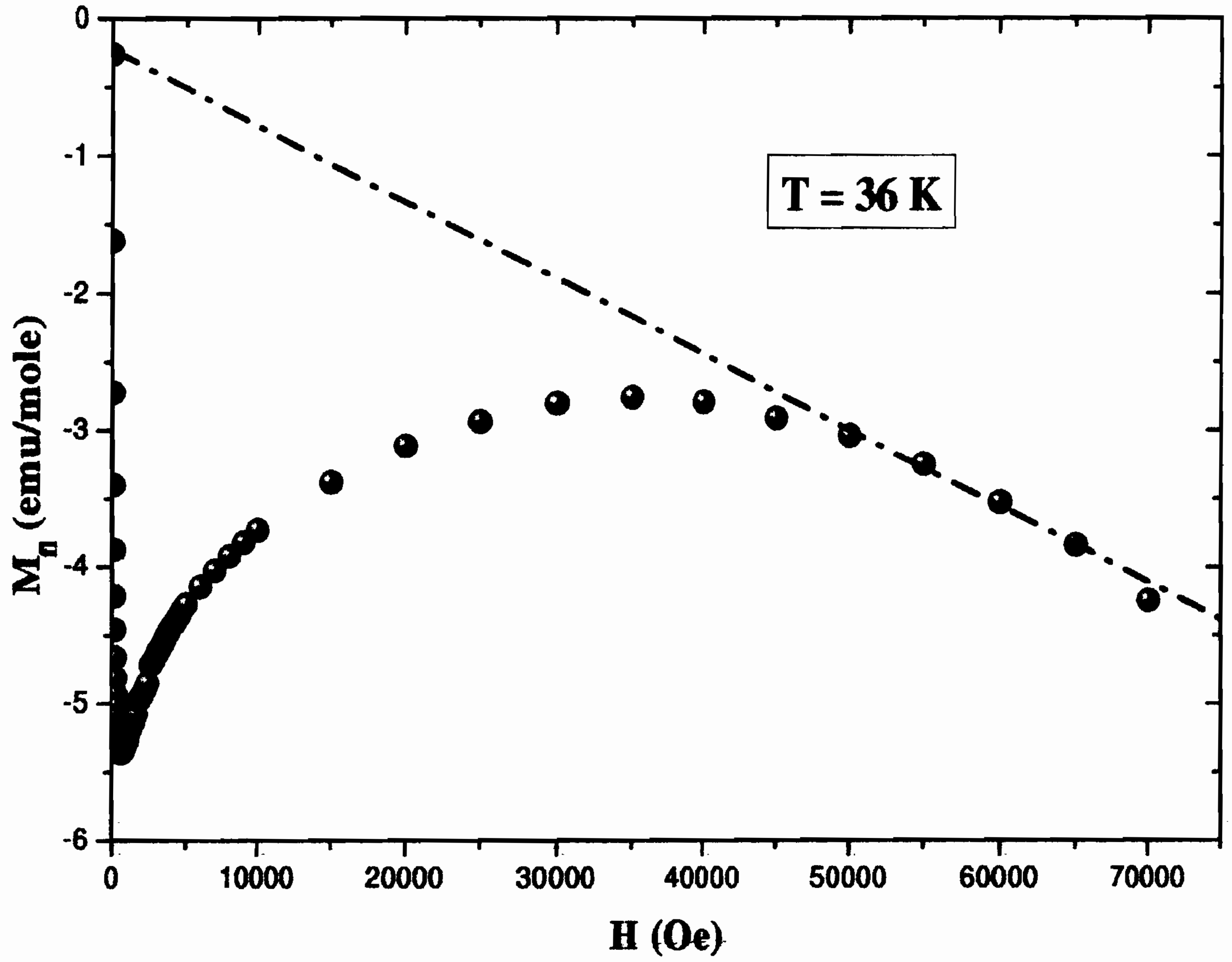

Figure 2.16: The magnetization curve in the range of H $= 0 \div 70000$ Oe of chain ordered underdoped YBCO compound. After the upturn the magnetization increase with the field and progressively takes the field dependence expected in the GL framework (dashed line).

Chapter 3

^{89}Y NMR study as a function of the doping amount

In the first part of this chapter the basic concepts useful to interprete the ^{89}Y NMR experiments are given. Then a brief recall of the theoretical background required for the deep understanding of the subsequent discussion is reported, for a model of localized magnetic moments (used for underdoped samples) and of delocalized carriers (for overdoped samples). In the third part of the chapter the experimental results of a systematic ^{89}Y NMR study, involving measurements of line width, Knight shift (K_S), echo dephasing time and spin-lattice relaxation time (T_1) are presented in YBCO-type SC's spanning from the underdoped to the overdoped regime, in the temperature range 1.6 – 300 K. The analysis of the data and summarizing conclusions are then given. In particular, the following aspects are addressed. The occurrence, in the underdoped regime, of low-energy magnetic excitations causing a divergence of the relaxation rates on cooling, accompanied by a concurrent broadening of the NMR line. The unusual relation between K_S and T_1 in the light of the evolution of the density of states with doping. It is shown how also a generalized spin susceptibility which includes charge and spin excitations fails in explaining same of the experimental findings, thus suggesting that a certain revision of commonly accepted view for the microscopic magnetic properties in YBCO family is still necessary.

3.1 Definition of the NMR quantities and experimental methodology

In NMR experiments the microscopic properties are detected by studying the nuclear magnetization and its time evolution towards the equilibrium. A nucleus j having spin $\mathrm{I} = \frac{1}{2}$ (like ^{89}Y) is subjected to a magnetic field $\vec{\mathrm{H}}_0$ at the nuclear site[1] and the relevant hamiltonian can be written

$$\mathcal{H} = \mathcal{H}_z + \mathcal{H}_{ne} + \mathcal{H}_d \tag{3.1}$$

where

$\mathcal{H}_z = -\gamma\hbar\vec{\mathrm{I}}\cdot\vec{\mathrm{H}}_0$ is the Zeeman hamiltonian (γ gyromagnetic ratio),

$\mathcal{H}_{ne} = \sum_i \vec{\mathrm{I}}_j \hat{A}_{ji} \vec{\mathrm{S}}_i$ is the hyperfine hamiltonian describing the interaction between the nuclear spin $\vec{\mathrm{I}}_j$ and electronic spin $\vec{\mathrm{S}}_\mathrm{i}$ with $\hat{A}_{ji}$ hyperfine coupling tensor,

$\mathcal{H}_d = \sum_{i<j} \hbar\gamma_i\gamma_j \vec{\mathrm{I}}_i \left[\frac{\vec{\mathrm{I}}_j}{r_{ij}^3} - \frac{3r_{ij}(\vec{\mathrm{I}}_j\cdot\vec{r}_{ij})}{r_{ij}^5}\right]$ is the dipole-dipole hamiltonian between the nuclear magnetic moments.

In a pulsed NMR experiment all the nuclei of one species in the samples are excited simultaneously by means of a transverse radiofrequency (RF) field pulse. The RF field H_1 (directed along a coil axis perpendicular to H_0) corresponds to a small rotating field and at resonance condition the precessional frequency of $\vec{\mu}_j$ is equal to ω_{RF}. By controlling the duration of the RF pulses the nuclear magnetization can be aligned along any direction. For a duration $\tau = \frac{\pi}{2}\frac{1}{\gamma H_1}$ the magnetization is brought in the xy-plane perpendicular to $\vec{\mathrm{H}}_0 \parallel z$. Following the $\frac{\pi}{2}$ pulse the free precession of the nuclear moments in the xy-plane induces a signal $s(t)$, called free induction decay (FID). This response in the time domain is collected and its Fourier transform yields the spectrum $f(\omega)$ in the frequency domain (see Fig. 3.1 part (a)). From the spectra at

---

[1] For nuclei at spin $\mathrm{I} > \frac{1}{2}$ the electric interaction between the nuclear quadrupole moment (Q) and electrical field gradient (EFG) on nuclear site has usually to be taken into account.

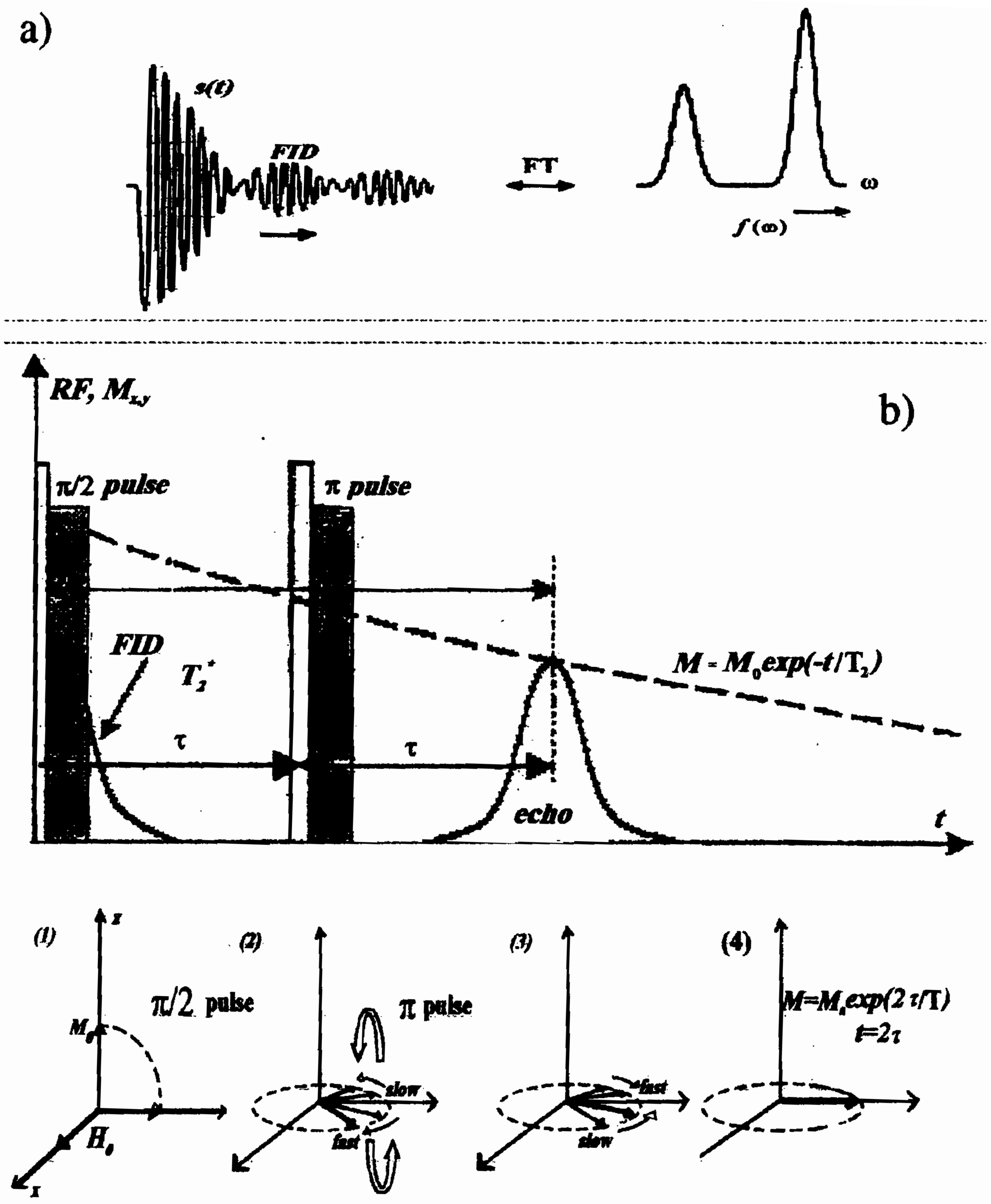

Figure 3.1: (a) The Fourier transform allows one to obtain the NMR spectra by means of the acquisition of free induction decay signal $s(t)$; (b) The formation of a spin echo by means of a $\pi/2-\pi$ pulse sequence. A schematic form of RF pulse and of the transverse magnetization signal is reported. Below it is shown that a $\pi/2$ pulse brings M_0 in the y direction (1), (2) the spin isochromats fan out, when a π pulse occurs at time τ slow and fast precessing spin interchange and the refocusing takes place (3); at time 2τ the echo signal is generated.

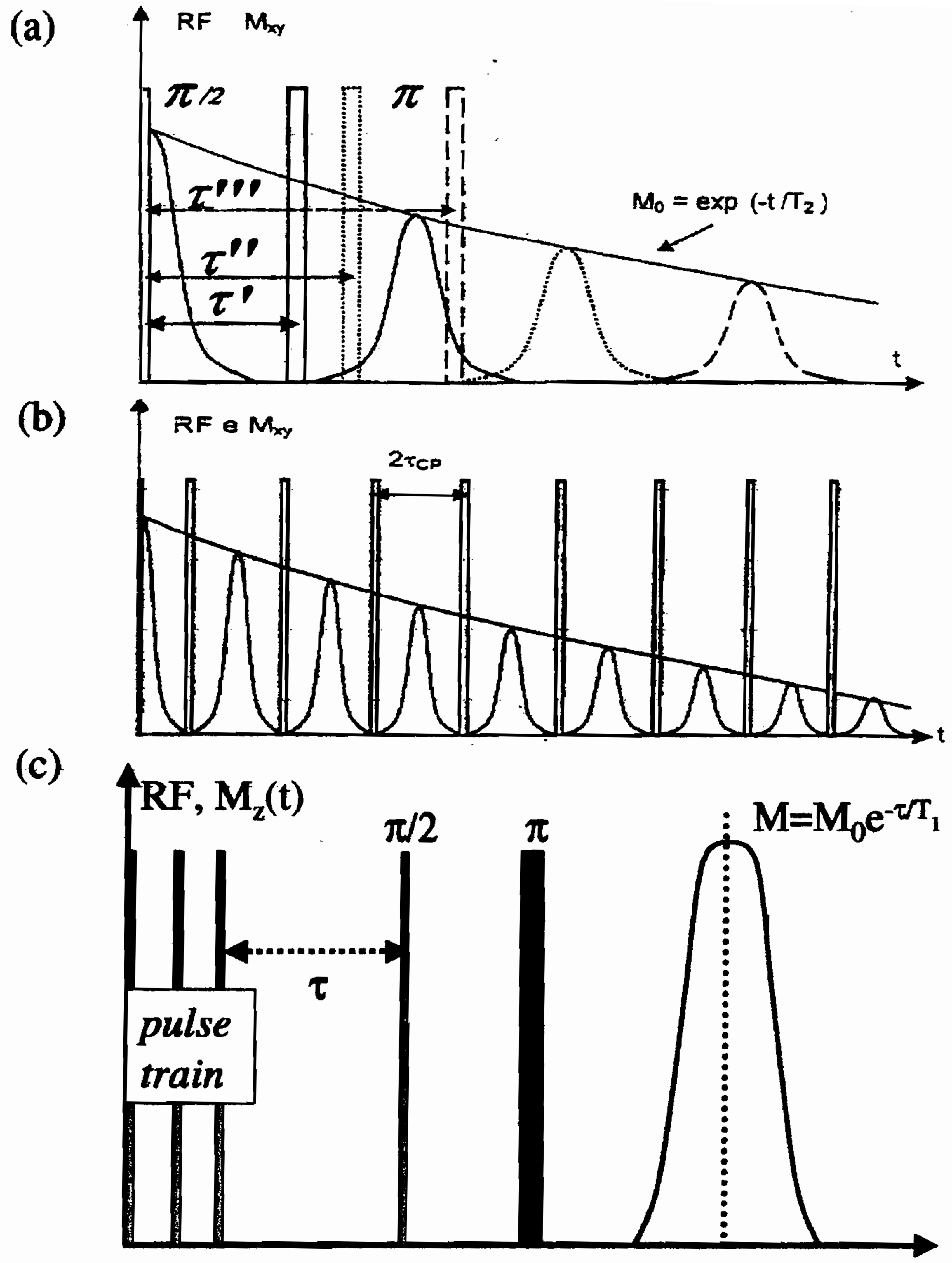

Figure 3.2: Scheme of Hahn (a) and CPMG (b) sequences and the resulting echoes. In part (c) of figure it is shown the sequence used when T_1 is long: the saturation train of $\pi/2$ pulse is followed by a $\pi/2$-π pulse sequence. The time τ in this case is the time in which the magnetization is partially reconstructed along z-axis.

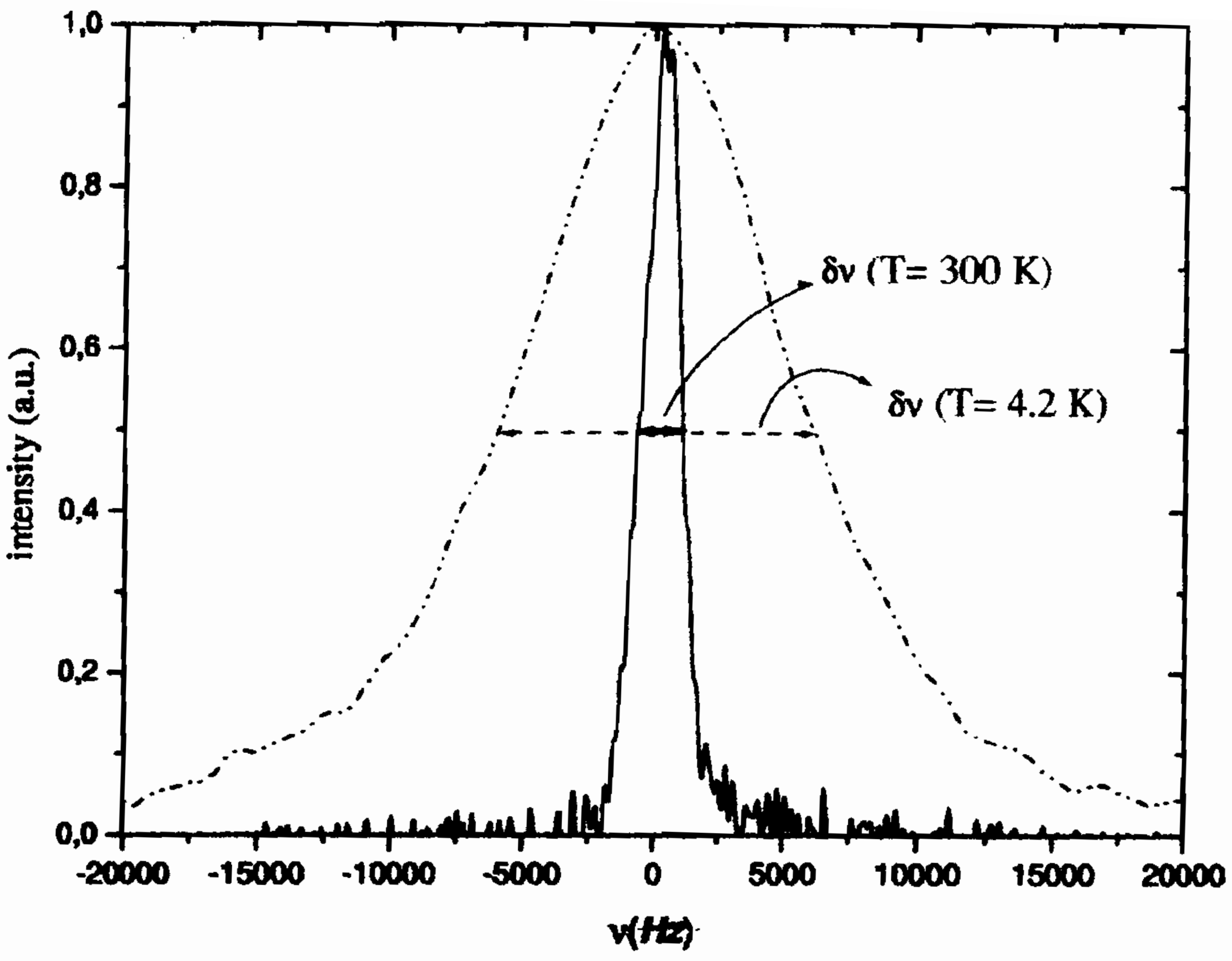

Figure 3.3: Normalized ^{89}Y NMR spectrum at T = 4.2 K (dashed line) and at T = 300 K (solid line) for YBCO:Ca with x=0.25 and y=6.1. *$\delta\nu$ is the full width at half intensity.* The increase of the line width on cooling (see also Fig. 3.6) is apparent.

different temperatures one can derive the behavior of two important quantities, the *line width*, $\delta\nu$, i.e. the spectral width at half intensity (see Fig. 3.3), *the shift*, K_T, of the line center with respect to a reference, usually the same nucleus in a compound dissolved in a solution (see Fig. 3.4).

Following a $\pi/2$ pulse the transverse component $M_\perp$, in the *xy*-plane, can decay as a result of two processes. The *irreversible* decay is controlled by the intrinsic spin-spin relaxation time T_2. The *reversible* (or inhomogeneous) decay results from a distribution of precessional frequency (due for example to an inhomogeneous magnetic field) controlled by a time constant usually called T_2^*. In the presence of both mechanisms, the irreversible decay of $M_\perp$ is obtained by applying a second RF π pulse at a time τ_m after the first $\pi/2$ pulse (Hahn sequence, see Fig. 3.1 part (b), and Fig. 3.2 part (a)). At the time $2\tau_m$ after the first pulse the echo signal is generated, in concomitance with the refocussing of the nuclear spins. In fact during the time interval τ_m the nuclear spins have been spread in the *xy*-plane as a consequence of the distribution of the precessional frequencies (see Fig. 3.1 part (b)). The decrease of the echo amplitude as a function of $2\tau_m$ yields the intrinsic T_2.

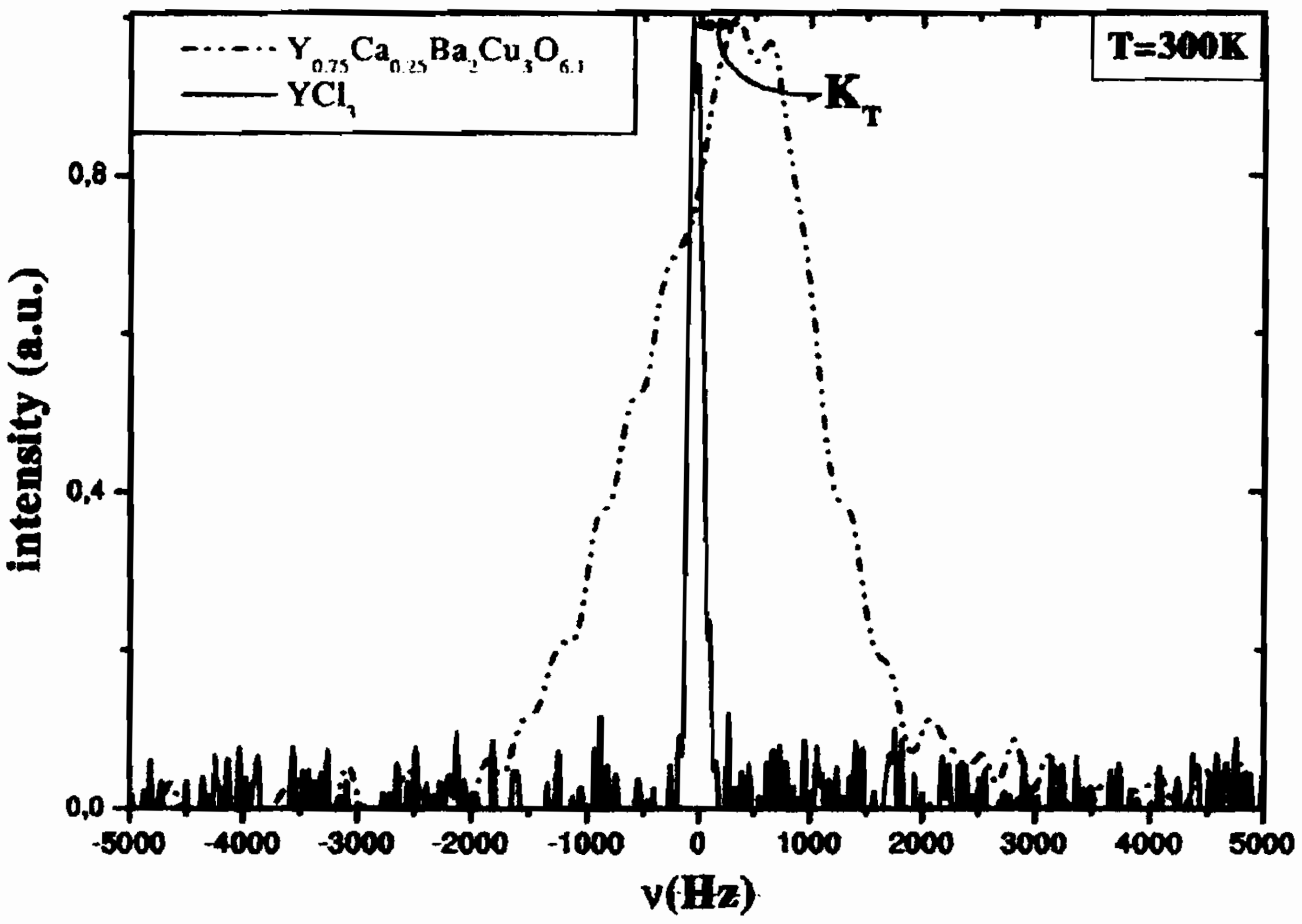

Figure 3.4: Shift of NMR spectrum, K_T, with respect to a reference line. The ^{89}Y NMR spectrum of YBCO:Ca (x=0.25, y=6.1) (dashed line) with respect to the one of YCl_3 (solid line) at T=300 K is reported. On the x-axis the 0 frequency corresponds to the resonance frequency of 19.608 MHz, in 9.4 T field.

Another sequence used to measure longer T_2 is the CPMG (Carr, Purcell, Meiboom, Gill), that originally consisted in a train of refocusing π-pulses separated by $2\tau_m$ smaller than T_2 in order to avoid the autodiffusion effects. A continuous reconstruction of the echo signal is obtained with this last technique (see Fig. 3.2 part (b)). The pulse NMR techniques offer simple and direct methods to measure the recovery of longitudinal magnetization towards the equilibrium condition after a given non equilibrium situation is induced by a sequence of RF pulses. The regrowth of the FID, or of the echo amplitude, towards its equilibrium value yields the recovery law, with a time constant T_1 inversely proportional to the relaxation transition probability W, that is related to the time-independent part of the interaction Hamiltonian. Generally for I = $\frac{1}{2}$ the recovery law for M_z is exponential: $M_z(t) = M_0[1 - e^{-\frac{t}{T_1}}]$. The magnetization is reestablished along z-axis due to the T_1 process and therefore it is not directly detectable being the pick-up coil sensitive only to the component of magnetization in the x-y plane. Therefore a second pulse is necessary to measure the spin-lattice relaxation time T_1. The basic idea is to perturb the magnetization from its equilibrium state with one pulse and examine its recovery along the z axis after a variable delay with another pulse, for example a $\pi/2$ pulse. Often the $\pi/2$ and π pulses yielding the echo signal are preceded by a saturating train of $\pi/2$ pulses (see Fig. 3.2 part (c)) in order to achieve full saturation of the line, thus avoiding the so-called spectral diffusion yielding an artificially fast recovery at short times. For details on basic NMR aspects in solid state physics see Ref. [76].

3.2 Basic theoretical background.

The theoretical expressions for the ^{89}Y NMR quantities defined in the previous Section, and used in the subsequent discussion, are recalled in the following, with direct reference to superconducting cuprates. In particular the quantities $2W \equiv \frac{1}{T_1}, \frac{1}{T_2}$ and K_T will be related to the generalized spin susceptibility $\chi(\vec{q}, \omega)$.

3.2.1 Line width

The NMR line shape can be due, in principle, to several contributions. The first one arises from the rigid dipolar lattice, namely the interactions with like ^{89}Y and unlike ^{63,65}Cu nuclei and yields a Gaussian line shape and it can be written in term of the second moment, M_2,

$$f(u) = \frac{1}{\sqrt{2\pi M_2}} e^{-\frac{u^2}{2M_2}} \tag{3.2}$$

with $u = \omega - \omega_R$ and ω_R effective resonance frequency or center of the line, or equivalently in the free induction decay FID (or half of the echo signal):

$$s(t) = e^{-\frac{M_2 t^2}{2}} \tag{3.3}$$

The evaluation of the second moment due to the dipolar interactions, in powdered samples of YBCO, has been given by Markert *et al.*[77]. If other sources of Gaussian broadening, such as field inhomogeneity, distribution of demagnetization factors, etc., are taken into account, the full width at half intensity (FWHI) $\delta\nu \simeq 2.36 M_2^{\frac{1}{2}}$ of the ^{89}Y NMR line above T_C can be expected around 1KHz. $\delta\nu$

should depend only little from doping and should be practically temperature independent, down to T_C.
In the superconducting state a further source of broadening of the ^{89}Y NMR spectra is due to the bulk distribution of the local field induced by the flux lines lattice. In fact the ^{89}Y tracks the local field modulation[78]. One will see that the increase in the line width in the low temperature range (see Sect. 3.3 and Fig. 3.6) in underdoped samples cannot be explained by taking into account only the contributions from the flux lines lattice. When a given source of fluctuations of the longitudinal field $h_z(t)$ is active, the line shape can be written

$$f(u) = \int_0^\infty e^{-iut} \left\langle e^{i\gamma \int_0^t h_z(t')dt'} \right\rangle dt \qquad (3.4)$$

The effective correlation time is

$$\tau_z \equiv \int_0^\infty \frac{\langle h_z(0)h_z(t')\rangle}{\langle h_z^2(0)\rangle} dt' \equiv \int_0^\infty g_z(t')dt' \qquad (3.5)$$

with $g_z(t)$ the correlation function. In the *slow motions condition*, when τ_z is larger than the inverse of $\delta\omega_z \approx \gamma\sqrt{\langle h_z^2\rangle}$ (*rigid lattice line width*), the contribution to the line shape $f(u)$ in Eq. 3.4 is Gaussian and the second moment $M_2' \equiv \langle \delta\omega_z^2 \rangle$ adds to the second moment M_2 in Eqs. 3.2 and 3.3. In the *fast motions condition*, when $\tau_z \ll [\langle\delta\omega_z^2\rangle]^{-\frac{1}{2}}$, $f(u)$ in Eq. 3.4 turns to the Lorentzian line shape, with line width

$$(\delta\omega)_L = \left\langle \delta\omega_z^2 \right\rangle \tau_z. \qquad (3.6)$$

Correspondingly the FID signal (and equivalently half of the echo signal) should be a mixture of Gaussian decay described by Eq. 3.3 and of an exponential decay. For fast motions the exponential decay of the FID (or of the echo amplitude, if a reversible fast decay is associated to an inhomogeneous broadening implying $T_2^* \ll T_2$) yields a time constant T_2' so that

$$\frac{1}{T_2'} = \frac{\gamma^2}{2} j_{zz}(0) \qquad (3.7)$$

where

$$j_{zz}(\omega) = \int_{-\infty}^{+\infty} dt\; e^{-i\omega t} \langle h_z(t)h_z(0)\rangle \qquad (3.8)$$

is the spectral density of the random modulation of the field.
In the previous equations $\delta\omega$ is the line width, FWHI, in rad s^{-1}.

3.2.2 Spin echo dephasing

The spin echo dephasing time T_2 (as measured in a two pulse $\pi/2-\tau_m-\pi-$ echo experiment, when a reversible fast decay is associated to an inhomogeneous broadening yielding $\mathrm{T}_2^* \ll \mathrm{T}_2$), can detect the dynamical effects modulating the local field $h_z(t)$. This detection is usually more effective than the one reflected in the line width and its description is more complex than that for the spin-lattice relaxation rate T_1^{-1} (see later on). Looking at the echo decay is particularly useful when the motions modulating $h_z(t)$ are slow. In this case in fact the contribution to T_1^{-1} is small and the contribution to the line width is not clearly resolved. The decay of the echo amplitude can be written[79, 80, 81]

$$h_e(2\tau_m) = h_e(0) \cdot e^{-\left(\frac{2\tau_m}{\mathrm{T}_2}\right)^n} \left[e^{-\left\langle\omega_z^2\right\rangle\tau_z^2 g(\tau_m,\tau_z)}\right] \tag{3.9}$$

with

$$g(\tau_m, \tau_z) = \frac{2\tau_m}{\tau_z} - \left(1 - e^{-\frac{\tau_m}{\tau_z}}\right) \cdot \left(3 - e^{-\frac{\tau_m}{\tau_z}}\right), \tag{3.10}$$

assuming, as usual, a stationary Gaussian random frequency modulation and an exponential correlation function for $h_z(t)$. In Eq. 3.9, n is in between 1 and 2, depending on the character (Gaussian or exponential) of the intrinsic contribution described by T_2. From the above Eqs. 3.9 and 3.10 one sees that even for *ultra-slow motion*, namely $\langle\delta\omega_z^2\rangle^{\frac{1}{2}} \cdot \tau_z \gg 1$, the echo dephasing still allows one to detect a motional effect, described by

$$h_e(2\tau_m) \propto e^{-\left(\frac{2\left\langle\delta\omega_z^2\right\rangle\tau_m^3}{3\tau_z}\right)} \tag{3.11}$$

even though the FID or the resonance line (as well as T_1^{-1}) are practically unaffected.
One should remark that, in principle, also spin-lattice interactions contribute to the dephasing of the echo.
A first contribution implies a *Redfield* term $e^{-\frac{t}{a\mathrm{T}_1}}$ in Eqs. 3.9,

3.10, 3.11, where a is a constant of order of unit and T_1 is the experimentally measured spin-lattice relaxation time. In view of the long values of T_1 measured for ^{89}Y (Fig.s 3.7, 3.8, 3.9) one can neglect this *Redfield* correction to the echo decay.
A second contribution to ^{89}Y spin-echo can arise from T_1-driven fluctuations of the un-like $^{63,65}Cu$ nuclei. When $T_1^{(Cu)}$ is of the order of the pulse separation τ_m between the pulses leading the ^{89}Y spin echo, one can expect[82, 83] a peak in the spin-echo dephasing rate (T_2^{-1}). In optimally doped YBCO the maximum effectiveness of this mechanism, which contributes with a exponential decay to $h_e(t)$, occurs around 60-70 K.[80, 81, 82]

3.2.3 Knight shift K_S

The total shift of the spectrum line is the sum $K_T = K_{0,\delta} + K_S$.
$K_{0,\delta}$ is given by the orbital and chemical shift contribution, it is temperature independent and it amounts to about 150 ppm with respect to the ^{89}Y resonance in the reference YCl_3[84]. K_S, or Knight shift, is related to electronic contribution. In the following $K_{0,\delta}$ will not be taken into account and for un-oriented powder samples only an isotropic shift K_S resulting from a scalar nuclei-electrons interaction will be considered.
K_S is conveniently related to the spin susceptibility:

$$K_S = \frac{D_T}{g\mu_B}\chi_{spin} = D_T g \mu_B \chi' \tag{3.12}$$

where D_T is a magnetic field (z-component) at the Y site and where the static spin susceptibility χ' (in eV^{-1} units) has been introduced, with $\chi_{spin} \equiv g^2\mu_B^2\chi'$.
K_S, depending on the interpretative model, can be obtained from the field induced polarization of delocalized Fermi-like carriers or from the static field $< h_z >$ at the Y site due to the localized magnetic moments $\gamma_e\hbar < \vec{S}_z >_{H,T}$ at the Cu^{2+} spin, $< h_z >$ is mostly due to the transferred hyperfine contribution, the dipolar part being negligible.

Model of *Localized magnetic moments*, LM

In cuprates the 3d electron band is rather narrow and in the tight binding models the magnetic properties are usually well described by a spin-localized scenario, with maximum spin density on the Cu(2) sites. In this case the field at the Y site can be written $< h_z >= \sum_{i=1}^{8} D_i < \vec{S_z^{(i)}} >_{H,T}$. D_i is about -4 KOe and χ' in Eq. 3.12 is the $q = 0, \omega = 0$ limit of the generalized spin susceptibility $\chi(\vec{q}, \omega)$ pertaining to the Cu^{2+} magnetic moments in strong AF correlation. This interpretative scenario of localized magnetic moments should be more suitable for strongly underdoped compounds.

Model of *Delocalized carriers*, DC

This somewhat opposite interpretative model assumes that doping drives the hybridization of 3d Cu electrons with the Fermi liquid of the itinerant hole carriers. D_T in Eq. 3.12 is the hyperfine contact term and it can be seen as $\frac{8\pi}{3} \langle u_k \rangle^2 g\mu_B$ ($\langle u_k \rangle$ being the average of the Bloch function for carriers at the Fermi surface). The static susceptibility χ' is usually written as[5]

$$\chi'(0,0) = \frac{\rho(E_F)}{1 - \mathcal{I}\rho(E_F)} \tag{3.13}$$

with $\rho(E_F)$ the density of states at the Fermi level and $\mathcal{I} \equiv \mathcal{I}_{q=0}$ coupling constant between carriers accounting for the AF correlation. $\mathcal{I}$ enhances the susceptibility of the bare holes and it can be doping-dependent. This latter model of delocalized carriers is likely to be more appropriate in the overdoped regime.
Finally it must be mentioned that the applicability of a model in which charge and spin excitations for conventional Fermions are embedded in an energy-dependent density of states has been discussed by Cooper and Loram[85]. In particular Williams *et al.*[86] have proposed a way to account for the evolution of K$_S$ with doping within the DC scenario. $\chi'(0,0)$ is substantially rewritten as the Pauli spin susceptibility

$$\chi'(0,0) = \mu_B \int_{-\infty}^{\infty} \rho(E) \left[-\frac{\partial f(E)}{\partial E} \right] dE \tag{3.14}$$

where μ_B is the Bohr magneton, $f(E)$ is the Fermi function and $\rho(E)$ is the density of states. One assumes that $\rho(E)$ is the sum of two contribution: an energy independent one (in two dimensions) and an energy dependent one, pinned at the Fermi level and growing with the doping (for $n_h \geq 0.17$). $\rho(E)$ can thus be written

$$\rho(E) = (1-y)\rho_k + y\rho_{\nu h}(E) \tag{3.15}$$

where $\rho_k = \frac{\hbar^2 k^2}{2m^*}$ is the free-electron energy-independent background; $\rho_{\nu h}$ is the contribution from a dispersion relation of the form $E(k) = -2t(\cos(k_x a) + \cos(k_y b)$, with t related to nearest-neighbor hopping probability: y is the "amplitude" of the energy dependent peak and its value depends on hole concentration[86].

3.2.4 Spin-lattice relaxation

The spin-lattice relaxation is driven by the fluctuations of the transverse components $h(t)$ of the local field h at the Y site. Generally it can be written

$$\frac{1}{\mathrm{T}_1} \equiv 2W = \frac{\gamma^2}{2} \int \langle h_+(t) h_-(0) \rangle \, e^{-i\omega_R t} dt \tag{3.16}$$

where $h_\pm$ are the transverse components of h and ω_R is the NMR resonance frequency. The relationship between the relaxation rate $1/\mathrm{T}_1$ and the dynamical spin susceptibility $\chi(\vec{q}, \omega)$ can be obtained from Eq. 3.16[5]

$$\mathrm{T}_1^{-1} = \frac{{}^{89}\gamma^2}{2N} k_B T \sum_{\vec{q}} A^2_{\vec{q}} \frac{\chi''_\pm(\vec{q}, \omega_m)}{\omega_m} \tag{3.17}$$

A_q are the FT's of the lattice functions specifying the position of the magnetic ions. A^2_q can be assumed independent from the orientation of the external magnetic field and in the *model of localized spins (LM)* is given by

$$A^2_{\vec{q}} = D^2_T \left\{ \cos^2 \frac{q_x a}{2} \cos^2 \frac{q_y b}{2} \cos^2 \frac{q_z d}{2} \right\} \tag{3.18}$$

where d is the distance between the CuO$_2$ planes. $\chi''(q, \omega)$ in Eq. 3.17 includes the term $g^2 \mu_B^2$. For ferromagnetic correlation among planes, $q_z = 0$ in Eq. 3.18. For *delocalized carriers* A^2_q is practically q-independent.

A rather general expression used in the interpretation of the NMR relaxation in HTSC is:

$$\left(\frac{\chi''(\vec{q},\omega)}{\omega}\right)_{\omega\rightarrow 0} = \chi(q,0)j_q(\omega) \tag{3.19}$$

where the static susceptibility is related to the collective amplitude of the normal excitations. In particular, assuming a correlation function of the exponential form with only a correlation time τ_z, the relaxation rate could indicatively be written in the form

$$\frac{1}{\mathrm{T}_1} = \omega_h^2 \cdot \frac{2\tau_z}{1+\omega_m^2\tau_z^2} \tag{3.20}$$

where $\omega_h = \gamma\sqrt{< h_\pm^2 >}$.
In the DC model one can analyze the data for T_1 starting from the relaxation rate for weakly interacting electrons

$$\frac{1}{\mathrm{T}_1} = \gamma^2 A^2 k_B T \pi\hbar \int \rho^2(E)\left(-\frac{\partial f}{\partial E}\right) dE \tag{3.21}$$

where $\rho(E)$ is the density of states. If $\frac{\partial f}{\partial E}$ is written as $\delta(E-E_F)$ and the conditions for ideal metal are used, one obtains the *Korringa* relation

$$\mathrm{T}_1^{-1} \propto \mathrm{T}(\rho(\mathrm{E_F}))^2 \propto \mathrm{K_S^2 T}. \tag{3.22}$$

In the framework of *DC model* with pinned $\rho(E)$ one should use the $\rho(E)$ given by Eq. 3.15. In Ref. [87] has been evidenced that, in contrast to experimental results, in the framework of this model T_1 should be sensitive to role of $(y\rho_{\nu h})$ more than $\mathrm{K_S}$.
As for $\mathrm{K_S}$ the problem is to find a proper expression for the dynamical susceptibility. A recent attempt to derive a form of $\chi(\vec{q},\omega)$, capable to fit the temperature dependence of ^{63,65}Cu and ^{89}Y T_1 in optimally doped is due to Zavidonov and Brinkmann[88], by using a two-times Green function method, within a framework of a t-J mode. $\chi(\vec{q},\omega)$ is formally similar, in the limit $\omega_m \rightarrow 0$ to the superposition of two rather general expressions usually written in term of amplitude and of decay rates of the excitations:

$$\frac{\chi''(\vec{q},\omega_m)}{\omega_m} = \frac{\chi_S(0,0)}{\Gamma_\mathrm{q}(0)} + \frac{\chi_S(0,0)}{\Gamma_\mathrm{q}(\mathrm{AF})} \tag{3.23}$$

Here $\chi_S(0,0)$ is the static susceptibility, while $\Gamma_q(0)$ and $\Gamma_q(AF)$ are decay rates which lead to a response function dominated by two kind of excitations and peaked at $q = 0$ and $q = q_{AF} = (\frac{\pi}{a}, \frac{\pi}{a})$, with a smooth q-dependence. It must be noted that in this theory[88] $\Gamma_q(0)$ and $\Gamma_q(AF)$ depend on the extra hole concentration. Furthermore it should be stressed that the $q = 0$ contribution is not simply associated to free holes but it includes excitations of charge and spin degrees of freedom. This remark is particularly relevant since, as observed by Nandor *et al.*[89] in optimally doped YBCO by means of high temperature measurements of ^{89}Y relaxation, the linear temperature dependence of T_1^{-1} strictly follows the Korringa law ($T_1^{-1} \propto K_S^2 \cdot T$) in spite of the fact that the Knight shift K_S (and hence the static hole susceptibility) drops by $12 \div 13\%$ between room temperature and 700 K. Finally we recall that the q-dependence of A_q^2 (Eq. 3.18) filters out the AF fluctuations, which instead dominate the behavior of the ^{63}Cu relaxation rate. This means that the ^{89}Y relaxation rate can be written, in practice, only in terms of the first contribution in Eq. 3.23:

$$\frac{1}{T_1} = {}^{89}\gamma^2 \cdot \frac{1}{2} \cdot D_T^2 \frac{1}{N} \sum_{\vec{q}} \frac{\chi_S}{\Gamma_q(0)} \tag{3.24}$$

(the form factor is practically q-independent for delocalized carriers, as already mentioned). By using as free parameter at T=0 the correlation length ξ_0 Zavidonov and Brinkmann[88] have been able to fit the experimental results for ^{89}Y T_1 in optimally doped YBCO, in the temperature range $100 \div 300$ K, obtaining $\xi_0 \approx 4.2$, in lattice units.

3.3 Experimental results

In this Section the experimental results of ^{89}Y NMR line width, Knight shift, the echo dephasing time and the spin-lattice relaxation time, in the temperature range $1.6 - 300$ K, are reported. ^{89}Y NMR measurements have been carried out by means of standard pulse technique in a field of 9.4 T. In the SC compounds of YBCO family, ^{89}Y nucleus, lacks of quadrupole moment and filters out[5] the AF correlation. For this reason ^{89}Y nucleus has been used in several NMR studies[90, 86, 91, 92] on YBCO compounds. The experimental results of this thesis work are often compared with those obtained by other research groups in optimally, underdoped and overdoped samples.

In Fig. 3.5 the Knight shifts (K_S) of the ^{89}Y resonance line with respect to a reference solution of YCl_3 are reported. K_S is obtained from the total shift by subtracting $K_{0,\delta} \sim 155$ ppm. The Knight shift displays the temperature dependence already noticed in previous works[93, 89, 29], with ($-K_S$) increasing from 100 ppm to 150 ppm on cooling from 300 K to T_C in overdoped samples, while ($-K_S$) decreases of about 100 ppm in the same temperature range in underdoped compounds.

The ^{89}Y NMR line width $\delta\nu$ was found practically temperature independent down to T_C in optimally doped and in overdoped compounds, showing only a little increase on cooling. Only in the superconducting phase the well-known marked broadening related to the vortex lattice[5] was detected in these samples. On the contrary, in underdoped compounds the line width $\delta\nu$ (see Fig. 3.6) shows a sizeable increase which starts above T_C. In the SC phase this broadening is further enhanced and it superimposes to the one expected from the field distribution associated to the vortexes. In fact in optimally doped YBCO for $T \rightarrow 0$ one has $\delta\nu_{FL} \propto \lambda_L(0)^{-2} \propto n_C \approx 9$KHz, λ_L being the London penetration length and n_C the number of carriers. In underdoped YBCO the $T = 0$ line broadening $\delta\nu_{FL}(0)$ (due to the vortex lattice) should decrease with respect to the optimally doped compound by a factor around the ratio of the correspondent transition temperatures. Thus in Fig. 3.6 the solid line is the schematic form of the broadening expected below T_C with $\delta\nu_{FL}(0)$ scaled by the factor (35 K/91 K) and going to zero for $T \sim T_C = 20$ K.[2] From Fig. 3.6 is thus evident that a further mechanism of line broadening occurs in the low temperature range of underdoped compounds and that it sets in well above $T_C(H)$. $T_C(H)$ has been estimated by SQUID measurements and by detuning of the NMR resonance circuit.

The spin lattice relaxation rates T_1^{-1} are separately reported as a

---

[2] The estimate of the linewidth, arising from supercurrents in the vortex lattice state in 9 T applied field, given by London model is approximated. Using the approach of E.H. Brandth[94] the linewidths can be calculated and the values are larger (until 50% in certain cases) respect the estimate made. It is noted, however, that the increasing of linewidth cannot anyway be due to vortexes because the broadening starts at T larger than $T_C(H)$ (see Fig. 3.6).

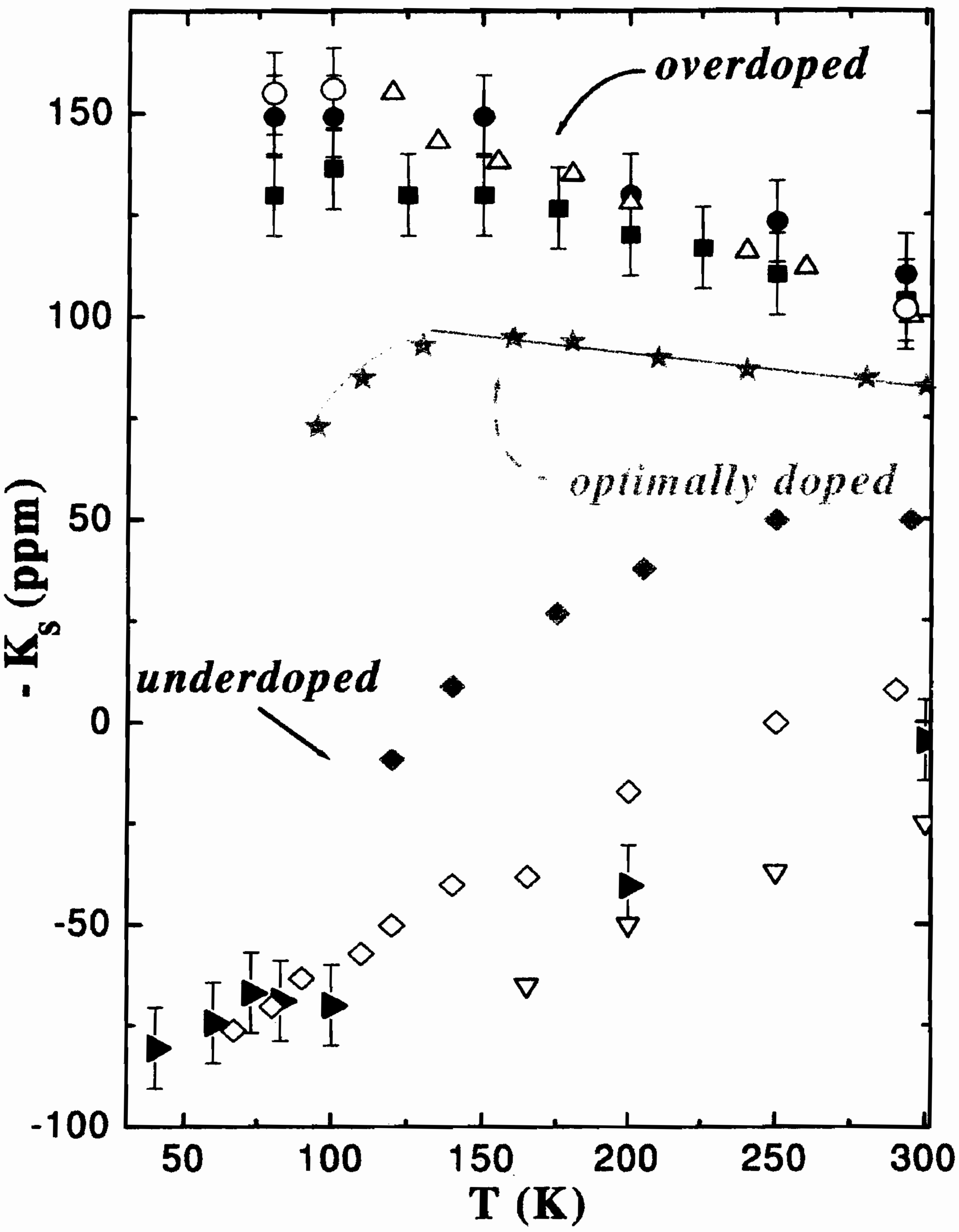

Figure 3.5: ^{89}Y NMR Knight shift (reference YCl$_3$) as a function of temperature in underdoped and overdoped regimes of $Y_{1-x}Ca_xBa_2Cu_3O_y$, for $y \approx 6.1$ and $y \approx 6.96$ respectively (►) $x = 0.25$, $T_C(0) = 35$ K; (■) $x = 0.10$, $T_C(0) = 74$ K;(○) $x = 0.10$, $T_C(0) = 70$ K; (•) $x = 0.05$, $T_C(0) = 82$ K. The data represented by ($\bigtriangledown$) and by ($\Diamond$) are from Ref. [29] for x=0.22 and $T_C(0)$ respectively 30 K and 59 K, while the ones represented by (♦) and (($\triangle$)) are from Ref.s [91, 92]. For comparison also the data in optimally doped YBCO (from Ref. [89]) are reported (★) with the sketchy behavior given by solid line. It must be noted that K_S is obtained from the total shift by subtracting $K_{0,\delta} \sim 155$ ppm.

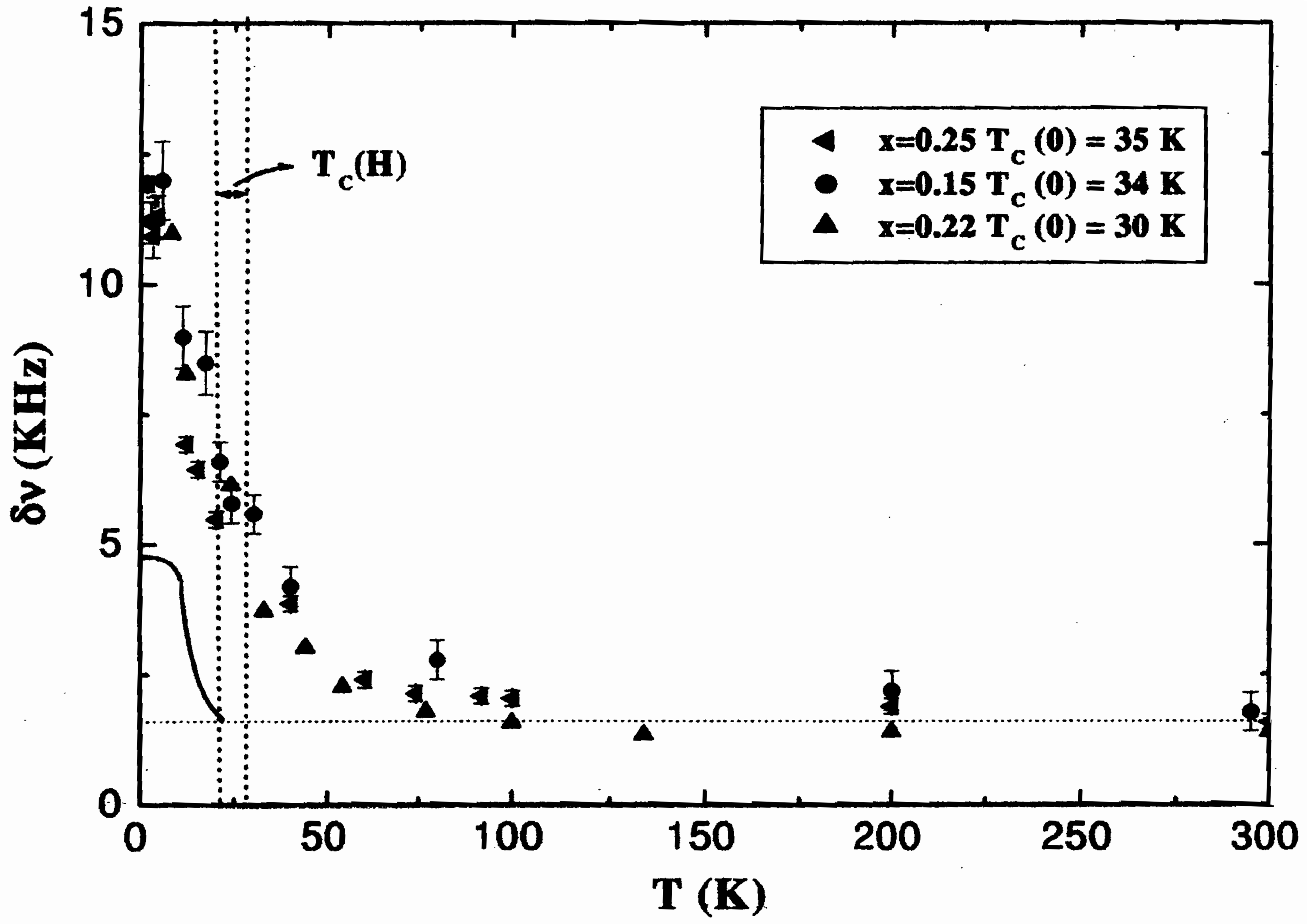

Figure 3.6: ^{89}Y NMR line width $\delta\nu$, in a field $H_0 = 9.4$ Tesla, as a function of temperature in the underdoped regime of $Y_{1-x}Ca_xBa_2Cu_3O_{6.1}$. The data indicated by (▲) are from Ref. [29]. The range of the superconducting transition temperature in the magnetic field is indicated. The solid line below $T_C(H)$ is a sketchy behavior of the contribution to the line width expected from the vortex lattice (see text).

function of temperature in the normal state (Fig. 3.7) and in the superconducting phases (Fig. 3.8 and 3.9), for typical overdoped and underdoped samples.

For the normal state the trend of T_1^{-1}, in overdoped samples, decreases linearly with T as in the Korringa relation (see Eq. 3.22), but in this case K_S is not independent on temperature. On the contrary K_S, as shown in Fig. 3.5 increases by a factor 15% from 100 K to 300 K. It must be reminded that the data reported in Fig. 3.5 are obtained from the total shift by subtracting $K_{0,\delta} \sim 155$ ppm. In underdoped samples the temperature behavior of the relaxation rate in the range $50 \leq T \leq 300$ K shows that the density of state

$\rho(E_F)$ (see Eq. 3.21) decreases on cooling. Thus, as one can see also from Knight shift measurements, the opening of a pseudo gap in the charge or spin excitations occurs in underdoped regime. Below T_C, by using Eq. 3.21 and writing $\rho(E)$ in the form pertaining to d-wave symmetry, yielding $\rho(E) \propto E$ for $E \rightarrow 0$, one would obtain $T_1^{-1} \propto T^3$ (see Ref. [5]). The fast decrease of relaxation rate in the superconducting phase is generally, in part, masked by the relaxation mechanism due to flux line motions which appear at temperature close to the irreversibility temperature. The trend just described is well followed by T_1^{-1} in overdoped samples. Below T_C the relaxation rate in overdoped samples (see Fig. 3.8) is approximately the one expected in SC phases once that a contribution from lattice vortex motions around the irreversibility temperature is taken into account (see the qualitative behavior reported as solid line in Fig. 3.8 and obtained by scaling the data found in YBCO124[95]). In underdoped compounds, on the contrary, the presence of a peak at low temperature is observed .

Before describing the measurements in underdoped regime, it is necessary to comment about the recovery laws. It must be remarked that in the normal phase they are all described by a single exponential, as expected for $\mathrm{I} = 1/2$ with a site-independent fluctuation dynamics or anyway when the condition of a common spin-temperature is achieved. For overdoped compounds a single exponential recovery law is detected also below T_C, as shown in the inset of Fig. 3.8. On the contrary, in underdoped compounds (Fig. 3.9) a fast relaxing component, of stretched exponential character, is found to arise progressively on cooling below about 60 K. In the inset of Fig. 3.9 a typical experimental finding for recovery law is reported. In Fig. 3.10 one can see that on cooling the weight of fast relaxing component increases, while the one of the slow relaxing component decreases. In the low temperature range the component at long T_1 follows approximately the temperature behavior expected for the usual temperature dependence of T_1 in superconducting phases. On the contrary the fast relaxing component in underdoped compounds shows a divergent behavior on cooling, with a maximum occurring at a temperature T_g around 7-8 K. In Fig. 3.9 is reported only the short component of T_1^{-1}, T_{1s}^{-1}, obtained as the time required to reduce the recovery to $e^{-\frac{1}{2}}$, once that the slower component of the recovery has been subtracted.

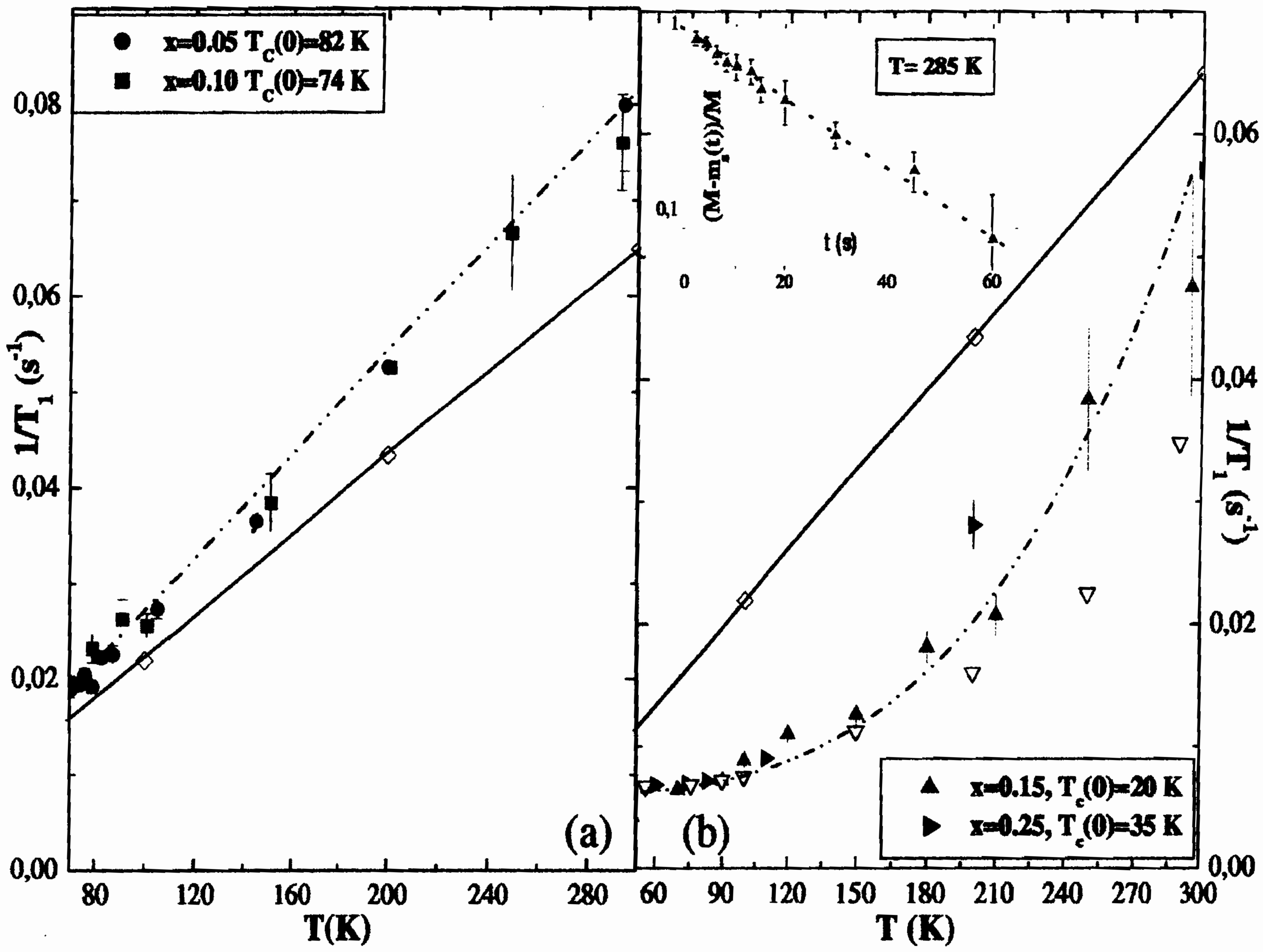

Figure 3.7: a) ^{89}Y NMR relaxation rate in the normal state, as a function of temperature, in the overdoped $Y_{1-x}Ca_xBa_2Cu_3O_{6,95}$ (part (a)) and underdoped $Y_{1-x}Ca_xBa_2Cu_3O_{6.1}$ (part (b)). The solid lines, in both graphics, represents relaxation rate according the theory from Ref. [88] for optimally doped YBCO, which yield a good fit of the experimental data (◇) by Nandor *et al.*[89]. The dashed line in part (a) is the best fit behavior of the data in overdoped compounds according to the law $T_1^{-1} \propto K_S^2 T$, in the hypothesis of K_S temperature independent (which is not correct, since a reduction of K_S by a factor about 15% from 100 K to 300 K occurs in overdoped compounds; see text and Fig. 3.5). In part b) the data ▽ for x=0.22 ($T_C(0) = 30$ K) are the ones reported in Ref. [29] and the dashed line tracks the effect of the spin gap opening occurring below about 350 K, in underdoped samples. In the inset a typical recovery plot detected in normal state is shown.

The echo dephasing time T_2 has been measured with the stan-

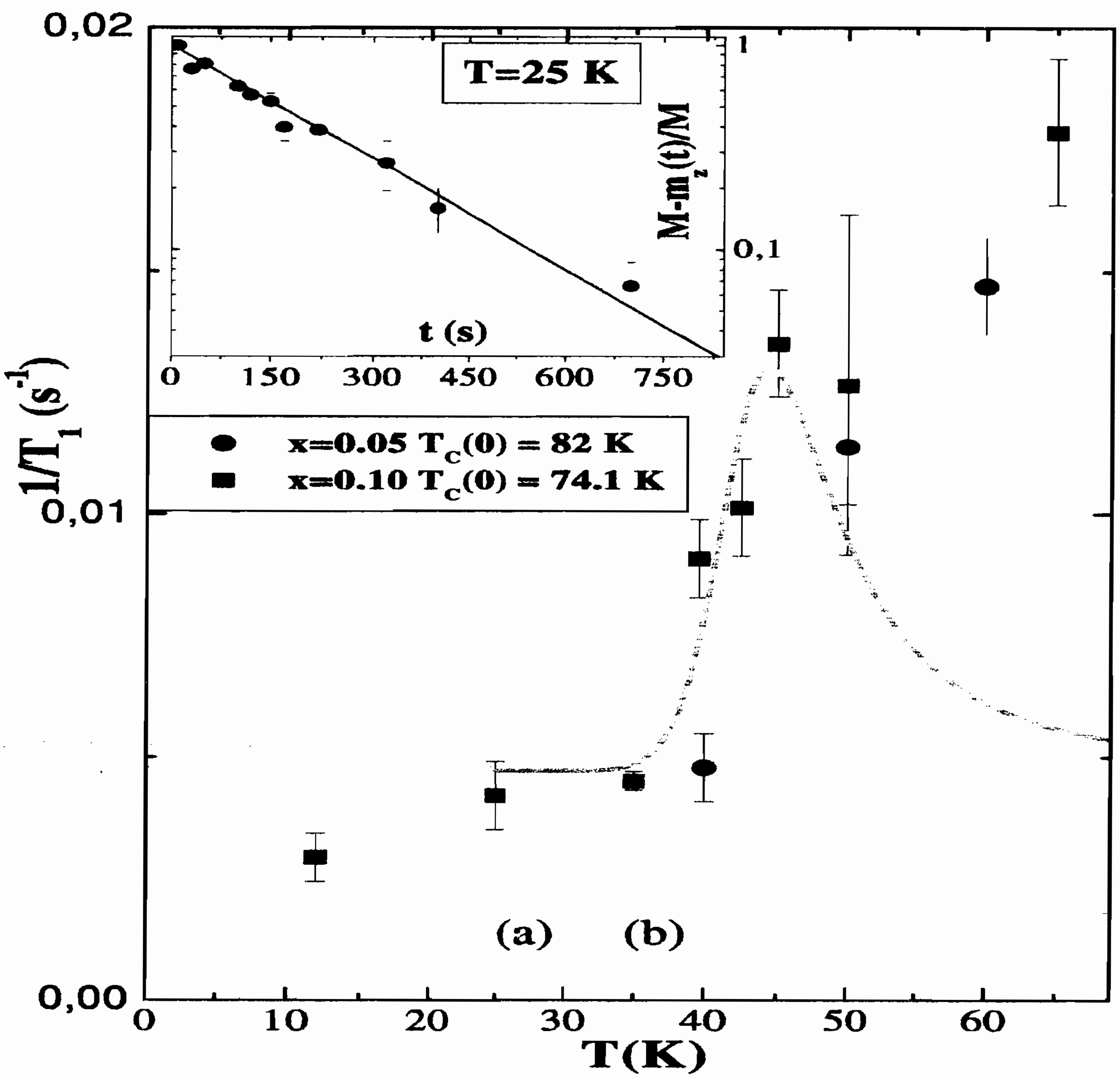

Figure 3.8: ^{89}Y relaxation rate, in the low temperature range in overdoped compounds. The inset evidences how the recovery law is a single exponential also below T_C in overdoped regime. The solid line is the sketchy behavior of contribution to the relaxation rate due to the thermal motions of flux lines, as qualitatively estimated from the data in Y124 (see Ref. [5, 95]).

dard $\pi/2 - \tau - \pi$ sequence and CPMG sequence. The results of T_2^{-1} as a function of temperature are reported in Fig. 3.11. It is worth noting that in CPMG T_2 measurements the suppression of the peak occurs, because the CPMG method filters out the dynamic contribution with characteristic time $\tau_z > \tau_m^{CPMG}$. In the inset the blowing of the $1/T_2$ data at low temperature better evidences a peak at $T \approx 7$ K and an increase for temperatures below

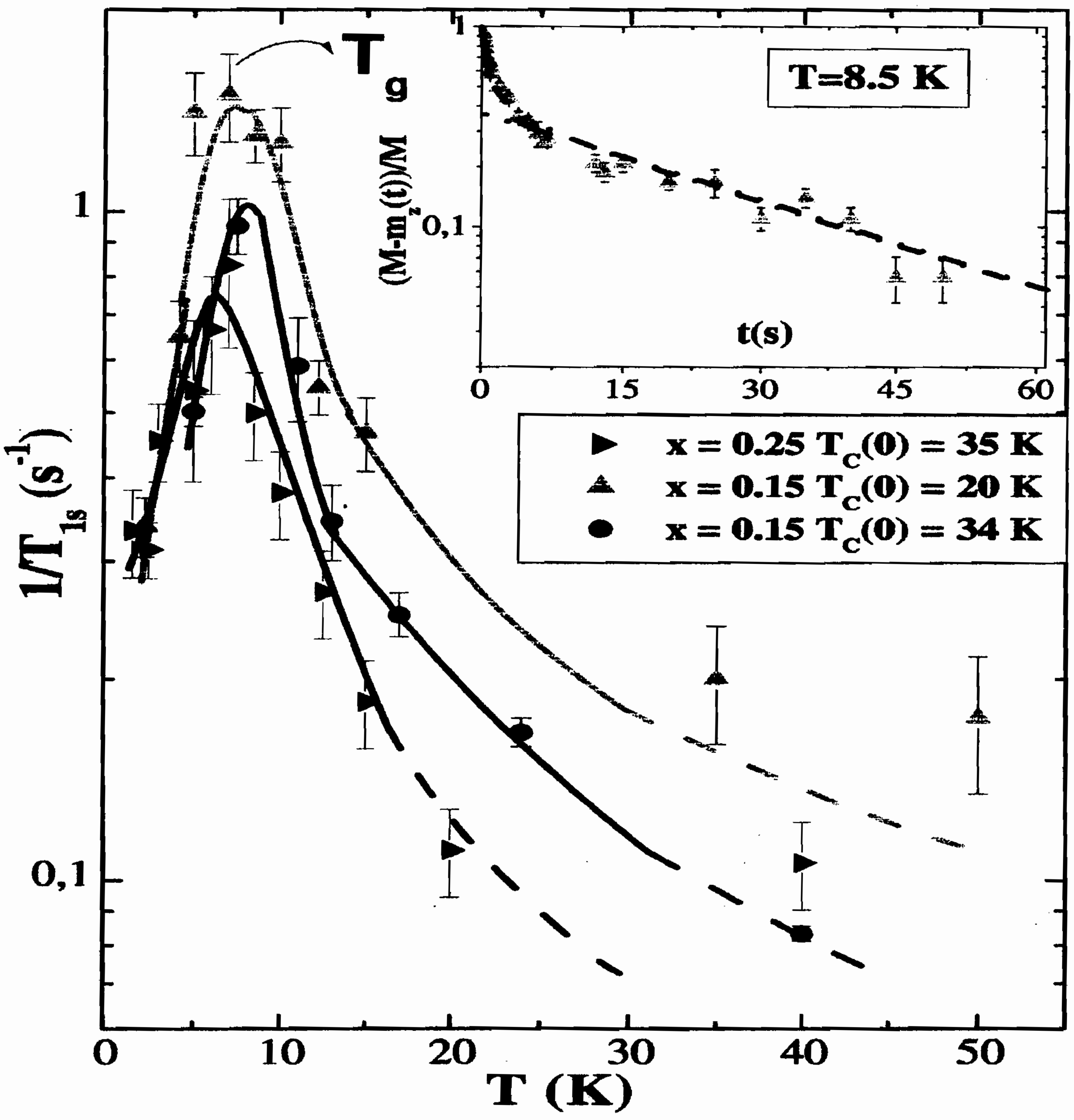

Figure 3.9: ^{89}Y relaxation rate, in the low temperature range of underdoped compounds. The inset evidences that in underdoped regime the fast-relaxing component to the recovery law is observed. T_{1s}^{-1} refers to the fast relaxing component of stretched exponential character (see inset), with T_{1s} taken as the value at which this component reduces to $1/\sqrt{e}$, where separation between fast and slow relaxing component was performed. The lines are guides for eyes.

4 K. In Fig. 3.12 the progressive change-over of the echo decay on cooling is shown. For fluctuation frequencies for the z-component of the local field of order of τ_m^{-1} the echo decay evidences a trend

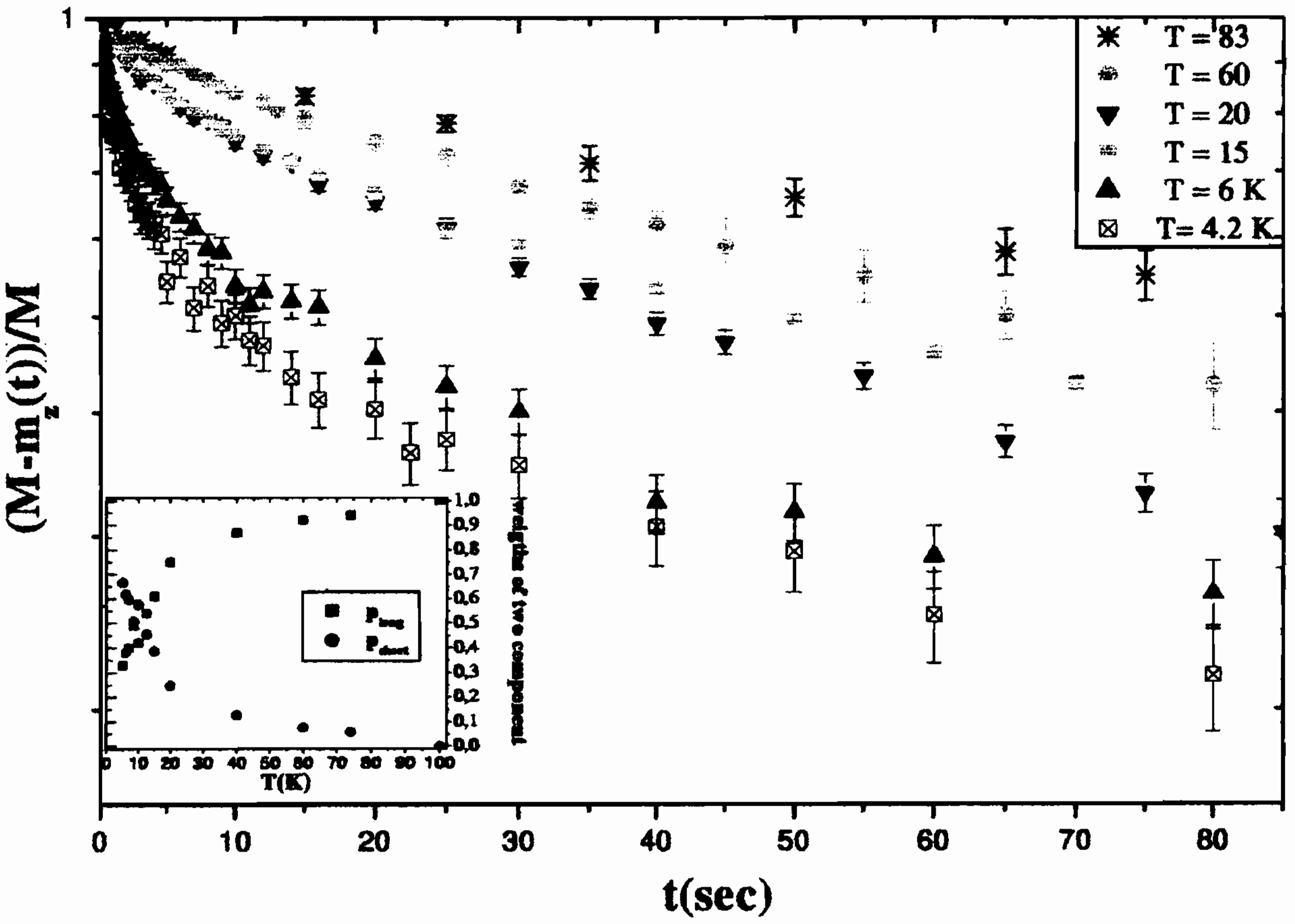

Figure 3.10: Comparison of the recovery laws at representative temperatures showing how they change on cooling. In the inset the weights of the fast and slow exponential components, as a function of temperature, are shown.

$\propto e^{-\left(\frac{\tau_m}{\tau_e}\right)^3}$, as expected in rigid lattice condition. Nevertheless, on further decrease of the temperature the echo decay changes again its form.

3.4 Analysis of the data and summarizing conclusions

The ^{89}Y NMR measurement allows one to investigate the whole phase diagram from underdoped to overdoped regime. By studying of characteristic NMR quantities as function of temperature in underdoped, optimally and overdoped compounds several phenomena have been pointed out[5]: the spin gap opening and the coexistence between superconductivity and magnetism in underdoped samples, the study of superconducting fluctuations above the critical temperature and the study of vortex lines and flux lines dynamics in

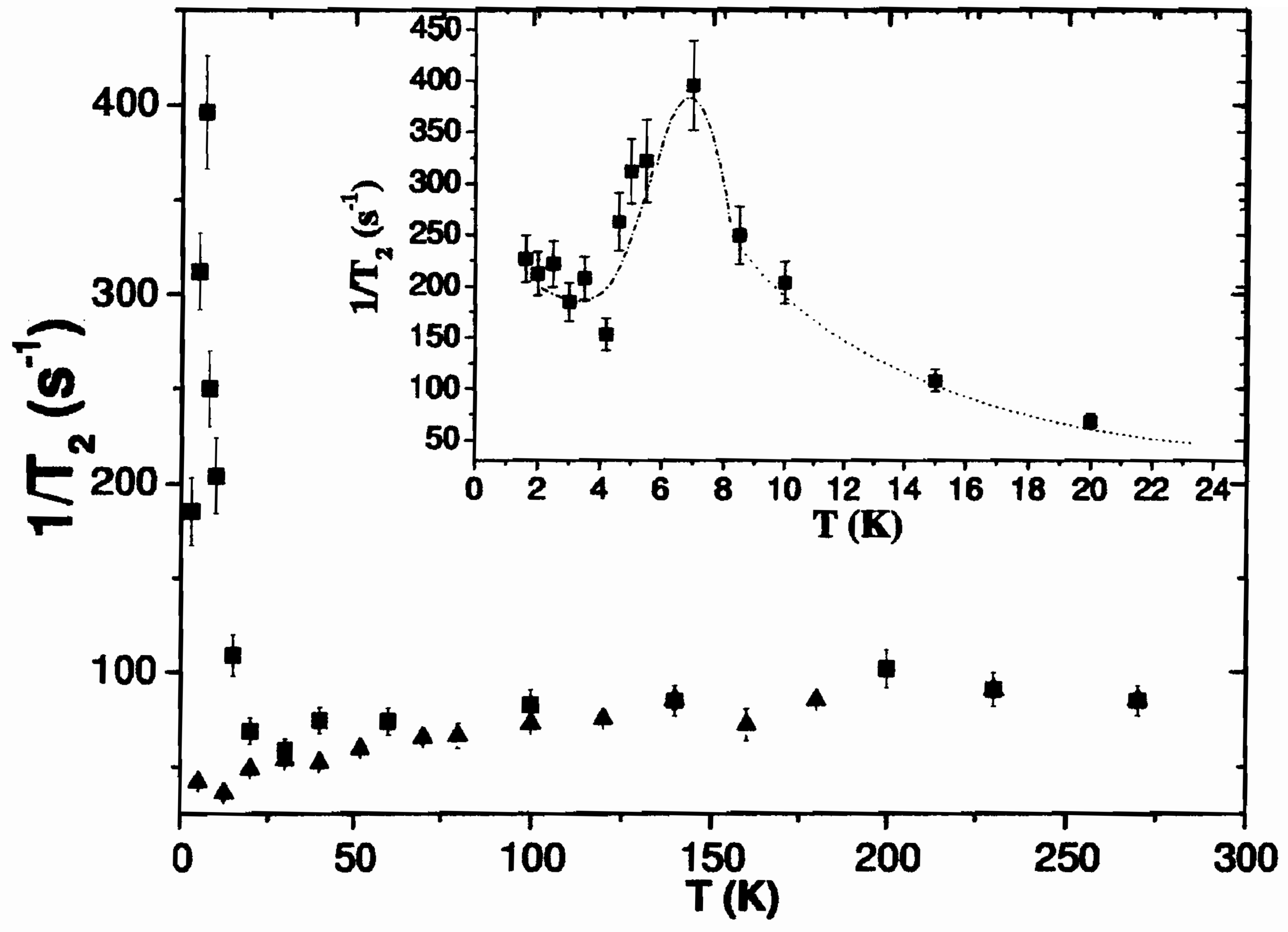

Figure 3.11: Inverse of the dephasing time of the spin echo in $Y_{0.75}Ca_{0.25}Ba_2Cu_3O_{6.1}$ for the Hahn (■) and for CPMG sequence (▲), as a function of temperature. In the inset the blow up of data for the Hahn echo in the low temperature range is shown.

superconductivity state. In this section an overview of the experimental results, presented in the previous Section, will be given. Two aspects will be broached in some details, the linear dependence of $(1/^{89}T_1)$ vs. T in overdoped and optimally doped compounds and the peak at low temperature for $(1/^{89}T_1)$ and $(1/^{89}T_2)$ in underdoped compounds.

Normal state

In the normal state of **underdoped** compounds, at temperature below T^* (that is $\sim$ 350 K), both T_1^{-1} and K_S decrease for decreasing temperature (see Fig. 3.5 and part (b) of Fig. 3.7). This departure from the linear temperature dependence of T_1^{-1} is in agreement with previous observations[84, 90, 86, 91, 92] and it has been ascribed to the spin-gap opening. For a Fermi-like spectrum of excitations, since $T_1^{-1} \propto \rho^2(E_F)$ (see Eq. 3.21), one could relate

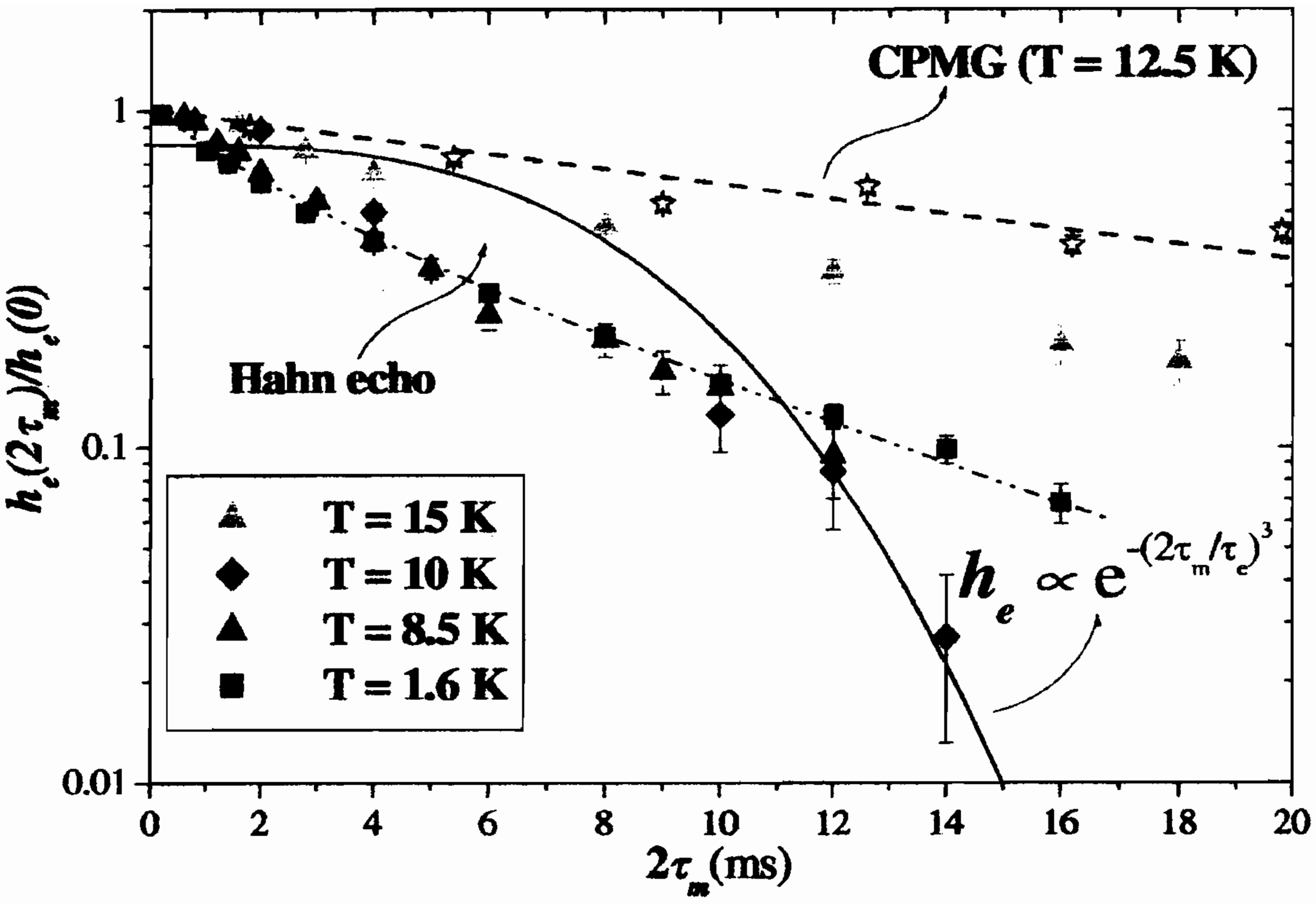

Figure 3.12: Normalized echo amplitude for representative temperatures. The echo decay changes progressively on cooling showing first a single exponential, then an exponential with cubic power, finally a stretched exponential law.

the spin-gap opening to a charge pseudo-gap, observed by means of various techniques[85]. However, the ^{89}Y NMR experimental findings indicate that a delocalized-carriers model can hardly be applied in the underdoped regime. Thus one is led to conclude that the spin-gap opening has to be related to a phenomenon of magnetic character, such as precursor superconducting fluctuations well beyond the Ginzburg-Landau scenario or antiferromagnetic fluctuations leading to a local situation similar to the one occurring in the parent AF, with a gap between the lower and upper Hubbard bands.

In **optimally** doped and **overdoped** compounds the relaxation rate depends linearly from temperature (see part (a) of Fig. 3.7). On the other hand this behavior does not agree with the Korringa law $\mathrm{T_1 T} \propto \mathrm{K_S^{-2}}$ (Eq. 3.22) since $\mathrm{K_S}$ in overdoped compounds is temperature dependent, decreasing by about $20 \div 25$ percent on increasing temperature from 80 K to 300 K (see Fig. 3.5) (a temperature independent contribution $\mathrm{K}_{0,\delta} \approx 150$ ppm is considered in this estimate). As mentioned in Sect. 3.2 the behavior of $\mathrm{K_S}$ has

been explained by Williams *et al.*[86] on the basis of a Fermi-gas like model for the density of states, including a peak growing in the overdoped regime (and a gap in the underdoped case) pinned at the Fermi level. This DC model, as qualitatively discussed in Ref. [87], cannot be used to analyze the data for T_1. On the basis of Eq. 3.15 $\rho_{vh}(E)$ was numerically extracted and by means of Eq. 3.21, T_1^{-1} has been evaluated. It was seen that T_1 should be more sensitive to the role of $(y\rho_{vh})$ than K_S. In recent papers Zavidonov *et al.*[88] have derived an expression for the generalized susceptibility that includes in a direct way the dependence on the extra hole concentration. In this theoretical picture[88] $\frac{\chi''_{\pm}(q,\omega)}{\omega}$ is not interpreted as arising from free holes but rather from collective excitations including charge and spin degree of freedom.
The data of ^{89}Y T_1 and K_S, shown in the previous Section, have been tested[96] with the theoretical behavior expected from Eq. 3.24 and χ_S and Γ_q from Ref. [88], in correspondence to a value $n_h = 0.21$ for hole concentration. The experimental behaviors are not very well reproduced (see Fig. 3.13). Only by altering the slope of K_S vs T to a certain extent, the temperature behavior of T_1^{-1} can be apparently well fitted, but in a limited temperature range.

Superconducting state

In the SC state the temperature dependence of T_1^{-1} in **overdoped** (and in **optimally** doped) YBCO (Fig. 3.8) substantially agrees with the one expected for spin-singlet and d-wave pairing, with a slight shoulder around $T \cong 50$ K which can be attributed to the flux-lines motions occurring around the irreversibility temperature. The behavior in **underdoped** compounds is dramatically different (Fig. 3.9). A sharp peak in T_1^{-1} is detected, with a maximum in the relaxation rate at $T_g \simeq 8$K, indicating that slowing down of the spin fluctuations in the range $\approx 20 \cdot 2\pi$MHz occurs. The recovery law is no longer a single exponential but rather turns to a stretched exponential. Therefore a further source of relaxation, superimposed to the usual one in the superconducting phase and not presented in overdoped samples, has to be taken into account. On general physical grounds, in view of the frequency and temperature dependence of T_1's and of the recovery law trend, one can write the relaxation

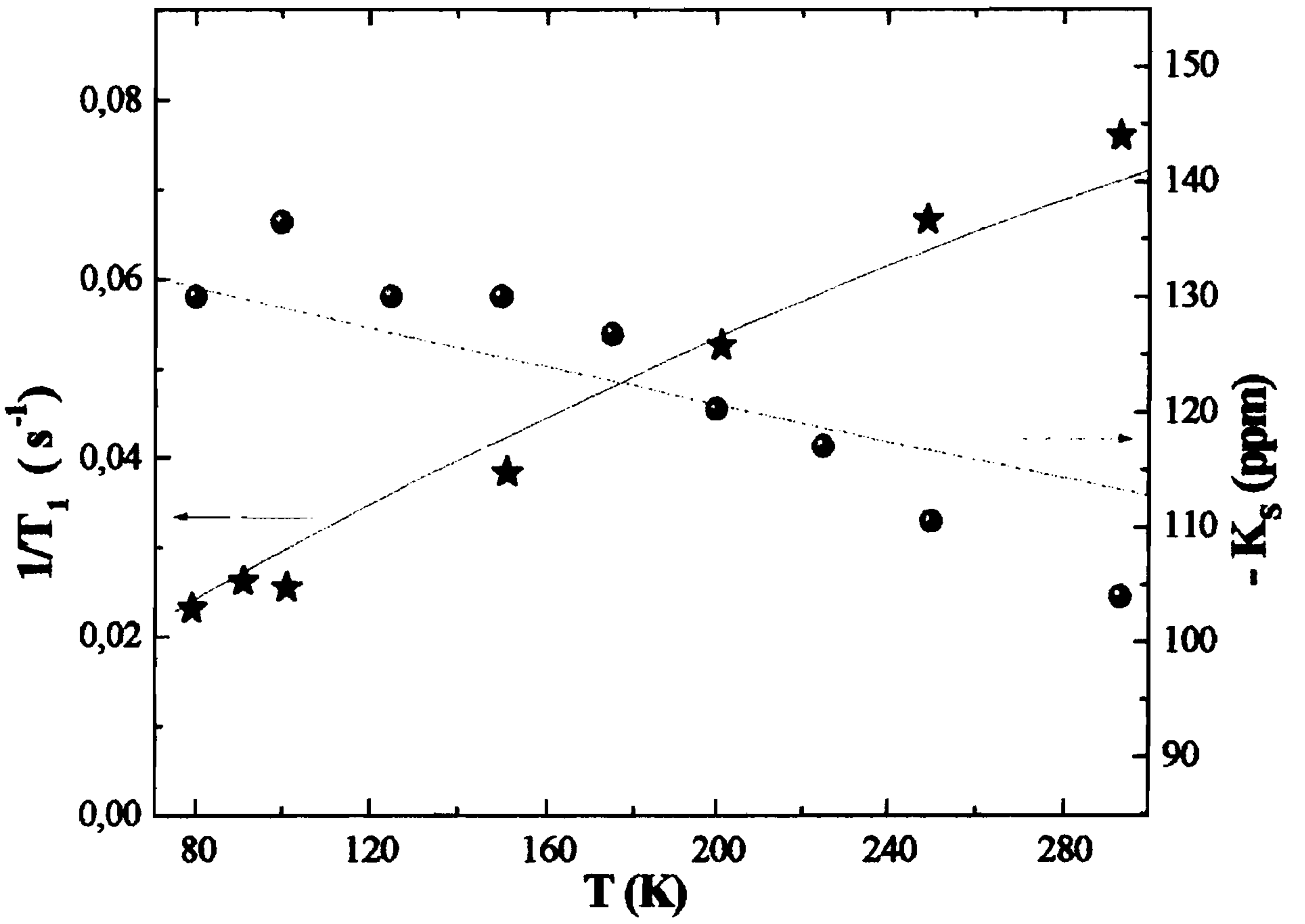

Figure 3.13: Tentative fits of T_1 and K_S on the basis of the generalized susceptibility given in Ref. [88] for $n_h = 0.21$.

rate (Eq. 3.20) in underdoped SC phase as follows:

$$2W = \gamma_n^2 < (h_\pm)^2 > j(\omega_m, \tau_e) \tag{3.25}$$

where $j(\omega_m, \tau_e)$ is the spectral density at $\omega_m = {}^{89}\gamma\ H_0$, and τ_e is the effective correlation time for transverse fluctuations of effective field at the nuclear site $\vec{h}_\pm$, with mean square amplitude $< (h_\pm)^2 >$. The stretched exponential recovery corresponds to

$$e^{-\left(\frac{t}{T_1^e}\right)^{\frac{1}{2}}} = \int_0^\infty p\left(\frac{1}{T_1}\right) e^{\left[-\frac{t}{T_1}\right]} d\left(\frac{1}{T_1}\right) \tag{3.26}$$

where $p\left(\frac{1}{T_1}\right) = \frac{T_1}{2\sqrt{\pi}\left(\frac{T_1}{T_1^e}\right)^{\frac{1}{2}}} e^{-\frac{T_1}{4T_1^e}}$ is a distribution function that can be related to the distribution of the energy barriers E and yielding an average correlation time

$$< \tau_e > = \tau_0 e^{\frac{<E>}{K_B T}}, \tag{3.27}$$

while

$$j(\omega_m,\tau_e)=\frac{<\tau_e>}{1+\omega_m^2<\tau_e>^2}. \tag{3.28}$$

In particular assuming a rectangular distribution of energy barrier, of width Δ, Eq. 3.28 can be written[97]

$$j(\omega_m,\tau_e)=\frac{1}{2\omega_m\frac{\Delta}{T}}\left[arctg(\tau_0\omega_m e^{\frac{(E+\Delta)}{T}})-arctg(\tau_0\omega_m e^{\frac{(E-\Delta)}{T}})\right] \tag{3.29}$$

In Fig. 3.14 the fit of the data in $Y_{0.75}Ca_{0.25}Ba_2Cu_3O_{6.1}$ according to this Equation in compared to the one for a single correlation time. From fit of the ^{89}Y T_1 data in the light of Eq.s 3.25-3.29 one can obtain

$$\tau_0\simeq 8\cdot 10^{-11}\ s, E=22\ \mathrm{K}\ \text{and}\ \Delta=16\ \mathrm{K} \tag{3.30}$$

The value of the average energy barrier for $Y_{0.85}Ca_{0.15}Ba_2Cu_3O_{6.1}$ is ~ 30 K (data not reported).

From the maxima in the relaxation rates (occurring at a temperature frequently indicated by T_g and called "spin-glass" freezing temperature) from Eqs. 3.25-3.28 one can extract the effective magnetic field at nuclear site

$$\sqrt{<h_\pm^2>}=\frac{1}{^{89}\gamma}\left(\frac{\omega_m}{T_1^{max}}\right)^{\frac{1}{2}} \tag{3.31}$$

In fact Eq.s 3.27 and 3.28 imply

$$j(\omega_m,<\tau_e(T_g)>)\simeq\frac{1}{\omega_m} \tag{3.32}$$

and substituting this result in Eq. 3.25, the Eq. 3.31 is obtained. For YBCO:Ca x=0.25 $\sqrt{<h_\pm^2>}\simeq 16$ Oe, for YBCO:Ca x=0.15 $\sqrt{<h_\pm^2>}\simeq 18$ Oe. It must be noted that while the average energy barriers are of the same order of the one in underdoped LASCO (see Ref. [98, 99] and Fig. 3.15), the effective field in Cu-O bilayer compounds is about an order of magnitude smaller than the one associated to a single "magnetic" layer. In fact $\sqrt{<h_\pm^2>}\simeq 150$ Oe in LASCO with x=0.1 (for experimental data see also Ref.

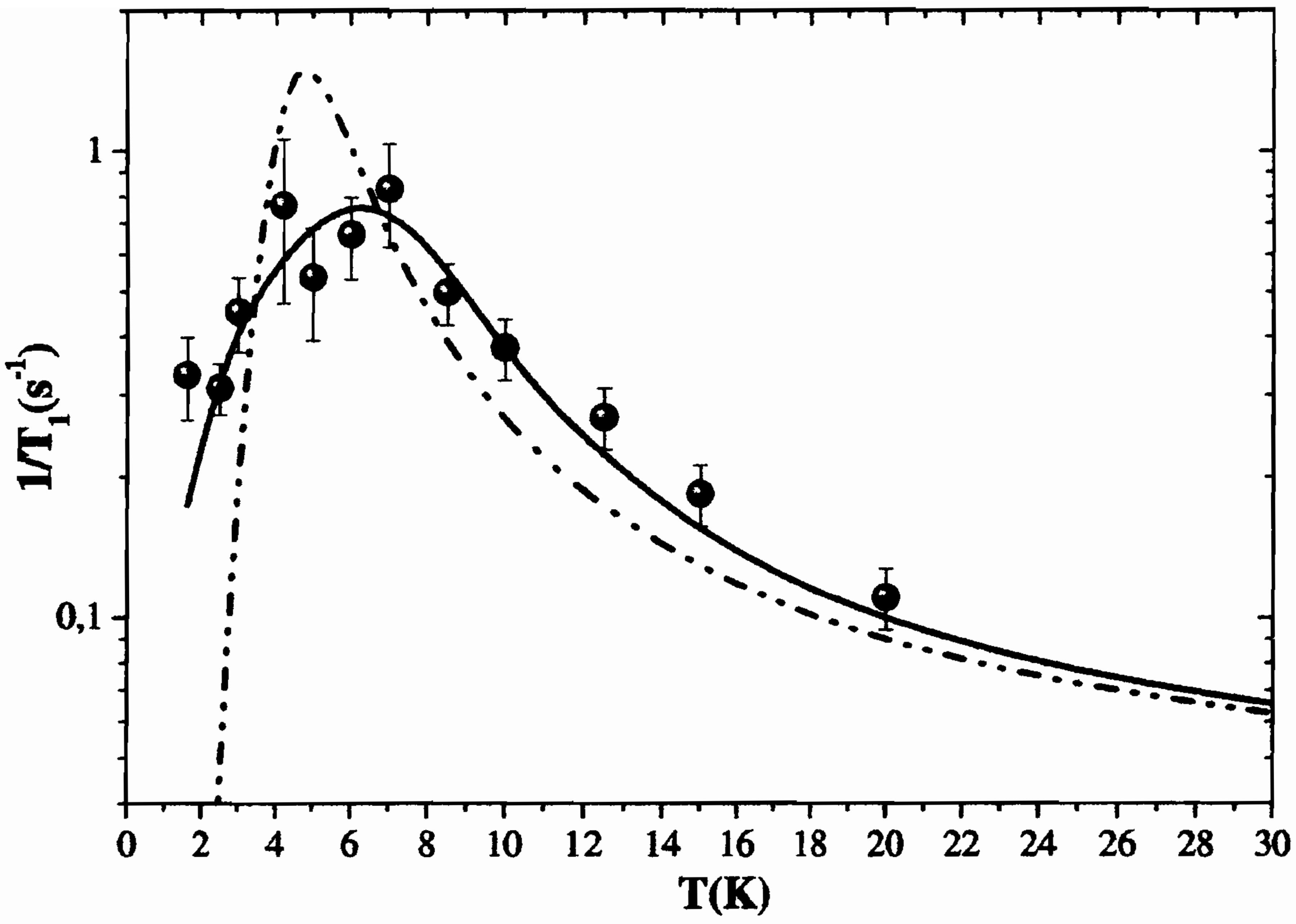

Figure 3.14: Fit of experimental results for T_1^{-1} in $Y_{0.75}Ca_{0.25}Ba_2Cu_3O_{6.1}$ for a single energy E (dashed line) and a rectangular distribution (solid line). The values derived from the solid line turn out $<E>= 22K$ $\Delta = 16K$ $\tau_0 = 5 * 10^{-10}$s.

[100, 101, 102]). For field generated by magnetic moments uncorrelated and approximately located onto the Cu-O plane, the field at the ^{89}Y nucleus should be larger than the one at the ^{139}La site by a factor around 2.5 (by assuming a dependence of the field from the inverse of third power of the distance). It is conceivable that the motion causing $h(t)$ must have opposite phases in the two planes of the bilayer compounds, thus yielding a kind of compensation at Y site. In other words in bilayer compounds the correlation between adjacent CuO_2 planes partially cancels out the effective fluctuating field at the Y site. From the data in Fig. 3.15 it appears that an external magnetic field, up to 23 Tesla, has practically no effect on the magnetic dynamics driving the relaxation process. This can immediately be realized by comparing the maxima in zero field (NQR) and in the field $H_0 = 23$ Tesla. The maxima approximately scale with the ratio of the measuring frequencies ($\omega_m \simeq 18$ MHz and $\omega_m \simeq 140$ MHz, respectively) in accordance to Eq. 3.27 for

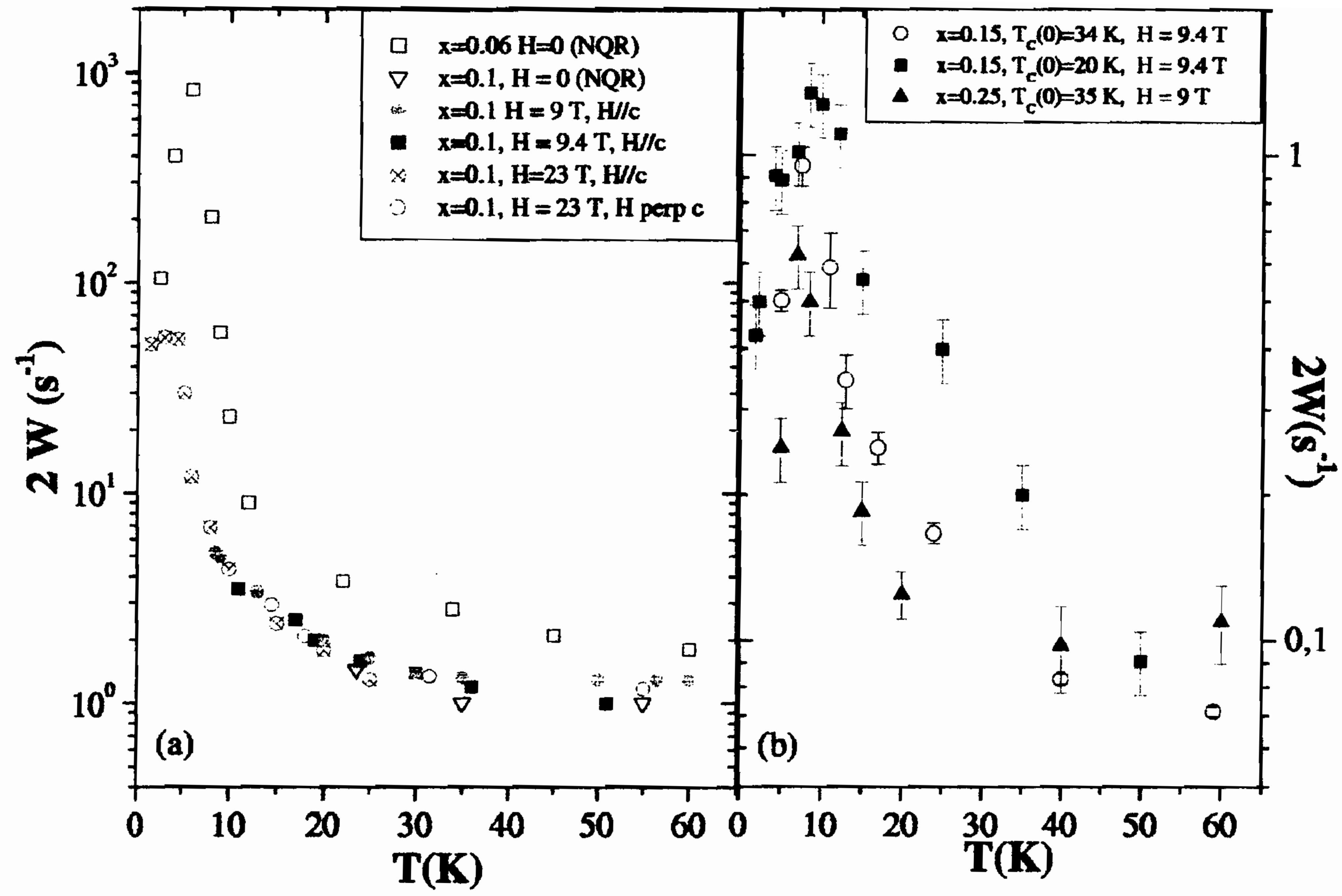

Figure 3.15: ^{139}La NMR-NQR relaxation rate in underdoped LASCO (single crystal) (part a) and ^{89}Y NMR relaxation rates in Ca-doped YBCO (part b). For LASCO samples the transition temperature $T_C(0)$ in zero field are $T_C(0) \approx 25$ K and $T_C(0) = 10$ K for Sr amount x=0.1 and x=0.06 respectively. For YBCO:Ca x is the Ca content (oxygen stoichiometry about 6.1, with some differences between the two samples at x $\simeq$ 0.15).

$\tau_e \simeq \omega_m^{-1}$. The magnetic field independence can hardly be justified if one assumes that the fluctuating fields $h(t)$ is due to magnetic dipoles. A field of 23 Tesla should introduce a marked anisotropy and then affect the spin dynamics in a considerable way, as it is known to occur for relaxation processes driven by the spin dynamics in ordered and in disordered systems.

In conclusion, one has to look for a source of fluctuating magnetic field that in a natural way implies a distribution of activation energies, activation energies of the same order in different compounds (namely YBCO and LASCO), phase relationship to grant compen-

sation of the effective field in between the Cu-O planes in bilayered compounds, independence from an external magnetic field.
These points can be explained assuming that the low energy spin excitations are not due to magnetic moments but rather related to sliding motions of orbital currents (id-CDW) coexisting with d-wave superconducting state. The phenomenological analysis given above is corroborated by the formal conclusions based on an extended t-J model including the Coulomb interactions[98]. In this description the hamiltonian is written

$$H = \sum t_{ij} \Phi_i^{pd,\sigma} \Phi_j^{\sigma,dp} + \frac{1}{2} \sum J_{ij} \left[s_i s_j - \frac{n_i n_j}{4} \right] + \frac{1}{2} \sum G_{ij} \delta_i \delta_j \tag{3.33}$$

where s_i is the number of extra-holes per unit cell and $\Phi_i^{pd,\sigma}$ ($\Phi_j^{\sigma,dp}$) the creation (annichilation) operator constructed on basis of singlet combination of cooper (d) and oxygen (p) states; J_{ij} is a measure of AF coupling between nearest neighbor sites i, j; t_{ij} is the hopping integral that describes the motion of electrons without causing a change in their spins; $n_i = \sum_\sigma \Phi_i^{\sigma\sigma}$, and the terms with G_{ij} is the Coulomb interaction. (For detail about this theory see Ref. [103, 104, 105]). The d-wave superconductivity can coexist with extend charge density wave (id-CDW), as shown in other works[106, 107, 108] and the correspondent ordered phase is a staggered pattern of orbital currents[109]. The quasi-particle damping resembles the situation in disordered superconductors, in agreement to nanoscale inhomogeneities (and then localization) which is known to occur in underdoped cuprates. From the fact that the relaxation rates are due to a progressive slowing down on cooling (with the slow motion condition below T_g) and not to a phase transition (see Ref. [98] for details) it can be concluded that the excitations are sliding currents motions. The current-current correlation functions are insensitive to the external magnetic field, since they involve correlation particle-hole type, proportional to the difference of Fermi functions with the same spin orientation. The stretched exponential character of the recovery law is the natural consequence of distribution in the pinning barriers for the sliding current motions. The strong reduction of the effective field at Y site compared to the value detected at the La site, is the consequence of the compensation due to the phase relationship of the currents circulating in the two $Cu - O_2$ planes of the bilayer YBCO compounds, as already mentioned.

Let us now discuss the results provided by the spin-echo dephasing measurements (Fig. 3.11). For $T \gtrsim 30$ K the data obtained from the Hahn or CPMG sequence practically coincide.

The difference between the Hahn and CPMG echoes dephasing time, at lower temperature, is a direct evidence, from a qualitative point of view, that some τ_z's have reached the range of milliseconds. In the low temperature region, where the spin lattice relaxation rate displays the peak around T_g, an enhancement of the decay rate of the Hahn echo around 8 K is observed, to be followed, below about 3 K, by an increase in T_2^{-1}. Correspondently, as it is shown in Fig. 3.12 the function $h_e(2\tau_m)$ shows significant changeovers. For $T \gtrsim 10$ K $h_e(2\tau_m)$ is practically exponential. Around $T \simeq 7$ K, where the maximum in the Hahn echo decay rate is detected, the decay function is about of the form $h_e(2\tau_m) \propto e^{-\frac{\tau_m}{\tau_e}^3}$. In the low temperature range, $T \lesssim 3K$, the function $h_e(2\tau_m)$ changes again to a form resembling the stretched exponential involved in the recovery law for T_1 below ~ 50 K.

Having obtained from the fitting of the T_1 data the temperature behavior of $\tau_e \equiv \tau_\pm$ (correlation time for the transverse fluctuation) (Eq.s 3.27 and of 3.30) one can first derive an estimate of the order of magnitude and the temperature behavior of the dynamical contribution to T_2^{-1} according to Eq. 3.7. By assuming $\tau_z \approx \tau_\pm$ and for $(\delta\omega_z)^2$ a value corresponding to effective field indicated by a fraction of the linewidth, say $\delta\nu \sim 1$ KHz, one realizes that the dynamical contribution to T_2^{-1}, according to Eq. 3.7, i.e. $\mathrm{T}_2^{-1} \approx (2\pi \cdot 10^3)^2\ \tau_0\ \mathrm{e}^{\frac{\mathrm{E}}{\mathrm{T}}} \approx 3.95 \cdot 10^7 \cdot\ 5 \cdot 10^{-10}\ \mathrm{e}^{\frac{22}{\mathrm{T}}}$, would become of the order of 100 s^{-1} only around 2.5 K, than rapidly increasing on cooling and flattening at $T \sim 1.2$ K. If the mean square value of fluctuating field $\sqrt{\langle h_z^2(t)\rangle}$ should be assumed of the order of the transverse one derived from T_1 data (15 Oe) again a value of $\mathrm{T}_2^{-1} \approx 200\ s^{-1}$ or more would be reached only below 3.5 K. The conclusion is that the slowing down of the spin dynamics causing the maximum in T_1^{-1} could be responsible of the slight increase in T_2^{-1} detected below about 2 K (see Fig. 3.11). The tendency to a stretched exponential for the decay function (Fig. 3.12) is a further support to this conclusion. Thus the peak in T_2^{-1} observed around 7 K has to be attributed to a spin dynamics different from the transverse one yielding the peak in T_1^{-1} at about the same temperature.

Extra peaks in the spin-echo dephasing rate have already been detected in optimally doped YBCO, around $T \simeq 30$ K (see Ref. [80] and references therein), including for NQR ^{63}Cu T_2, which would ruled out the hypothesis of a contribution due to vortex dynamics. In view of the complex phase diagram that has been argued to characterize the low temperature phases of underdoped cuprates, with a variety of low-energy excitations[111, 107, 106, 109, 110] one cannot disregard the hypothesis of the "extra peak" in T_2^{-1} indicative of a novel type of dynamics driving the transverse fluctuations of the local field at the Yttrium site. For our case, a "conventional" source of the peak in T_2^{-1} can be envisage in the vortex dynamics. In strongly underdoped YBCO124, the effective correlation time describing vortex motions has been proved[95] to diverge on cooling below T_C, reaching the msec range at about 10 K, with an (extrapolated) irreversibility temperature around 0.2 -0.3 T_C. For an order of magnitude estimate of the contribution to the echo decay from the vortex lattice motion one can write

$$(T_2^{-1})_{FL} \sim \gamma^2 < \Delta H^2 > \frac{2\tau_{FL}}{1 + (\frac{\tau_m}{\tau_{FL}})^2} \tag{3.34}$$

The maximum in $(T_2^{-1})_{FL}$ is expected at the temperature where τ_{FL} is of the order of the characteristic "measuring" time τ_m in the Hahn echo. Then a very small amplitude $\sqrt{\Delta H^2} \sim 0.2$ Oe of the dynamical ripple of the local field distribution accounts for the experimental results $(T_2^{-1})_{max} \sim 400\ s^{-1}$ at $T \simeq 7$ K (Fig. 3.11). One could also speculate that a temperature behavior of ^{63}Cu T_1 of the form similar to the one for ^{89}Y could induce a contribution to T_2^{-1} strictly analogous to the one observed at about 50-60 K in optimally doped YBCO[82]. It must be stressed that the measurements of ^{63}Cu T_1 are prevented in the low temperature range by shortening of T_2 (wipe-out phenomenon, see Ref. [100]).

Finally we comment about the line-width data, reported in Fig. 3.6. The broadening of the line initiates in a temperature range where no effects of the vortices nor "static" contribution from the slowing-down of the spin dynamics discussed above are active. As already pointed out[101, 29] it is feasible that the broadening results from a stripe-like modulation in a practically time-independent local field. This site dependent field in the neighbourhood of "stripes" prevents the occurrence of common spin-temperature, thus justifying the non-exponential recovery law in the spin-lattice and spin-spin relaxation measurements.

Appendices

Appendix A

Superconducting Diamagnetic Fluctuations in BCS superconductors: the example of MgB_2.

In this appendix a study of the fluctuating diamagnetism in MgB_2 by means of high resolution SQUID magnetization measurements is reported in order to allow the comparison between the behavior in BCS superconductors and in HT_CSC.

The fluctuating diamagnetism is strongly enhanced in high temperature superconductors with respect to conventional SC's because of the high temperature range and of the anisotropy of cuprates[1]. The fluctuating diamagnetism (FD) can be detected also in in low-temperature conventional BCS superconductors by means of SQUID magnetization measurements. The broadening of the transition due to SF and the effect of the magnetic field in quenching the fluctuating Cooper pairs has been studied by Tinkham[2] through measurements of M_{fl} at constant field as a function of temperature, in metals. From the measurements of M_{fl} vs T of Gollub et al.[42] one can actually deduce the occurrence of an upturn in the field dependence: for $H \ll H_{up}$ the diamagnetic magnetization increases with H while for $H \gtrsim H_{up}$ the field tends to suppress the fluctuating magnetization. Because of the relatively small value of M_{fl} in conventional BCS superconductors, the isothermal magnetization

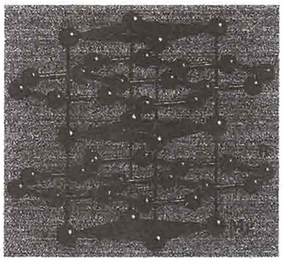

Figure A.1: Schematic MgB_2 crystal structure.

curves M_{fl} vs H could hardly be studied in detail in the past years. The recently discovered superconductor MgB_2[112], although being of conventional BCS character has two characteristics that enhance SF's and therefore the value of M_{fl} at $T = T_C(0)$: the high value of the transition temperature and an anisotropic spectrum of the fluctuations[43], similarly to cuprate superconductors as we shall see.

MgB_2 has a hexagonal crystal structure with boron layers interleaved by magnesium layers (see Fig. A.1) and may be regarded as layered having sheets of metallic boron with strong covalent intralayer bonding, separated by Mg layers with ionic interlayer B-Mg bonding. The strong B-B bonding induces strong electron-phonon interaction, so that the superconductivity in MgB_2 is mainly due to charge carriers in the boron planes. The sample we have investigated was prepared by Palenzona et al. (University of Genova), starting from high purity B and Mg powders, heated at 950 °C for 24 hs.

The zero field transition temperature of the sample is $T_C = T_C(0) = 39.07 \pm 0.04$ K, as estimated by FC magnetization curves at H = 1 Oe (see Fig. A.2).

The isothermal magnetization curves, $-M_{fl}$ vs H, in the temperature range $T_C(0) \lesssim T \lesssim T_C(0) + 0.5$ K, have been detected. Zero field cooled (ZFC) magnetization curves have been compared to field cooled (FC) data, obtained by cooling to a given temperature in the presence of different fields. The isochamp magnetization curves, $-M_{fl}$ vs T, in low field have been performed. A temperature-independent paramagnetic magnetization was detected in the range 100-40 K, yielding a volume Pauli susceptibility around 2×10^{-7}. The diamagnetic magnetization around T_C was

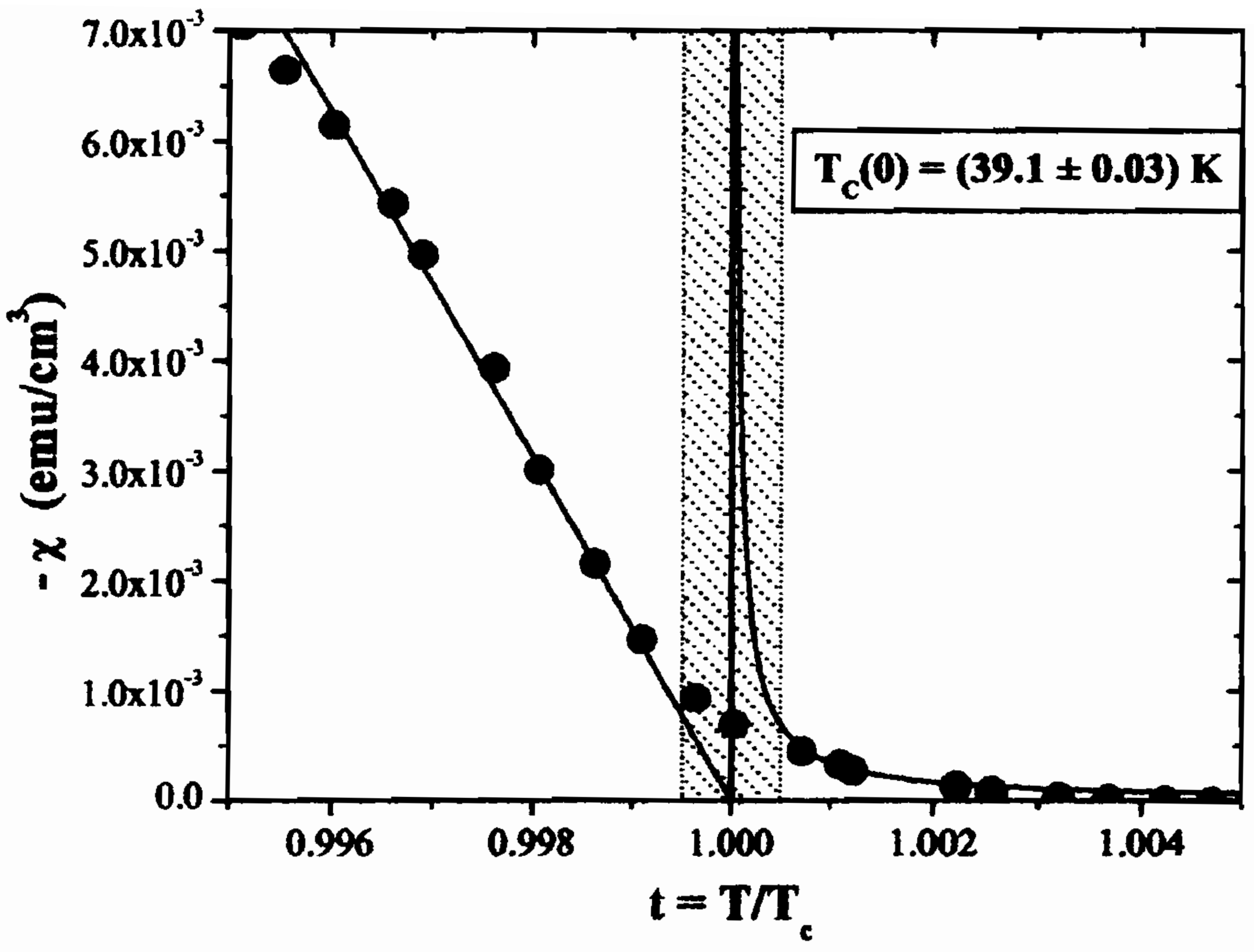

Figure A.2: $-\chi = -M_{fl}/H$ vs $t = T/T_C$ from FC magnetization at H = 1 Oe. For $T < T_C, \chi \propto (1-t)$, for $T > T_C, \chi \propto \frac{1}{(t-1)}$. The dashed area is approximately the region where the rounding of the transition occurs, because of the superconducting fluctuations.

obtained from the raw data by subtracting the paramagnetic magnetization, as well as the temperature-independent correction due to the sample holder.

Zero dimensional model and analysis of the isothermal magnetization curves

In Fig. A.3 the isothermal magnetization curves are shown. The departure from the results obtained in framework of GL model[2] (see Sect. 2.1.2), $M_{fl}(T = T_C) \propto H^{1/2}$ and $M_{fl}(T \gg T_C) \propto H$, valid in the limit of evanescent field, is evident. The upturn field $H_{\rm up}(T)$, as well as the maximum negative value reached by M_{fl} at $H_{\rm up}$, are functions of temperature. A simple qualitative justification of these experimental findings can be obtained assuming that the fluctuation-induced SC droplets are spherical, with a diameter of the order of the coherence length $\xi(T)$. It is noted that those droplets are the ones actually yielding the most effective diamagnetic screening[42].

The fluctuating diamagnetism (FD) due to metastable SC droplets of diameter 2R can be described on the basis of the London equation:

$$\nabla^2 \vec{h} = \frac{1}{\lambda^2} \vec{h}, \tag{A.1}$$

with

$$\lambda^2 = \frac{mc^2}{4\pi e^2 n_s}, \tag{A.2}$$

$n_s \equiv |\psi|^2$ (pair density). $\vec{h}$ represents the microscopic value of the magnetic flux density[1]. Applying the Eq. A.1 in a case of a spherical droplet one obtains

$$M \simeq -H_{ext} \frac{1}{40\pi} \frac{R^2}{\lambda^2}, \tag{A.3}$$

where λ can be derived by GL energy functional in Gaussian approximation neglecting the field. The cost in energy to produce one SC droplet is $E \approx \alpha |\psi|^2 \frac{4}{3}\pi R^3$, with $\alpha = \frac{\hbar}{2m\xi^2(T)} \propto \varepsilon$. Being $E \sim k_B T$ it results

$$|\psi|^2 \approx \frac{k_B T \xi^2(T)}{\frac{4}{3}\pi R^3 2m}, \tag{A.4}$$

from Eq.A.2

$$\lambda^2 = \frac{2m^2 c^2 \frac{4\pi}{3} R^3}{4\pi e^2 k_B T \xi^2(T)}. \tag{A.5}$$

From A.3:

$$\chi = \frac{M}{H_{ext}} = -\frac{1}{40\pi} \left[\frac{R}{\lambda}\right]^2 = \tag{A.6}$$

$$-\frac{1}{40\pi} \frac{3R^2 e^2 k_B T \xi^2(T)}{2m^2 c^2 R^3} \simeq -\frac{1}{10} \pi^2 \frac{k_B T}{\Phi_0^2} \frac{\xi^2(T)}{R}.$$

Thus smaller droplets imply large susceptibility. On the other hand droplets with $R \lesssim \xi(T)$ involve marked order parameter gradients

---

[1] It must be noted that the usual definition of the London penetration depth: $\lambda^2 = \frac{mc^2}{4\pi e^2 n_s}$ is identical to equation 2.4 considering $n_s \equiv |\psi|^2 \equiv \left(-\frac{\alpha}{\beta}\right)$. The London model is a phenomenological two fluid model in which the Maxwell equations are applied together with the definition of superconductor as a perfect conductor and the request of time-independent magnetic fields to describe the Meissner effect (see Eq. A.1 and see Ref. [2]). It is worth noting that the London theory does not take into account non local electrodynamic effects, consequently it can describe only superconductor with short coherence length (i.e. HTcSC).

and cause the free energy increase because of the kinetic terms in $F_{GL}[\psi]$ functional. Thus it can be concluded that the FD is, principally, due to droplets with $R \sim \xi(T)$.

It is possible to calculate in an exact way the free energy functional $F_{LG}[\psi]$ for all values of temperature T (including the critical region) and field H, ($H < H_{C2}$), in the assumption that to these droplets can be applied the *0-D approximation*, valid rigorously only for diameter $d << \xi(T)$.[2] In this case the order parameter ψ does not depend on the space variables so $\psi_0 = \psi\sqrt{V}$ (V=volume droplets), therefore the $\nabla\psi$ goes to zero. The whole effect of the magnetic field, choosing the gauge $\vec{\nabla} \cdot \vec{A} = 0$, is to decrease the critical temperature[1, 4]:

$$T_C(H) = T_C(0)\left(1 - \frac{4\pi^2\xi_0^2}{\Phi_0^2} < A^2 >\right). \tag{A.7}$$

where $< A^2 >$ is the average of A^2 over the sample volume.

In this case the free energy in the framework of GL can be written

$$\mathcal{F}[\psi(0)] = \alpha\left|\psi_0\right|^2 + \frac{\beta}{2V}\left|\psi_0\right|^4 \tag{A.8}$$

The partition function

$$\mathcal{Z}_0 = \int D[\psi]e^{-\frac{\mathcal{F}[\psi(0)]}{k_BT}} \tag{A.9}$$

in polar coordinates, is

$$\mathcal{Z}_0 = \pi\int d|\psi_0|^2 e^{-\frac{\left(\alpha|\psi_0|^2 + \frac{\beta}{2V}|\psi_0|^4\right)}{k_BT}} =$$

$$= \sqrt{\frac{\pi^3 V k_B T}{\beta}}\left[e^{x^2}(1 - \mathrm{erf}(x))\right]\Big|_{x=\alpha\sqrt{\frac{V}{2\beta k_BT}}}. \tag{A.10}$$

---

[2] It is worth noting that the zero dimensional case cannot be applied directly to the usual experimental situation, in which ψ is not constant over the sample volume and one or more sample dimensions are greater than ξ. However a macroscopic sample can be treated as composed of tiny, independent particles, whose size is limited by a correlation length of fluctuating, $\sim \xi$. In Ref. [113] the behavior of M_{fl} at constant field as a function of a temperature has been studied in aluminum particles of size less than 1000 Å(zero dimensional limit).

Above the critical region the asymptotic expression for the $\mathrm{erf}(x)$[3] can be used and one finds

$$F_0 = -k_B T \ln \frac{\pi\sqrt{2}}{\alpha_0\left(\varepsilon + \frac{4\pi^2\xi_0^2}{\Phi_0} < A^2 >\right)} \tag{A.12}$$

with $\alpha_0 = \frac{1}{4mT_C}\frac{1}{\xi_0^2}$ and $\alpha = \alpha_0\left(\varepsilon + \frac{4\pi^2\xi_0^2}{\Phi_0} < A^2 >\right)$, according to Eq. A.7.
For spherical particle

$$< A^2 >= \frac{1}{10} H^2 d^2 \tag{A.13}$$

and the expression for 0D fluctuating magnetization, valid for all fields $H < H_{C2}$, becomes

$$\begin{aligned} M_{fl}^{0D}(\varepsilon, H) &= -\frac{\partial F_0(\varepsilon, H)}{\partial H} = . \\ &= -\frac{k_B T \frac{2}{5}\frac{\pi^2\xi_0^2}{\Phi_0^2} d^2 H}{\left(\varepsilon + \frac{\pi^2\xi_0^2}{5\Phi_0^2} H^2 d^2\right)}. \end{aligned} \tag{A.14}$$

This Eq. can be extended by setting d equal to $\xi(T)$, in the consideration that the droplets of diameter $d = \xi(T)$ are those yielding the most effective diamagnetic screening as we have proved above. Then Then

$$M_{fl}^{0D} = -k_B T \frac{\frac{2\pi^2\xi_0^4}{5\Phi_0^2\varepsilon}}{\left(\varepsilon + \frac{\pi^2\xi_0^4 H^2}{5\Phi_0^2\varepsilon}\right)} H. \tag{A.15}$$

From this equation the value of field at which the magnetization has a minimum and the magnetization at that field turns out

$$H_{up} = \frac{\sqrt{5}\Phi_0\varepsilon}{\pi\xi_0^2} \tag{A.16}$$

---

[3] The error function

$$\mathrm{erf}(z) = 2\pi^{-\frac{1}{2}} \int_0^z e^{-y^2} dy \tag{A.11}$$

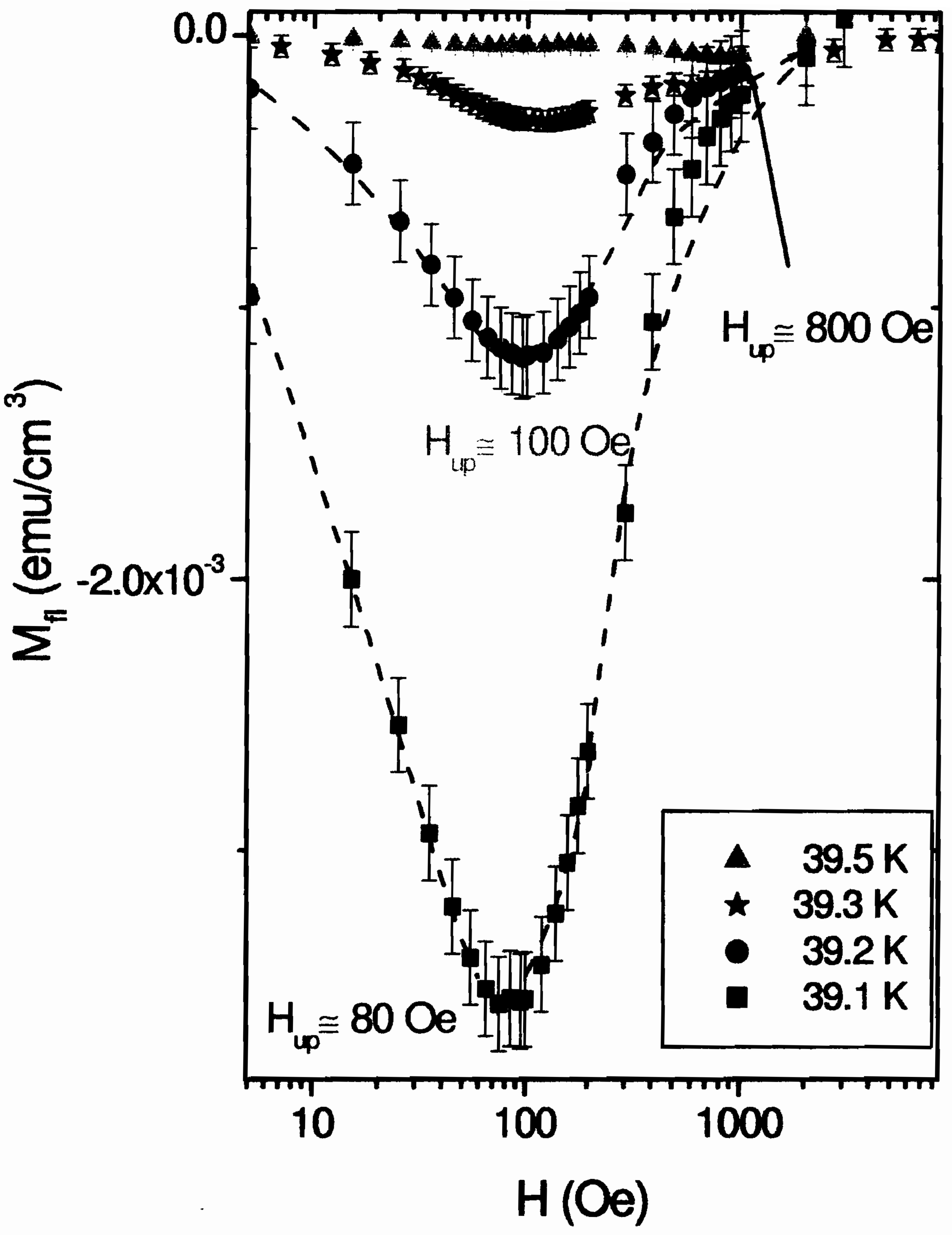

Figure A.3: ZFC isothermal magnetization curves in MgB_2 at different temperatures. While in the limit $H \rightarrow 0$ one has $-M_{fl}(T \simeq T_C) \propto H^{1/2}$ and $M_{fl}(T >> T_C) \propto H$, for field $H \gtrsim 100$ Oe the departure from the behavior expected in the framework of GL theories in finite field is dramatic. The dashed lines are guide for eye that qualitatively follow Eq. A.15-A.17.

$$M_{up} = -\frac{k_B T \pi}{\sqrt{5}} \frac{\xi_0}{\Phi_0} \varepsilon^{-1}. \qquad \text{(A.17)}$$

In Fig. A.3 the ZFC magnetization curves of MgB_2 are reported It must be noted that no difference is found between FC and ZFC magnetization curves.
It is worth noting that for $\xi(0) \simeq 5 \div 10$ Å and ε in the range $10^{-1} - 10^{-2}$, H_{up} is expected to be in the range of 10 Tesla. Thus the magnetization curves observed in YBCO samples (see Fig.s 2.6, 2.7) cannot be ascribed to the breakdown of the GL approach of the type commonly observed in BCS superconductors. Furthermore in those cases the value of H_{up} does not depend on temperature and ZFC-FC magnetizations are different.

Analysis of rescaled magnetization curves. Anisotropic spectrum of the superconducting fluctuations.

In Fig. A.4 the value of the scaled magnetization $m = -M_{\text{fl}}(T)/H^{1/2}T$ is reported as a function of the magnetic field. For $T \sim T_C$, $m_c = m(T = T_C)$ decays with the field and reaches half of the value $m(H \to 0)$ at about $H_s = 100$ Oe. For temperature far from $T_C(0)$ and small field, the magnetization tends to the linear increase with H and then $m \propto H^{1/2}$, while for larger H the departure from the behavior expected in the framework of Gaussian GL theories in finite fields is dramatic. In Fig. A.5 the scaled volume magnetization $m = -M_{fl}/H^{1/2}T_C$ versus the reduced temperature $\varepsilon = (T - T_C(0))/T_C(0)$ is reported, for MgB_2, and, for comparison, for optimally doped oriented powder of YBCO. The transition to the superconducting phase is very sharp (total transition width less than 0.2 K). Outside from the critical region below T_C, as expected[2, 42], m linearly decreases on increasing temperature, corresponding to a diamagnetic susceptibility going as $(1 - T/T_C(H))$. In the vicinity of $T_C(H)$ ($T \gtrsim T_C(H)$) the rounding of the transition due to critical fluctuations[42] originates an almost exponential temperature dependence for m.

In according to scaling arguments[43] (see Sect. 2.1.4), the Eq. 2.32 for 3D anisotropic system can be rewritten

$$m_c = \frac{M_{\text{fl}}(\mathrm{T_C})}{\sqrt{H} \cdot \mathrm{T_C}} = \frac{k_{\mathrm{B}}}{\Phi_0^{3/2}} \times m^{an}(\infty) = \frac{k_{\mathrm{B}}}{\Phi_0^{3/2}} \times (-0.324) \times \gamma \qquad \text{(A.18)}$$

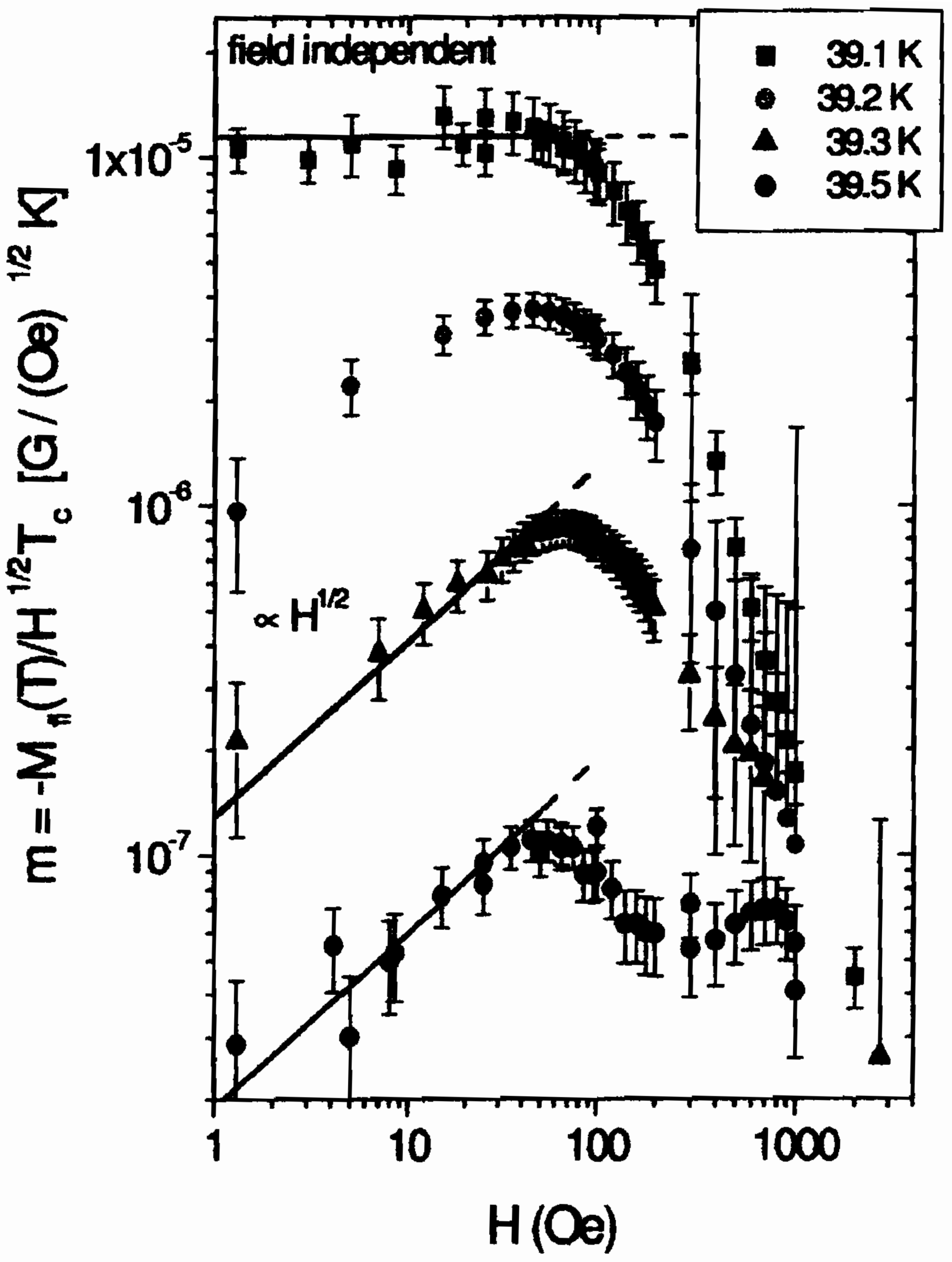

Figure A.4: Field dependence of the scaled magnetization at typical temperatures. For $T \simeq T_C$ (squares) the law $M(T_C) \propto H^{1/2}$ is verified, for $H \lesssim 50$ Gauss and for $T \gtrsim T_C + 0.2K$ (triangles and circles) one has $-M_{fl} \propto H$, again only for $H \lesssim 50$ Gauss.

where $\gamma = \xi_{\parallel}/\xi_{\perp}$ while the field should be along the c-axis[42, 114].

From the data for m reported in Fig. A.5 one sees that the results obtained in MgB_2 are consistent with a spectrum of SF with a strong enhancement factor. For a quantitative estimate, one can compare the value of m with the one in grain-oriented YBCO placed in magnetic field along the c-axis. It turns out that the absolute value of the scaled magnetization is slightly field dependent also in YBCO, where the crossing of $m(T)$ for different fields at $T_C(0)$ seems to be well verified[47] for $H \gtrsim 100$ Oe (see Fig. 2.4). While our data coincide with the one in Ref. [47] for H=1000 Oe, a sig-

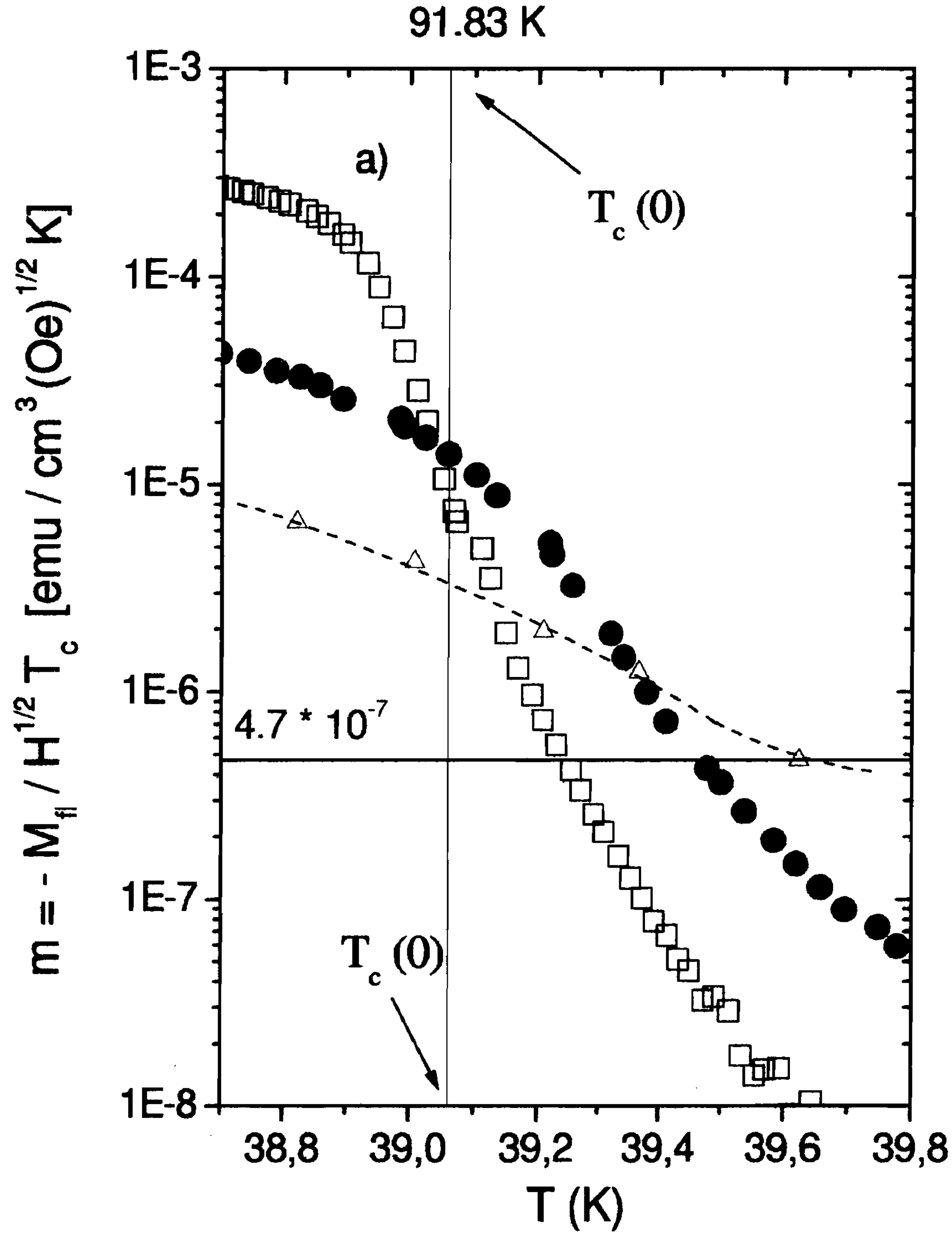

Figure A.5: Scaled magnetization $m = -M_{\text{fl}}/H^{1/2}T_C$ in MgB_2 around the superconducting transition temperature in a field of 1 Oe (empty squares), reported as a function of the reduced temperature $\varepsilon = (T - T_C(0))/T_C(0)$. For comparison (see text) the data in oriented powder of optimally doped YBCO for field along the c-axis are reported, for $H = 3$ Oe (full circles) and for $H = 1000$ Oe (empty triangles), with the dashed line for the eye. The value of the scaled magnetization expected at $T_C(0)$ for isotropic 3D systems and Gaussian fluctuations, 4.7×10^{-7}, is indicated.

nificative increase of m appear when the field is reduced to 3 Oe. By using our data in small field and comparing the results for m at $T_C(0)$ in powdered MgB_2 and in YBCO, where $\gamma \simeq 7$, in the light of Eq. A.18 one deduces an anisotropic factor of the same order in both cases. It should be remarked that the anisotropy degree of MgB_2 is still uncertain, with reports giving values unexpectedly large particularly for powders, ranging from 5 to 9[112]. Recent measurements of fluctuation conductivity show a two-dimensional nucleation in MgB_2[115],in accordance with the anisotropic spectrum of fluctuations.

Appendix B

The theoretical picture for the precursor fluctuating diamagnetism in underdoped and overdoped compounds.

In the following the theoretical description[72, 73] for phase fluctuations of the local order parameter in a layered liquid of vortices, by taking into account the presence of mesoscopic superconducting "islands" is given. The SC islands can be above or below the local irreversibility temperature and the relevant differences occur, as it will be shown.

The order parameter contribution to the free energy functional is

$$\mathcal{F}_{LD}\left[\theta\right] = \frac{1}{2a^2s}\sum_l \int d^2r \left\{ a^2 J_{\shortparallel} \left(\nabla_{\shortparallel}\theta - \frac{2ie}{c\hbar}\mathbf{A}_{\shortparallel} \right)^2 + J_{\perp}[1-\cos(\theta_{l+1}-\theta_l)] \right\} \tag{B.1}$$

where $J_{\shortparallel} = \dfrac{\pi\hbar^2 n_h}{4m_e}$ and $J_\perp = 2\pi\mathcal{J}n_h$ are the order parameter phase coupling constants on the plane and between planes respectively and s is the distance between layers.

The presence of superconducting droplets above the local transition temperature is assumed, and the phase of the order parameter can fluctuate, producing thermal excitations (vortex and antivortex pairs in 2D, vortex loops in anisotropic model). The potential vector $\mathbf{A}_{\shortparallel}$ in Eq. B.1 describes both the magnetic field applied parallel to the c - axis and the one induced by fluctuations. By following the 2D Coulomb gas theory, at each vortex is associated an effective charge $q_v = \sqrt{2\pi J_{\shortparallel}}$ and a vortex-antivortex pair has an energy $E_0 = q_v^2 \ln\left(\dfrac{\mathcal{L}}{\xi_{ab}}\right)$, playing the role of an activation energy and thus yielding Eq. 2.35. In order to refer to the anisotropic 3D model the vortex lines (or the vertical elements of the vortex loops) are correlated along the c - axis for a length $n_3 \cdot s$ and a correction to q_v will be found selfconsistently.

By considering, as usual, the partition function $Z = \int D\theta \exp(-\beta\mathcal{F}_{LD}[\theta])$ with $\beta = \dfrac{1}{k_B T}$, the susceptibility is

$$\chi = \frac{\partial M_{fl}}{\partial H} = \frac{\partial^2 F_{LD}}{\partial H^2} = \frac{1}{\beta}\left[\frac{1}{Z}\frac{\partial^2 Z}{\partial H^2} - \left(\frac{1}{Z}\frac{\partial Z}{\partial H}\right)^2\right] \tag{B.2}$$

Since

$$\frac{1}{Z}\frac{\partial Z}{\partial H} = -\beta \int \frac{\partial \mathcal{F}_{LD}}{\partial H} e^{-\beta\mathcal{F}_{LD}(\vartheta)} D\vartheta \equiv -\beta \left\langle \frac{\partial \mathcal{F}_{LD}}{\partial H} \right\rangle \tag{B.3}$$

and

$$\begin{aligned} -\frac{1}{\beta}\frac{1}{Z}\frac{\partial^2 Z}{\partial H^2} &= \int \frac{\partial^2 \mathcal{F}_{LD}}{\partial H^2} e^{-\beta\mathcal{F}_{LD}(\vartheta)} D\vartheta + \\ &-\beta \int \left(\frac{\partial \mathcal{F}_{LD}(\vartheta)}{\partial H}\right)^2 e^{-\beta\mathcal{F}_{LD}} D\vartheta = \\ &\equiv \left\langle \frac{\partial^2 \mathcal{F}_{LD}}{\partial H^2} \right\rangle - \beta \left\langle \left(\frac{\partial \mathcal{F}_{LD}}{\partial H}\right)^2 \right\rangle \end{aligned} \tag{B.4}$$

χ is obtained as the sum of three contributions

$$\chi = \left\langle \frac{\partial^2 \mathcal{F}_{LD}}{\partial^2 H} \right\rangle^2 - \beta \left\langle \left(\frac{\partial \mathcal{F}_{LD}}{\partial H}\right)^2 \right\rangle + \beta \left(\left\langle \frac{\partial \mathcal{F}_{LD}}{\partial H} \right\rangle \right)^2 \qquad \text{(B.5)}$$

where $\langle\rangle$ means the thermal average.

Choosing the gauge $A_z = 0$, z being the c-axis direction, $\vec{A}_{\shortparallel}(\vec{r}) = (-yH, 0)$ in the Fourier space: $\frac{\partial}{\partial H} = -\frac{i}{q}\frac{\partial}{\partial A}$ and $\frac{\partial^2}{\partial H^2} = +\frac{i}{q^2}\frac{\partial^2}{\partial A^2}$ and the homogeneous susceptibility is given by

$$\chi = \lim_{q \to 0} \frac{K(q)}{q^2} \qquad \text{(B.6)}$$

where[1]

$$K(q) = \frac{J_{\shortparallel}}{s}\left(\frac{2\pi}{\Phi_0}\right)^2 \left[\frac{J_{\shortparallel}}{k_B T}(P(q) - Q(q)) - 1\right] \qquad \text{(B.7)}$$

In fact

$$\left\langle \frac{\partial^2 \mathcal{F}}{\partial A^2} \right\rangle = -\frac{J_{\shortparallel}}{s}\left(\frac{2\pi}{\Phi_0}\right)^2 \qquad \text{(B.8)}$$

$$\left(\left\langle \frac{\partial \mathcal{F}_{LD}}{\partial A} \right\rangle \right)^2 \equiv \frac{J_{\shortparallel}}{s}\left(\frac{2\pi}{\Phi_0}\right)^2 Q(q) \qquad \text{(B.9)}$$

$$\left\langle \left(\frac{\partial \mathcal{F}_{LD}}{\partial A} \right)^2 \right\rangle \equiv \frac{J_{\shortparallel}}{s}\left(\frac{2\pi}{\Phi_0}\right)^2 P(q) \qquad \text{(B.10)}$$

In Eq. B.7 $P(q)$ involves the current-current correlation function

$$P(q) = \frac{1}{NL^2} \sum_{l,l'} \int d^2\rho \int d^2\rho' e^{[i\vec{q}\cdot(\vec{r}-\vec{r}')]} \qquad \text{(B.11)}$$
$$\left\langle \left(\nabla_x \theta_l(\rho) - \frac{2\pi}{\Phi_0} A_{\shortparallel,x}(\vec{r}) \right) \left(\nabla_x \theta_{l'}(\rho') - \frac{2\pi}{\Phi_0} A_{\shortparallel,x}\left(\vec{r}'\right) \right) \right\rangle$$

---

[1] In Eq.8, 9b, 10b of the paper in Ref. [72] there are typing errors. The corresponding corrected Equations are B.7, B.12, B.17

with N representing the number of layers and $L^2 = \pi R_d^2$, R_d being the average radius of the superconducting islands, with coordinate $\vec{r} = (\vec{\rho}, ns)$.

The x-component of the phase gradient is given by the same expression used in magnetostatics in order to calculate the magnetic field of a system of current loops and lines:

$$\nabla_x \theta_l(\rho) = s \sum_{m_1, l_1} \frac{y - R_y(m_1, l_1)}{\left| |\vec{\rho} - \vec{R}(m_1, l_1)|^2 + s^2 (l - l_1)^2 \right|^{3/2}} t(m_1, l_1), \tag{B.12}$$

where $t(m_1, l_1) = \pm 1$ and $\vec{R}(m_1, l_1)$ labels the position of each "pancake" m_1 on the layer l_1.

Three terms are obtained by the evaluation of Eq. B.11: $P_{\theta\theta}(q)$, $P_{AA}(q)$ and $P_{\theta A}(q)$ (the two terms due to the correlation between $\nabla_x \theta$ and $A_{\shortparallel, x}$ give the same contribution being $P_{\theta A}(q) = P_{A\theta}(q) = P_{\theta A}(-q)$). The first one involves the positional correlation function of the vortex line elements. In order to calculate it, Sewer and Beck[60] introduced the static structure factor of a disordered vortex liquid. Because of the weak interlayer coupling harmonic deviations of the vortex lines (or loops) along the z direction are taken into account. This model can be used to describe also the vortex system in the glassy phase, below the irreversibility line temperature and therefore the same expression for $P_{\theta\theta}(q)$ is used here. It must be noted that in the theory in Ref. [60] χ depends only on the regular part of structural factor. The cross correlation between $\nabla_x \vartheta$ and $A_{\shortparallel, x}$ are supposed to vanish due to the disordered structure of the vortex system above the melting temperature. But if there are SC droplets this disordered structure is not random and the cross correlation between phase and field is not zero. One has

$$P_{\theta\theta} = \frac{4\pi^2}{q^2} S(q) =$$

$$\frac{4\pi}{q^2} \left\{ \underbrace{N^2 \left(\frac{L^2 H}{\Phi_0} \right)^2}_{S(q=0)} + N L^2 n_v S_c(q) [1 + 2 \cdot X(q)] \right\} \tag{B.13}$$

where S(q) is the structural factor defined by

$$S(q) = \sum_{s,n,s',n'} t(s,n)t(s',n') \left\langle e^{\{i\vec{q}\cdot[\vec{R}(s,n)-\vec{R}(s',n')]\}} \right\rangle \tag{B.14}$$

n_v is the areal density of vertical vortex-line elements, and $S_c(q)$ is the 2 D Coulomb gas structural factor. Then

$$P_{\theta\theta} = \frac{4\pi}{q^2} \left\{ N^2 \left(\frac{L^2 H}{\Phi_0} \right)^2 + \right.$$

$$\left. +NL^2 n_v \underbrace{\frac{q^2}{q^2 + \frac{2\pi n_v q_v^2}{k_B T}}}_{S_C(q)} \cdot \left[1 + 2 \underbrace{\frac{1 - e^{\frac{-k_B T n_3 s^2 \gamma^2}{4 J_{\shortparallel}} q^2}}{e^{\frac{k_B T s^2 \gamma^2}{4 J_{\shortparallel}} q^2} - 1}}_{X(q)} \right] \right\} \tag{B.15}$$

The first step to evaluate the regular part of $S(q)$ is to consider the extreme limit of totally decoupled layers, treating the vortex structure as a neutral two-component Coulomb gas (given by an equal number of thermal vortices and antivortices) plus a one component gas (the field induced vortices) in a neutralizing background (given by the external flux). The second step is to assume that a single vortex line in position s' in layer n is correlated with a vortex line in s' with $n' \neq n$. Furthermore the correlation is the same for all vortex line s' and extends only over a distance $\xi_3 = n_3 s$ (weak coupling). Finally the vortex lines behave like harmonic strings with an effective stiffness given approximately by $\approx \frac{J_\perp}{s} \equiv \frac{J_{\shortparallel}}{s\gamma^2}$.
The evaluation of the term $P_{AA}(q)$ is straightforward:

$$P_{AA}(q) = \frac{\pi^2}{36} (\frac{HL^2}{\Phi_0}) L^2 q^2 \tag{B.16}$$

The further contribution $P_{\theta A}(q)$, appearing due to the cross correlation between $\nabla_x \theta$ and $A_{\shortparallel,x}$ (and disregarded in Ref. [60]), cannot be neglected below the vortex lattice melting temperature, where irreversibility effects occur. In this case one obtains

$$P_{\theta A}(q) + P_{\theta A}(-q) = 2\frac{sH}{L}\frac{(2\pi)^2}{\Phi_0}\left(\frac{Lq\cos\frac{Lq}{2} - 2\sin\frac{Lq}{2}}{q^2}\right)$$

$$\sum_{l,l'} e^{(-qs|l-l'|)} \cdot \left\langle \sum_{m_1,l_1} t\left(m_1, l_1\right) \cos\left[iql_1 R_y\left(m_1, l_1\right)\right] \right\rangle .$$

The thermal average is performed in the assumption that the vortices are uniformly distributed in the planes (the detail of calculus is in note[2]):
$\left\langle\sum_{m,l} t\left(m,l\right) \cos iqlR_y\left(m,l\right)\right\rangle = \sum_m t(m) < \cos qR(m) >= \frac{HL^2}{\Phi_0} - q^2\frac{L^4H}{24\Phi_0} + o(q^3)$. The expansion of $P_{\theta A}(q)$ in powers of qL gives

$$P_{\theta A}(q) = -\frac{2\pi^2}{3}\left(\frac{HL^2}{\Phi_0}\right)^2 + \frac{2L^2}{45}\pi^2\left(\frac{HL^2}{\Phi_0}\right)q^2 \qquad \text{(B.17)}$$

The function $Q(q)$ in Eq. B.7, related to the third term of Eq. B.5, again neglected in Ref. [60], can be calculated, yielding

$$Q(q) = (2\pi)^2\left(\frac{HL^2}{\Phi_0}\right)^2\left[\frac{1}{q^2L^2} + \frac{1}{144\times 4}q^2L^2 + \frac{1}{12}\right] \qquad \text{(B.18)}$$

---

[2] To derive Eqs. B.17 and B.18 the following thermal average must be calculated: $\left\langle\sum_{m,l} t\left(m,l\right) \cos iqlR_y\left(m,l\right)\right\rangle = \sum_m \langle t(m)\rangle - \frac{1}{2}q^2\sum_m < R^2(m) > +o(q^3)$. Indicating with N_+ (N_-) the number of vortex line elements parallel (antiparallel) to the field the first term gives $N_+ - N_- = \frac{HL^2}{\Phi_0}$. The sum in the second term can be split in two parts which separately count the vortex line elements parallel and antiparallel to the field: $\sum_m t(m) < R_y^2(m) >= \sum_{m+} < R_y^2(m) > - \sum_{m-} < R_y^2(m) >$. One can assume that the vortices are uniformly distributed in the planes and that the y components of their positions are distributed on a line, separated each other by a distance $\Delta L = \frac{L}{N_+}$.Then, the $i-$th vortex is in the mean position $< R_i >= \Delta L i = \frac{\Delta L}{N_+}i$, with $i = -\frac{N_+}{2}\cdots\frac{N_+}{2}$. $\sum_{m_\pm} < R(m_\pm)^2 >= \sum_{i=-\frac{N_\pm}{2}}^{\frac{N_\pm}{2}} \frac{L^2}{N_\pm^2}i^2 = \frac{L^2}{12N_\pm}\left(N_\pm + 2\right)\left(N_\pm + 1\right)$. By considering $N_\pm >> 1$ one finally finds $\sum_m t(m) < R_y^2(m) >\approx \frac{L^2}{12}(N_+ - N_-)$. Then the first equation in this note can be written $\sum_m t(m) < \cos qR(m) >= \frac{HL^2}{\Phi_0} - q^2\frac{L^4H}{24\Phi_0} + o(q^3)$

It should be noted that the first term in Q, diverging for $q \rightarrow 0$, exactly cancels out the q^{-2} term in the expansion of $P_{\theta\theta}(q)$ which appears from the structure factor.

By using Eqs. B.16, B.17, B.18 and Eq. B.5 from B.7 one finally obtains

$$K(q) = \frac{J_{\parallel}}{s}\left(\frac{2\pi}{\Phi_0}\right)^2\left[\frac{2\pi J_{\parallel}}{q_v^2}(1+2n_3) - \left(\frac{H}{H^*}\right)^2\delta - 1\right] +$$

$$\left\{-\frac{k_B T}{s\Phi_0^2}\frac{1}{(1+2n_3)}\left[1+\left(\frac{H}{H^*}\right)^2\delta\right]^2\left[\frac{1}{n_v}+\frac{s^2\gamma^2(1+n_3)}{\left[1+\left(\frac{H}{H^*}\right)^2\delta\right]}\right] +\right.$$

$$\left.+\frac{47\pi R_d^2}{540}\frac{J_{\parallel}}{s}\left(\frac{2\pi}{\Phi_0}\right)^2\left(\frac{H}{H^*}\right)^2\delta\right\}q^2 \qquad \text{(B.19)}$$

with $\delta = \frac{3\pi^2}{4}\frac{J_{\parallel}}{k_B T}$ and $H^* = \frac{\Phi_0}{\pi R_d^2}$ is an effective "critical" field depending on the island size (for $T \geq T_{irr}$ the numerical factor is $\pi^2/3$, γ is the anisotropic factor defined by $\gamma = \frac{J_{\parallel}}{J_{\perp}}$.

To avoid unphysical divergences in the calculation of the susceptibility from Eq. B.6, the first term in square brackets of Eq. B.19 has to be zero, giving a renormalization of q_v due to both the anisotropy of the system and the presence of applied magnetic field. Then

$$q_v^2(H) = \frac{q_v^2(1+2n_3)}{\left[1+\left(\frac{H}{H^*}\right)^2\delta\right]}. \qquad \text{(B.20)}$$

In view of the field-dependent vortex charge, the pair energy (in the limit $H < H^*$) becomes

$$E = \frac{E_0}{\left[1+\left(\frac{H}{H^*}\right)^2\delta\right]}. \qquad \text{(B.21)}$$

Thus the thermally-excited vortex pair density turns out slightly field dependent. This field dependence, formally derived here, is significantly different from the one assumed in Ref. [60].

Finally the diamagnetic susceptibility is obtained in the form

$$\begin{aligned}\chi \;=\;& -\frac{k_B T}{s\Phi_0^2}\frac{1}{(1+2n_3)}\left[1+\left(\frac{H}{H^*}\right)^2\delta\right]^2\left\{\frac{1}{n_v}+\frac{s^2\gamma^2(1+n_3)}{\left[1+\left(\frac{H}{H^*}\right)^2\delta\right]}\right\}+\\ &+\frac{47\pi R_d^2}{540}\frac{J_{\parallel}}{s}\left(\frac{2\pi}{\Phi_0}\right)^2\left(\frac{H}{H^*}\right)^2\delta \end{aligned} \qquad \text{(B.22)}$$

The main differences between this susceptibility in Eq.B.22 and the one given in Ref. [60] consists in the presence of the factor $\left(\frac{H}{H^*}\right)^2$ and of the third, positive term. This term can cause an inversion in the sign of the susceptibility corresponding to an upturn in the magnetization curves. This phenomenon depends on the dimension of the islands and $\chi = 0$ (i.e. the occurrence of the upturn) requires $R_d > R_0$ where R_0 depends on some characteristics of the material. It must be reminded that the inversion in the sign of the susceptibility is related to the third term in Eq. B.22 and thus to the term $P_{\theta A}(q)$, since the amount of impurities and/or imperfections acting as nucleation centers might also play a role.

Appendix C

Effect of the magnetic field on the superconducting fluctuations as reflected in the NMR relaxation rate.

In the Chapter 2 the fluctuating diamagnetism when the transition temperature T_C is approached from above (T_C^+) has been studied by means of the analysis of the diamagnetic susceptibility χ_{dia} as a function of temperature and field. The role of the superconducting fluctuation (SF) on the spin susceptibility χ_{spin}, pertaining to itinerant carriers in AF correlation, in principle can be studied through nuclear spin-lattice relaxation and from Knight shift (K_S) measurements.
In this appendix an overview of the studies about the field dependence of SF, as observed in the dynamical spin susceptibility $\chi(\vec{q}, \omega)$ in the high temperature superconductors of the YBCO family, is given.
In particular the effect of the magnetic field on the density states (DOS) contribution to the relaxation rate W is analyzed in some more detail. In the first part of this Appendix some expressions already used in Chapter 3 are rewritten, taking into consideration also ^{63,65}Cu nucleus. Then the effects of SF on the NMR quantities are described through an heuristic interpretation of the theoretical results obtained with the diagrammatic techniques. The experimental results recently obtained in optimally doped YBCO are

reviewed and discussed.

General expressions for the relaxation rate and shift in $\mathrm{HT_CSC}$

The electronic properties of metals and superconductors can be explored through the hamiltonian

$$H_{hyp} = \hbar\gamma_n \sum_J \vec{I}_n \hat{A}_J \vec{S}_J \qquad (C.1)$$

coupling a given nucleus n to the on-site and to the neighboring electronic spin $\vec{S}_J$. $\hat{A}$ includes a scalar isotropic term A_{iso} and an anisotropic dipolar term $\hat{A}_{dip}$. In $\mathrm{HT_CSC}$ the longitudinal and transverse components of $\hat{A}$, for nuclei such as Cu, O, Y, La etc. are presently rather well known (see Refs. [5, 116]). In the presence of a magnetic field H_0, or of spontaneous ordering, one has $\langle S\rangle_{H,T} \neq 0$ and therefore a further magnetic field at the nucleus arises, implying the Knight shift, K_S, of the NMR (or NQR) frequency. The Knight shift, originally introduced as due to the spin contributions from delocalized electrons in metals, in HT_CSC is often generalized to include all the contributions from $\langle S\rangle_{H,T}$. By neglecting the temperature independent chemical shift and the effect of the demagnetization field, one can write

$$(K_S)_{\alpha\alpha} = \frac{1}{g\mu_B} \sum_J \left(\hat{A}_J\right)_{\alpha\alpha} \chi_{spin} \qquad (C.2)$$

with $\chi_{spin} = \frac{\chi_{mole}}{N_A n}$, χ_{mole} molar susceptibility in cm^3/mole, and n number of magnetic units (e.g. $\mathrm{CuO_2}$ in $\mathrm{HT_CSC}$) in the unit cell, N_A Avogadro number. In terms of dynamical generalized susceptibility $\chi(\vec{k},\omega)$ in Eq. C.2 one has

$$\chi_{spin} = g^2\mu_B^2\chi'(k=0,\omega=0) \qquad (C.3)$$

where the static homogeneous susceptibility includes $S(S+1)/3$. In the framework of models where delocalized carriers are considered, interaction among carriers is taken into account within the usual RPA (Random Phase Approximation). Then

$$\chi'(k=0,\omega=0) = \frac{1}{4}\frac{\rho(E_F)}{\left[1-\frac{1}{2}\mathcal{I}\rho(E_F)\right]} \qquad (C.4)$$

where $\rho(E_F)$ is the density of states at Fermi level (per unit cell) and $\mathcal{I} \equiv \mathcal{I}_{\mathrm{q}=0}$ is the coupling constant between electrons.
The time-dependent part of the hyperfine Hamiltonian C.1 drives the nuclear spin-lattice relaxation through the fluctuations of the local "field" at nucleus related to $\vec{S}_j(t)$. A general expression for the relaxation rate is

$$W = \frac{1}{2}\hbar k_B T \gamma_n^2 \cdot \sum_{\vec{k}} \left[A_{xx}(\vec{k})A_{xx}(-\vec{k}) + A_{yy}(\vec{k})A_{yy}(-\vec{k})\right] \cdot \cdot \frac{\chi''_{\pm}(\vec{k},\omega_0)}{\omega_0} \tag{C.5}$$

where ω_0 can be the electronic or the nuclear frequency, z is the quantization axis (H_0 for NMR, V_{zz} for NQR) and

$$A_{\beta\beta}(\vec{k}) = \sum_J (A_J)_{\beta\beta} e^{-\vec{k}\cdot\vec{r_J}} \tag{C.6}$$

is the Fourier transform of the transverse components of $\hat{A}$. In the limit $\omega_0 \longrightarrow 0$ one has

$$\frac{\chi''(\vec{k},\omega)}{\omega} \approx \frac{\chi''(\vec{k},0)}{\Gamma_{\vec{k}}} = \frac{|S_{\vec{k}}|^2}{k_B T}\frac{1}{\Gamma_{\vec{k}}} \tag{C.7}$$

when $\Gamma_{\vec{k}}$ is the decay rate of the collective spin fluctuations.

Physical picture of the NMR effects due to SF.

From the definition of SC current density $\vec{J} = 2e|\psi|^2\frac{\hbar}{m}\vec{\nabla}\vartheta$, the paraconductivity can be derived in the form[4]

$$\sigma_{fl} = \frac{(e^*)^2}{2m}\sum_{\vec{k}} < |\psi_{\vec{k}}|^2 > \tau_{\vec{k}} \tag{C.8}$$

When compared to Drude conductivity $\sigma_D = (e^2/m)n_e\tau$, one sees that $< |\psi_{\vec{k}}|^2 >$ plays the role of the density of carriers with correspondent life time $\tau_{\vec{k}}$ instead of electron collision time, τ. One could remark the similarity of Eq. C.8 to the expression for NMR-NQR relaxation rate in the vicinity of a phase transition, namely

$W \propto \sum_{\vec{k}} < |\psi_{\vec{k}}|^2 > /\Gamma_{\vec{k}}$, where $\psi_{\vec{k}}$ is the collective component of the critical variable and $\Gamma_{\vec{k}}$ is a decay rate. (It should be noted that the above expression holds only in the limit $\omega_{NMR} \ll \Gamma_{\vec{k}}$ and different component of $\chi''(\vec{k}, \omega)$ are actually involved in σ_{fl} and in W).

In principle there are three relaxation processes involving the fluctuating pairs. One can discuss them within a Fermi liquid scenario, without specifying the electron-electron interaction (the only requirement is that the charge and spin excitations are of fermionic character). This approach has been proved successful in describing several quantities affected by SF[1]. The direct and most singular contribution, with a direct correspondence to the idea of a fluctuating pair, is the **Aslamazov-Larkin (AL)** one. It contributes to σ_{fl} but it is ineffective for the nuclear spin-lattice relaxation. In fact, if a given electron of a fluctuating pair reverses its spin to cause nuclear relaxation, then is no longer possible to assign a spin label to the pair.

The **Maki-Thompson (MT)** contribution results from a purely quantum process and it can be seen[117] as implying the pairing of electron with itself at a previous stage of motion, along intersecting trajectories. It requires diffusive motion and in principle it might be thought very sensitive to pair-breaking mechanism as, for instance, a magnetic field. A negative SF term comes from the **density of states (DOS) reduction** when electrons are subtracted to create pairs. In the following a heuristic description of the way the above mentioned SF terms affect NMR quantities is given. The formal derivation of these effects by diagrammatic techniques is given in Ref. [1] and in the references reported therein.

From Eqs. C.2, C.3 and Eq. C.4 (with $\mathcal{I} = 0$ for simplicity) and by taking into account that from 2D integration of Eq. 2.10 the number of fluctuating pairs per unit volume is

$$n_C = \sum_k \left\langle |\psi_{\vec{k}}|^2 \right\rangle = 2n_e \frac{T_C}{T_F} \ln \frac{1}{\varepsilon} \tag{C.9}$$

while $\chi(0,0) = \frac{n_e - 2n_C}{E_F}$. The Knight shift in the presence of SF and the limit of negligible field can be then written

$$K_S^{SF} \propto \chi^0(0,0) \left[1 - 2\frac{T_C}{T_F} \ln \frac{1}{\varepsilon}\right] \tag{C.10}$$

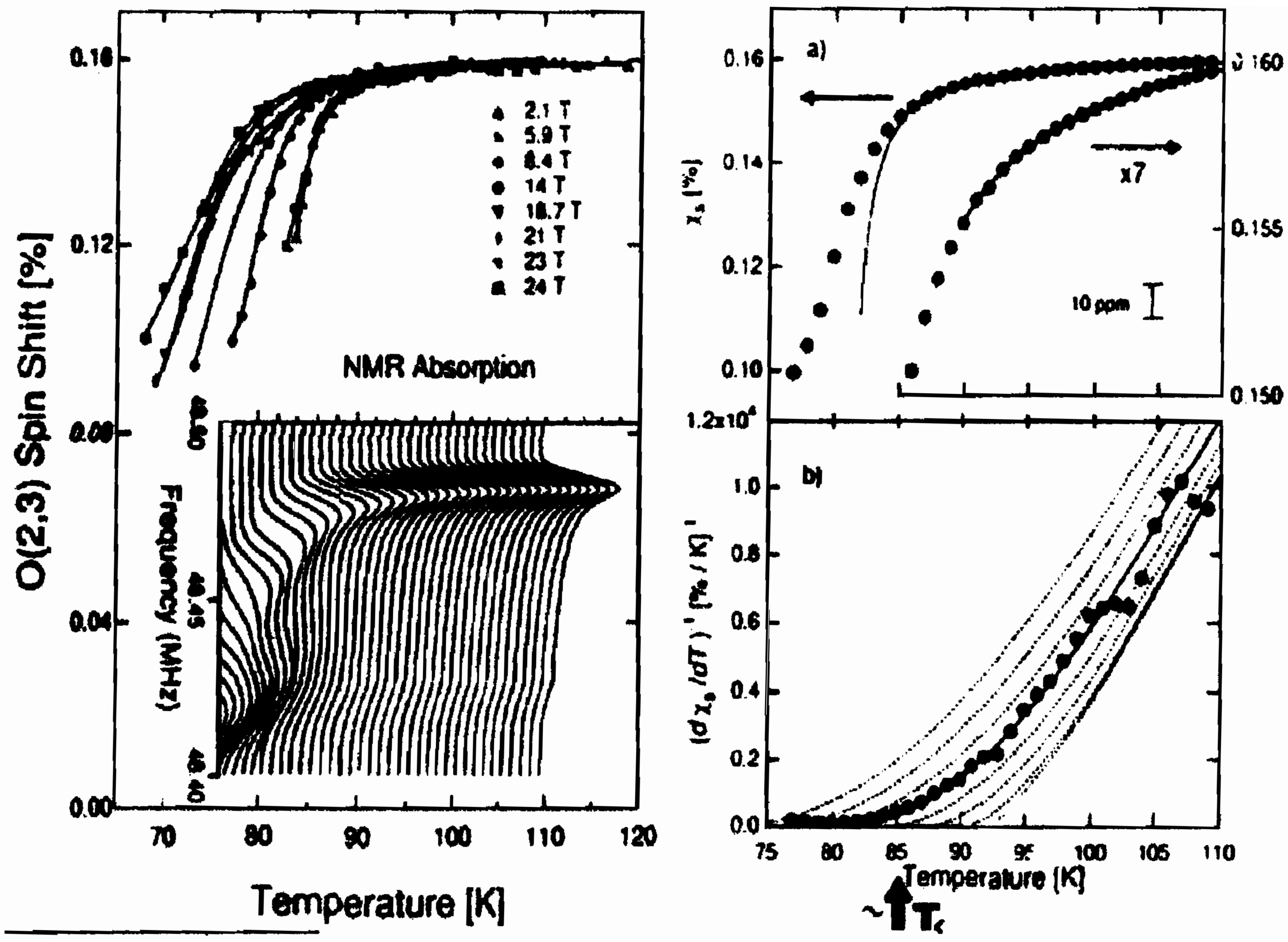

Figure C.1: ^{17}O NMR spectra in YBCO and deduced temperature behavior of the spin susceptibility for $T \to T_C^+$ showing the reduction due to DOS contribution from SF. (Ref. [118]).

with $\varepsilon = (T - T_C(0))/T_C(0)$. It is noted that the field H is necessary to carry out the measure and in principle one should expect a field-dependence of the correction term to the spin susceptibility $\chi^0(0,0)$ in the absence of SF in Eq. C.10. Only one experimental evidence of the correction to K_S in the vicinity of T_C seems to be found in the literature[118] (Fig. C.1). From ^{17}O NMR high resolution spectra in $YBa_2Cu_3O_7$, in fields ranging from 2.1 up to 24 Tesla, and from the smooth crossover in K_S close to $T_C(H)$, a field-dependent SF contribution to the spin susceptibility has been claimed. In part b) on the right side of the figure it is shown how the 2D regime of SF, implying $\left(\frac{d\chi_{spin}}{dT}\right)^{-1} \propto (T - T_C(H))$, is abandoned for $T \leq 96$ K. The theoretical interpretation of the data in Fig. C.1 has been given by Bachman et al[118]. It can be observed that their data can be qualitatively justified by Eq. C.10, when a field-effect in suppressing the SF and/or a crossover of 2D fluctuations towards a 3D regime is assumed to occur.

In regards of the "dynamical" effects involving the life time , the *DOS contribution* to the spin-lattice relaxation rate can be obtained by 2D integrating Eq. 2.16, taking into account Eq. 2.15. Then[117, 45]

$$\left\langle \tau^{DOS} \right\rangle = \sum_{\vec{k}} \frac{\tau_{GL}}{1+\xi^2 k^2} = \hbar\rho(E_F)\frac{1}{4}\left(\frac{\hbar}{E_F\tau}\right)\ln\frac{1}{\varepsilon} \qquad \text{(C.11)}$$

(τ electron collision time). In Eq. C.11 one notes the correction to the Fermi-gas effective correlation time $\hbar\rho(E_F)$.
The *MT contribution* corresponds to the integration of a decay rate of diffusive character on approaching the critical temperature at a phase transition:[117, 45]

$$\left\langle \tau^{MT} \right\rangle = \sum_{\vec{k}} \frac{1}{(Dk^2 + \tau_\phi^{-1})\varepsilon}\left(\frac{1}{1+k^2\xi^2}\right) \qquad \text{(C.12)}$$

where $D = \frac{v_F^2}{2}\tau$ is the carrier diffusion constant, with τ mean collision time and $\hbar/\tau_\phi$ a depairing energy heuristically introduced (as usual for diffusive-like excitations in 2D) to avoid the divergence of the spectral density for $\omega \longrightarrow 0$. For s-wave orbital symmetry the 2D integration of Eq. C.12 yields[117, 45]

$$\left\langle \tau^{MT} \right\rangle = \hbar\rho(E_F)\frac{\hbar}{4\tau E_F}\frac{1}{(\varepsilon-\gamma_\phi)}\ln\frac{\varepsilon}{\gamma_\phi} \qquad \text{(C.13)}$$

where $\gamma_\phi = \frac{\xi^2(0)}{\tau_\phi D}$ is a pair breaking parameter. One should remark that the exact estimate[1] implies $\pi/8$ instead of $\frac{1}{4}$ in Eq. C.13, while also $\langle\tau_{DOS}\rangle$ (Eq. C.11) has a little numerical difference. By taking into account Eqs. C.13 and C.11 and considering Eq.s C.5, and C.7 one can write for the relaxation rate due to SF

$$W^{SF} \approx W^0\left\{\frac{\pi\hbar}{8E_F\tau}\frac{1}{\varepsilon-\gamma}\ln\frac{\varepsilon}{\gamma_\phi} - \frac{0,8\hbar}{E_F\tau}\ln\frac{1}{\varepsilon}\right\} \qquad \text{(C.14)}$$

W^0 the one in absence of SF. One can expect that close to T_C the 2D $\longrightarrow$ 3D dimensionality crossover occurs. To extend Eq. C.14 to a layered system one has to integrate over a corrugated cylinder

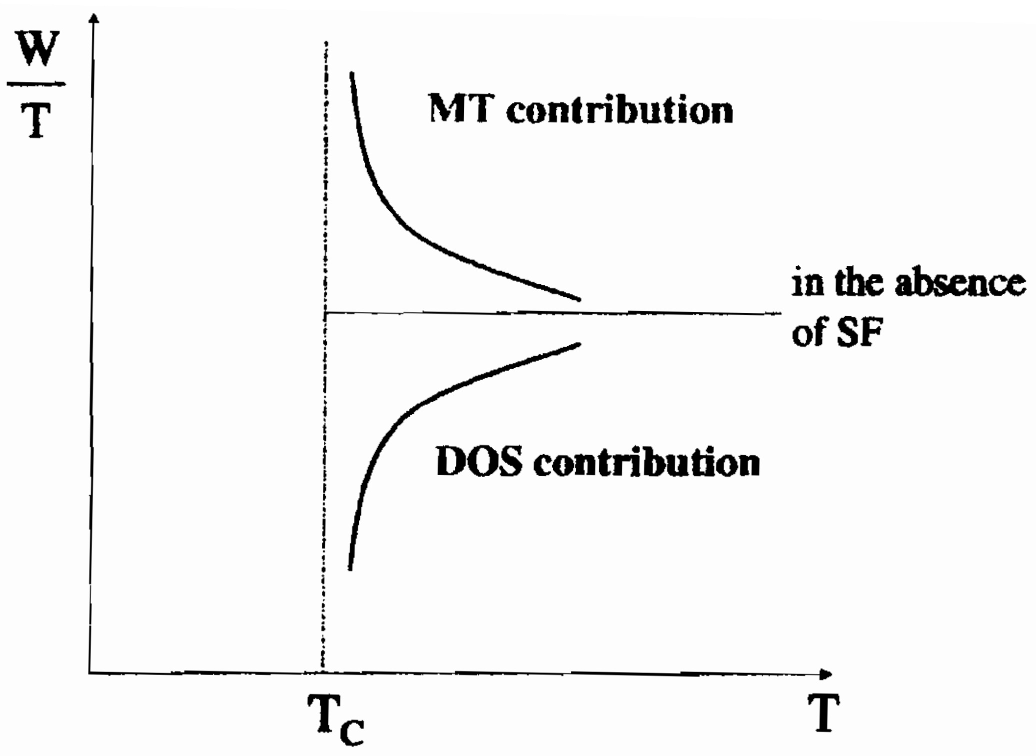

Figure C.2: Sketchy behavior of the temperature dependence of W for $T \to T_C^+$.

and this corresponds to substitute[1] $\ln \varepsilon^{-1}$ by $2\ln 2/\sqrt{\varepsilon}+\sqrt{\varepsilon+r}$ and $ln(\varepsilon/\gamma_\phi)$ by $2\ln\left\{(\sqrt{\varepsilon}+\sqrt{\varepsilon+r})/(\sqrt{\gamma_\phi}+\sqrt{\gamma_\phi+r})\right\}$, with $r = \frac{2\xi_C^2(0)}{d^2}$ anisotropy parameter (d interlayer distance). The temperature dependence of W expected, in principle, in the vicinity of T_C^+ is sketched in Fig. C.2.

Since the MT term could be qualitatively thought as being strongly affected by a magnetic field, in order to avoid the compensation between MT and DOS terms in Eq. C.14, it was formerly suggested [119] to compare W in zero field (NQR) with the NMR one. Although this work[119] deserves the credit to have opened the NQR-NMR studies of SF, the basic idea turned out too naive. In fact the MT term is strongly sensitive to impurities and furthermore the effect of the magnetic field on both $< \tau_{MT} >$ and $< \tau_{DOS} >$ was later on[120] found much more complex.

NMR - NQR T_1 results in optimally doped YBCO: field dependence of the DOS term.

Direct measurements[121, 122] of ^{63}Cu NMR-NQR relaxation in quasi-optimally doped YBCO have subsequently indicated that little, if any, field dependence of ^{63}Cu W occurred for $T \approx T_C + 2K$, up to fields of 14 Tesla. In underdoped YBCO$_{6+x}$ and in YBCO124 the NQR and NMR W's were found[53, 123] to differ only in the range $T_C(0) \div T_C(H)$. The results for ^{63}Cu relaxation rate in optimally doped YBCO ($T_C(0) = 92$ K), for different magnetic fields,

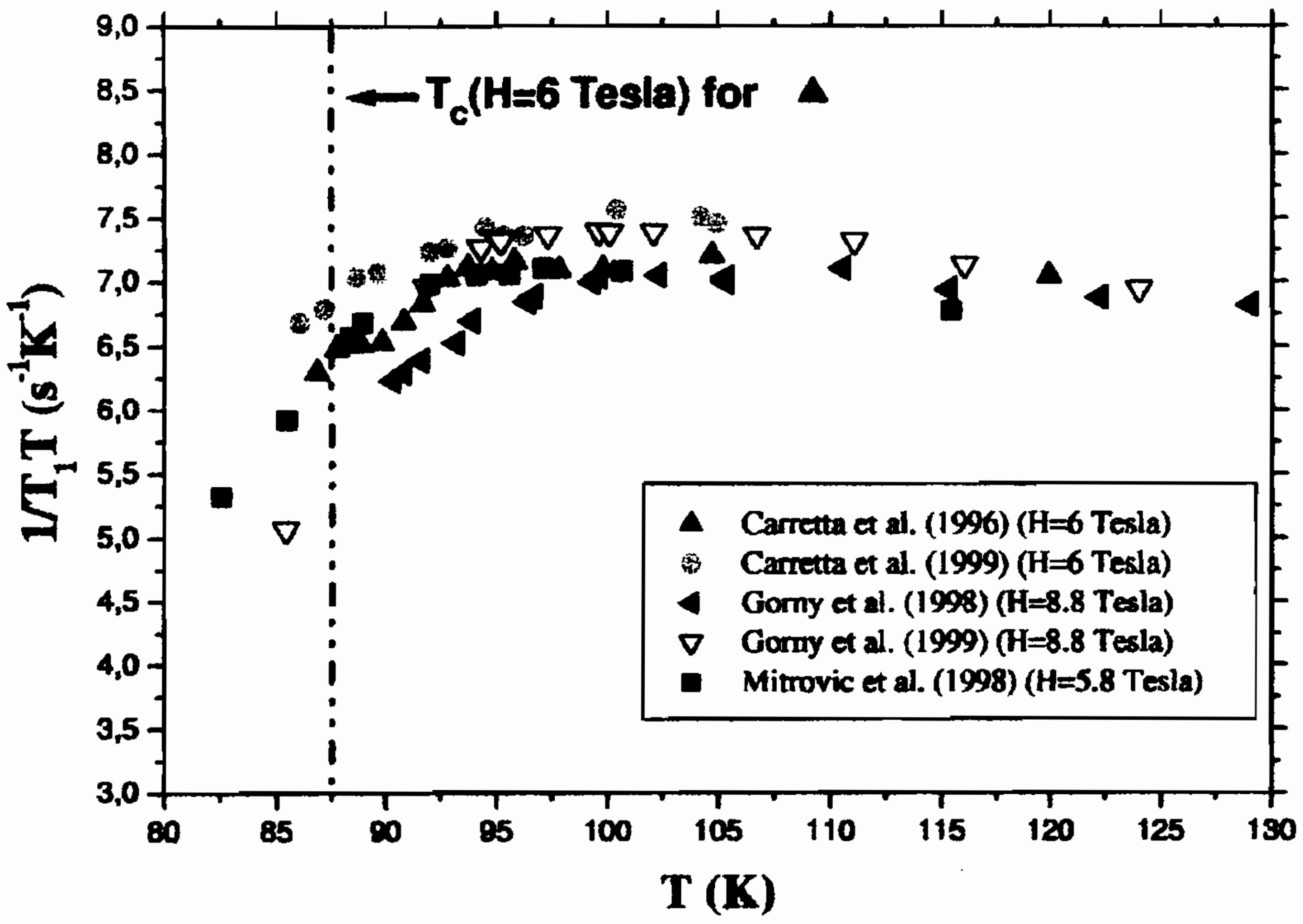

Figure C.3: ^{63}Cu NMR relaxation rates in YBCO at different magnetic fields, around the transition temperature (data from Ref.s [124, 121, 122, 53]).

are collected in Fig. C.3. From these data one concludes that below about 100 K an upturn in the temperature dependence of (W/T) occurs, indicative of a DOS contribution from SF with little, if any, field dependence.

The field dependence of the SF is a rather delicate issue. In particular, for the quantity $W \propto \sum_{\vec{k}} \left(\frac{\chi''(\vec{k},\omega)}{\omega} \right)_{\omega=0}$ involved in the relaxation rate, one has complicate interplays with the temperature, the anisotropy parameter r, the phase breaking times τ and τ_ϕ and of the ratio $\beta = H/H_{C2}$ (see Eq. C.14 for the case of zero field). Furthermore, it is still under debate if the long-wave length approximation in the order parameter fluctuations and the assumption of $\omega = 0$ for W can be safely made.

An analytical treatment for the effect of the magnetic fields on SF and W for layered 3D superconductors has been carried out[120], in the assumption of long wave-length fluctuations and for $H << H_{C2}$. From this treatment various field and temperature crossovers are expected for W^{SF}, with an interplay of the MT and DOS term depending from the role of the impurities. However, for both DOS and MT terms the field dependence is not marked, at least for $T \approx T_C + 1K$. In Fig. C.4 illustrative temperature behaviors, for

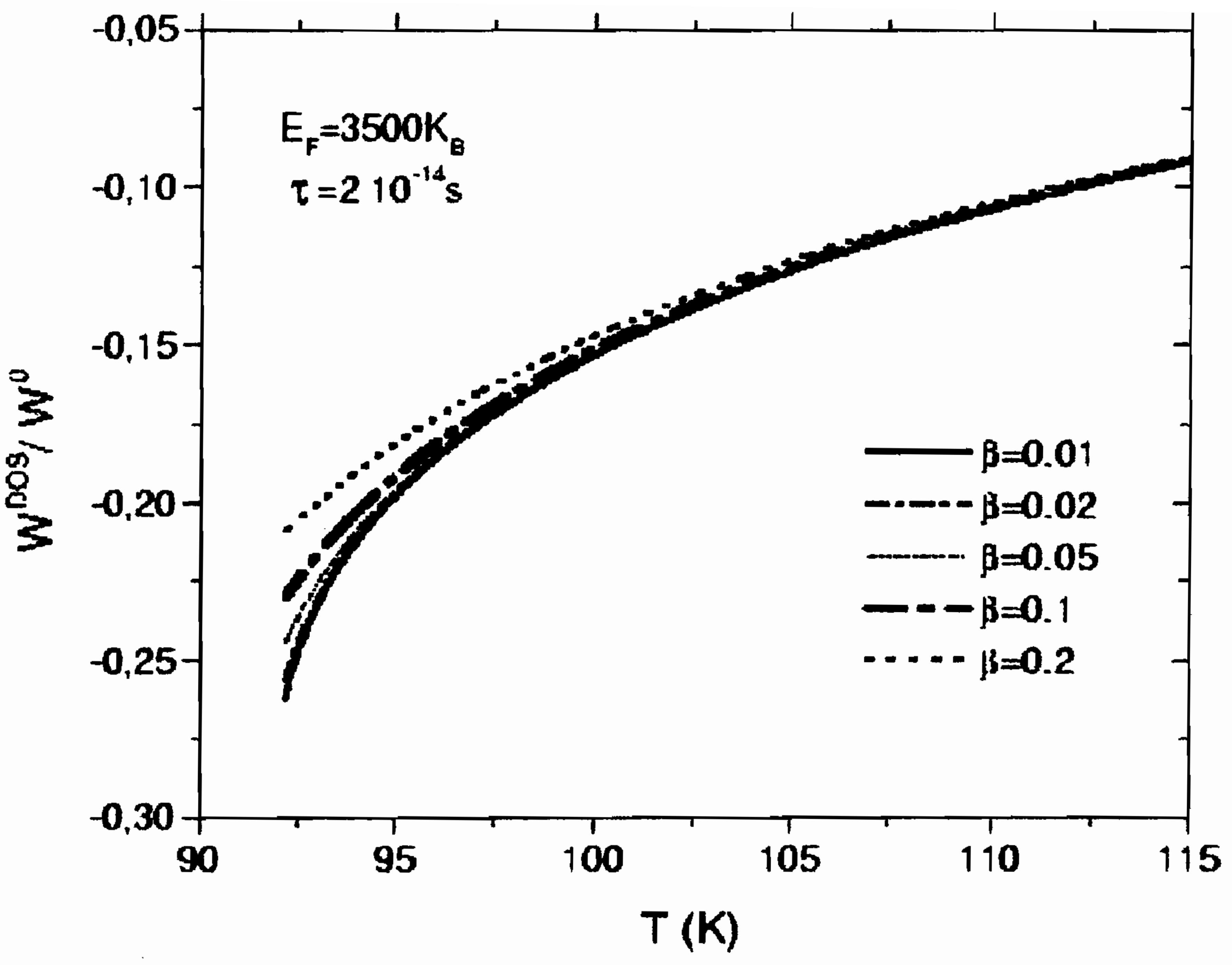

Figure C.4: Theoretical temperature dependence of the DOS contribution to the relaxation rate, normalized to the one in the absence of SF, for different fields [Ref. [120]]. $\beta \equiv H/H_{C2}(0)$.).

various fields, of (W^{DOS}/W_0) are reported.

In Fig. C.5 the field dependence of (W^{DOS}/W_0) at given temperatures (solid lines, valid for $\beta = H/H_{C2} \leq 0.2$) is compared with experimental findings.

These results show that in YBCO a DOS term due to SF is likely to occur in the vicinity of T_C. However, its field dependence is not strong, at least for values of the magnetic field small compared to H_{C2}, namely in the region where the assumptions required for the analytical treatment should hold. It is still possible that in strong magnetic fields dynamical and/or short wave-length fluctuations play a non negligible role. On the other hand, strong fields should extend the temperature range where the fluctuations have 3D character.

More recent measurements [125] indicate no field dependence of ^{63}Cu W, while a field dependent DOS contribution is observed for ^{17}O NMR W (see Fig. C.6). This result shows that near T_C the

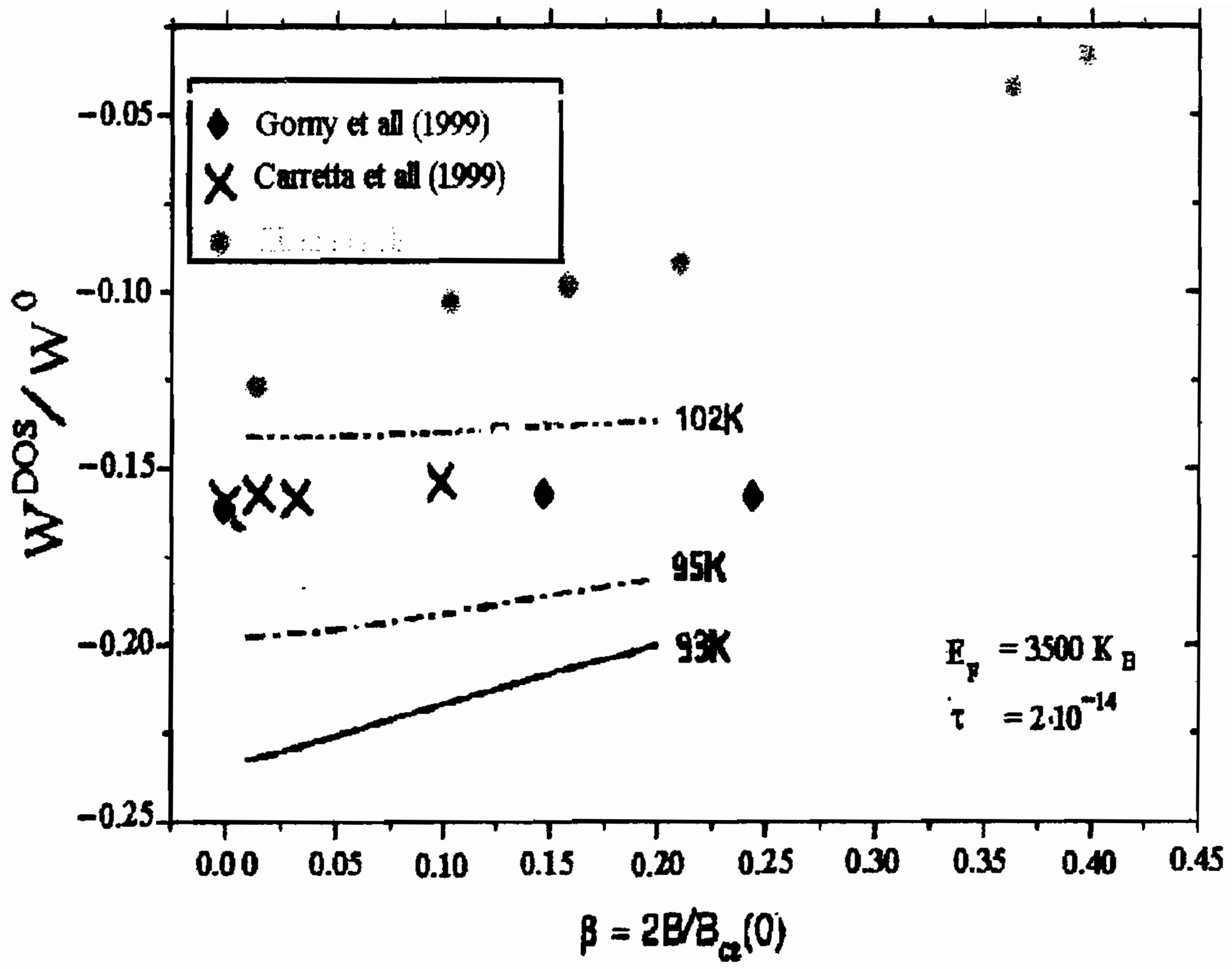

Figure C.5: Theoretical field dependence of the DOS contribution to the relaxation rate and comparison with some experimental results (data taken from Ref.s [121, 122, 123, 53]), for $T \approx T_C{+}2K$. $\beta \equiv H/H_{C2}(0)$.).

electronic spin susceptibility responds to a magnetic field differently in different parts of the Brillouin zone. (It must be noted that in Eq. C.5 for W there are different form factors for different nuclei). Near $\vec{k} = (\pi, \pi)$ antiferromagnetic spin fluctuations dominate the spin susceptibility, which is insensitive to SF. In the region away from $\vec{k} = (\pi, \pi)$, the one detected by means ^{17}O relaxation measurements the susceptibility is affected by SF. Furthermore this observation is a support to the two-bands scenario, with carriers excitations (to which oxygen nucleus is more sensitive) little coupled to Cu^{2+} spin excitations.

Further work is still necessary, considering very pure samples, possibly single crystals, to unravel the intriguing effects of the magnetic field on the SF contribution to NMR relaxation rates around T_C.

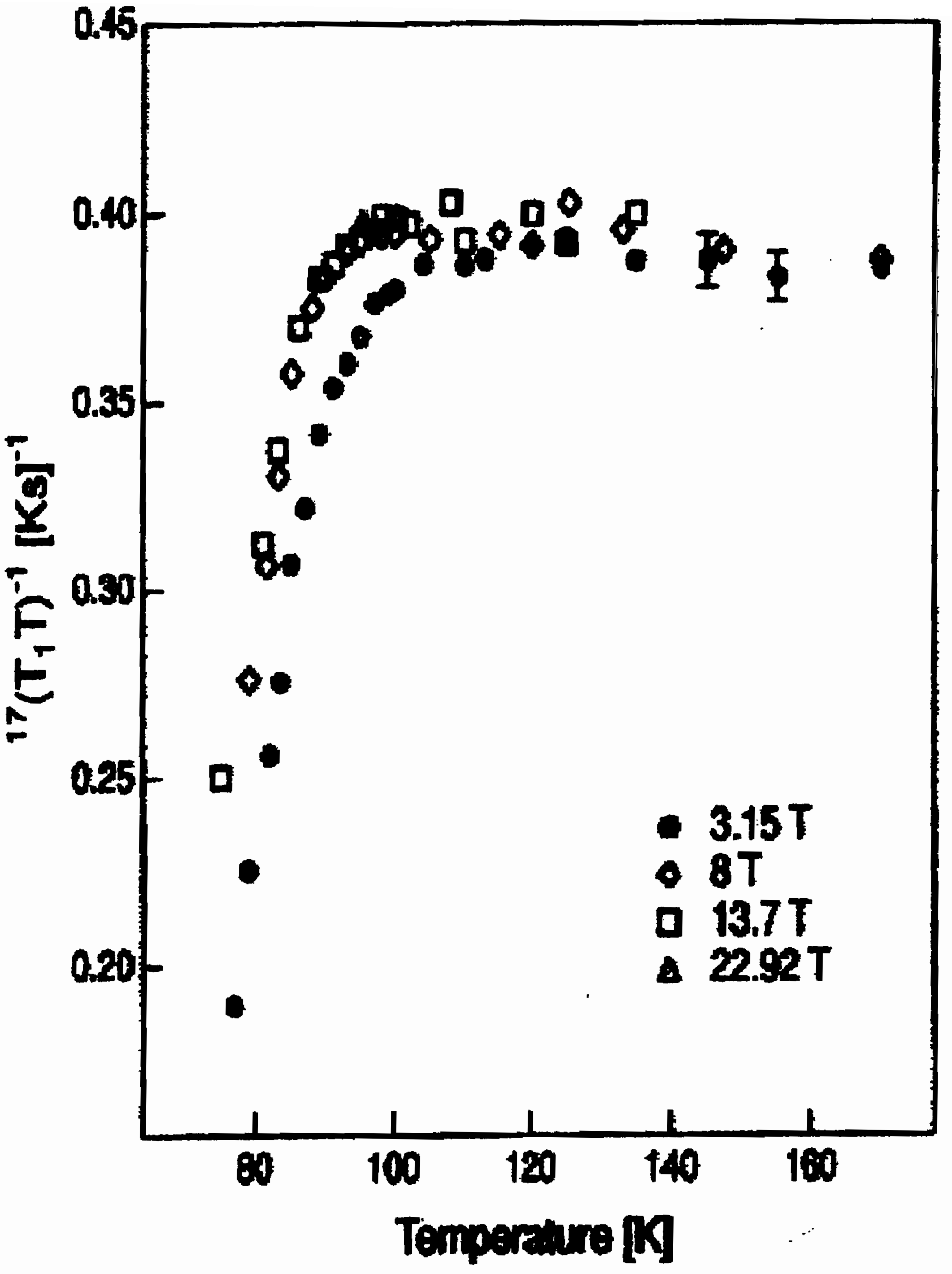

Figure C.6: ^{17}O spin lattice relaxation rate as a function of temperature in different magnetic fields. [Data from Ref. [125]].

Bibliography

[1] A.A. Varlamov, G. Balestrino, E. Milani and D.V. Livanov, **Adv. Phys. 48**, 655 (**1999**); see also "*Fluctuation Phenomena in High Temperature Superconductors*", Edited by M. Ausloos and A.A. Varlamov, Kluwer Academic Publishers, Netherlands (**1997**).

[2] M. Tinkham "*Introduction to Superconductivity*" Mc Graw-Hill, New York (**1996**).

[3] J. Kurkijarvi, V. Ambegaokar and G. Eilenberger, **Phys. Rev. B 5**, 868 (**1972**).

[4] A.I. Larkin and A.A. Varlamov, "*Fluctuation Phenomena in Superconductors*" in "*Physics of conventional and non-conventional superconductors* " Eds. K.H. Bennemann and J.B. Ketterson, Springer Verlag (**2002**).

[5] A. Rigamonti, F. Borsa and P. Carretta, **Rep. Progr. Physics 61**, 1367-1439 (**1998**). Other review articles are referred in this report. For the overdoped regime, in particular in Tl-based compounds, see A. Trokiner in "The gap symmetry and fluctuations in high T_C superconductors", Ed. by Bok *et al.*, Plenum Press, p.331 (**1998**).

[6] M.K. Wu, J.R. Ashburn, C.J. Torng, P.H. Hor, R.L. Meng, L. Gao, Z.J. Huang, Y.Q. Wang, and C.W. Chu, **Phys. Rev. Lett. 58**, 908 (**1987**).

[7] A. Manthiram and J.B. Goodenough **Physica C 159**, 760 (**1989**).

[8] A. Vecchione, P. Tedesco, M. Gombos, M. Polichetti and S. Pace, Inst. Phys. Conf. Ser. **167**, 143 (**2000**); A. Vecchione, M. Gombos, P. Tedesco and S. Pace, **Int. J. Mod. Phys. B 14**, 2670 (**2000**); M. Gombos, A. Vecchione, P. Tedesco, D. Zola, U. Gambardella and S. Pace, **IEEE Trans. on Appl. Super. 11**, 3517 (**2001**); M. Gombos, A. Vecchione, S. Pace, P. Tedesco and D. Zola, **Physica C 372**, 1141 (**2002**).

[9] G. Calestani, A. Migliori,P. Manca and P. Sirugu, **Il Nuovo Cimento 19**, 1075 (**1997**).

[10] P. Manca, S. Sanna, G. Calestani, A. Migliori, R. De Renzi and G. Allodi, **Phys. Rev. B 61**, 15450 (**2000**).

[11] P. Carretta, **Physica C 292**, 286 (**1997**)

[12] P. Carretta, A. Lascialfari, A. Rigamonti, A. Rosso and A.A. Varlamov, **Phys. Rev. B 61**, 12420 (**2000**)

[13] J.L. Tallon, C. Bernhard H. Shaked R.L. Hitterman and J. D. Jorgensen, **Phys. Rev. B 51** , 12911 (**1995**).

[14] J.L. Tallon and N.E. Flower, **Physica C 204**, 237 (**1993**).

[15] R.J. Cava, **Physica C 165**, 419 (**1990**).

[16] J.M. Tranquada, *et al.* **Phys. Rev. B 38**, 2477 (**1988**); J.M. Tranquada in "Earlier and Recent Aspects of Superconductivity" Eds. J.G. Bednorz and K.A. Müller, Springer Series in Solid-State Sciences 90 (**1991**).

[17] G. Calestani in "*High temperature superconductivity. Models and measurements*", pp. 387. Proceedings of the 1994 GNSM school, Vietri sul Mare, Italy, edited by M. Aquarone (**1996**).

[18] J.D. Jorgensen, B.W. Veal, A.P. Paulikas, L.J. Nowicki, G.W. Crabtree, H. Caus and W.K. Kwok, **Phys. Rev. B 41**, 1863 (**1990**).

[19] K. Hatada and H. Shimizu, **Physica C 304**, 89 (**1998**).

[20] E.M. McCarron III, M.K. Crawford and J.B. Parise, **J. Solid State Chem 78**, 192 (**1989**); J.B. Parise and E.M. McCarron III, **J. Solid State Chem. 83**, 188 (**1989**).

[21] V.P.S. Awana, S.K. Malik, M.B. Yelon, **Physica C 262**, 272 (**1996**); V.P.S. Awana and A.V. Narlikar, **Phys. Rev. B 49**, 6353 (**1994**); V.P.S. Awana and A.V. Narlikar, **Modern Phys. Lett. B. 10**, 845 (**1996**).

[22] B. Fisher, J. Genossar, C.G. Kuper, L. Patlagan, G.M. Reisner,and A. Knizhnik, **Phys. Rev. B 47**, 6054 (**1993**).

[23] C. Legros-Glebel, J.F. Marrucco, E. Vincent, D. Favrot, B. Poumellac, B. Touzelin, M. Gupta and H. Alloul, **Physica C 175**, 279 (**1991**).

[24] T. Watanabe, M. Fujiwara, N. Suzuki, **Physica C 252**, 100 (**1995**).

[25] X.S. Wu, S.S. Jiang, J. Lin, J.S. Liu, W.M. Chen, X. Jin, **Physica C 309**, 25-32 (**1998**).

[26] Z.J. Wu, Q.B. Meng, S.Y. Zhang, **Phys. Rev. B 58**, 958 (**1998**).

[27] A.J. Vega, M.K. Crawford, E.M. Mc Carron and W.E. Farnet, **Phys. Rev. B 40**, 8878 (1989).

[28] Ch. Niedermayer C. Bernard, T. Blasius, A. Golnik, A. Moodenbaugh and J.I. Budnick, **Phys. Rev. Lett. 80**, 3843 (**1998**).

[29] P.M. Singer and T. Imai, **Phys. Rev. Lett. 88**, 187601 (**2002**).

[30] J. Bobroff, H. Alloul, S. Ouazi, *et al.*, **Phys. Rev. Lett. 89**, 157002 (**2002**).

[31] J. Bardeen, L.N. Cooper and J.R. Schrieffer, **Phys. Rev. 108**, 1175 (**1957**).

[32] L.P.Gor'kov, **Soviet Phys. JETP 9**, 1364 (**1959**), from Zh. Eksperim. i. Teor. Fiz. 36, 1918 (1959).

[33] E.M. Lifšits L.P. Pitaevskij "*Fisica statistica*", part II, "*Teoria dello stato condensato*", chapter V, Editori Riuniti, Edizioni Mir (**1981**)

[34] C. Baraduc, A. Buzdin, J.Y. Henry, J.P. Brison and L. Puech, **Physica C 248**, 138 (**1995**).

[35] A.E. Koshelev, **Phys. Rev. B 50**, 506 (**1994**).

[36] A. Buzdin and V. Dorin, in "*Fluctuation Phenomena in High Temperature Superconductors*", Edited by M. Ausloos and A.A. Varlamov, Kluwer Academic Publishers, Netherlands, p. 335 (**1997**).

[37] L.N. Bulaevskii, M.Ledvij and V.G. Kogan, **Phys. Rev. Lett. 68**, 3773 (**1992**).

[38] V.G. Kogan, M. Ledvij, A.Yu. Simonov, J.H. Cho, and D.C. Johnston, **Phys. Rev. Lett. 70**, 1870 (**1993**).

[39] L. Romanò in "*High temperature superconductivity. Models and measurements.*", p. 387. Proceedings of the 1994 GNSM school, Vietri sul Mare, Italy, Edited by M. Aquarone (**1996**).

[40] L.N. Bulaevskii, **Int. J. Mod. Phys. B 4**, 1849 (**1990**).

[41] T.M. Mishonov, "Fluctuational torque for high-T_C superconductors in strong magnetic field" in *Physics and Materials Science of High Temperature Superconductors*, **NATO ASI E 181**, 37 (**1990**), Edited by R. Kossowsky, S. Methfessel and D. Wohlleben (Kluwer Academic Publishers, Dordrecht).

[42] J.P. Gollub, M.R. Beasley, R. Callarotti and M. Tinkham, **Phys. Rev. B 7**, 3039 (**1973**).

[43] A. Lascialfari, T. Mishonov, A. Rigamonti, P. Tedesco, A. Varlamov, **Phys. Rev. B 65**, R180501 (**2002**)

[44] A.Z. Patašinskij, V.L. Pokrovskij "*Teoria delle fluttuazioni nelle transizioni di fase*", Editori riuniti, edizioni Mir (**1985**)

[45] A. Rigamonti and P. Tedesco, Lecture Notes at the INFM National School in Structure of Matter (Villa Gualino, Torino, September 2000) and **Scientifica Acta**, University of Pavia, **XV**, 49 (**2000**).

[46] M.A. Hubbard, M.B. Salamon and B.W. Veal, **Physica C 259**, 309 (**1996**).

[47] A. Junod, J.Y. Genoud, G. Triscone and T. Schneider, **Physica C 294**, 115 (**1998**).

[48] T. Schneider and H. Keller, **Int. J. Mod. Phys. B 8**, 487 (**1993**) and references therein; T. Schneider and H. Keller, **Physica C 207**, 336 (**1993**); see also T. Schneider and J.M. Singer, in "*Phase Transitions Approach to High Temperature Superconductivity*", Chapter 6, Imperial College Press (**2000**).

[49] S. Salem-Sugui and E.Z. Dasilva, **Physica C 235**, 1919 (**1994**).

[50] A. Lascialfari, P. Tedesco and I. Zucca, **Int. J. Mod. Phys. B** (**2002**).

[51] P. Carretta, A. Lascialfari, A. Rigamonti, F. Teodoli, F. Bolzoni and F. Licci, **Int. J. Mod. Phys. B 14**, 2815 (**2000**).

[52] P. Carretta, A. Lascialfari, A. Rigamonti, A. Rosso and A.A. Varlamov, **Phys. Rev. B 61**, 12420 (**2000**).

[53] P. Carretta, A. Lascialfari, A. Rigamonti, A. Rosso and A.A. Varlamov, **Int. J. Mod. Phys. B 13**, 1123 (**1999**).

[54] K.Kanoda, T. Kawagoe, M. Hasumi, T. Takahashi, S. Kagoshima and T. Mizoguchi, **J. Phys. Soc. Japan 57**, 1554 (**1988**).

[55] D. Babic, J.R. Cooper, J.W. Hodby and Chen Changkang, **Phys. Rev. B 60**, 698 (**1999**).

[56] B. Rosenstein, B.Y. Shapiro, R. Prozorov, A. Shaulov, Y. Yeshurun, **Phys. Rev. B 63**, 134501 (**2001**).

[57] U.Welp, S. Fleshler, W. K. Kwok, R. A. Klemm, V. M. Vinokur, J. Downey, B. Veal, and G. W. Crabtree, **Phys. Rev. Lett. 67**, 3180 (**1991**).

[58] C. Tórron, A. Diaz, A. Pomar, J.A. Veira and F. Vidal, **Phys. Rev. B 49**, 13143 (**1994**)

[59] J. Mosqueira, C. Carballeira, M.V. Ramallo, C. Torron, J. Veira and F. Vidal, **Europhys. Lett. 53**, 632 (**2001**).

[60] A. Sewer and H. Beck, **Phys. Rev. B 64**, 014510 (**2001**).

[61] Y. Yeshurun, A.P. Malozemoff, A. Shaulov, **Rev. Mod. Phys. 68**, 911 (**1996**).

[62] I. Iguchi, T. Yamaguchi and A. Sugimoto, **Nature 412**, 420 (**2001**)

[63] C. Bergemann, A.W. Tyler, A.P. Mackenzie, J.R. Cooper, S.R. Julian and D.E. Farrell, **Phys. Rev. B 57**, 14387 (**1998**).

[64] Z. Akase, Y. Tomokiyo, Y. Tanaka and M. Watanabe, **Physica C 339**, 1 (**2000**).

[65] E.W. Hudson, S.H. Pan, A.K. Gupta, K.W. Ng, J.C. Davis, **Science 285**, 88 (**1999**).

[66] M. Gutmann, S.J.L. Billinge, E.L. Brosha and G.H. Kwei, **Phys. Rev. B 61**, 11762 (**2000**).

[67] E. Bozin, G. Kwei, H. Takagi and S. Billinge, **Phys. Rev. Lett. 84**, 5856 (**2000**).

[68] Yu.N. Ovchinnikov, S.A. Wolf and V.Z. Kresin, **Phys. Rev. B 63**, 064524 (**2001**).

[69] E.Z. Kuchinskii and M.V. Sadowskii, **JETP 90**, 535 (**2000**), also in **cond-mat/9910261**.

[70] E.V.L. De Mello, E.S. Caixeiro and J.L. Gonzales, **cond-mat 0110519** (24 Oct **2001**); ibidem, **cond-mat 0110479** (22 Oct **2001**)

[71] Yu.N. Ovchinnikov, S.A.Wolf and V.Z. Kresin, **Phys. Rev. B 60**, 4329 (**1999**).

[72] A. Lascialfari, A. Rigamonti, L. Romanò, P. Tedesco, A. Varlamov, and D. Embriaco, **Phys. Rev. B 65**, 144523 (**2002**).

[73] L. Romanò, **Int. J. Mod. Phys. B**, (**2002**).

[74] C. Carballeira, J. Mosqueria, A. Revcolevschi and F. Vidal, **Phys. Rev. Lett. 84**, 3157 (**2000**).

[75] A. Lascialfari, A. Rigamonti, I. Zucca, L. Romanò, **Phys. Rev. Lett.**, submitted

[76] C.P. Slichter "*Principles of Magnetic Resonance*" Springer-Verlag (**1990**).

[77] J.T. Markert, T.W. Noh, S.E. Russek and R.M. Cotts, **Solid State Comm. 63**, 847 (**1987**).

[78] H. Brom and H. Alloul, **Physica C 177**, 293 (**1991**). See also Ref. [5] and references there in.

[79] M. Takigawa and G. Saito, **J. Phys. Soc. Japan 55**, 1233 (**1986**). In this paper the theoretical treatment leading to the analogous of Eq. 3.9 is developed for the time dependence of an anisotropic shift.

[80] C.H. Recchia, J.A. Martindale, C.H. Pennington, W.L. Hults and J.L. Smith, **Phys. Rev. Lett. 78**, 3543 (**1997**).

[81] C.H. Recchia, K. Gorny and C.H. Pennington, **Phys. Rev. B 54**, 4207 (**1996**).

[82] R.E. Walsteadt and S.W. Cheong, **Phys. Rev. B 51**, 3163 (**1995**).

[83] M. Takigawa, W.L. Hults and J.L. Smith, **Phys. Rev. Lett. 71**, 2650 (**1993**)

[84] H. Alloul, A. Mahajan, H. Casalta and O. Klein, **Phys. Rev. Lett. 70**, 1171 (**1993**).

[85] J.R. Cooper and J.W. Loram, **J. Phys. France 6**, 2237 (**1996**).

[86] G.V.M. Williams, J.L. Tallon, R. Michalak and R. Dupree, **Phys. Rev. B 54**, R6909 (**1996**); ibidem, **Phys. Rev. B 57**, 8696 (1998).

[87] P. Carretta, A. Lascialfari, A. Rigamonti, F. Tedoldi, F. Bolzoni, F. Licci, **Int. J. Mod. Phys. B 14**, 2815 (**2000**).

[88] A.Yu. Zavidonov and D. Brinkman, **Phys. Rev. B 63**, 132506 (**2001**); see also by the same authors **Phys. Rev. B 58**, 12486 (**1998**); A.Yu. Zavidonov, I.A. Larionov and D. Brinkman, **Phys. Rev. B 61**, 15462 (**2000**); D. Brinkman and A.Yu. Zavidonov, **Z. Naturforsch. 57 a**, 479 (**2002**).

[89] V.A. Nandor et al., **Phys. Rev. B 60**, 6907 (**1999**); see also T. Auler, M.Horvatic, J.A. Gillet, C.Berthier, Y. Berthier, P. Segransan and J.Y. Henry, **Phys. Rev. B 56**, 11294 (**1997**).

[90] A.G. Kontos, R. Dupree and Z.P. Han, **Physica C 247**, 1 (**1995**) and references therein.

[91] G.V.M. Williams and J.L. Tallon, **Phys. Rev.B 57**, 10984 (**1998**)

[92] G.V.M. Williams, J.L. Tallon and J.W. Loram, **Phys. Rev. B 58**, 15053 (**1998**)

[93] J.L. Tallon, J.W. Loram, G.V.M. Williams, J.R. Cooper, I.R. Fisher, J.D. Johnson, M.P. Staines and C. Bernhard, **Phys. Status Solidi (b) 215**, 531 (**1999**).

[94] E.H. Brandth, **Phys. Rev. Lett. 78**, 2208 (**1997**)

[95] M. Corti, B.J. Suh, F.Tabak, A. Rigamonti, F.Borsa, M.Xu, B. Dabrowski, **Phys. Rev. B 54**, 9469 (**1996**)

[96] P. Carretta, A. Lascialfari , A. Rigamonti, P. Tedesco, F. Tedoldi and I.A. Larionov, **Phys. Rev. B** submitted.

[97] A. Rigamonti and S. Torre, **Phys. Rev. B 33**, R2024 (**1986**)

[98] M. Eremin and A. Rigamonti, **Phys. Rev. Lett. 88**, 037002 (**2002**)

[99] A. Rigamonti, M. Eremin, A. Campana, P. Carretta, M. Corti, A. Lascialfari, P.Tedesco, **Int. J. Mod. Phys. B** (**2002**).

[100] M.-H. Julien, A. Campana, A. Rigamonti et al., **Phys. Rev. B 63**, 144508 (**2001**) and references therein.

[101] A. Campana, P. Carretta, M. Corti, A. Lascialfari, A. Rigamonti and F. Licci, **Int. J. Mod. Phys. B 14**, 2797 (**2000**).

[102] P. Carretta, A. Lascialfari, A. Rigamonti, P. Tedesco, F. Tedoldi, **Int. J. Mod. Phys.**, (**2002**).

[103] M.V. Eremin et al., **Solid State Comm. 92**, 511 (1994).

[104] M.V. Eremin et al., **JEPT Lett. 85**, 963 (**1997**)

[105] M. Eremin et al., **Phys. Rev. B 64**, 214512 (**2001**)

[106] E. Cappelluti and R. Zeyher, **Phys. Rev. B 59**, 6475 (**1999**).

[107] M.V. Eremin and I.A. Larionov, **JEPT letters 68**, 611 (**1998**).

[108] G. Amoretti et al., **Physica C 221**, 227 (**1994**).

[109] S. Chakravarty, R.B. Loughlin, D.K. Morr and Ch. Nayak, **Phys. Rev. B 63**, 094503 (**2001**)

[110] H.A. Mook, P.Dai and F.Dogan, **Phys. Rev. B 64**, 012501 (**2001**).

[111] Y. Sidis et al. **Phys. Rev. Lett. 86**, 4100 (**2001**).

[112] For a topical review of superconducting properties in MgB_2 see C. Buzea and T. Yamashita, **cond-mat/0108265**, also in **Superconductors, Science & Technology 14**, R115 (**2001**).

[113] R. A. Buhrman and W. P. Halperin, **Phys. Rev. Lett. 30**, 692 (**1973**)

[114] T. Mishonov and E. Penev, **Intern. J. Mod. Phys. B 14**, 3831 (**2000**); Comment on "First Observation for a Cuprate Superconductor of Fluctuation-Induced Diamagnetism well Inside the Finite-Magnetic-Field Regime", **cond-mat/0007178**.

[115] A.S. Sidorenko, L.R. Tagirov, A.N. Rossolenko, N.S. Sidorov, V.I. Zdravko, V.V. Ryazanov, M. Klemm, S. Horn and R. Tidecks, **JETP Lett. 76**, 17 (**2002**) from Pis'ma v Zh. Eksperim. i Teor. Fiz. 76, 20 (2002).

[116] B. Berthier, M.H. Julien, M. Horvatic and Y. Berthier, **J. Phys. I. 6**, 2205 (**1996**).

[117] A. Rigamonti and A. Varlamov, **Istituto Lombardo (Rend. Sc.) B 131**, 291 (**1997**).

[118] H.N. Bachman, V.F. Mitrović, A,P. Reyes, W.P. Halperin, M. Eschring, J.A. Sauls, A. Kleinhammes, P. Kurns and N.G. Moulton, **Phys. Rev. B 60**, 7591 (**1999**).

[119] P. Carretta, D.V. Livanov, A. Rigamonti and A.A. Varlamov, **Phys. Rev. B 54**, R9682 (**1996**).

[120] P. Mosconi, A.Rigamonti and A. Varlamov, **Appl. Magn. Resonance**, 19, 345 (**2000**).

[121] K. Gorny et al., **Phys. Rev. Lett. 82**, 177 (**1999**).

[122] P. Carretta, private communication.

[123] G. Zheng et al., **Phys. Rev. B 60**, R9947 (**1999**).

[124] V.F. Mitrović, H.N. Bachman, W.P. Halperin, M. Eschring, and J.A. Sauls, **Phys. Rev. Lett. 82**, 2784 (**1999**).

[125] V.F. Mitrović, H.N. Bachman, W.P. Halperin, A.P. Reynes, P. Kuhns and W.G. Moulton, **Phys. Rev. B 66**, 014511 (**2002**).

Acknowledgements

I express my gratitude to Prof. Attilio Rigamonti for his constant guidance and for his patience during the writing of this thesis. Most of all I thank him for his contagious enthusiasm in disclosing the secrets of nature.

I am grateful to Dr. Alessandro Lascialfari for his assistance during the experiments and for the scientific discussions which contribute greatly to the results described in this thesis.

I thank Dr. Fabio Tedoldi for his introductory help with NMR measurements and Mr. Sergio Aldovrandi for his daily technical support and for his good humor. I thank also Dr. Laura Linati for her help in solving technical problems during the measurements at Centro Grandi Strumenti. I am grateful to Prof. Pietro Carretta and Prof. Maurizio Corti for their helpfulness. I wish to thank also Dr. Cristiana Mozzati and Dr. Pietro Galinetto for their help with SQUID measurements.

My sincere thanks to Prof. Sandro Pace, who motivated me to accept the PhD studentship in Pavia and for the use of the facilties for the synthesis and characterization of the samples at the Department of Physics of the University of Salerno. I thank Dr. Antonio Vecchione and Dr. Marcello Gombos for their help in the synthesis and characterization of the samples as well as for their sincere friendship. I am grateful to Prof. Leonardo Marchese for the permission to use the SEM and EDS facilities at Politecnico di Alessandria and Dr. Alberto Frache for his assistance during the measurements.

I thank Dr. Paolo Ghigna and Dr. Lorenzo Malavasi for their complete helpfulness and the use of the chemical laboratories at Dipartimento di Chimica Fisica Università di Pavia, and also for the use of the X-ray powder diffractometer. I am grateful to Prof. Joseph Spalek and Dr. Michal Rams (Physical Institute of the Jag-

ellonian University in Cracow) for their warm welcome in Cracow and for giving me free access to their SQUID instruments for AC measurements.
Moreover, I thank Prof. Andrei Varlamov and Dr. Laura Romanó for the interesting scientific discussions occurred during the preparation of some of the published papers.
Finally I thank Dr. Vesna Mitrovic (CNRS, Grenoble) who read the manuscript, for her accurate comments and useful suggestions.

Relativistic mean field theory of nuclear structure

Andrea Meucci

Dipartimento di Fisica Nucleare e Teorica,
Università di Pavia
and Istituto Nazionale di Fisica Nucleare,
Sezione di Pavia, Italy

TALK GIVEN ON NOVEMBER 13, 2000

I. INTRODUCTION

The study of atomic nuclei has been the goal of nuclear physics since the formulation of quantum mechanics. Since early experimental probes of the nucleus were limited to energies less than the nucleon mass ($M \simeq 939$ MeV), the nucleus has conventionally been treated as a quantum mechanical, many-body problem of non relativistic nucleons interacting through a two-body potential and described by the Schrödinger equation. The two-body potential is fitted to the measured properties of the deuteron and to low energy nucleon-nucleon (NN) scattering data; one then attempts to predict the properties of the nuclei with A$\geq$3. This is a very difficult problem, because the NN potential is spin dependent, short-ranged, and with a repulsive central core [1,2]. However, reliable approaches, such as Faddeev equations, correlated hyperspherical harmonics, variational Monte Carlo, and Green's function Monte Carlo methods, have been developed for solving the non relativistic nuclear many-body problem for nuclei with A$\leq$10 [3].

A completely different procedure is necessary to study nuclei at higher energies and with greater precision than ever before. For example, electron-nucleus scattering at large momentum transfer at TJNAF and ultra relativistic heavy ion collision at RHIC involve physics that cannot be described by the Schrödinger equation, such as relativistic motion of the nucleus, dynamical meson exchange, baryon resonances, etc. We know that QCD is the fundamental theory of the strong interactions, and then it is the natural instrument to describe this new physics. Unfortunately the QCD coupling is strong at energy scales of existing nuclear data, and QCD predictions are not available.

In contrast, since at present energies hadronic degrees of freedom are experimentally observed, we can develop a theory based on these variables. The calculations can be fitted to the available nuclear and scattering data, and extrapolated to the new experimental situations stated above. Our goal is then to formulate an effective hadronic description of nuclei, that is consistent with quantum mechanics, special relativity, causality, and symmetries of the strong interaction. We start from an effective Lagrangian density and build a relativistic quantum field theory. Unfortunately, because of the strong coupling it cannot be treated using perturbation theory. However, the mean field approach is a reasonable approximation, at least to describe static properties of finite nuclei. Of course, the effective Lagrangian is completely phenomenological but, unlike the non relativistic NN potential, its parameters are directly adjusted to nuclear matter and finite nuclei properties.

In this work the basic formalism of the relativistic mean field theory (RMFT) is presented. Emphasis is put on the derivation of the formulas for the description of ground state properties of finite nuclei. The reader, who is interested in a detailed discussion of these theoretical techniques, is referred to the excellent review articles and books existing on this subject [4–8]. Several computer codes are easily available in literature [9–12].

In Section II we introduce the simple RMF model containing nucleons, Lorentz scalar and vector mesons σ and ω, and the isovector vector meson ρ. The mean field and the no sea approximation are also described. In Section III we discuss applications of the RMFT for the description of atomic nuclei. The Dirac and the Klein-Gordon equations for the nucleon and the meson fields are derived. In Section IV we present the solutions of the RMFT equations for spherical nuclei with closed shell and for deformed nuclei. In particular, we concentrate on the description of binding energies and of nuclear and charge radii. In Section V we present our conclusions.

II. THE RELATIVISTIC MEAN FIELD MODEL

A. The interacting fields

The relativistic mean field theory is a phenomenological description of nuclei. The nucleons are treated as point-like particles described by Dirac spinors

$$\Psi = \begin{pmatrix} \Psi_+ \\ \Psi_- \end{pmatrix} , \tag{1}$$

interacting through the exchange of point-like particles called mesons. The number of these mesons, the values of their masses, coupling constants, and quantum numbers are determined to reproduce the experimental data.

The simplest meson is surely the pion, which carries the quantum numbers J=0, T=1, and P=−1 for angular momentum, isospin, and parity. However, because of its negative parity, the corresponding meson field does not conserve parity on the Hartree level. Of course, two and any even number of pions contribute to positive parity fields. Even if it seems possible to form mean fields starting from meson pairs, such an idea would considerably complicate the theory. Therefore we introduce introduce a phenomenolgical σ meson with quantum number J=0, T=0, and P=1. The corresponding field is the scalar field $\sigma(x)$ which produces an attractive force between the nucleons.

The exchange of vector mesons determines the repulsive part of the interaction. The most important vector meson is the ω meson with quantum numbers J=1, T=0, and P=−1, which originates the vector field $\omega^\mu(x)$. The Coulomb repulsion is described by the time-like component of the vector potential $A^\mu(x)$ due to photon exchange between the nucleons. In addition, the nuclear force depends on the isospin caused by the exchange of ρ mesons with quantum numbers J=1, T=1, and P=−1. They are described by an isovector vector field $\vec{\rho}^{\,\mu}(x)$.

In order to simplify the equations many authors use only the $\sigma(x), \omega^\mu(x), A^\mu(x)$, and $\vec{\rho}^{\,\mu}(x)$ fields, and neglect all other possible meson fields. They are, however, less important to describe ground state properties and their effect can be taken into account by a suitable choice of the parameters for the other mesons.

B. The mean field approximation

We introduce the mean field approximation for the simple model of nucleons interacting through a scalar field. It is described by the Lagrangian density

$$\begin{aligned}\mathcal{L} &= \mathcal{L}_{\mathrm{N}} + \mathcal{L}_{\mathrm{meson}} + \mathcal{L}_{\mathrm{int}} \\ &= \overline{\Psi}\Big(\mathrm{i}\gamma_\mu \partial^\mu - M\Big)\Psi + \frac{1}{2}\Big(\partial_\mu \sigma\, \partial^\mu \sigma - m_\sigma^2 \sigma^2\Big) - g_\sigma\, \overline{\Psi}\sigma\Psi\ , \end{aligned} \tag{2}$$

where Ψ and σ are the nucleon and scalar meson field operators, while $\partial^\mu \equiv \partial/\partial x_\mu$ is the four dimensional generalization of the gradient operator.

In the mean field approximation we remove all the quantum fluctuations of the meson fields and use their expectation values, which are classical fields

$$\hat{\sigma} \rightarrow \langle\sigma\rangle \equiv \sigma\ . \tag{3}$$

The nucleons move as independent particles in the meson fields. This means that the nucleon field operator can be expanded in terms of single particle states and the densities become sums over the single particle wave functions. It is clear that we should in principle take into account the negative energy solution for a fully relativistic description; that means that we should evaluate the vacuum polarization effects to all orders. However, since nucleons and mesons are composite particles and not constituent of a basic field theory, we can reasonably neglect those effects, and restrict the sum to the occupied particle states $i = 1...\mathrm{A}$. This is called the *no sea* approximation where we have for the scalar density ρ_{s}

$$\rho_{\mathrm{s}} = \sum_{i=1}^{\mathrm{A}} \overline{\Psi}_i \Psi_i\ . \tag{4}$$

III. THE RELATIVISTIC MEAN FIELD EQUATIONS

We now extend the RMFT to study atomic nuclei. The starting point is the Lagrangian density [15]

$$\begin{aligned}\mathcal{L} = {} & \overline{\Psi}\Big(\mathrm{i}\gamma_\mu\partial^\mu - M\Big)\Psi + \frac{1}{2}\Big(\partial_\mu\sigma\,\partial^\mu\sigma - m_\sigma^2\sigma^2\Big) - U(\sigma) \\ & - \frac{1}{4}\Omega_{\mu\nu}\Omega^{\mu\nu} + \frac{1}{2}m_\omega^2\omega_\mu\omega^\mu - \frac{1}{4}\vec{R}_{\mu\nu}\vec{R}^{\mu\nu} + \frac{1}{2}m_\rho^2\vec{\rho}_\mu\vec{\rho}^{\,\mu} - \frac{1}{4}F_{\mu\nu}F^{\mu\nu} \\ & - g_\sigma\overline{\Psi}\sigma\Psi - g_\omega\overline{\Psi}\gamma_\mu\omega^\mu\Psi - g_\rho\overline{\Psi}\gamma_\mu\vec{\tau}\vec{\rho}^{\,\mu}\Psi - e\frac{1+\tau_3}{2}\overline{\Psi}\gamma_\mu A^\mu\Psi\ , \qquad (5)\end{aligned}$$

where M, m_σ, m_ω, and m_ρ are the nucleon and meson masses, $g_\sigma, g_\omega, g_\rho$, and $e^2/(4\pi) = 1/137.036$ are the corresponding coupling constants for the mesons and the photon. $U(\sigma)$ is a non linear self-interaction of the σ meson, i.e.,

$$U(\sigma) = \frac{1}{3}g_2\,\sigma^3 + \frac{1}{4}g_3\,\sigma^4\ . \qquad (6)$$

The field tensors of the mesons and of the photon are

$$\begin{aligned}\Omega^{\mu\nu} &= \partial^\mu\omega^\nu - \partial^\nu\omega^\mu\ , & (7)\\ \vec{R}^{\mu\nu} &= \partial^\mu\vec{\rho}^{\,\nu} - \partial^\nu\vec{\rho}^{\,\mu}\ , & (8)\\ F^{\mu\nu} &= \partial^\mu A^\nu - \partial^\nu A^\mu\ . & (9)\end{aligned}$$

The mean field approximation is introduced at this point by treating the fields as classical fields. The equations of motion can be derived from the Euler-Lagrange equations of motion [13], i.e.,

$$\partial_\mu\left(\frac{\partial\mathcal{L}}{\partial\partial_\mu q} - \frac{\partial\mathcal{L}}{\partial q}\right) = 0\ . \qquad (10)$$

These result in a set of coupled differential equations, namely the Dirac equation with potential terms for the nucleons

$$\left[\gamma_\mu\left(\mathrm{i}\partial^\mu + g_\omega\omega^\mu + g_\rho\vec{\tau}\vec{\rho}^{\,\mu} - e\frac{1+\tau_3}{2}A^\mu\right) - M + g_\sigma\sigma\right]\Psi_i = 0\ , \quad (11)$$

and the Klein-Gordon equations with source terms for the mesons

$$\left[\Box + m_\sigma^2\right]\ \sigma = -g_\sigma \rho_{\mathrm{s}} - g_2\sigma^2 - g_3\sigma^3\ , \tag{12a}$$

$$\left[\Box + m_\omega^2\right]\ \omega^\mu = g_\omega j^\mu\ , \tag{12b}$$

$$\left[\Box + m_\rho^2\right] \vec{\rho}^{\ \mu} = g_\rho \vec{j}^{\ \mu}\ , \tag{12c}$$

$$\Box A^\mu = e j_{\mathrm{c}}^\mu\ . \tag{12d}$$

The sources of the meson fields are defined the nucleon densities and currents:

- the scalar density

$$\rho_{\mathrm{s}} = \sum_{i=1}^{A} n_i \overline{\Psi}_i \Psi_i\ , \tag{13}$$

- the baryon current

$$j^\mu = \sum_{i=1}^{A} n_i \overline{\Psi}_i \gamma^\mu \Psi_i\ , \tag{14}$$

- the isovector current

$$\vec{j}^{\ \mu} = \sum_{i=1}^{A} n_i \overline{\Psi}_i \gamma^\mu \boldsymbol{\tau} \Psi_i\ , \tag{15}$$

- and the electromagnetic current

$$j_{\mathrm{c}}^\mu = \sum_{i=1}^{A} n_i \overline{\Psi}_i \frac{1+\tau_3}{2} \gamma^\mu \Psi_i\ . \tag{16}$$

Since we want to describe nuclear stationary states all time derivatives and all space vector components of densities and fields vanish. The single particle wave functions separate as $\Psi_i(\boldsymbol{r},t) = \Psi_i(\boldsymbol{r})\exp\{\mathrm{i}\varepsilon_i t\}$. Furthermore, we assume that the nucleon single-particle states do not mix isospin, so only the third component of the isospin vectors is necessary. Finally, we obtain a simplified set of equations (stationary RMF equations). The Dirac equation (11) reduces to

$$[-\mathrm{i}\boldsymbol{\alpha}\cdot\boldsymbol{\nabla} + V + \beta\,(M+S)]\,\Psi_i = \varepsilon_i\Psi_i \ , \tag{17}$$

where S and V are the scalar and vector potentials which are defined by the meson fields

$$S = g_\sigma\sigma \ , \tag{18}$$

$$V = g_\omega\omega^0 + g_\rho\tau_3\rho_3^0 + e\frac{1+\tau_3}{2}A^0 \ . \tag{19}$$

The scalar potential contributes to the nucleon effective mass as

$$M^* = M + S \ . \tag{20}$$

The Klein-Gordon equations (12) for the mesons reduce to

$$\left[-\nabla^2 + m_\sigma^2\right]\ \sigma = -g_\sigma\rho_{\mathrm{s}} - g_2\sigma^2 - g_3\sigma^3 \ , \tag{21a}$$

$$\left[-\nabla^2 + m_\omega^2\right]\omega^0 = g_\omega\rho_{\mathrm{B}} \ , \tag{21b}$$

$$\left[-\nabla^2 + m_\rho^2\right]\rho_3{}^0 = g_\rho\rho_3 \ , \tag{21c}$$

$$-\nabla^2 A^0 = e\rho_{\mathrm{c}} \ . \tag{21d}$$

The nucleon densities are:

- the scalar density

$$\rho_{\mathrm{s}} = \sum_{i=1}^{\mathrm{A}} n_i\overline{\Psi}_i\Psi_i \ , \tag{22}$$

- the baryon density

$$\rho_{\mathrm{B}} = \sum_{i=1}^{\mathrm{A}} n_i \Psi_i^\dagger \Psi_i \ , \tag{23}$$

- the isovector density

$$\rho_3 = \sum_{i=1}^{\mathrm{Z}} n_i \Psi_i^\dagger \Psi_i - \sum_{i=1}^{\mathrm{N}} n_i \Psi_i^\dagger \Psi_i \ , \tag{24}$$

- and the charge density

$$\rho_{\mathrm{c}} = \sum_{i=1}^{\mathrm{A}} n_i \Psi_i^\dagger \frac{1+\tau_{3i}}{2} \Psi_i \ . \tag{25}$$

The occupation numbers n_i are introduced to account for pairing, which is important for open shell nuclei. If we neglect pairing they take the value 1 for levels below the Fermi surface and 0 for levels above. In the presence of pairing the occupation numbers are obtained in the constant gap approximation [14] through the expression

$$n_i = \frac{1}{2}\left[1 - \frac{\varepsilon_i - \lambda}{\sqrt{(\varepsilon_i - \lambda)^2 + \Delta^2}}\right] \ , \tag{26}$$

where ε_i is the single particle energy for the state i. The chemical potential λ for protons (neutrons) is obtained requiring $\sum_i n_i = Z(N)$. The sum is taken over proton (neutron) states. The gap parameter Δ is taken from the odd-even mass difference

$$\Delta = \frac{1}{2}\left\{E(N+2) - E(N+1) - [E(N+1) - E(N)]\right\} \ . \tag{27}$$

The RMF equations for the fields $\Psi_i, \sigma, \omega^0, \rho_3^0$, and A^0 can be solved in a self consistent way. Starting from an initial guess for the potentials S and V, we solve the Dirac equations (17) for the spinors

Ψ_i. We then calculate the densities $\rho_\mathrm{s}, \rho_\mathrm{B}, \rho_3$, and ρ_c and solve the Klein-Gordon equations (21) to get a new set of potential terms. The procedure is repeated until convergence is achieved. Once the solution has been found we can compute observables such as the total energy of the system

$$E = \sum_{i=1}^{\mathrm{A}} \varepsilon_i - \frac{1}{2} \int \mathrm{d}\boldsymbol{r} \left(g_\sigma \rho_\mathrm{s} \sigma + \frac{1}{3} g_2 \sigma^3 + \frac{1}{2} g_3 \sigma^4 + g_\omega \rho_\mathrm{B} \omega^0 \right.$$
$$\left. + g_\rho \rho_3 \rho_3^0 + e \rho_\mathrm{c} A^0 \right) . \qquad (28)$$

IV. THE SOLUTION OF THE RMF EQUATIONS

A. Spherical nuclei

If we restrict to spherical symmetric nuclei the meson fields depend only on the radius r. The four component spinor solution of the Dirac equation (17) is written

$$\Psi_{nkt} = \begin{pmatrix} g_{nkt}(r)\ \Phi_{km}\ \xi_t \\ \mathrm{i}\ f_{nkt}(r)\ \Phi_{-km}\ \xi_t \end{pmatrix} , \qquad (29)$$

where n is the radial quantum number and k determines both the total and the angular momentum quantum numbers. Φ_{km} is a spin 1/2 spherical harmonic wave function

$$\Phi_{km} = \sum_{m_l, m_s} \left(\frac{1}{2}\ l\ m_s\ m_l \mid j\ m \right) Y_{l,m_l} X_{\frac{1}{2},m_s} , \qquad (30)$$

where

$$j = |k| - \frac{1}{2} , \qquad (31)$$
$$l = k \ \left(\text{if} \quad k > 0\right) , \quad \text{or} \quad l = -k - 1 \ \left(\text{if} \quad k < 0\right) . \qquad (32)$$

ξ_t is a two component isospinor (we take $t = 1/2$ for protons and $t = -1/2$ for neutrons). The normalization of the radial wave functions g and f is given by

$$\int \mathrm{d}r\, r^2 \left(|g|^2 + |f|^2\right) = 1 \,. \tag{33}$$

The Dirac equation (17) becomes a coupled first order equation for the upper and lower components

$$\left(\partial_r + \frac{k_i+1}{r}\right) g_i + \left(M^* - V + \varepsilon_i\right) f_i = 0 \,, \tag{34a}$$

$$\left(\partial_r - \frac{k_i-1}{r}\right) f_i + \left(M^* + V - \varepsilon_i\right) g_i = 0 \,, \tag{34b}$$

where $\partial_r \equiv \partial/\partial r$ and M^* and V were defined in Eqs. (19) and (20). Given the wave functions we can sum over all the occupied states to obtain the spherical densities

$$\rho_{\mathrm{s}}^{\mathrm{sph}} = \sum_{i=1}^{\mathrm{A}} n_i \frac{2j_i+1}{4\pi} \left(|g_i|^2 - |f_i|^2\right) \,, \tag{35a}$$

$$\rho_{\mathrm{B}}^{\mathrm{sph}} = \sum_{i=1}^{\mathrm{A}} n_i \frac{2j_i+1}{4\pi} \left(|g_i|^2 + |f_i|^2\right) \,, \tag{35b}$$

$$\rho_{3}^{\mathrm{sph}} = \sum_{i=1}^{\mathrm{A}} n_i \tau_{3i} \frac{2j_i+1}{4\pi} \left(|g_i|^2 + |f_i|^2\right) \,, \tag{35c}$$

$$\rho_{\mathrm{C}}^{\mathrm{sph}} = \sum_{i=1}^{\mathrm{A}} n_i \frac{1+\tau_{3i}}{2} \frac{2j_i+1}{4\pi} \left(|g_i|^2 + |f_i|^2\right) \,. \tag{35d}$$

The Klein-Gordon equations for the meson fields are

$$\left[-\partial_r^2 - \frac{2}{r}\partial_r + \frac{l\,(l+1)}{r^2} + m_\sigma^2\right] \sigma = -g_\sigma \rho_{\mathrm{s}}^{\mathrm{sph}} - g_2\sigma^2 - g_3\sigma^3 \,, \tag{36a}$$

$$\left[-\partial_r^2 - \frac{2}{r}\partial_r + \frac{l\,(l+1)}{r^2} + m_\omega^2\right] \omega^0 = g_\omega \rho_{\mathrm{B}}^{\mathrm{sph}} \,, \tag{36b}$$

$$\left[-\partial_r^2 - \frac{2}{r}\partial_r + \frac{l\,(l+1)}{r^2} + m_\rho^2\right] \rho_3^0 = g_\rho \rho_3^{\mathrm{sph}} \,, \tag{36c}$$

TABLE I. Various sets of meson parameters NL1, NL2, NL3, and NLSH for the Lagrangian density of Eq. (5). From Ref. [15]

		NL1	NL2	NL3	NLSH
M	[MeV]	938	938	939	939
m_σ	[MeV]	492.250	504.890	508.194	526.059
m_ω	[MeV]	783.000	780.000	782.501	783.000
m_ρ	[MeV]	763.000	763.000	763.000	763.000
g_σ		10.138	9.111	10.217	10.4444
g_ω		13.285	11.493	12.868	12.945
g_ρ		4.976	5.507	4.474	4.383
g_2	[fm^{-1}]	-12.172	-2.304	-10.431	-6.9099
g_3		-36.265	-13.783	-28.885	-15.8337

$$\left[-\partial_r^2 - \frac{2}{r}\partial_r + \frac{l\,(l+1)}{r^2}\right] A^0 = e\rho_c^{\mathrm{sph}}\ . \tag{36d}$$

In the RMF description of spherical nuclei, $l = 0$ in the Klein-Gordon equations. The above set of equations (34-36) is solved self-consistently as we described in Section III. The solutions depend on the parameters of the Lagrangian density (5). The meson masses, the coupling constants, and the parameters of the non linear interaction $U(\sigma)$ are obtained by fitting of experimental data of a few finite spherical nuclei and of nuclear matter. The nuclear properties fitted are the ground state binding energy, the charge radius, and (if available) the neutron radius. The nuclear matter properties considered are the empirical equilibrium density, the binding energy per particle, the incompressibilty, the asymmetry parameter, and the effective mass.

In Table I we list the values of several sets of parameters which have been proposed. Once the parameters have been specified, we can calculate the properties of many closed shell nuclei. In Table II we show the results for the binding energy per nucleon, the charge radius, and the nuclear r.m.s. radius for ^{16}O, ^{40}Ca, ^{48}Ca, ^{90}Zr, and ^{208}Pb obtained using the sets NLSH and NL3.

In Figs. 1 through 6 we display the charge density, the scalar and vector potentials, and the effective mass M^*/M for ^{16}O, ^{40}Ca, and ^{208}Pb. In finite nuclei these fields assume a Woods-Saxon shape: they are approximately constant in the nuclear interior, apart from small mean field fluctuations, and vanish outside the nucleus. The model distinguishes in the nucleus a large attractive scalar field S and a large repulsive vector field V. In Fig. 7 we compare the predicted single particle spectrum for ^{208}Pb with experimental data for low-lying states derived from neighboring nuclei. The RMF calculations reveal a shell structure; the level ordering and the gap between the last occupied and the first unoccupied level are well reproduced. It is important to stress that, as no parameters are fitted to the spectrum, we derive the level structure of the shell model from bulk nuclear properties.

B. Deformed nuclei

We extend the above equations (34-36) to deal with axially symmetric nuclei [12]. Since the densities are still invariant with respect to rotation around the symmetry axis, it is useful to work with the cylindrical coordinates

$$x = r_\perp \cos\phi\ , \qquad y = r_\perp \sin\phi\ , \qquad \text{and} \qquad \mathrm{z}\ , \tag{37}$$

where the z axis is taken as the symmetry axis. The Dirac spinor can be written

$$\begin{aligned} \Psi_i &= \begin{pmatrix} g_i(\boldsymbol{r},t) \\ \mathrm{i}f_i(\boldsymbol{r},t) \end{pmatrix} \\ &= \frac{1}{\sqrt{2\pi}} \begin{pmatrix} g_i^+(z,r_\perp)\exp\{(\Omega_i - 1/2)\,\phi\} \\ g_i^-(z,r_\perp)\exp\{(\Omega_i + 1/2)\,\phi\} \\ \mathrm{i}f_i^+(z,r_\perp)\exp\{(\Omega_i - 1/2)\,\phi\} \\ \mathrm{i}f_i^-(z,r_\perp)\exp\{(\Omega_i + 1/2)\,\phi\} \end{pmatrix} X_{t_i}(t)\ , \end{aligned} \tag{38}$$

TABLE II. The binding energy per nucleon, charge radius, and nuclear r.m.s. radius for ^{16}O, ^{40}Ca, ^{48}Ca, ^{90}Zr, and ^{208}Pb, obtained with the set NLSH and NL3, compared with the experimental data. From Ref. [12].

	Nucleus	B/A [MeV]	r_{ch} [fm]	r_{nuc} [fm]
^{16}O	NLSH	-8.022	2.733	2.582
	NL3	-8.051	2.761	2.612
	expt	-7.976	2.730	
^{40}Ca	NLSH	-8.500	3.470	3.344
	NL3	-8.550	3.488	3.362
	expt	-8.552	3.450	
^{48}Ca	NLSH	-8.648	3.474	3.500
	NL3	-8.649	3.483	3.516
	expt	-8.667	3.451	
^{90}Zr	NLSH	-8.701	4.261	4.240
	NL3	-8.704	4.270	4.252
	expt	-8.710	4.258	
^{208}Pb	NLSH	-7.885	5.515	5.614
	NL3	-7.887	5.524	5.633
	expt	-7.868	5.503	

where Ω_i is the eigenvalue of the projection of the single particle angular momentum $\jmath$ over the z axis and t_i is the third component of the isospin. For each solution with positive Ω_i we have the time reversed solution with the same energy

$$\begin{aligned}\Psi_i &\equiv \left\{g_i^+, g_i^-, f_i^+, f_i^-, \Omega_i\right\} \\ &\to \Psi_{\bar{i}} = T\Psi_i \equiv \left\{-g_i^-, g_i^+, f_i^-, -f_i^+, -\Omega_i\right\} . \end{aligned} \tag{39}$$

The wave functions $g_i^\pm(z, r_\perp)$ and $f_i^\pm(z, r_\perp)$ are solutions of the Dirac equations

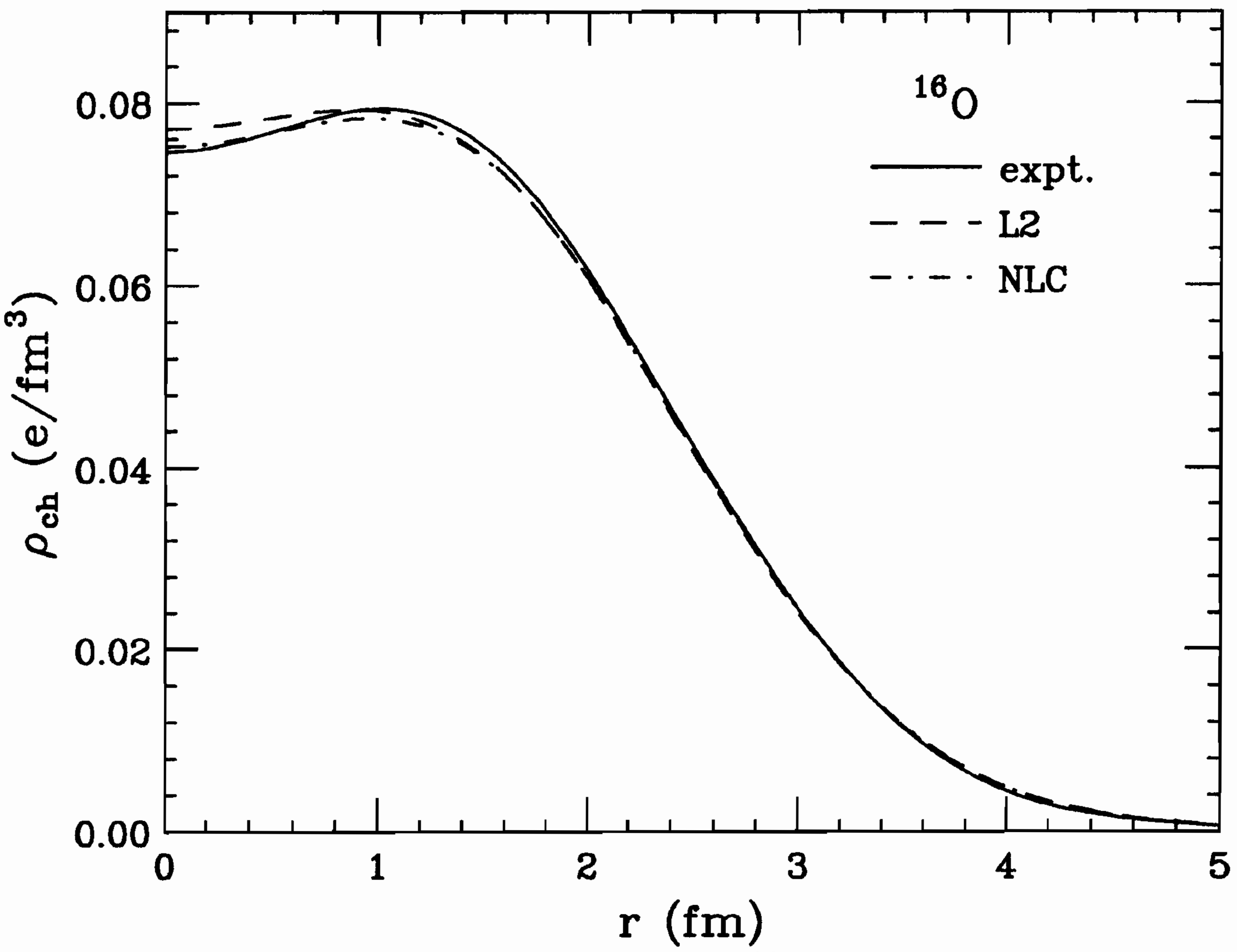

FIG. 1. Charge density distributions for ^{16}O. The experimental curve is from Ref. [16]. The Dirac-Hartree calculations for parameter set L2 give the dashed curve, while those from set NLC give the dot-dashed curve. From Ref. [6].

$$(M^* + V)\, g_i^+ + \partial_z f_i^+ + \left(\partial_{r_\perp} + \frac{\Omega + 1/2}{r_\perp}\right) f_i^- = \varepsilon_i g_i^+ \,, \tag{40a}$$

$$(M^* + V)\, g_i^- - \partial_z f_i^- + \left(\partial_{r_\perp} - \frac{\Omega - 1/2}{r_\perp}\right) f_i^+ = \varepsilon_i g_i^- \,, \tag{40b}$$

$$(M^* - V)\, f_i^+ + \partial_z g_i^+ + \left(\partial_{r_\perp} + \frac{\Omega + 1/2}{r_\perp}\right) g_i^- = -\varepsilon_i f_i^+ \,, \tag{40c}$$

$$(M^* - V)\, f_i^- - \partial_z g_i^- + \left(\partial_{r_\perp} + \frac{\Omega - 1/2}{r_\perp}\right) g_i^+ = -\varepsilon_i f_i^- \,. \tag{40d}$$

Thanks to time reversal symmetry, the contributions to the densities of the two time reversed states i and $\bar{\imath}$ are identical. Therefore the densities are

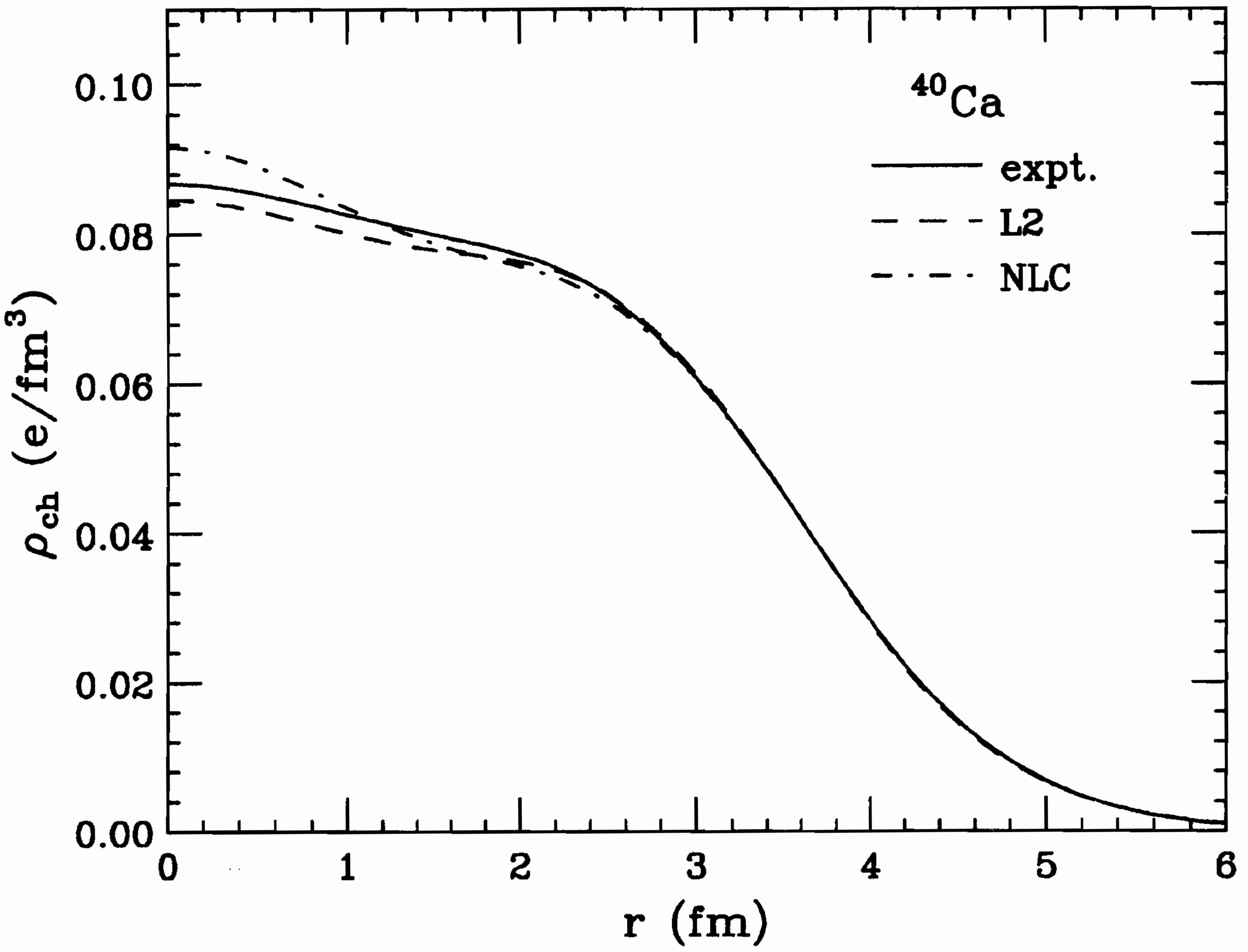

FIG. 2. The same as in Fig. 1, but for ^{40}Ca.

$$\rho_{\rm s} = 2\sum_{i=1} n_i \left[\left(|g_i^+|^2 + |g_i^-|^2\right) - \left(|f_i^+|^2 + |f_i^-|^2\right)\right] , \tag{41a}$$

$$\rho_{\rm B} = 2\sum_{i=1} n_i \left[\left(|g_i^+|^2 + |g_i^-|^2\right) + \left(|f_i^+|^2 + |f_i^-|^2\right)\right] , \tag{41b}$$

and the same for ρ_3 and $\rho_{\rm c}$. The sum runs only over the positive Ω_i states. The Klein-Gordon equations in cylindrical coordinates determine the fields

$$\left[-\frac{1}{r_\perp}\partial_{r_\perp} r_\perp \partial_{r_\perp} - \partial_z^2 + m_\sigma^2\right] \sigma = -g_\sigma \rho_{\rm s} - g_2\sigma^2 - g_3\sigma^3 , \tag{42a}$$

$$\left[-\frac{1}{r_\perp}\partial_{r_\perp} r_\perp \partial_{r_\perp} - \partial_z^2 + m_\omega^2\right] \omega^0 = g_\omega \rho_{\rm B} , \tag{42b}$$

$$\left[-\frac{1}{r_\perp}\partial_{r_\perp} r_\perp \partial_{r_\perp} - \partial_z^2 + m_\rho^2\right] \rho^0 = g_\rho \rho_3 , \tag{42c}$$

$$\left[-\frac{1}{r_\perp}\partial_{r_\perp} r_\perp \partial_{r_\perp} - \partial_z^2\right] A^0 = e\rho_{\rm c} . \tag{42d}$$

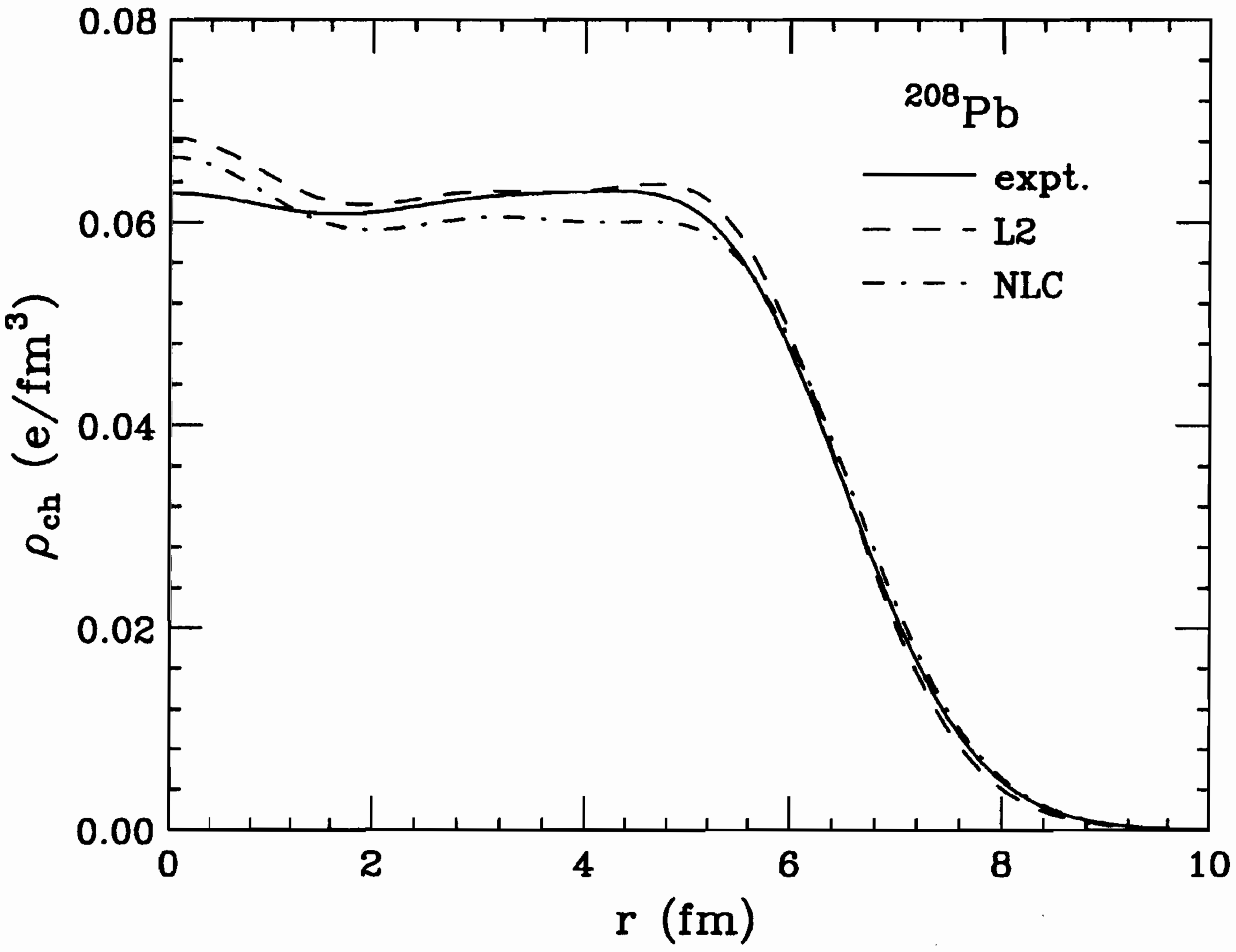

FIG. 3. The same as in Fig. 1, but for ^{208}Pb.

The calculations are usually performed expanding $g_i^\pm$ and $f_i^\pm$ in terms of the eigenfunctions of a deformed axial symmetric oscillator potential

$$V_{\rm osc}(z, r_\perp) = \frac{1}{2} M\omega_z^2 z^2 + \frac{1}{2} M\omega_\perp^2 r_\perp^2 \ . \tag{43}$$

The eigenfunctions of the deformed harmonic oscillator can be written explicitly as

$$\begin{aligned}\Phi_\alpha(z, r_\perp, \phi, s, t) &= \Phi_{n_z}(z)\Phi_{n_r}^{m_l}(r_\perp)\frac{1}{\sqrt{2\pi}} \exp\{im_l\phi\} X_{m_s}(s) X_{t_\alpha}(t) \\ &= \Phi_\alpha(\boldsymbol{r}, s) X_{t_\alpha}(t) \ , \end{aligned} \tag{44}$$

where $\Phi_{n_z}(z)$ and $\Phi_{n_r}^{m_l}(r_\perp)$ are expressed by the Hermite and associated Laguerre polynomials. The solutions of the Dirac equation in the axially symmetric case are expanded as

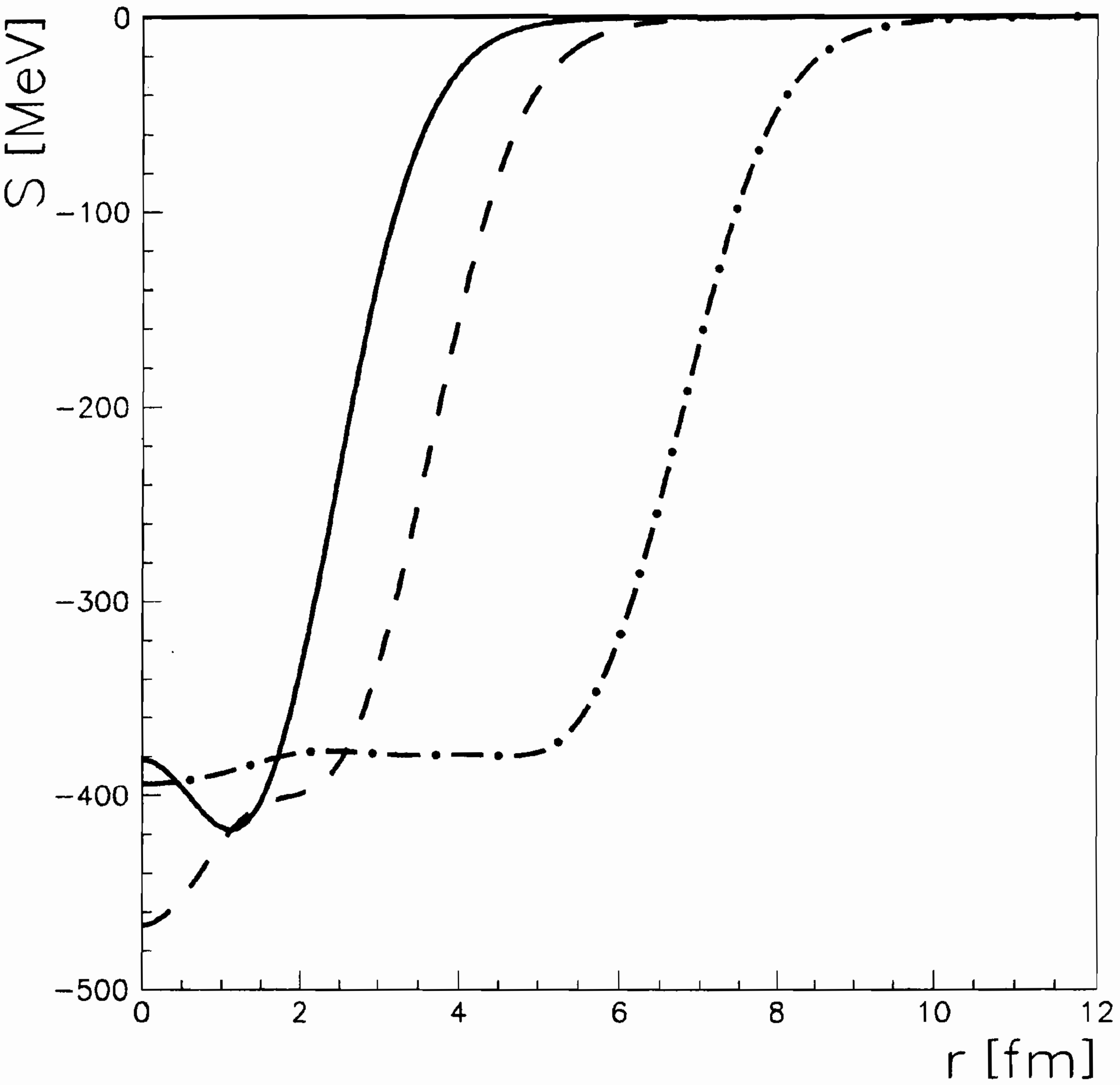

FIG. 4. Scalar potential $S = g_\sigma \sigma$ for ^{16}O (solid line), ^{40}Ca (dashed line), and ^{208}Pb (dot-dashed line) obtained with the set NLSH and the code ADFG of Ref. [10].

$$g_i(\boldsymbol{r}, s, t) = \sum_{\alpha}^{\alpha_{\max}} g_\alpha^{(i)} \Phi_\alpha(\boldsymbol{r}, s) X_{t_i}(t) \ , \tag{45a}$$

$$f_i(\boldsymbol{r}, s, t) = \sum_{\overline{\alpha}}^{\overline{\alpha}_{\max}} f_{\overline{\alpha}}^{(i)} \Phi_{\overline{\alpha}}(\boldsymbol{r}, s) X_{t_i}(t) \ . \tag{45b}$$

The Dirac equation reduces to a symmetric matrix diagonalization, while the Klein-Gordon equations for the meson fields become an inhomogeneous set of linear equations. For the Coulomb field, due

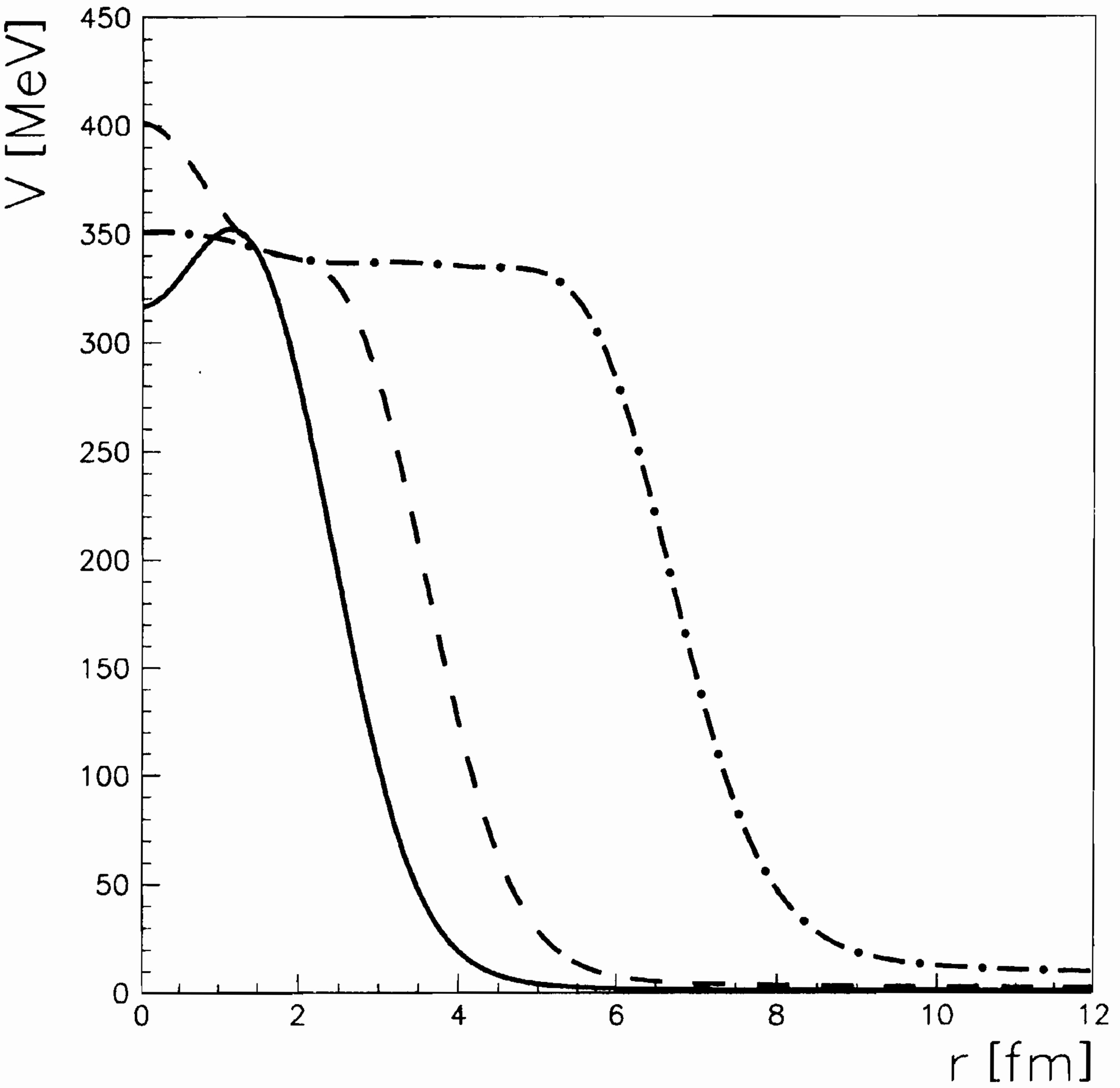

FIG. 5. Vector potential $V = g_\rho \rho_3^0 + g_\omega \omega^0 + eA^0$ for proton states of ^{16}O (solid line), ^{40}Ca (dashed line), and ^{208}Pb (dot-dashed line) obtained with the set NLSH and the code ADFG of Ref. [10].

to its long range character, the Green function method is used. Details of the calculations can be found in Ref. [12].

In Fig. 8 we show the isotopic dependence of the deviation of the theoretical mass calculated in RMF theory from the experimental values for Sn isotopes. The theoretical results were obtained using the sets NL1, NLSH, and NL3. All parametrizations give a very good description of the experimental masses.

In Table III we compare the results for some deformed rare earth

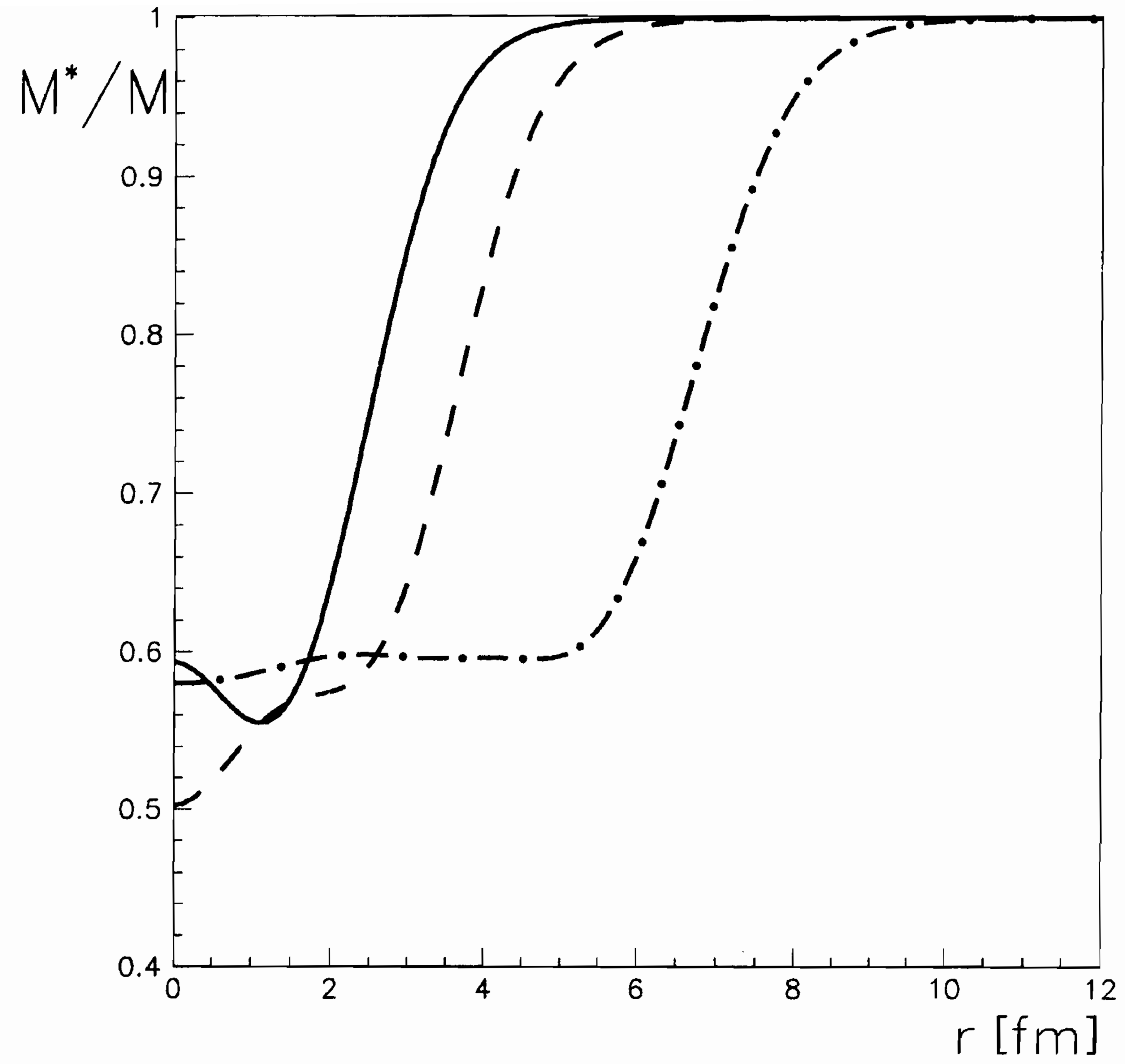

FIG. 6. Effective mass M^*/M for ^{16}O (solid line), ^{40}Ca (dashed line), and ^{208}Pb (dot-dashed line) obtained with the set NLSH and the code ADFG of Ref. [10].

and actinide nuclei obtained with parametrization NL3 with available experimental data. We find an excellent agreement between RMF theory results and observed data. This is mainly due to the non linear coupling between the σ mesons in Eq. (6). Otherwise it is impossible to reproduce the proper spin-orbit splitting, which is necessary to describe nuclear deformation.

We recall that the quadrupole $Q_{\mathrm{n,p}}$ and hexadecupole $H_{\mathrm{n,p}}$ moments for neutrons and protons are related to the expectation values

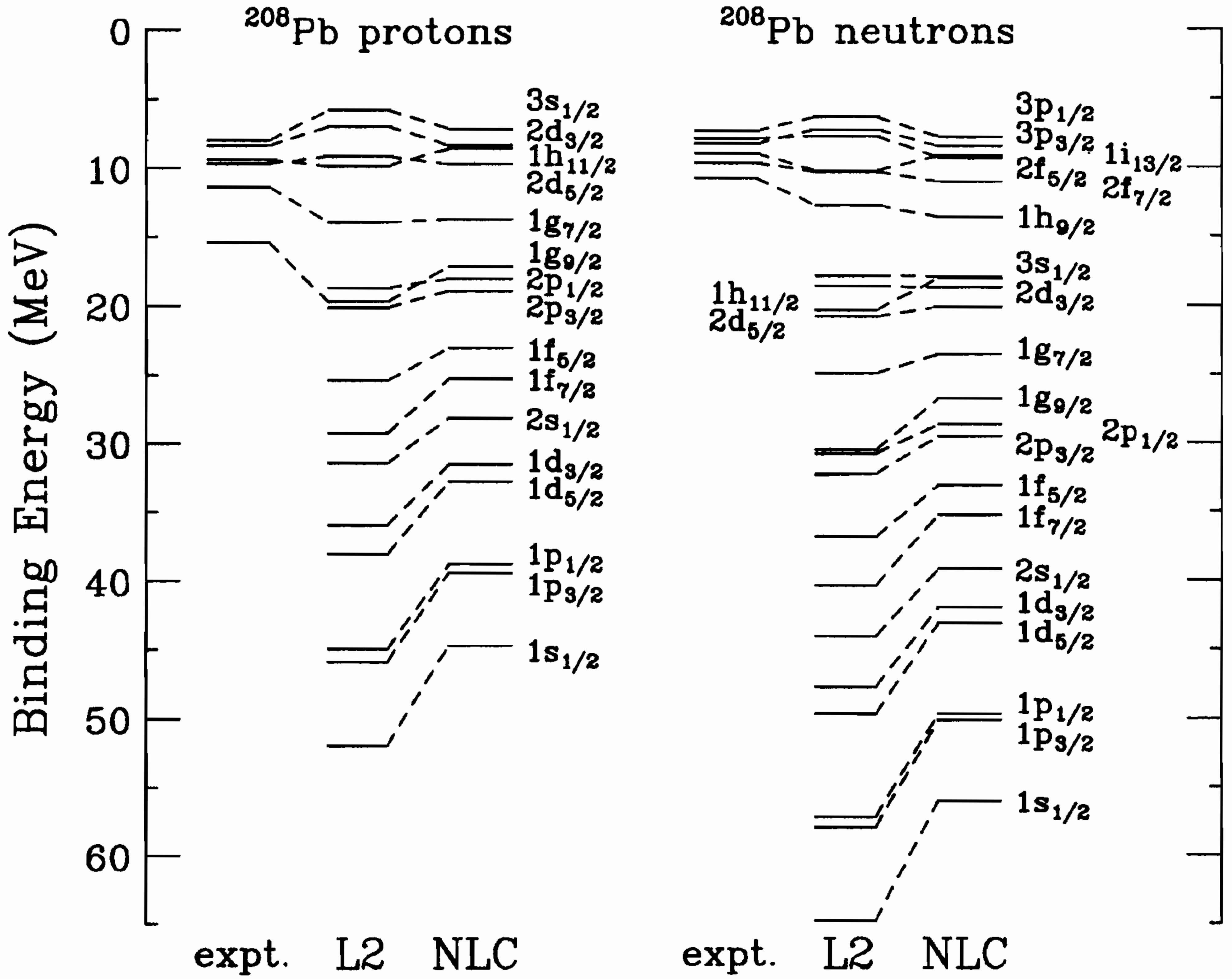

FIG. 7. Predicted spectrum for occupied single particle levels in ^{208}Pb obtained with the set L2 and NLC. The experimental values for low-lying states derived from neighboring nuclei are also shown. From Ref. [6].

of the spherical harmonics by

$$\langle r^2 Y_{20}(\vartheta, 0)\rangle_{\mathrm{n,p}} = \frac{1}{2}\sqrt{\frac{5}{4\pi}}\, Q_{\mathrm{n,p}} \,, \tag{46}$$

$$\langle r^4 Y_{40}(\vartheta, 0)\rangle_{\mathrm{n,p}} = \frac{1}{8}\sqrt{\frac{9}{4\pi}}\, H_{\mathrm{n,p}} \,. \tag{47}$$

The quadrupole deformation parameter β is obtained from the calculated quadrupole moment through

$$Q = Q_{\mathrm{n}} + Q_{\mathrm{p}} = \frac{3}{4\pi}\sqrt{\frac{16\pi}{5}}\, A R_0^2 \beta \,, \tag{48}$$

where $R_0 = 1.2A^{1/3}$.

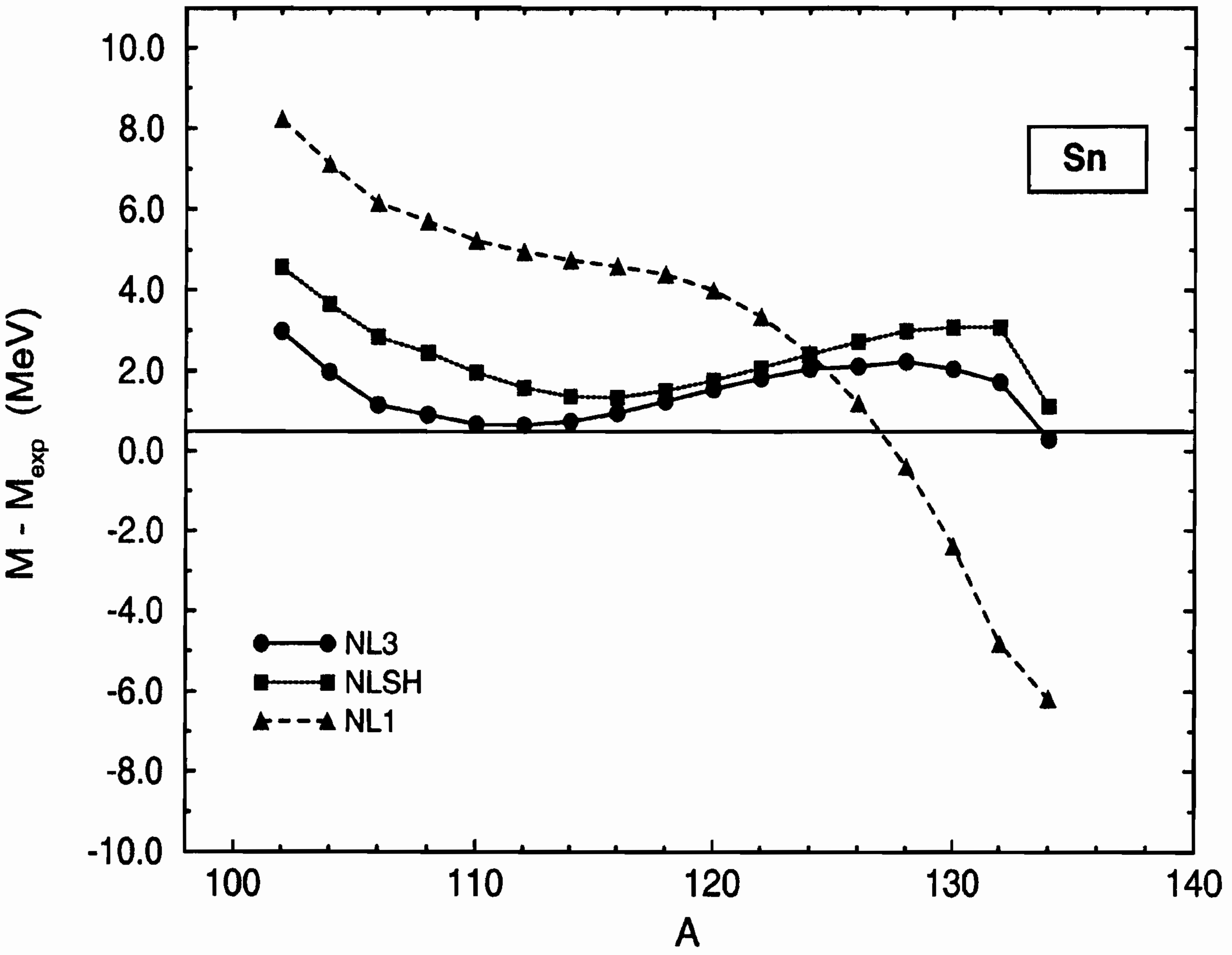

FIG. 8. The deviation of the theoretical masses of Sn isotopes calculated in RMFT with NL1, NLSH, and NL3, from the experimental values. From Ref. [15].

V. CONCLUSIONS

In this work we have introduced an effective meson-baryon field theory to describe finite nuclei. The model includes the spin properties in a natural way and distinguishes in the nucleus a large attractive scalar field S and a large repulsive vector field V. The number of adjustable parameters used in RMFT is limited as compared to non relativistic descriptions based on realistic NN potential. The RMFT equations have been solved in a mean field approximation to yield static properties (binding energies, nuclear radii, densities, spectra, etc.) for spherical nuclei with closed shell and for axial symmetric deformed nuclei. The agreement with experimental data

TABLE III. Total binding energies (BE), charge radii (r_{ch}), quadrupole deformation parameters (β), proton quadrupole moments (Q_{p}), and proton hexadecupole (H_{p}) moments for some deformed rare earth and actinide nuclei with the parametrization NL3. The values in parentheses are the experimental data. From Ref. [15].

	BE [MeV]	r_{ch} [fm]	β	Q_{p} [barn]	H_{p} [barn^2]
^{152}Sm	-1294.49	5.177	0.301	5.63	0.48
	(-1294.05)	(5.099)	(0.306)	(5.78)	(0.46)
^{158}Gd	-1296.40	5.176	0.342	7.14	0.48
	(-1295.90)	(5.172)	(0.348)	(7.36)	(0.39)
^{162}Dy	-1342.09	5.227	0.347	7.54	0.45
	(-1324.11)	(5.210)	(0.341)	(7.36)	(0.27)
^{166}Er	-1352.06	5.272	0.349	7.87	0.36
	(-1351.57)	(5.303)	(0.342)	(7.70)	(0.27)
^{174}Yb	-1406.15	5.336	0.328	7.77	0.04
	(-1406.60)	(5.410)	(0.325)	(7.58)	(0.22)
^{232}Th	-1766.29	5.825	0.251	9.23	1.06
	(-1766.69)	(5.790)	(0.261)	(9.62)	(1.22)
^{236}U	-1790.67	5.873	0.275	10.60	1.16
	(-1790.42)		(0.282)	(10.80)	(1.30)
^{238}U	-1801.39	5.892	0.283	10.93	1.07
	(-1801.69)	(5.854)	(0.286)	(11.12)	(1.38)

is excellent and shows that RMFT can provide us a quantitative description of ground state properties of nuclei.

ACKNOWLEDGMENTS

I am grateful to my friend and colleague Sabrina Casanova for providing me a copy of the code `TIMORA` [9].

[1] R. Machleidt, Phys. Rev. C **63**, 024001 (2001)

[2] R. Machleidt and I. Slaus, J. Phys. G: Nucl. Part. Phys. **27**, R69 (2001)

[3] J. Carlson and R. Schiavilla, Rev. Mod. Phys. **70-3**, 743 (1998).

[4] B. D. Serot and J. D. Walecka, Adv. Nuc. Phys. **16**, 1 (1986).

[5] B. D. Serot, Rep. Prog. Phys. **55**, 1855 (1992).

[6] B. D. Serot and J. D. Walecka, Int. J. Mod. Phys. **E 6**, 515 (1997).

[7] P. G. Reinhard, Rep. Prog. Phys. **52**, 439 (1989).

[8] P. Ring, Prog. Part. Nucl. Phys. **37**, 193 (1996).

[9] C. J. Horowitz, D. P. Murdoch, and B. D. Serot, in *Computational Nuclear Physics I: Nuclear Structure*, edited by K. Langanke, J. A. Maruhn, and S. E. Koonin (Springer-Verlag, Berlin, 1991).

[10] W. Pöschl, D. Vretenar, A. Rummel, and P. Ring, Comput. Phys. Commun. **101**, 75 (1997).

[11] W. Pöschl, D. Vretenar, and P. Ring, Comput. Phys. Commun. **103**, 217 (1997).

[12] P. Ring, Y. K. Gambhir, and G. A. Lalazissis, Comput. Phys. Commun. **105**, 77 (1997).

[13] F. Mandl and G. Shaw, *Quantum Field Theory*, (John Wiley and Sons, Chichester, 1993).

[14] D. Vautherin, Phys. Rev. C **7**, 296 (1973).

[15] G. A. Lalazissis, J. König, and P. Ring, Phys. Rev. C **55**, 540 (1997).

[16] H. de Vries, C. W. de Jager, and C. de Vries, At. Data Nucl. Tables **36**, 495 (1987).

	STUDY OF THE CHARACTERISTICS OF RESISTIVE PLATE CHAMBERS IN THE RD5 EXPERIMENT - L. Pontecorvo (RD5 Coll.)	pag. 145
	OPERATION OF RESISTIVE PLATE CHAMBERS WITH PURE CF_3BR - R. Cardarelli	pag. 159
	WLDC: A DRIFT CHAMBER WITH A PAD RPC FOR MUON DETECTION AT LHC H. Faissner, Th. Moers, R. Priem, B. Razen, D. Rein, H. Reithler, D. Samm, R. Schleichert, H. Schwarthoff, H. Tuchscherer, H. Wagner	pag. 167
	GLASS ELECTRODE SPARK COUNTER - G. Bencivenni, G. Felici, E. Iacuessa, C. Gustavino, M. D'Incecco	pag. 181
	RPC READOUT FOR PARTICLE ASTROPHYSICS - M. Bonori, U. Contino, F. Massa	pag. 193
	RESULTS OF TESTS OF PROTOTYPE RESISTIVE PLATE CHAMBERS - I. Crotty, J. Lamas Valverde, G. Laurenti, M.C.S. Williams, A. Zichichi	pag. 199
	GLASS ELECTRODES RPC: PERFORMANCE AND WORKING MODEL - M. Bonori, U. Contino, F. Massa	pag. 207
	FAST PARALLEL RPC READOUT SYSTEM - A. Lanza, G. Liguori, P. Torre, M. Ambrosio, G.C. Barbarino, M. Iacovacci, A. Lauro, G. Osteria, G. Agnetti, O. Catalano, L. Scarsi	pag. 219
	DATA ACQUISITION SYSTEMS DEVELOPED AT CAEN - F. Catarsi, C. Landi, G. Franchi, M. Lippi	pag. 225
Volume IX - n. 1 15/4/1994	RETICOLI DISORDINATI: IL MODELLO DI ANDERSON - R. Farchioni	pag. 1
	BREVE INTRODUZIONE ALLA TEORIA QUANTISTICA DELLA STIMA - M. Paris	pag. 23
	SUSY - M. Cacciari	pag. 36
	MASSE DEL QUARK TOP E DEL BOSONE DI HIGGS NEL MODELLO STANDARD - F. Piccinini	pag. 79
	DIELETTROFORESI: LIEVITAZIONE A CONTROLLO REAZIONATO - L. Laboranti	pag. 97
Volume IX - n. 2 15/11/94	PROPRIETÀ FISICHE DI CLUSTER METALLICI - V. Bellani	pag. 1
	APPLICAZIONI DI RETI NEURALI ALLA FISICA DELLE ALTE ENERGIE - P. Vitulo	pag. 18
	CRITTOGRAFIA QUANTISTICA - C. Macchiavello	pag. 47
	IL "PARADOSSO" DEI GEMELLI - M. Cacciari	pag. 64
	TRANSIZIONI DI FASE NEL PRIMO UNIVERSO - S. Rolli	pag. 77
	SULLA STABILITÀ DINAMICA DELLA BICICLETTA - M. Paris	pag. 102
Volume X - n. 1 15/3/95	FISICA DELLE INTERAZIONI FONDAMENTALI CON NEUTRONI FREDDI A. Guglielmi	pag. 1
	EFFETTO DELLA DISPERSIONE SPAZIALE SULL'ASSORBIMENTO ECCITONICO DEI CRISTALLI - G. Panzarini	pag. 79
	IL CAMPO ELETTRICO GENERATO DA UNA CARICA PUNTIFORME IN MOVIMENTO IN UN MEZZO ISOTROPO - U. Bellotti	pag. 105
Volume X - n. 2 15/6/95	SPETTROSCOPIA VIBRAZIONALE A RISOLUZIONE TEMPORALE - P. Calvi	pag. 1
	IL CONTROLLO DEI SISTEMI CAOTICI - M. Maris	pag. 25
	ASPETTI SPERIMENTALI DELLA FISICA DEI MESONI *B* A LEP - L. Viola	pag. 59
	AN INTRODUCTION TO THE PERTURBATIVE QCD POMERON AND TO JET PHYSICS AT LARGE RAPIDITIES - V. Del Duca	pag. 91
Volume X - n. 3 15/12/95	DIFFUSIONE DI LUCE DA SUPERFICI RUGOSE - M. Patrini	pag. 1
	PRINCIPI E APPLICAZIONI DELLE SPETTROSCOPIE A DIFFRAZIONE DI ELETTRONI - L. Rossi	pag. 25
	IONI DI TERRE RARE IN SEMICONDUTTORI - E. Pavarini	pag. 49
	PERDITA DI ENERGIA PER IONIZZAZIONE - P. Montagna	pag. 85
Volume XI - n. 1 15/6/96	TOPICS IN RESISTIVE PLATE CHAMBERS - R. Santonico	pag. 1
	THE AVALANCHE TO STREAMER TRANSITION IN RPC'S - R. Cardarelli, R. Santonico, V. Makeev	pag. 11
	A MODEL OF AVALANCHE TO STREAMER TRANSITION IN PPC/RPC DETECTORS - P. Fonte	pag. 25
	NEW DEVELOPMENTS OF RPC: SECONDARY ELECTRON EMISSION AND MICROSTRIP READOUT - E. Cerron Zeballos, I. Crotty, P. Fonte, D. Hatzifotiadou, J. Lamas Valverde, V. Peskov, M.C.S. Williams, A. Zichichi	pag. 45
	THE RPC SYSTEM FOR THE CMS EXPERIMENT AT LHC- G. Wrochna	pag. 63
	RPC TRIGGER DESIGN FOR THE FUTURE EXPERIMENT CMS - G. De Robertis, M. Gorski, M. Konecki, J. Krolikowski, I.M. Kudla, M. Lewandowski, F. Loddo, K. Pozniak, A. Ranieri, G. Wrochna	pag. 79
	THE LEVEL-1 MUON TRIGGER ALGORITHM OF THE ATLAS EXPERIMENT - A. Nisati	pag. 91
	RESISTIVE PLATE COUNTERS FOR THE BELLE DETECTOR AT KEKB - N. Morgan	pag. 101
	PRELIMINARY DESIGN OF THE BABAR DETECTOR FOR MUONS AND NEUTRAL HADRONS AT PEP II - N. Cavallo	pag. 115
	THE RPC FORWARD-BACKWARD TRIGGER SYSTEM OF THE L3 EXPERIMENT - P. Paolucci	pag. 129
	PERFORMANCES OF THE RPC TRIGGER SYSTEM IN THE L3	

Volume XIII - n. 1 15/4/98	I BUCHI NERI: OSSERVAZIONE NEI SISTEMI STELLARI BINARI - G. Bonomi	pag. 1
	SPETTROMETRIA DI MASSA A IONI SECONDARI - R. Rolli	pag. 17
	FUNZIONI DI STRUTTURA IN ELETTRODINAMICA QUANTISTICA - E. Poli	pag. 45
	CALORIMETRIA CON FIBRE AL QUARZO - N. Moggi	pag. 71
	LA FRIZIONE DINAMICA IN SCENARI DI INTERESSE ASTROFISICO - A. Pallavicini	pag. 93
Volume XIII - n. 2 15/5/98	IV International Workshop on : RESISTIVE PLATE CHAMBERS AND RELATED DETECTORS - Sergio P. Ratti, Riccardo De Asmundis	pag. 1 pag.393
Volume XIV - n. 1 15/5/99	CORRELAZIONI NELLA PRODUZIONE MULTIPLA DI PARTICELLE A $\sqrt{s}$ = 630 E 1800 GeV - Niccolò Moggi	pag. 1
	FUNZIONI DI STRUTTURA IN QCD PERTURBATIVA – Fabrizio Gangemi	pag. 23
	I BUCHI NERI: OSSERVAZIONE NEI SISTEMI STELLARI BINARI - G. Bonomi	pag. 51
	QUANTIZZAZIONE BRS DELLE TEORIE DI GAUGE – Andrea Pallavicini	pag. 85
	CP VIOLATION IN THE Bo SECTOR – Amedeo Perazzo	pag. 101
Volume XV - n. 1 15/10/00	PROVE SPERIMENTALI DELLA QUANTIZZAZIONE DELLA CARICA ELETTRICA – D. Iannuzzi	pag. 1
	SURVIVAL PROBABILITY OF LARGE RAPIDITY GAPS IN $\bar{p}p$ COLLISION – M.M. Block, F. Halzen	pag. 35
	SPIN SUSCEPTIBILITY AND DIAMAGNETIC SUSCEPTIBILITY AT THE SUPERCONDUCTING TRANSITION. EFFECTS OF MAGNETIC FIELD AND DOPING-DEPENDENCE IN YBCO COMPOUNDS – A. Rigamonti, P. Tedesco	pag. 49
	RECENTI SVILUPPI SULLA REGOLA DI SOMMA DI COULOMB NEI NUCLEI – A. Meucci	pag. 87
Volume XVI - n. 1 15/03/01	MAGNETIC CORRELATIONS AND SPIN DYNAMICS IN PURE AND DOPED HALDANE CHAINS: ^{89}Y NMR IN $Y_{2-y}Ca_yBaNi_{1-x}Mg_xO_5$ – F. Tedoldi	pag. 1
	A FACILITY FOR THE STUDY OF PARTICLE-INDUCED INFRARED EMISSION IN NOBLE GASES – D. Iannuzzi	pag. 93
Volume XVI - n. 2 25/07/01	PARTICLE INDUCED INFRARED EMISSION IN GASES, LIQUIDS, AND CRYSTALS - D. Iannuzzi	pag. 1
Volume XVII - n. 1 15/12/02	NONADIABATIC SUPERCONDUCTIVITY: FROM THEORY TO MATERIALS - P. Paci	pag. 1